



Wrocław University  
of Science and Technology



**Collins Aerospace**  
An **RTX** Business

---

**PHD THESIS**

**THE IMPACT OF DYNAMIC LOADS ON TRANSMISSION SHAFTS OF  
THE CIVIL AIRCRAFT**

**by Michał Ptak, MSc, Eng.**

Wrocław University of Technology Supervisor  
Jerzy Czmochocki, Assoc. Prof., PhD, Eng.

Collins Aerospace Company Supervisor  
Marcin Cis, MSc, Eng.

WROCLAW 2023



## **ACKNOWLEDGEMENTS**

The accomplishment of the doctoral dissertation was supported by the "Doktorat Wdrożeniowy" program financed by the Polish Ministry of Education and Science, edition 3<sup>rd</sup>, grant no. DWD/3/36/2019.

I am most sincerely grateful to MSc. Eng. Marcin Cis for his expert advice, sharing his experience and extensive knowledge in the aerospace and automotive industry in the fields of dynamic analysis and programming, as well as for his kind and friendly interest in my research.

I would like to thank Assoc. Prof. PhD Eng. Jerzy Czmochoński for all his support during my research and helping me get acquainted with the scientific community.

I would like to thank MSc. Eng. Dariusz Kiełbowicz for his support with benchmarking my tools and algorithm with MSC CAE Fatigue software and contact with the developer of this software to discuss some of the limitations of legacy techniques for vibration damage estimation.

I wish to express my sincere gratitude to my mother, Krystyna Ptak, for her support and motivating me to work hard on my PhD.

I also wish to express my sincere gratitude to Miss Weronika Kowalińska, for her patience, general support and faith in me during my PhD studies.

---

## CONTENTS

<u>ACKNOWLEDGEMENTS</u> .....	2
<u>CONTENTS</u> .....	3
<u>ABBREVIATIONS</u> .....	18
<u>CHAPTER 1 INTRODUCTION</u> .....	19
<u>CHAPTER 2 VIBRATION FATIGUE DAMAGE PREDICTION UNDER STOCHASTIC LOADING IN THE FREQUENCY DOMAIN THEORETICAL BACKGROUND</u> .....	23
2.1 The Narrow Band method – developed by Bendat and Rice .....	24
2.2 The Dirlik method – a general solution for narrow and wide band processes .....	27
2.3 The Wide Band method – developed by Steinberg.....	29
2.4 The Lalanne/Rice method – a general solution for narrow-band and wide-band signals	33
2.5 Review of other methods for PDF estimation.....	34
2.5.1 The Tunna Solution of PDF estimation .....	34
2.5.2 The Wirsching Method of vibration fatigue damage estimation .....	34
2.5.3 The Chaudhury & Dover Solution of vibration fatigue damage estimation .....	34
2.5.4 The Hancock Solution of vibration fatigue damage estimation .....	35
<u>CHAPTER 3 VIBRATION FATIGUE DAMAGE PREDICTION UNDER STOCHASTIC LOADING IN THE FREQUENCY DOMAIN – ALGORITHM, PROGRAMMING AND COMPUTATION</u> .....	36
3.1 Algorithm for vibration damage estimation in the frequency domain - introduction.....	39
3.2 Spectral Moment estimation using different numerical integration methods.....	45
3.2.1 The Cumulative Trapezoidal integration method.....	45
3.2.2 Numerical integration methods used – summary.....	48
3.3 Created Python algorithm verification against the commercial MSC tool – CAE Fatigue	49
3.3.1 Sample description .....	50
3.3.2 Material properties case study.....	53
3.3.3 Algorithms benchmarked against commercial software .....	55
3.4 Lalanne method modification .....	62
3.4.1 Integration of the PDF for Dirlik, Lalanne and Narrow Band methods .....	62
3.4.2 Introduction modification of the Lalanne PDF function.....	64
<u>CHAPTER 4 VIBRATION FATIGUE DAMAGE PREDICTION UNDER STOCHASTIC LOADING – COMBINED FREQUENCY AND TIME DOMAIN CONSIDERATION</u> .....	67

---

4.1	Time signal generation from the PSD Response function .....	67
4.2	Time series Rainflow Cycle Counting algorithm .....	70
<b>CHAPTER 5 <u>COMBINED TIME AND FREQUENCY DOMAINS FOR VERIFICATION AND MODIFICATION OF THE LEGACY THEORY</u> .....</b>		<b>75</b>
5.1	Signal statistics in the time domain as a benchmark of the signal statistic in the frequency domain - research results.....	75
5.2	Narrow Band method modification .....	80
5.3	Vibration damage estimation with modified integration of spectral moments - results .	81
5.4	Populational research complementary to the Dirlik method .....	86
5.4.1	White noise random signal analysis .....	87
5.4.2	Wide band random signal analysis .....	96
5.4.3	Narrow Band random signal analysis .....	105
5.4.4	Summary and conclusion of the populational research .....	114
<b>CHAPTER 6 <u>DEVELOPING A METHOD FOR VIBRATION DAMAGE ESTIMATION UNDER COMBINED RANDOM AND DETERMINISTIC LOADING</u>.....</b>		<b>117</b>
6.1	Research for developing a new method - introduction .....	117
6.2	The Legacy method – vibration damage estimation under combined stochastic and deterministic loading in the frequency domain .....	119
6.3	Combined frequency and time domains vibration damage estimation under combined stochastic and deterministic loading – a new proposed method .....	121
6.4	Comparison of results obtained for the legacy method and the proposed method .....	126
6.5	Additional considerations made on the proposed method .....	127
6.5.1	White noise random signal analysis .....	127
6.5.2	Wide band random signal analysis .....	134
6.5.3	Narrow Band random signal analysis .....	141
6.5.4	Summary and conclusion for using the new proposed method .....	148
<b>CHAPTER 7 <u>USAGE DEVELOPED ALGORITHMS FOR VIBRATION DAMAGE PREDICTION OF AIRCRAFT TRANSMISSION SHAFTS</u>.....</b>		<b>149</b>
7.1	The transmission shaft geometry model and discrete model description.....	149
7.2	Correlation of the numerical environment with test results .....	151
7.3	Impact of stochastic dynamic loading on exemplary transmission shaft assessment using the developed methods – damage estimation under stochastic loading.....	153
7.3.1	Frequency domain damage estimation.....	153

---

7.3.2	Combined frequency and time domains damage estimation under stochastic loading .....	158
7.4	The impact of combined stochastic and deterministic dynamic loading on exemplary transmission shaft assessment – damage estimation under combined stochastic and deterministic loading.....	161
7.4.1	Frequency domain damage estimation under combined stochastic and deterministic loading .....	162
7.4.2	Combined time and frequency domain damage estimation under combined stochastic and deterministic loading.....	163
CHAPTER 8	<u>CONCLUSIONS AND FURTHER RESEARCH</u> .....	168
BIBLIOGRAPHY	.....	171

---

## FIGURES

Figure 1-1 Transmission shafts architecture in a slot and flap system [1] .....	20
Figure 1-2 Spectral density of signal strength for individual standard curves .....	21
Figure 2-1 The Narrow Band solution – all positive peaks are matched with corresponding troughs of similar magnitude, hence the green signal is transformed into a red signal .....	24
Figure 2-2 The wide-band time signal, following Gaussian distribution [6] .....	29
Figure 2-3 Upward zero crossing E[P] and peaks E[P] in the time series spectrum [8] .....	30
Figure 2-4 The narrow-band signal shape in the time and frequency domains, $\gamma \in 0.95; 1$ , [8]..	30
Figure 2-5 The wide-band signal shape in the time and frequency domains, $\gamma \in 0.5; 0.95$ , [8]..	31
Figure 2-6 The white noise signal shape in the time and frequency domains, $\gamma < 0.5$ , [8].....	31
Figure 2-7 The sinusoidal signal shape in the time and frequency domains, $\gamma = 1$ , [8] .....	31
Figure 2-8 The number of cycles histogram for the Steinberg method (3 bins method) for the narrow band signal [6].....	32
Figure 2-9 An example of the Rainflow cycle histogram based on the PSD of signal peaks for the Lalanne/Rice method [6] .....	33
Figure 3-1 Structure of the result repository in the Abaqus output database (.odb) file .....	36
Figure 3-2 PSD Response derivation based on the Transfer Function and PSD input loading .....	38
Figure 3-3 Part 1 of the algorithm for vibration damage assessment in the frequency domain ..	39
Figure 3-4 Part 2 of the algorithm for vibration damage assessment in the frequency domain ..	40
Figure 3-5 Part 3.1 of the algorithm for vibration damage assessment in the frequency domain, Dirlik method implementation .....	41
Figure 3-6 Part 3.2 of the algorithm for vibration damage assessment in the frequency domain, Bendat/Rice method implementation.....	42
Figure 3-7 Part 3.3 of the algorithm for vibration damage assessment in the frequency domain, Steinberg method implementation .....	43
Figure 3-8 Part 3.4 of the algorithm for vibration damage assessment in the frequency domain, Lalanne method implementation.....	44
Figure 3-9 The 0 Spectral moment obtained by the cumulative trapezoidal integration method of the transfer function .....	45
Figure 3-10 The 1 <sup>st</sup> Spectral moment obtained by the cumulative trapezoidal integration method of the transfer function .....	46
Figure 3-11 The 2 <sup>nd</sup> Spectral moment obtained by the cumulative trapezoidal integration method of the transfer function.....	46
Figure 3-12 The 4 <sup>th</sup> Spectral moment obtained by cumulative trapezoidal integration method of transfer function .....	47
Figure 3-13 Sample of the geometry used for the analysis .....	50

---

Figure 3-14 The geometry, discrete model, and graphical support representation of a sample taken for visualisation of the research results .....	50
Figure 3-15 Discrete FEM model graphical representation details .....	51
Figure 3-16 Best-fit S-N curves for notched, $K_t=3.0$ , fatigue behaviours of 17-4PH (H1025) stainless steel bar, longitudinal and long transverse directions [49] .....	53
Figure 3-17 The S-N curve for vibration fatigue consideration for 17-4PH (H1025) $K_t = 3$ .....	54
Figure 3-18 Visualisation of Dirlik Damage using a developed Python Algorithm at sample geometry using the Abaqus visualisation module and in-house script – white noise signal	56
Figure 3-19 Visualisation of Dirlik Damage obtained in the MSC CAE Fatigue commercial software environment – white noise signal .....	57
Figure 3-20 Visualisation of Dirlik Damage using the developed Python Algorithm at sample geometry using the Abaqus visualisation module and in-house script – wide band signal..	58
Figure 3-21 Visualisation of Dirlik Damage obtained in the MSC CAE Fatigue commercial software environment – wide band signal .....	59
Figure 3-22 Visualisation of Dirlik Damage using a developed Python Algorithm at sample geometry using the Abaqus visualisation module and in-house script – narrow band signal .....	60
Figure 3-23 Visualisation of Dirlik Damage obtained in the MSC CAE Fatigue commercial software environment – narrow band signal .....	61
Figure 3-24 Lalanne PDF in the function of a stress variable.....	62
Figure 3-25 Narrow Band Bendat PDF in the function of a stress variable .....	63
Figure 3-26 Dirlik PDF in the function of a stress variable.....	63
Figure 3-27 Error function $\text{erf}(x)$ and complementary error function – $\text{erfc}(x)$ , graphical representation .....	64
Figure 3-28 Modified Lalanne PDF in the function of a stress variable .....	65
Figure 3-29 Graphical comparison of Lalanne PDF – $LAL(s)$ and modified Lalanne PDF – $LALm(s)$ in the function of a stress variable .....	65
Figure 4-1 The process of recreating time signals from the frequency using the Monte Carlo method .....	67
Figure 4-2 The complex conjugate symmetry of the $\theta$ function .....	69
Figure 4-3 Rainflow Method graphical representation [59] .....	70
Figure 4-4 Flowchart of the Rainflow Cycle Counting Algorithm in the time domain.....	71
Figure 4-5 System response time history from the IFFT and Monte Carlo Methods – white noise signal .....	72
Figure 4-6 Initial time series processing extracting peak and trough for the Rainflow Counting Algorithm – white noise signal .....	72
Figure 4-7 Rainflow Cycle Counting Algorithm Histogram – white noise signal.....	72

---

Figure 4-8 System response time history from the IFFT and Monte Carlo Methods – wide band signal .....	73
Figure 4-9 Initial time series processing extracting peak and trough for the Rainflow Counting Algorithm – wide band signal .....	73
Figure 4-10 Rainflow Cycle Counting Algorithm Histogram – wide band signal .....	73
Figure 4-11 System response time history from the IFFT and Monte Carlo Methods – narrow band signal.....	74
Figure 4-12 Initial time series processing extracting peak and trough for the Rainflow Counting Algorithm – narrow band signal .....	74
Figure 4-13 Rainflow Cycle Counting Algorithm Histogram – narrow band signal.....	74
Figure 5-1 PSD response function for sample 1, irregular factor 0.975 .....	76
Figure 5-2 PSD response function for sample 11, irregular factor 0.486 .....	77
Figure 5-3 PSD response function for sample 16, irregular factor 0.258 .....	77
Figure 5-4 Graphical representation of the proposed reduced integration of spectral moments	82
Figure 5-5 Damage values for the searched population for the white noise signal, with a signal clipped at 3 standard deviations, block size $N=2^{12}$ .....	87
Figure 5-6 The best fitted distribution for damage values for the searched population for the white noise signal, with a signal clipped at 3 standard deviations, block size $N=2^{12}$ – Generalised Extreme Value distribution .....	88
Figure 5-7 Damage values for the searched population for the white noise signal, with a signal clipped at 3 standard deviations, block size $N=2^{14}$ .....	88
Figure 5-8 The best fitted distribution for damage values for the searched population for the white noise signal, with a signal clipped at 3 standard deviations, block size $N=2^{14}$ – Generalised Extreme Value distribution .....	89
Figure 5-9 Damage values for the searched population for the white noise signal, with a signal clipped at 3 standard deviations, block size $N=2^{16}$ .....	90
Figure 5-10 The best fitted distribution for damage values for the searched population for the white noise signal, with a signal clipped at 3 standard deviations, block size $N=2^{16}$ – Exponentiated Weibull distribution .....	90
Figure 5-11 Damage values for the searched population for the white noise signal, with a signal clipped at 3 standard deviations, block size $N=2^{18}$ .....	91
Figure 5-12 The best fitted distribution for damage values for the searched population for the white noise signal, with a signal clipped at 3 standard deviations, block size $N=2^{18}$ – Normal distribution .....	91
Figure 5-13 Damage values for the searched population for the white noise signal, with a signal clipped at 5 standard deviations, block size $N=2^{12}$ .....	92
Figure 5-14 The best fitted distribution for damage values for the searched population for the white noise signal, with a signal clipped at 5 standard deviations, block size $N=2^{12}$ – Exponentiated Weibull distribution .....	92

---

Figure 5-15 Damage values for the searched population for the white noise signal, with a signal clipped at 5 standard deviations, block size $N=2^{14}$ .....	93
Figure 5-16 The best fitted distribution for damage values for the searched population for the white noise signal, with a signal clipped at 5 standard deviations, block size $N=2^{14}$ – Generalised Extreme Value distribution .....	93
Figure 5-17 Damage values for the searched population for the white noise signal, with a signal clipped at 5 standard deviations, block size $N=2^{16}$ .....	94
Figure 5-18 The best fitted distribution for damage values for the searched population for the white noise signal, with a signal clipped at 5 standard deviations, block size $N=2^{16}$ – Generalised Extreme Value distribution .....	94
Figure 5-19 Damage values for the searched population for the white noise signal, with a signal clipped at 5 standard deviations, block size $N=2^{18}$ .....	95
Figure 5-20 The best fitted distribution for damage values for the searched population for the white noise signal, with a signal clipped at 5 standard deviations, block size $N=2^{18}$ – Exponentiated Weibull distribution .....	95
Figure 5-21 Damage values for the searched population for the wide band signal, with a signal clipped at 3 standard deviations, block size $N=2^{12}$ .....	96
Figure 5-22 The best fitted distribution for damage values for the searched population for the wide band signal, with a signal clipped at 3 standard deviations, block size $N=2^{12}$ – Exponentiated Weibull distribution .....	97
Figure 5-23 Damage values for the searched population for the wide band signal, with a signal clipped at 3 standard deviations, block size $N=2^{14}$ .....	97
Figure 5-24 The best fitted distribution for damage values for the searched population for the wide band signal, with a signal clipped at 3 standard deviations, block size $N=2^{14}$ – Generalised Extreme Value distribution .....	98
Figure 5-25 Damage values for the searched population for the wide band signal, with a signal clipped at 3 standard deviations, block size $N=2^{16}$ .....	98
Figure 5-26 The best fitted distribution for damage values for the searched population for the wide band signal, with a signal clipped at 3 standard deviations, block size $N=2^{16}$ – Generalised Extreme Value distribution .....	99
Figure 5-27 Damage values for the searched population for the wide band signal, with a signal clipped at 3 standard deviations, block size $N=2^{18}$ .....	99
Figure 5-28 The best fitted distribution for damage values for the searched population for the wide band signal, with a signal clipped at 3 standard deviations, block size $N=2^{18}$ – Generalised Extreme Value distribution .....	100
Figure 5-29 Damage values for the searched population for the wide band signal, with a signal clipped at 5 standard deviations, block size $N=2^{12}$ .....	100
Figure 5-30 The best fitted distribution for damage values for the searched population for the wide band signal, with a signal clipped at 5 standard deviations, block size $N=2^{12}$ – Generalised Extreme Value distribution .....	101

---

Figure 5-31 Damage values for the searched population for the wide band signal, with a signal clipped at 5 standard deviations, block size $N=2^{14}$ .....	102
Figure 5-32 The best fitted distribution for damage values for the searched population for the wide band signal, with a signal clipped at 5 standard deviations, block size $N=2^{14}$ – Generalised Extreme Value distribution .....	102
Figure 5-33 Damage values for the searched population for the wide band signal, with a signal clipped at 5 standard deviations, block size $N=2^{16}$ .....	103
Figure 5-34 The best fitted distribution for damage values for the searched population for the wide band signal, with a signal clipped at 5 standard deviations, block size $N=2^{16}$ – Generalised extreme distribution.....	103
Figure 5-35 Damage values for the searched population for the wide band signal, with a signal clipped at 5 standard deviations, block size $N=2^{18}$ .....	104
Figure 5-36 The best fitted distribution for damage values for the searched population for the wide band signal, with a signal clipped at 5 standard deviations, block size $N=2^{18}$ – Generalised Extreme Value distribution .....	104
Figure 5-37 Damage values for the searched population for the narrow band signal, with a signal clipped at 3 standard deviations, block size $N=2^{12}$ .....	105
Figure 5-38 The best fitted distribution for damage values for the searched population for the narrow band signal, with a signal clipped at 3 standard deviations, block size $N=2^{12}$ – Generalised Extreme Value distribution .....	106
Figure 5-39 Damage values for the searched population for the narrow band signal, with a signal clipped at 3 standard deviations, block size $N=2^{14}$ .....	107
Figure 5-40 The best fitted distribution for damage values for the searched population for the narrow band signal, with a signal clipped at 3 standard deviations, block size $N=2^{14}$ – Normal distribution .....	107
Figure 5-41 Damage values for the searched population for the narrow band signal, with a signal clipped at 3 standard deviations, block size $N=2^{16}$ .....	108
Figure 5-42 The best fitted distribution for damage values for the searched population for the narrow band signal, with a signal clipped at 3 standard deviations, block size $N=2^{16}$ – Generalised Extreme Value distribution .....	108
Figure 5-43 Damage values for the searched population for the narrow band signal, with a signal clipped at 3 standard deviations, block size $N=2^{18}$ .....	109
Figure 5-44 The best fitted distribution for damage values for the searched population for the narrow band signal, with a signal clipped at 3 standard deviations, block size $N=2^{18}$ – Exponentiated Weibull distribution .....	109
Figure 5-45 Damage values for the searched population for the narrow band signal, with a signal clipped at 5 standard deviations, block size $N=2^{12}$ .....	110
Figure 5-46 The best fitted distribution for damage values for the searched population for the narrow band signal, with a signal clipped at 5 standard deviations, block size $N=2^{12}$ – Generalised Extreme Value distribution .....	110

---

Figure 5-47 Damage values for the searched population for the narrow band signal, with a signal clipped at 5 standard deviations, block size $N=2^{14}$ .....	111
Figure 5-48 The best fitted distribution for damage values for the searched population for the narrow band signal, with a signal clipped at 5 standard deviations, block size $N=2^{14}$ – Generalised Extreme Value Distribution .....	111
Figure 5-49 Damage values for the searched population for the narrow band signal, with a signal clipped at 5 standard deviations, block size $N=2^{16}$ .....	112
Figure 5-50 The best fitted distribution for damage values for the searched population for the narrow band signal, with a signal clipped at 5 standard deviations, block size $N=2^{16}$ – Generalised Extreme Value Distribution .....	112
Figure 5-51 Damage values for the searched population for the narrow band signal, with a signal clipped at 5 standard deviations, block size $N=2^{18}$ .....	113
Figure 5-52 The best fitted distribution for damage values for the searched population for the narrow band signal, with a signal clipped at 5 standard deviations, block size $N=2^{18}$ – Generalised Extreme Value Distribution .....	113
Figure 5-53 Damage correction for different numbers of block size in IFFT – white noise signal .....	115
Figure 5-54 Damage correction for different numbers of block size in IFFT – wide band signal	116
Figure 5-55 Damage correction for different numbers of block size in IFFT – narrow band signal .....	116
Figure 6-1 Sine waves sweep simultaneous with a random background.....	118
Figure 6-2 Sine sweep system response in the time domain, sweep rate $K=0.095367$ Hz/s .....	122
Figure 6-3 Superimposed stochastic and deterministic responses in the time domain .....	123
Figure 6-4 Sine sweep system response in the time domain, sweep rate $K\cdot 2=0.190735$ Hz/s ...	124
Figure 6-5 Sine sweep system response in the time domain, sweep rate $K\cdot 4=0.38147$ Hz/s .....	124
Figure 6-6 Algorithm flow chart for damage estimation under combined stochastic and deterministic loading in the time domain .....	125
Figure 6-7 Damage values for the searched population for the white noise signal, with a signal clipped at 3 standard deviations, block size $N=2^{12}$ .....	128
Figure 6-8 The best fitted distribution for damage values for the searched population for the white noise signal, with a signal clipped at 3 standard deviations, block size $N=2^{12}$ – Normal distribution .....	128
Figure 6-9 Damage values for the searched population for the white noise signal, with a signal clipped at 3 standard deviations, block size $N=2^{14}$ .....	129
Figure 6-10 The best fitted distribution for damage values for the searched population for the white noise signal, with a signal clipped at 3 standard deviations, block size $N=2^{14}$ – Exponentiated Weibull distribution .....	129
Figure 6-11 Damage values for the searched population for the white noise signal, with a signal clipped at 3 standard deviations, block size $N=2^{16}$ .....	130

---

Figure 6-12 The best fitted distribution for damage values for the searched population for the white noise signal, with a signal clipped at 3 standard deviations, block size $N=2^{16}$ – Exponentiated Weibull distribution .....	130
Figure 6-13 Damage values for the searched population for the white noise signal, with a signal clipped at 5 standard deviations, block size $N=2^{12}$ .....	131
Figure 6-14 The best fitted distribution for damage values for the searched population for the white noise signal, with a signal clipped at 5 standard deviations, block size $N=2^{12}$ – Generalised Extreme Value distribution .....	131
Figure 6-15 Damage values for the searched population for the white noise signal, with a signal clipped at 5 standard deviations, block size $N=2^{14}$ .....	132
Figure 6-16 The best fitted distribution for damage values for the searched population for the white noise signal, with a signal clipped at 5 standard deviations, block size $N=2^{14}$ – Exponentiated Weibull distribution .....	132
Figure 6-17 Damage values for the searched population for the white noise signal, with a signal clipped at 5 standard deviations, block size $N=2^{16}$ .....	133
Figure 6-18 The best fitted distribution for damage values for the searched population for the white noise signal, with a signal clipped at 3 standard deviations, block size $N=2^{16}$ – Exponentiated Weibull distribution .....	133
Figure 6-19 Damage values for the searched population for the wide band signal, with a signal clipped at 3 standard deviations, block size $N=2^{12}$ .....	134
Figure 6-20 The best fitted distribution for damage values for the searched population for the wide band signal, with a signal clipped at 3 standard deviations, block size $N=2^{12}$ – Exponentiated Weibull distribution .....	135
Figure 6-21 Damage values for the searched population for the wide band signal, with a signal clipped at 3 standard deviations, block size $N=2^{14}$ .....	136
Figure 6-22 The best fitted distribution for damage values for the searched population for the wide band signal, with a signal clipped at 3 standard deviations, block size $N=2^{14}$ – Exponentiated Weibull distribution .....	136
Figure 6-23 Damage values for the searched population for the wide band signal, with a signal clipped at 3 standard deviations, block size $N=2^{16}$ .....	137
Figure 6-24 The best fitted distribution for damage values for the searched population for the wide band signal, with a signal clipped at 3 standard deviations, block size $N=2^{16}$ – Exponentiated Weibull distribution .....	137
Figure 6-25 Damage values for the searched population for the wide band signal, with a signal clipped at 5 standard deviations, block size $N=2^{12}$ .....	138
Figure 6-26 The best fitted distribution for damage values for the searched population for the wide band signal, with a signal clipped at 5 standard deviations, block size $N=2^{12}$ – Exponentiated distribution .....	138
Figure 6-27 Damage values for the searched population for the wide band signal, with a signal clipped at 5 standard deviations, block size $N=2^{14}$ .....	139

---

Figure 6-28 The best fitted distribution for damage values for the searched population for the wide band signal, with a signal clipped at 5 standard deviations, block size $N=2^{14}$ – Exponentiated Weibull distribution .....	139
Figure 6-29 Damage values for the searched population for the wide band signal, with a signal clipped at 5 standard deviations, block size $N=2^{16}$ .....	140
Figure 6-30 The best fitted distribution for damage values for the searched population for the wide band signal, with a signal clipped at 3 standard deviations, block size $N=2^{16}$ – Exponentiated Weibull distribution .....	140
Figure 6-31 Damage values for the searched population for the narrow band signal, with a signal clipped at 3 standard deviations, block size $N=2^{12}$ .....	141
Figure 6-32 The best fitted distribution for damage values for the searched population for the narrow band signal, with a signal clipped at 3 standard deviations, block size $N=2^{12}$ – Generalised Extreme Value distribution .....	142
Figure 6-33 Damage values for the searched population for the narrow band signal, with a signal clipped at 3 standard deviations, block size $N=2^{14}$ .....	143
Figure 6-34 The best fitted distribution for damage values for the searched population for the narrow band signal, with a signal clipped at 3 standard deviations, block size $N=2^{14}$ – Exponentiated Weibull distribution .....	143
Figure 6-35 Damage values for the searched population for the narrow band signal, with a signal clipped at 3 standard deviations, block size $N=2^{16}$ .....	144
Figure 6-36 The best fitted distribution for damage values for the searched population for the narrow band signal, with a signal clipped at 3 standard deviations, block size $N=2^{16}$ – Exponentiated Weibull distribution .....	144
Figure 6-37 Damage values for the searched population for the narrow band signal, with a signal clipped at 5 standard deviations, block size $N=2^{12}$ .....	145
Figure 6-38 The best fitted distribution for damage values for the searched population for the narrow band signal, with a signal clipped at 5 standard deviations, block size $N=2^{12}$ – Generalised Extreme Value distribution .....	145
Figure 6-39 Damage values for the searched population for the narrow band signal, with a signal clipped at 5 standard deviations, block size $N=2^{14}$ .....	146
Figure 6-40 The best fitted distribution for damage values for the searched population for the narrow band signal, with a signal clipped at 5 standard deviations, block size $N=2^{14}$ – Generalised Extreme Value Distribution .....	146
Figure 6-41 Damage values for the searched population for the narrow band signal, with a signal clipped at 5 standard deviations, block size $N=2^{16}$ .....	147
Figure 6-42 The best fitted distribution for damage values for the searched population for the narrow band signal, with a signal clipped at 3 standard deviations, block size $N=2^{16}$ – Generalised Extreme Value Distribution .....	147
Figure 7-1 Transmission shaft simplified geometry and graphical representation of the control point and boundary condition .....	149
Figure 7-2 Discrete model, element C3D8R, 8-nodes linear brick, reduced integration .....	150

---

Figure 7-3 Red curve – The Huber-Mises-Hencky stress quadratic shape function, the blue curve Huber-Mises-Hencky stress linear shape function .....	150
Figure 7-4 Test resonance characteristics of the transmission shaft .....	151
Figure 7-5 FEM resonance characteristics obtained from the corelated numerical environment (critical damping 2.1%) .....	152
Figure 7-6 Vibration damage estimation using the Dirlik method with reduced spectral moments integration for PSD Response clipped at five standard deviations using the author’s tool	156
Figure 7-7 Vibration damage estimation using the Dirlik method with reduced spectral moments integration for PSD Response clipped at three standard deviations the author’s tool .....	156
Figure 7-8 Graphical representation of damage deviation for different IFFT frequency resolutions for a signal clipped at three standard deviations .....	159
Figure 7-9 Graphical representation of damage deviation for different IFFT frequency resolutions for a signal clipped at five standard deviations .....	160
Figure 7-10 A combined stochastic and deterministic response of the transmission shaft in the time domain.....	163
Figure 7-11 Rainflow Cycle Counting histogram for combined stochastic and deterministic loading .....	164
Figure 7-12 Graphical representation of damage deviation under combined stochastic and deterministic loading for different IFFT frequency resolutions for a signal clipped at three standard deviations .....	166
Figure 7-13 Graphical representation of damage deviation under combined stochastic and deterministic loading for different IFFT frequency resolutions for a signal clipped at five standard deviations .....	166
Figure 7-14 Graphical representation of damage deviation under combined stochastic and deterministic loading for different IFFT frequency resolutions for a non-signal clipped response .....	167

---

**TABLES**

Table 2-1 The solution method for application summary ..... 23

Table 3-1 Spectral moments integration using different integration methods ..... 48

Table 3-2 Steel 17-4PH (H1025) material properties used for demonstrational analysis ..... 51

Table 3-3 PSD input curve definition used to obtain the white noise PSD response signal ..... 56

Table 3-4 Damages values for different methods used for vibration damage assessment in the frequency domain for the white noise signal..... 57

Table 3-5 PSD input curve definition used to obtain the wide band PSD response signal..... 58

Table 3-6 Damage values for different methods used for vibration damage assessment in the frequency domain for the wide band signal..... 59

Table 3-7 PSD input curve definition used to obtain the narrow band PSD response signal..... 60

Table 3-8 Damage values for different methods used for vibration damage assessment in the frequency domain for the narrow band signal..... 61

Table 3-9 Exemplary signal statistics in frequency domain parameters ..... 62

Table 3-10 Dirlik empirical variables for PDF estimation..... 63

Table 3-11 Damages based on the legacy and proposed Lalanne PDF ..... 66

Table 5-1 PSD response spectrum definition parameters ..... 76

Table 5-2 Signal statistics in frequency domain parameters across irregular factor values, full spectral moment integration..... 78

Table 5-3 Signal statistics in frequency domain parameters across irregular factor values, reduced spectral moment  $m_1, m_2, m_4$  integration ..... 79

Table 5-4 Summary of damage for the narrow band, wide band and wide noise signal for full and reduced integration of spectral moments – signal clipped at five standard deviations..... 84

Table 5-5 Summary of damage for the narrow band, wide band and wide noise signal for full and reduced integration of spectral moments – signal clipped at five standard deviations..... 85

Table 5-6 Statistical parameters for a white noise signal clipped at 3 standard deviations, block size  $N=2^{12}$  ..... 88

Table 5-7 Statistical parameters for a white noise signal clipped at 3 standard deviations  $N=2^{14}$  89

Table 5-8 Statistical parameters for a white noise signal clipped at 3 standard deviations  $N=2^{18}$  90

Table 5-9 Statistical parameters for a white noise signal clipped at 3 standard deviations  $N=2^{18}$  91

Table 5-10 Statistical parameters for a white noise signal clipped at 5 standard deviations, block size  $N=2^{12}$  ..... 92

Table 5-11 Statistical parameters for a white noise signal clipped at 5 standard deviations, block size  $N=2^{14}$  ..... 93

Table 5-12 Statistical parameters for a white noise signal clipped at 5 standard deviations, block size  $N=2^{16}$  ..... 94

Table 5-13 Statistical parameters for a white noise signal clipped at 5 standard deviations, block size  $N=2^{18}$  ..... 95

---

Table 5-14 Statistical parameters for a wide band signal clipped at 3 standard deviations, block size $N=2^{12}$ .....	97
Table 5-15 Statistical parameters for a wide band signal clipped at 3 standard deviations $N=2^{14}$	98
Table 5-16 Statistical parameters for a wide band signal clipped at 3 standard deviations $N=2^{16}$	99
Table 5-17 Statistical parameters for a wide band signal clipped at 3 standard deviations $N=2^{18}$ .....	100
Table 5-18 Statistical parameters for a wide band signal clipped at 5 standard deviations, block size $N=2^{12}$ .....	101
Table 5-19 Statistical parameters for a wide band signal clipped at 5 standard deviations, block size $N=2^{14}$ .....	102
Table 5-20 Statistical parameters for a wide band signal clipped at 5 standard deviations, block size $N=2^{16}$ .....	103
Table 5-21 Statistical parameters for a wide band signal clipped at 5 standard deviations, block size $N=2^{18}$ .....	104
Table 5-22 Statistical parameters for a narrow band signal clipped at 3 standard deviations, block size $N=2^{12}$ .....	106
Table 5-23 Statistical parameters for a narrow band signal clipped at 3 standard deviations $N=2^{14}$ .....	107
Table 5-24 Statistical parameters for a narrow band signal clipped at 3 standard deviations $N=2^{16}$ .....	108
Table 5-25 Statistical parameters for a narrow band signal clipped at 3 standard deviations $N=2^{18}$ .....	109
Table 5-26 Statistical parameters for a narrow band signal clipped at 5 standard deviations, block size $N=2^{12}$ .....	110
Table 5-27 Statistical parameters for a narrow band signal clipped at 5 standard deviations, block size $N=2^{14}$ .....	111
Table 5-28 Statistical parameters for a narrow band signal clipped at 5 standard deviations, block size $N=2^{16}$ .....	112
Table 5-29 Statistical parameters for a narrow band signal clipped at 5 standard deviations, block size $N=2^{18}$ .....	113
Table 6-1 Comparison damage evaluated using the spectral method in the frequency domain (legacy method) and new proposed method (damage evaluated in the time domain).....	126
Table 6-2 Statistical parameters for a white noise signal clipped at 3 standard deviations, block size $N=2^{12}$ .....	128
Table 6-3 Statistical parameters for a white noise signal clipped at 3 standard deviations $N=2^{14}$ .....	129
Table 6-4 Statistical parameters for a white noise signal clipped at 3 standard deviations $N=2^{16}$ .....	130
Table 6-5 Statistical parameters for a white noise signal clipped at 5 standard deviations, block size $N=2^{12}$ .....	131

---

Table 6-6 Statistical parameters for a white noise signal clipped at 5 standard deviations, block size $N=2^{14}$ .....	132
Table 6-7 Statistical parameters for a white noise signal clipped at 5 standard deviations, block size $N=2^{16}$ .....	133
Table 6-8 Statistical parameters for a wide band signal clipped at 3 standard deviations, block size $N=2^{12}$ .....	135
Table 6-9 Statistical parameters for a wide band signal clipped at 3 standard deviations $N=2^{14}$	136
Table 6-10 Statistical parameters for a wide band signal clipped at 3 standard deviations $N=2^{16}$ .....	137
Table 6-11 Statistical parameters for a wide band signal clipped at 5 standard deviations, block size $N=2^{12}$ .....	138
Table 6-12 Statistical parameters for a wide band signal clipped at 5 standard deviations, block size $N=2^{14}$ .....	139
Table 6-13 Statistical parameters for a wide band signal clipped at 5 standard deviations, block size $N=2^{16}$ .....	140
Table 6-14 Statistical parameters for a narrow band signal clipped at 3 standard deviations, block size $N=2^{12}$ .....	142
Table 6-15 Statistical parameters for a narrow band signal clipped at 3 standard deviations $N=2^{14}$ .....	143
Table 6-16 Statistical parameters for a narrow band signal clipped at 3 standard deviations $N=2^{16}$ .....	144
Table 6-17 Statistical parameters for a narrow band signal clipped at 5 standard deviations, block size $N=2^{12}$ .....	145
Table 6-18 Statistical parameters for a narrow band signal clipped at 5 standard deviations, block size $N=2^{14}$ .....	146
Table 6-19 Statistical parameters for a narrow band signal clipped at 5 standard deviations, block size $N=2^{16}$ .....	147
Table 7-1 S-N curve definition for steel 17-4PH (H1025) [49] .....	153
Table 7-2 PSD input curves for Loop 1 and Loop 2 of vibration damage consideration .....	154
Table 7-3 Summary of vibration damage estimation results for Loop 1 of consideration .....	155
Table 7-4 Summary of vibration damage estimation results for Loop 2 of consideration .....	157
Table 7-5 Summary of damage results for the combined frequency and time domains vibration damage estimation .....	159
Table 7-6 Stochastic and deterministic signal definition for vibration damage estimation under combined loading .....	161
Table 7-7 Summary of damage under combined stochastic and deterministic loading using frequency domain methods (time domain results presented as a reference) .....	162
Table 7-8 Damage summary for combined stochastic deterministic dynamic loading for a signal clipped at 3, 5 standard deviations and a non-clipped response .....	165

## **ABBREVIATIONS**

<b>Term / Acronym</b>	<b>Definition</b>
RMS	Root Mean Square of a given variable
PDF	Probability Density Function
PDFD	Probability Density Function based on the Dirlik approach
NB	Probability Density Function based on the Bendat Rice approach
LAL	Probability Density Function based on the Lalanne approach
STGB	Probability Density Function based on the Steinberg approach
IFFT	Inverse Fast Fourier Transformation
f	frequency
$m_i$	i spectral moment- (0 <sup>th</sup> , 1 <sup>st</sup> , 2 <sup>nd</sup> or 4 <sup>th</sup> )
S-N	Stress versus number of cycles – fatigue curve definition for the stress life method
RTCA	Radio Technical Commission for Aeronautics
$\sigma$	The mean value of a signal
FEM	Finite Element Method
LALm	Modified Probability Density Function based on the Lalanne legacy approach

## **CHAPTER 1     INTRODUCTION**

The initial research focused on a study of the legacy techniques and use of commercial software for vibration damage estimation in the aerospace industry, based on my experience in Collins Aerospace Company. Many civil and military projects need to meet specific requirements, taking into account specific cases – for which commercial software is at the initial stage of development or does not provide a solution for the considered cases (specific load combination, e.g., simultaneous acting sine sweep with random loading) or the provided solution is just a rough, conservative consideration. Working for many years on numerous aerospace projects before I started the research, I noticed that some methods used in the industry seem very conservative – I noticed that some units required redesigning, as they did not meet the dynamic load requirement. All the cases quoted in Collins Aerospace Company are the basis for initiating research, which allow for more robust vibration damage prediction to limit the cost of design and testing aerospace units, which need to meet the vibration loading requirements. This is also needed in terms of economical and safety aspects.

The introduced research focused on creating tools and methods, which can be used commercially for sizing aircraft and helicopter units for dynamic load requirements based on new developed methods or legacy methods modified based on research results. The aim for new tools, algorithms and scripts is to provide more robust techniques than currently used by the company – allowing to predict failures more accurately, reduce the design process time and reduce the volume of cost excessive testing of real units.

The research has been narrowed to impact stochastic dynamic loading and deterministic harmonic loading (for combined stochastic and deterministic loading scenario) on aircraft units – as these cases reported the highest number of issues in Collins Aerospace Company. As an example of using developed tools and methods I chose the transmission shafts of an aircraft. Transmission shafts are one of the most affected by the dynamic loading units of aircrafts and helicopters. The last step of the research introduces the process of assessment dynamic load impact on an exemplary transmission shaft using the legacy technique and new developed techniques – based on research results presented in this document and results of tests conducted on real shafts. The results of real shaft testing have been used to obtain a correlated FEM model.

It is worth noting that the transmission shaft example was used as demonstrational for consideration, but the created tools and methods can be used for all aerospace units – this generalisation is a great benefit for the whole company, as it does not narrow the research results just to the Actuation System Department (which is responsible for High Lift System aircraft transmission shafts).

The research focused on dynamic loads affecting transmission shafts in the slat and flap transmission systems (see Figure 1-1) – one slat transmission shaft was chosen as an example.

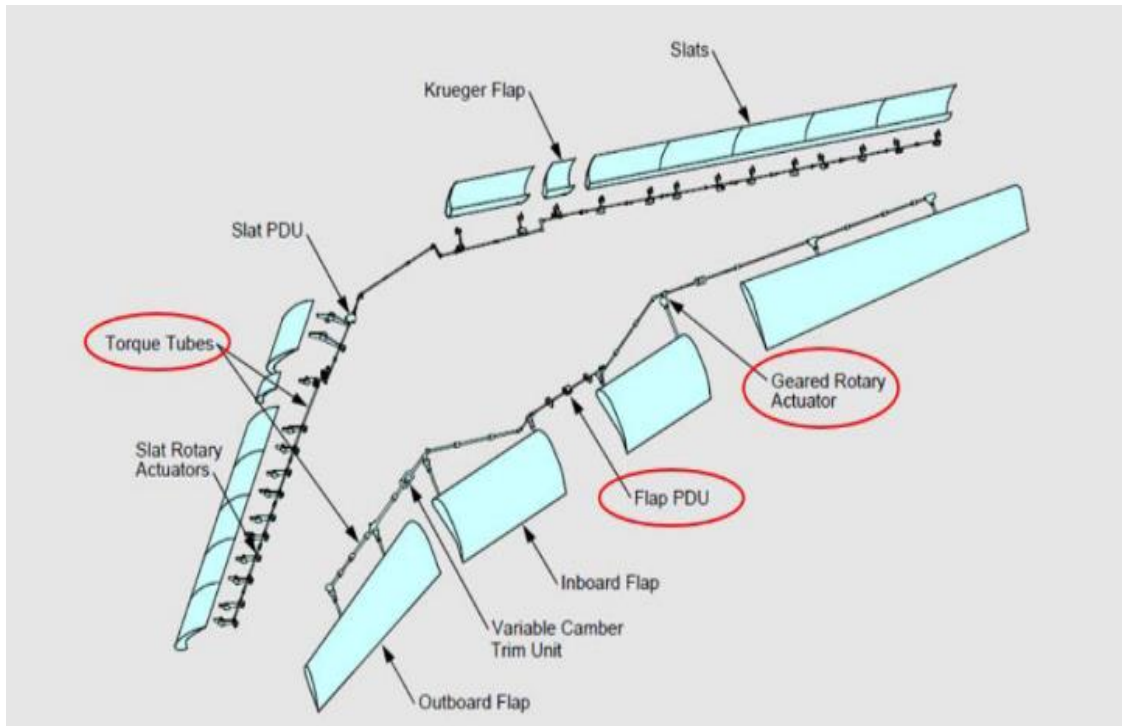


Figure 1-1 Transmission shafts architecture in a slot and flap system [1]

The RTCA aviation standard DO-160G [2] (Environmental Conditions and Test Procedures for Airborne Equipment) regulates the requirements of individual aircraft also with regards to vibration in individual zones of the aircraft. As mentioned above, this document focuses on two load cases random vibration cases on an aircraft related to take-off, flight and landing described by the function of power spectral density and deterministic harmonic loading (used for a combined stochastic and deterministic loading scenario).

Tools and methods developed in this document aim to assess the impact of dynamic loads on the transmission shafts of an aircraft as an exemplary usage. Transmission shafts are a torque transmitter from a power drive unit to the panels of slats and flaps. The example of the architecture of both systems (see Figure 1-1) shows the arrangement of transmission shafts connected to individual angular and planetary gears of the slat and flap systems. The significance of this system is important for the aircraft to obtain lift force during take-off and landing. These systems allow to increase the lift force of the aircraft at low speeds, making it easier for the aircraft to take off and maintain stability when approaching landing. In addition, these systems allow for the braking distance to be reduced, due to the aerodynamic drag caused during landing, which translates into less effort on the landing gear and the aircraft brakes, and a reduction in the braking distance.

Random vibrations are normally described in the form of the Power Spectra Density (PSD) function, separately for each vibration zone of the aircraft in the form of appropriate curves (see Figure 1-2 as an example). In the case of transmission shafts, C / C1 curves (blue dash curve in Figure 1-2) are used for locations in the aircraft fuselage, while for location on the wing of the aircraft more restrictive E / E1 curves (red curve in Figure 1-2) are used, which is due to the greater susceptibility of the aircraft wing to vibrations of different sources. The component exposure time to individual load profiles is 3h for each orthogonal direction.

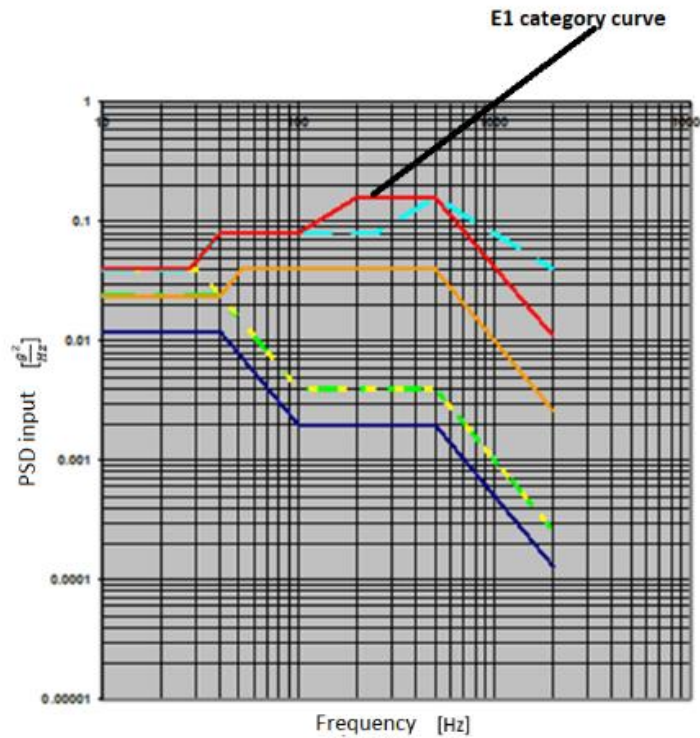


Figure 1-2 Spectral density of signal strength for individual standard curves, ref [2]

The more critical E / E1 curves indicate the maximum spectral density of the signal power in the 200 – 500Hz frequency bandwidth, equal to  $0.16g^2 / Hz$ . In this document different values of the PSD input curve were used to obtain the various PSD responses based on one transfer function – limiting the research time.

Research presented in this document has been divided into two parts:

- 1) Vibration damage assessment under stochastic loading – used in civil and military aircrafts.
- 2) Vibration damage assessment under combined stochastic and deterministic loading – used in military aircraft and helicopters.

Research introduced in this paper focuses on modification of the legacy technique for vibration damage estimation using the Dirlik, Bendat, Lalanne and Steinberg methods introduced in Chapter 2. Additionally, the research expands Dirlik's considerations – focusing on assessment of vibration damage using the Monte Carlo and IFFT methods. All the considerations aim to provide a more robust technique of vibration damage prediction for stochastic loading and enabling estimation of the mean value of damage and the damage range for considered probability and IFFT frequency resolution – rather than evaluating just the mean value of damage – an approach used by legacy methods.

In terms of the second aspect of the research (vibration damage assessment under combined stochastic and deterministic loading) an algorithm was created for the legacy technique – based on frequency domain consideration. Justification will be presented that the frequency method used for this load scenario implies conservatism in damage estimation. The next step of the research is developing a new and more robust method for vibration damage assessment under combined stochastic and deterministic loading. Use of combined frequency and time domain consideration is proposed, in order to superimpose a random and deterministic signal and process Rainflow Cycle Counting algorithm in the time domain for final damage estimation (not using Rainflow Cycle Counting in the frequency domain as for the legacy method). Additionally, for the new method, we also provide the opportunity to assess the mean damage and damage range (which depend on IFFT block size –  $N$  – see equation Eq. 4.5 ).

The considerations presented in this document allow for the development of a more robust technique for vibration damage estimation under random loading and combined random and deterministic harmonic loading, which can be adopted for commercial usage in Collins Aerospace Company, and which will be the basis for creation of in-house software.

---

## CHAPTER 2 VIBRATION FATIGUE DAMAGE PREDICTIONS UNDER STOCHASTIC LOADING IN THE FREQUENCY DOMAIN THEORETICAL BACKGROUND

This section presents the review of the frequency domain-based methods for vibration damage estimation, which are now the basis for the commercial software and tools used for commercial application. The aim of this research is to develop a methodology that would allow for the prediction of vibration damage, help to understand the testing of civil as well as military aircraft systems, and assess the possibility of under-testing. The research and conclusions presented in publications [3], [4], [5], [6], [7], [8], [9], [10], [11], [12], [13] and [14] are focused on a combined computer technique method and FEM analysis predicting the vibration damage. The above referenced papers are milestones in this field of study and help to implement theoretical considerations initiated by precursors like Bendat [15], [16] and [17], Dirlik [18] and Rice [19], Lanne [20], [21] and [22] and Steinberg [23]. The Steinberg method was developed for electronic applications [23], while the Wirsching [24], Chaudhury & Dover [25] and Hancock [26] methods are used for offshore applications. The Tunna method of vibration damage estimation under stochastic loading was developed for railway engineering equipment in the United Kingdom [27]. A summary of the solution methods for vibration damage estimation under stochastic loading for applications is presented in Table 2-1.

Solution method for applications			
General Use	Electronic Equipment	Offshore	Railway Engineering Equipment
Dirlik	Steinberg	Wirsching	Tunna
Lanne	Chaudhury & Dover	Hancock	-
Narrow Band (Bendat/ Rice Method)	-	Chaudhury & Dover	-

Table 2-1 Solution method for application summary

This paper focuses on further developing the Dirlik approach by using two combined methods: Monte Carlo and FEM simulation on predefined samples and Python programming language, which is the basis for this study. The research combines the Dirlik theoretical consideration on signal statistics in a time and frequency domain with studies made by Bishop and Halfpenny, who were the precursors of theoretical consideration in commercial software such as MSC CAE Fatigue [28] and [29] and HBM-nCode [30]. Therefore, research is focused on developing the theoretical background to describe the vibration damage phenomena under stochastic loading and developing code that allows for the use of commercial software such as Abaqus to evaluate the transfer function of the system. The transfer function can be multiplied by the PSD input to derive a system response using interpolation in the frequency domain and then estimate the damage based on the material allowable and exposure time to random loading. Another crucial aspect will be the introduction of complex time domain considerations using the Monte Carlo simulation approach (see Chapter 4) to benchmark the legacy methods and provide a new opportunity for precise vibration damage estimation for aircraft duty and test duty used during testing real units.

## 2.1 Narrow Band method – developed by Bendat and Rice

In the 20<sup>th</sup> century in the early sixties, Julius Bendat [15], [16], [17] developed a theory that was a milestone for the vibration fatigue prediction for systems exposed to stochastic loading. The Bendat method was used by Dirlik during the development of semi-empirical theory for more general use (from narrow band to white noise signals).

In the early 1950s, Rice [19] provided proof that the Probability Density Function (PDF) of peaks in vibration narrow band spectrum matched the Rayleigh distribution, defined by equation Eq. 2.1 as the bandwidth reduced.

$$P(\alpha) = \frac{\alpha}{\sigma^2} e^{-\frac{\alpha^2}{2\sigma^2}} \quad \text{Eq. 2.1}$$

where:

$\sigma$  – the signal standard deviation value

$\alpha$  – an independent variable e.g., complex Huber Mises Hencky stress

Two signals (with frequency  $f_1$  and  $f_2$ ) superposed to one – the red curve Figure 2-1 results in a time domain signal with frequency  $(f_1 + f_2)$  for narrow band solution, which is attenuated by a low frequency beat signal with frequency  $(f_1 - f_2)$ . The oscillation equation and the beat frequency equation can be demonstrated by trigonometry identities Eq. 2.2 [6].

$$\sin(2\pi f_1 t) + \sin(2\pi f_2 t) = 2 \cos\left(2\pi t \frac{f_1 - f_2}{2}\right) \sin\left(2\pi t \frac{f_1 + f_2}{2}\right) \quad \text{Eq. 2.2}$$

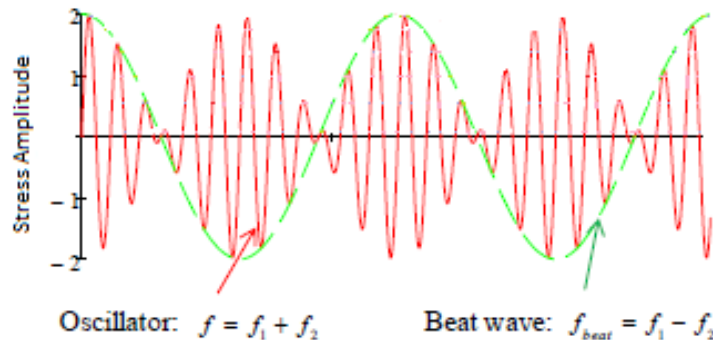


Figure 2-1 Narrow Band solution – all positive peaks are matched with corresponding troughs of similar magnitude, hence the green signal is transformed to the red signal, [6]

Following this assumption Bendat derived that the PDF function of Rainflow ranges of a signal also follows the Rayleigh distribution, and therefore the Rainflow range of a signal is defined by twice the peak amplitude. The narrow band solution assumes that all positive peaks are matched with corresponding troughs from a signal with similar magnitude, hence the green signal is transformed to the red signal – see Figure 2-1. This causes the PDF of Rainflow to be twice the PDF of the peaks. This approach used for the wide band process will therefore be conservative, and for some commercial software, such as CAE Fatigue [29], the number of peaks is replaced by an upward zero crossing variable to reduce the pessimism in the damage estimation [29].

The second step of the Bendat solution [19], [31], [32] and [33] is to use a series of equations in order to estimate the number of cycles per unit (e.g. second) of exposure to the signal. Rice defines the number of peaks  $E[P]$  and upward zero crossings  $E[0]$  for signal statistics in the frequency domain as per the following equations Eq. 2.3, Eq. 2.4:

$$E[0] = \sqrt{\frac{m_2}{m_0}} \quad \text{Eq. 2.3}$$

Where:

$m_2$  – is the second spectral moment

$m_0$  – is the zero spectral moment

$$E[P] = \sqrt{\frac{m_4}{m_2}} \quad \text{Eq. 2.4}$$

Where:

$m_4$  – is the fourth spectral moment

The spectral moments:  $m_0$ ,  $m_2$ ,  $m_4$  are the 0<sup>th</sup>, 2<sup>nd</sup>, 4<sup>th</sup> and are the area under the PSD response of the system. These can be derived by integration of the general equation for spectral moment as defined in the following equation Eq. 2.5:

$$m_n = \int_0^{\infty} f^n \cdot S(f) df \quad \text{Eq. 2.5}$$

Where:

$m_n$  – is the n spectral moment

f – is the considered frequency

$S(f)$  – is the PSD Response Function of the system or the single side PSD of stress amplitude at a particular frequency [Hz]  $f_i \in (f_{min}; f_{max})$ .

Note: the zero spectral moment represents the mean square value of the time domain signal or the RMS (Root Mean Square).

Bendat's final narrow band solution of the Rainflow range histogram based on PDF can be expressed by the following equation Eq. 2.6:

$$NB(S) = \left( \frac{S}{4m_0} e^{\frac{-S^2}{8m_0}} \right) \cdot dS \quad \text{Eq. 2.6}$$

Where:

S – is the stress at the considered histogram bin

Therefore, the number of cycles can be defined by equation Eq. 2.7:

$$n_{Narrow\_Band} = NB(S) \cdot T \cdot E[P] \quad \text{Eq. 2.7}$$

Where:

T- is the time of exposure on random loading

The first element of equation Eq. 2.6 is the Rayleigh probability distribution. T is the total time of exposition to a random load with predefined PSD input.

## 2.2 The Dirlik method – a general solution for the narrow and wide band processes

Following the Rice [19] approach the PDF of peaks can be derived from the weighted sum of the Gaussian and Rayleigh distribution. In his thesis Dirlik reasoned that the PDF of peaks is not equal to the PDF of Rainflow ranges and derived separate equations for both variables [18]. Dirlik proposed an empirical solution to estimate the desired PDF of Rainflow ranges based on extensive computer simulation using the Monte Carlo technique. Nevertheless, Dirlik's solution was derived on a relatively short record of data, i.e., 10 times for each considered predefined spectrum. This approach doesn't tell us much about the stochastic process and can therefore miss the proper estimated lives. Additional research in this matter has been introduced in section Chapter 4.

The Dirlik method also defines the PDFD(S) function based on a series of empirical estimated variables defined as in equation Eq. 2.8:

$$PDFD = \left( \frac{D_1}{Q} e^{\frac{Z}{Q}} + \frac{D_2 Z}{R^2} e^{\frac{-Z^2}{2R^2}} + D_3 Z e^{\frac{-Z^2}{2}} \right) \cdot \frac{dS}{2RMS} \quad \text{Eq. 2.8}$$

The variable definition is as follow:

Irregular factor Eq. 2.9:

$$\gamma = \frac{m_2}{\sqrt{m_0 \cdot m_4}} \quad \text{Eq. 2.9}$$

The normalised Dirlik stress variable (note: Dirlik's normalised stress variable is two times that of Bendat's normalised stress variable) Eq. 2.10:

$$Z = \frac{S}{2\sqrt{m_0}} \quad \text{Eq. 2.10}$$

The 'mean frequency' Eq. 2.11:

$$X_m = \frac{m_1}{m_0} \cdot \sqrt{\frac{m_2}{m_4}} \quad \text{Eq. 2.11}$$

The remaining Dirlik empirical variables Eq. 2.12 through Eq. 2.16:

$$D_1 = \frac{2(X_m - \gamma^2)}{1 + \gamma^2} \quad \text{Eq. 2.12}$$

$$D_2 = \frac{1 - \gamma - D_1 + D_1^2}{1 + \gamma^2} \quad \text{Eq. 2.13}$$

$$D_3 = 1 - D_1 - D_2 \quad \text{Eq. 2.14}$$

$$Q = \frac{1.25 \cdot (\gamma - D_2 \cdot R - D_3)}{D_1} \quad \text{Eq. 2.15}$$

$$R = \frac{\gamma - X_m - D_1^2}{1 - \gamma - D_1 + D_1^2} \quad \text{Eq. 2.16}$$

The Dirlik method is based on research and development made by Rice and Bendat, and therefore the Dirlik PDF (PDFD) is also based on the weighted sum of the Gaussian and Rayleigh exponential probability distribution. The Dirlik method has been ranked as more robust than the Narrow-Band Bendat and Steinberg methods, and similar as with robustness as Lalanne [10].

### 2.3 The Wide Band method – developed by Steinberg

As stated in section 2.1, the Narrow-Band approach for wide-band signal tends to be conservative, therefore other techniques need to be considered for damage prediction for better accuracy and less conservatism in the created algorithms.

Figure 2-2 presents the typical wide-band signal, where the high frequency sinusoidal signal is superimposed with a low frequency signal. The signal has a Gaussian distribution of peaks in the spectrum.

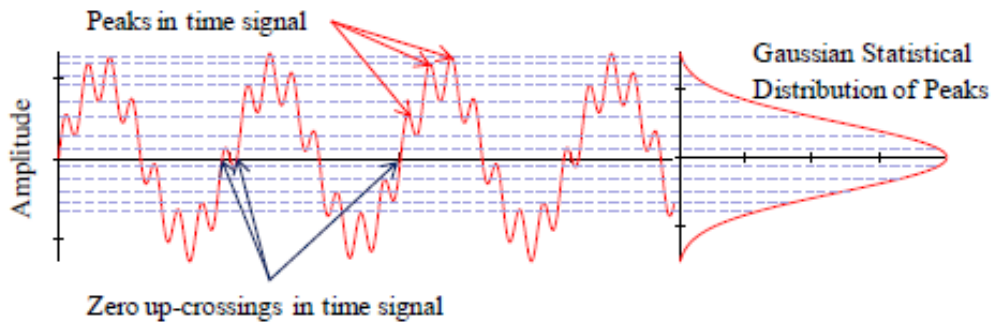


Figure 2-2 Wide-band time signal, which follows Gaussian distribution [6]

In that case the irregular factor Eq. 2.9 decreases and the statistical distribution from Rayleigh Eq. 2.1 becomes Gaussian distribution as defined in equation Eq. 2.17.

$$P(\alpha) = \frac{1}{\sigma\sqrt{2\pi}} e^{-\frac{\alpha^2}{2\sigma^2}} \quad \text{Eq. 2.17}$$

Note: the parameter description is analogical to that in equation Eq. 2.1.

As we can see, the irregular factor  $\gamma$  is inversely proportional to the number of peaks as seen in equations Eq. 2.3, Eq. 2.4, Eq. 2.9, and therefore it can be defined in equation Eq. 2.18. This was also noticed by Rice in his work and has been offered for use [19].

$$\gamma = \frac{E[0]}{E[P]} = \frac{m_2}{\sqrt{m_0 \cdot m_4}} \quad \text{Eq. 2.18}$$

Graphically, a signal statistic in the time domain can be presented as in Figure 2-3.

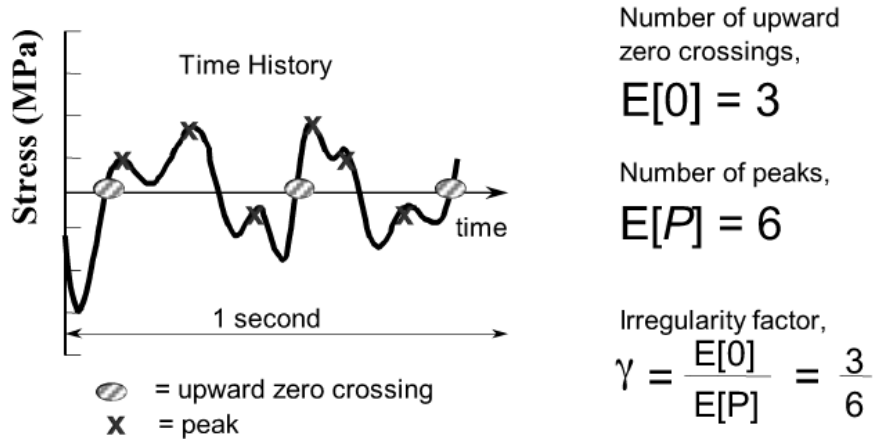


Figure 2-3 Upward zero crossing  $E[0]$  and peaks  $E[P]$  in the time series spectrum [8]

Therefore, the PDF of peaks is related to the bandwidth of a considered signal, and furthermore the wide-band signal peaks following the Gaussian distribution Eq. 2.17, opposed to the narrow-band signal, which peaks follow the Rayleigh distribution Eq. 2.1.

Irregular factors for a narrow-band signal tend towards unity – in this case all peaks in the spectrum occur above the mean of the signal, as opposed to the wide-band signal, where the irregular factors tend to zero – peaks in the spectrum occur symmetrically around the signal mean value.

The narrow-band process can be presented graphically as in Figure 2-4, and a typical wideband signal can be presented as in Figure 2-5. A white noise process can be a part of the wide-band process if the irregular factor is below 0.5, as in Figure 2-6. Figure 2-7 also shows a sinusoidal signal when the irregular factor is equal 1.

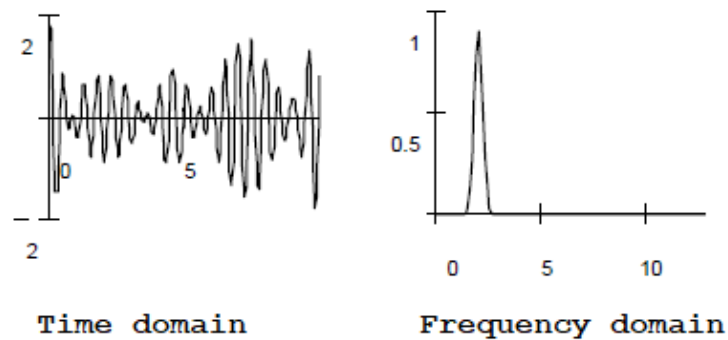


Figure 2-4 The narrow-band signal shape in the time and frequency domains,  $\gamma \in (0.95; 1)$ , [8]

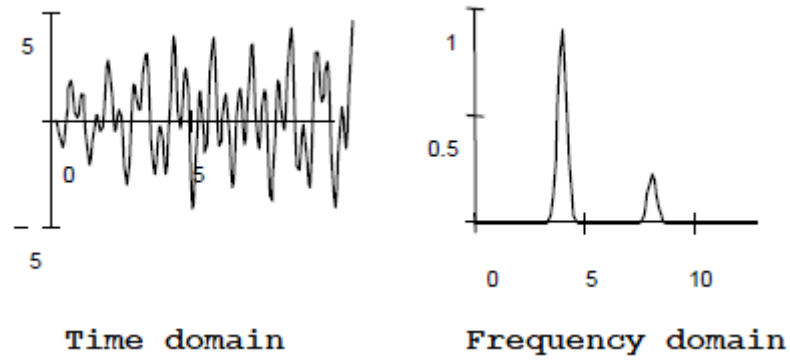


Figure 2-5 The wide-band signal shape in the time and frequency domains,  $\gamma \in (0.5; 0.95)$ , [8]

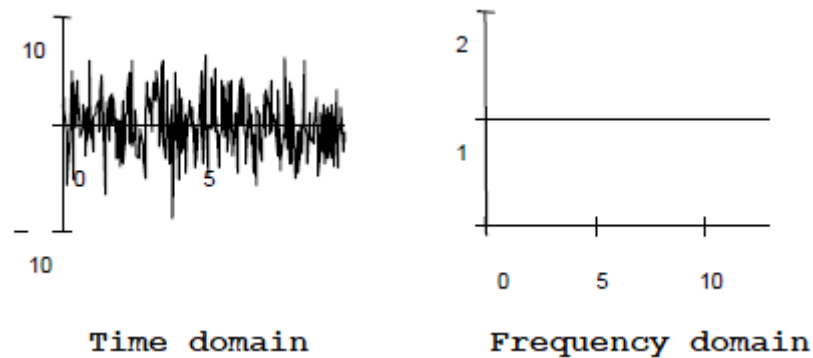


Figure 2-6 The white noise signal shape in the time and frequency domains,  $\gamma < 0.5$ , [8]

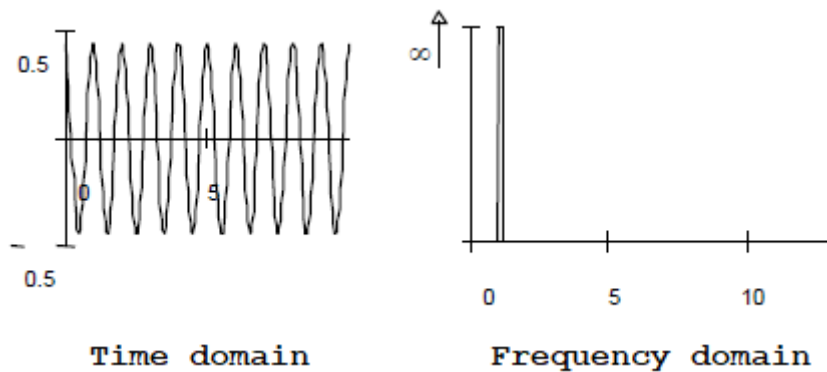


Figure 2-7 The sinusoidal signal shape in the time and frequency domains,  $\gamma = 1$ , [8]

Steinberg [11] and [23] others assume that the PDF of Rainflow ranges tends to be of Gaussian distribution. His approach was not to define PDF Rainflow ranges as a continuous histogram, but as discrete values based on three multiples of RMS – Root Mean Square amplitudes and is widely used in electronic equipment when there is good correlation with electronics testing. The histogram bins are calculated at stress amplitudes  $S=2 \cdot \text{RMS}$ ,  $S=4 \cdot \text{RMS}$  and  $S=6 \cdot \text{RMS}$ , the PDF of Rainflow ranges can be define as follows Eq. 2.19:

$$\text{STGB} = \begin{pmatrix} 0.683 \\ 0.271 \\ 0.043 \end{pmatrix} \quad \text{Eq. 2.19}$$

Therefore, the number of cycles for the three bins defined as introduced above are defined by equation Eq. 2.20, [23].

$$n_{Steinberg} = STGB \cdot E[P] \cdot T \tag{Eq. 2.20}$$

The number of cycles histogram for the Steinberg method for an example narrow band signal is presented in Figure 2-8.

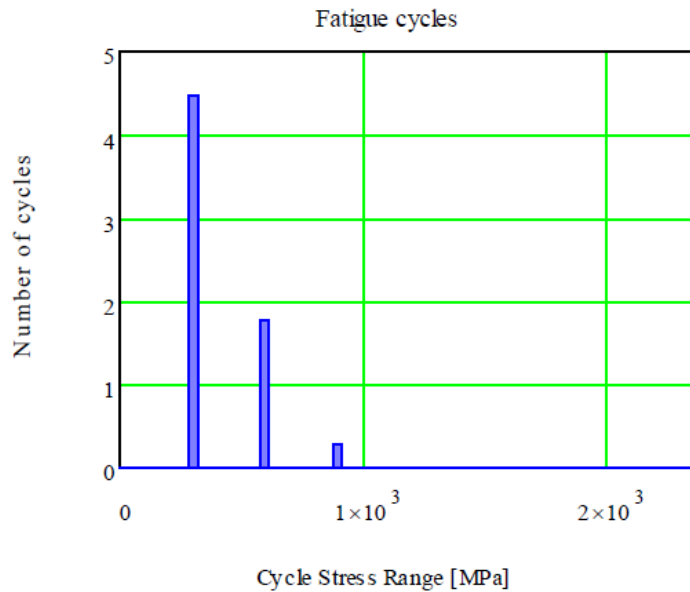


Figure 2-8 The number of cycles histogram for the Steinberg method (3 bins method) for the narrow band signal [6]

The Steinberg approach is more dedicated to hand calculation for electronic equipment, with simplification made by the author to make this method relatively accurate for the single slope S-N curve. In other scenarios a discrete value of Rainflow ranges can decrease the arbitration on different segments with different S-N curve slopes [6].

## 2.4 The Lalanne/Rice method – a general solution for narrow-band and wide-band signals

In his consideration Lalanne [6], [20], [21] and [22] has a similar approach to Rice [19] and concludes that for sufficiently long periods of time the PDF Rainflow ranges tend towards the PDF of signal peaks. Therefore, the weighted sum of the Gaussian and Rayleigh distribution will be correct for the derivation of the PDF of Rainflow ranges (Note: Dirlik, in his work [18], considered two different equations for the PDF of Rainflow ranges and the PDF of signal peaks).

The PDF of Rainflow ranges or PDF of signal peaks was defined as the following equation Eq. 2.21 [6] for Lalanne approach (LAL):

$$LAL = \frac{1}{RMS} \left\{ \frac{\sqrt{1-\gamma^2}}{\sqrt{2\pi}} e^{\frac{-S^2}{2m_0(1-\gamma^2)}} + \frac{S\gamma}{2RMS} e^{\frac{-S^2}{2m_0}} \left[ 1 + \operatorname{erf} \left( \frac{S\gamma}{\sqrt{2m_0(1-\gamma^2)}} \right) \right] \right\} \cdot dS \quad \text{Eq. 2.21}$$

Here S is the stress for each considered bin in the histogram (centre of the bin or average value – integral),  $\gamma$  – the irregular factor is defined by Eq. 2.18,  $\operatorname{erf}(x)$  is defined as the Gaussian error function and can be written as follows Eq. 2.22:

$$\operatorname{erf}(x) = \frac{2}{\sqrt{\pi}} \cdot \int_0^x e^{-t^2} dt \quad \text{Eq. 2.22}$$

The Lalanne and Rice approaches are treated as equally robust as the Dirlik approach [6], with one advantage that it is less empirical than the Dirlik approach. The number of cycles for the Lalanne method is solved numerically, like for the Dirlik method, and is based on the following equation Eq. 2.23:

$$n_{Lalanne} = LAL \cdot E[P] \cdot T \quad \text{Eq. 2.23}$$

An example of a cycle counting histogram is presented in Figure 2-9.

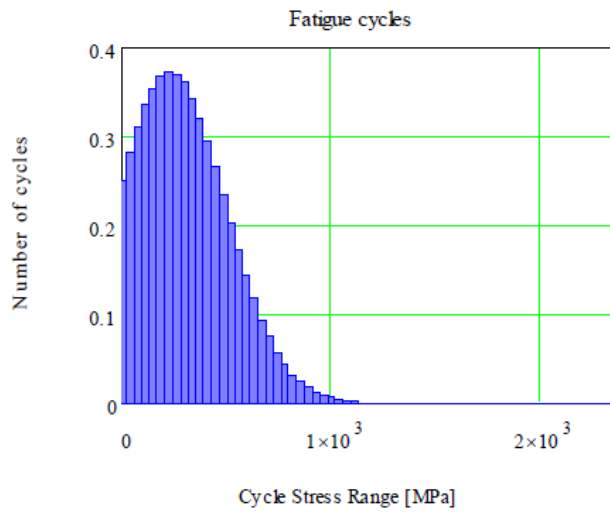


Figure 2-9 Example of a Rainflow cycle histogram based on a PSD of signal peaks for the Lalanne/Rice method [6]

## 2.5 Review of other methods for PDF estimation

This section introduces other methods of Rainflow Cycle Counting in the frequency domain for specific use.

### 2.5.1 Tunna Solution of PDF estimation

The Tunna [27] solution is similar to narrow-band, and details can be found in section 2.1. The PDF function for the Tunna solution is presented in Eq. 2.24. The Tunna solution was originally developed as a railway solution and therefore will not be used in creating counting algorithms.

$$p(S)_{Tunna} = \left( \frac{S}{4\gamma^2 m_0} e^{\frac{-S^2}{8m_0\gamma^2}} \right) \quad \text{Eq. 2.24}$$

### 2.5.2 The Wirsching Method of vibration fatigue damage estimation

The number of allowable cycles for the Wirsching [24] solution can be estimated using the following equation Eq. 2.25:

$$E[D]_{Wirsching} = E[D]_{Narrowband} (a(m) + [1 - a(m)](1 - \varepsilon)^{c(m)}) \quad \text{Eq. 2.25}$$

Where the Wirsching variable is defined as:

$$a(m) = 0.926 - 0.033m$$

$$c(m) = 1.587m - 2.323$$

$m$  – slope of the S-N curve in logarithmic coordination

$E[D]$  variables can be defined also by equation Eq. 2.26.

$$E[D] = E[P] \frac{T}{K} S_{eq}^m \quad \text{Eq. 2.26}$$

$$S_{eq} = \left[ \int_0^{\infty} S^m p(S) dS \right]^{1/m} \quad \text{Eq. 2.27}$$

Where:

$K$  – is the constant proportionality between stress and deformation

The Wirsching solution was developed as an offshore solution, therefore it will also not be a part of the research quoted in this document.

### 2.5.3 The Chaudhury & Dover Solution of vibration fatigue damage estimation

The number of allowable cycles for the Chaudhury & Dover [25] solution can be estimated using the following equation Eq. 2.28:

$$S_{eq}^{Chaundry\&Dover} = (2\sqrt{2m_0}) \left[ \frac{\varepsilon^{m+2}}{2\sqrt{\pi}} \Gamma\left(\frac{m+1}{2}\right) + \frac{\gamma}{2} \Gamma\left(\frac{m+2}{2}\right) + \text{erf}(\gamma) \frac{\gamma}{2} \Gamma\left(\frac{m+2}{2}\right) \right]^{1/m} \quad \text{Eq. 2.28}$$

---

where:

$$\text{erf}(\gamma) = 0.3012\gamma + 0.4916\gamma^2 + 0.9181\gamma^3 - 2.3534\gamma^4 - 3.3307\gamma^5 + 15.6524\gamma^6 - 10.7846\gamma^7$$

and  $\Gamma\left(\frac{m+2}{2}\right)$  is the Gamma function — a tabular function used to avoid a numerical approach for integration.

The Chaudhury & Dover solution was developed as an offshore solution; therefore, it will also not be a part of the research quoted in this document.

#### **2.5.4 The Hancock Solution of vibration fatigue damage estimation**

The number of allowable cycles for the Hancock [26] solution can be estimated using the following equation Eq. 2.25:

$$S_{eq\_Hancock} = (2\sqrt{2m_0}) \cdot [\gamma\Gamma\left(\frac{m}{2} + 1\right)]^{1/m} \quad \text{Eq. 2.29}$$

The Hancock solution was developed as an offshore solution; therefore, it will also not be a part of the research quoted in this document.

### CHAPTER 3 VIBRATION FATIGUE DAMAGE PREDICTIONS UNDER STOCHASTIC LOADING IN THE FREQUENCY DOMAIN – ALGORITHM, PROGRAMMING AND COMPUTATION

In this section we look at the computer technique used for vibration damage assessment. The Abaqus solver has been chosen as the solver used for FEM calculation, i.e., the transfer function of system estimation [34].

The first step of the algorithm is importing the complex stress tensor value from the '.odb' field output database as defined in Figure 3-1. The imported results are the value of stress calculated in the integration point of element and extrapolated to the element nodal location. Therefore, the Abaqus default keyword needs to be changed from the default integration point to the element nodal location.

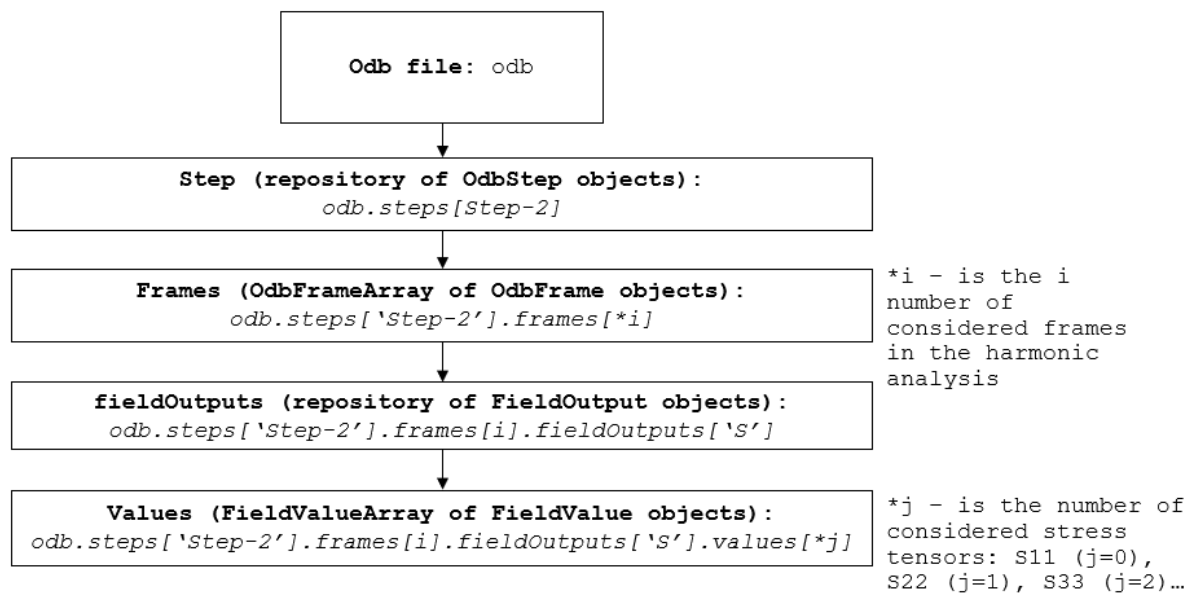


Figure 3-1 The structure of the result repository in the Abaqus output database (.odb) file

The PSD Response function based on complex stress tensors (real and imaginary values), which are used for the evaluation of Huber-Mises-Hencky –  $\sigma_{\text{HMH}}$  stress based on equation Eq. 3.1

$$\sigma_{\text{HMH}} = \frac{1}{2} [(\sigma_{11} - \sigma_{22})^2 + (\sigma_{22} - \sigma_{33})^2 + (\sigma_{11} - \sigma_{33})^2 + 6(\sigma_{23}^2 + \sigma_{31}^2 + \sigma_{12}^2)] \quad \text{Eq. 3.1}$$

Where each stress tensor components are evaluated as equation Eq. 3.2.

$$\sigma_{ij} = \text{Re}(\sigma_{ij}) + i\text{Im}(\sigma_{ij}) \quad \text{Eq. 3.2}$$

Where:

$\text{Re}(\sigma_{ij})$  – is the real part of the stress tensors

$\text{Im}(\sigma_{ij})$  – is the imaginary part of the stress tensors

The imaginary and real value for each frame – cumulative frequency value for the considered bandwidth, need to be imported by e.g. a loop through all the frames from step 2, which is a harmonic analysis at the considered frequency bandwidth (note: step 1 is the modal analysis for finding the resonance frequency in the considered spectrum used, then for creating the transfer function during harmonic analysis of the system for unit loading, e.g. a 1g sinusoidal signal input at unit basis).

To prevent importing the result from e.g., boundary condition region, where the quoted damage would make the result much less readable, programming tools have been developed for importing only the considered 'set' of elements, which can be an outer shaft surface, or an element in the stress concentration region, e.g., at the filet radius. This approach also decreases the computation time, especially at the stage of importing the result from the output database (.odb).

The stress-based approach is used for demonstrating the algorithm, and additionally this approach is widely used in the related research ([3] through [14]), and commercial software as nCode [30] and MSC CAE Fatigue [28], as isotropic material. Future research will also focus on developing an algorithm using the Critical Plane approach, which is treated as a more robust approach for multiaxial fatigue damage assessment ([28], [29], [30], [35], [36], [37] and [38], although much more computationally expensive.

Additionally, further research will focus also on the possibility to use the proposed method in synergy with the energetic fracture mechanics model, as used in [39], [40] and [41], where the Cohesive Zone Model is used for assessing damage and life prediction.

It should be mentioned that this method is originally developed for isotropic, metallic material, and any other consideration to use this method for orthotropic material will be a subject of future research.

Note: In this paper the stress life method is introduced as an example. Further research will focus on using the strain life method, using e.g. Morrow or Smith-Watson-Topper Mean Stress Correction and Neuber correction [42], [43] and [44].

The main aim of the development is to use commercial software for transfer function estimation as a reference level of load, e.g., a 1g harmonic analysis, and then import the results from an .odb file to Python algorithms for the next stage of computation on the frequency domain. The derived transfer function  $H(f)$  is then multiplied by the PSD input  $G(f)$  defined for the considered test duty and obtained PSD Response function in the frequency domain, see equation Eq. 3.3 for multiple input, equation Eq. 3.6 for single input and Figure 3-2 for graphical representation of the derivation PSD response function.

$$S(f) = \sum_{i=1}^n \sum_{j=1}^n H_i(f) G_{ij}(f) H_j(f) \quad \text{Eq. 3.3}$$

$$S(f) = H(f) \cdot G(f) \quad \text{Eq. 3.4}$$

The obtained PSD Response function is the input for the signal statistic in the frequency domain process, as introduced in section Chapter 2 of this paper.

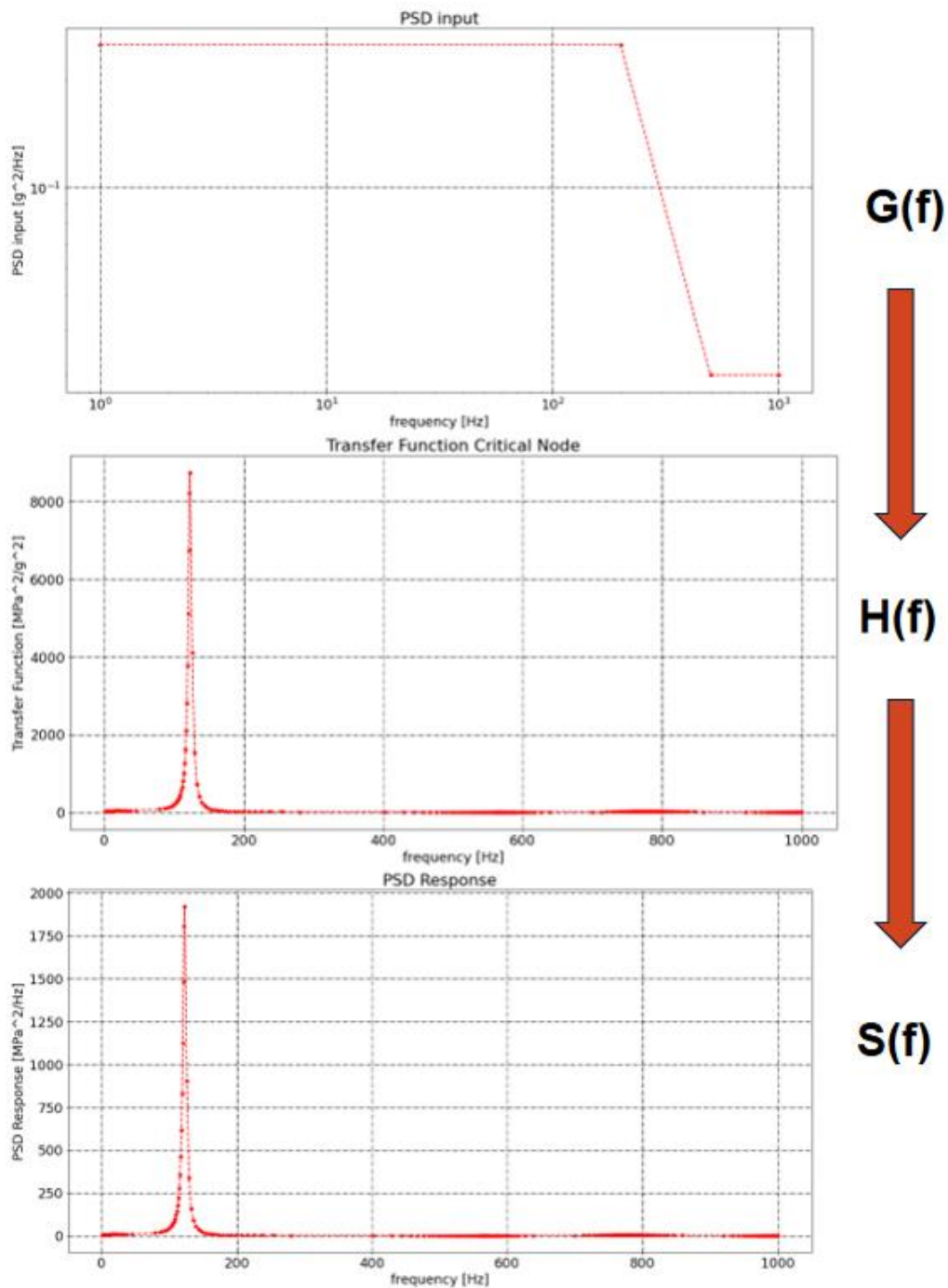


Figure 3-2 PSD Response derivation based on the Transfer Function and PSD input loading

### 3.1 Algorithm for vibration damage estimation in the frequency domain - introduction

This section introduces algorithms for vibration damage estimation using the Dirlik, Lalanne and Narrow Band Bendat methods . Figure 3-3 shows the first part of the algorithm, which aims to derive the transfer function of the considered unit (this can be represented by e.g., complex von Mises-Huber-Hencky stress).

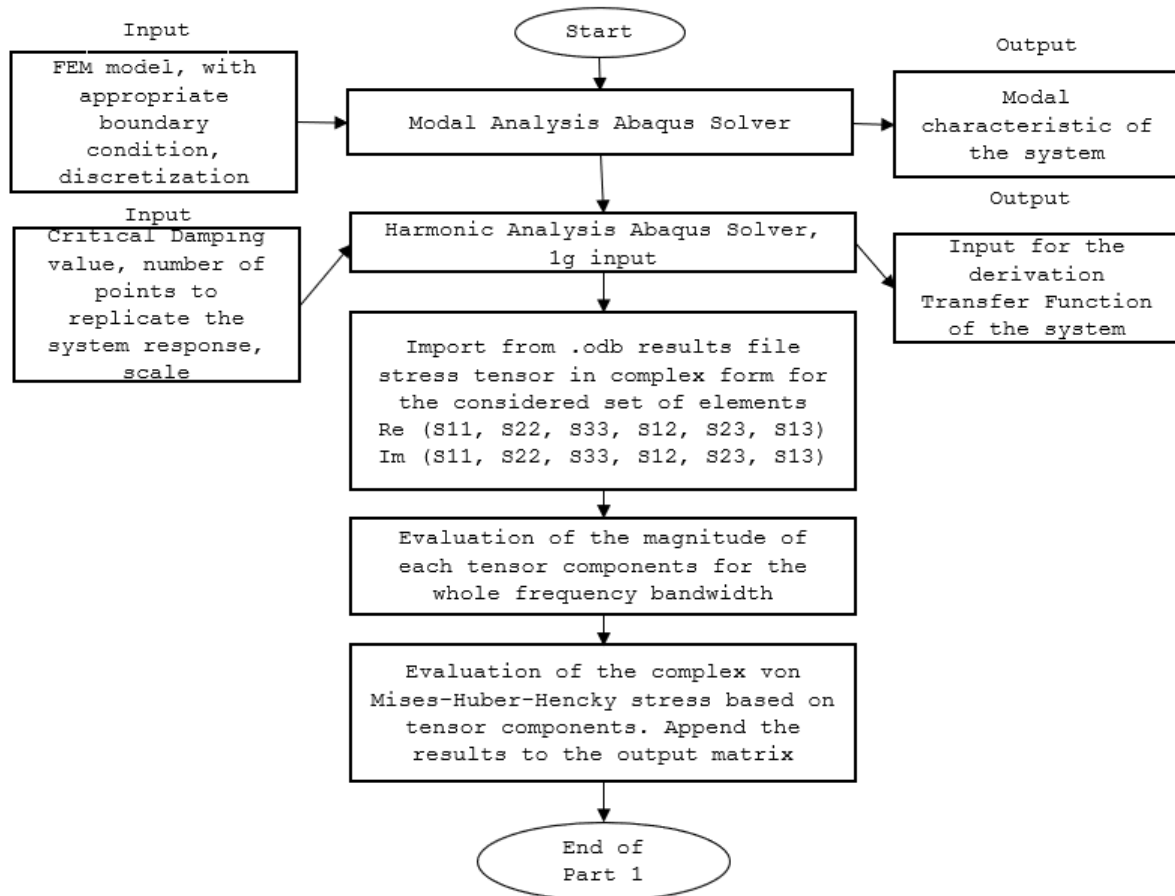


Figure 3-3 Part 1 of the algorithm for vibration damage assessment in the frequency domain

The second part of the algorithm (see Figure 3-4) focuses on the derivation PSD response function based on the given PSD input function. In this loop, the signal statistic in the frequency domain is processing – evaluation of spectral moments and signal statistic parameters are introduced in Chapter 2. Additionally, this part of the algorithm evaluates the variable used by this particular method for evaluation of the PDF function.

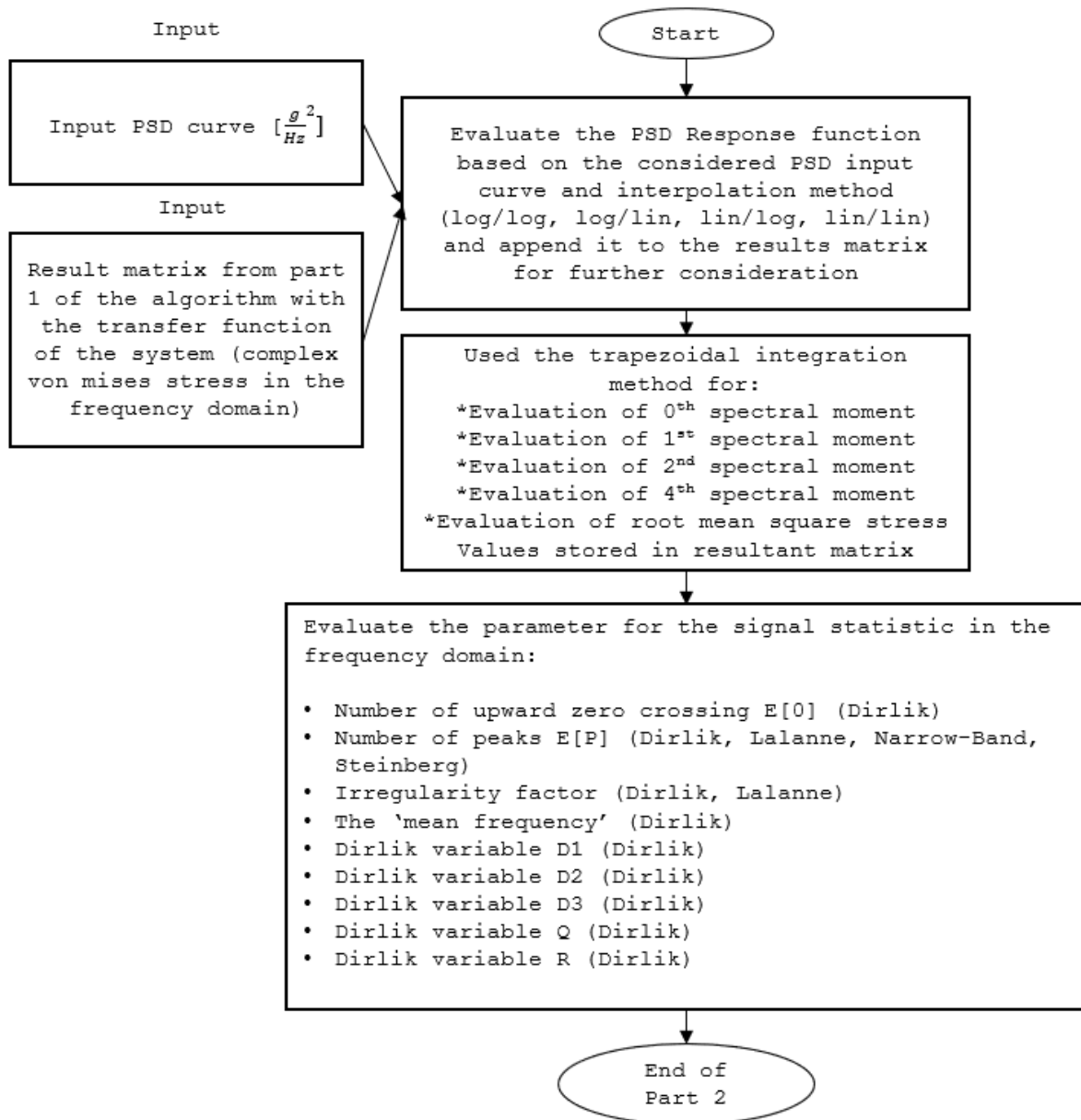


Figure 3-4 Part 2 of the algorithm for vibration damage assessment in the frequency domain

Figure 3-5, Figure 3-6, Figure 3-7 and Figure 3-8 introduce the third part of the algorithm (the final one), which consists of evaluation of the PDF function and damage estimation for the Dirlik, Bendat, Steinberg and Lalanne methods, respectively.

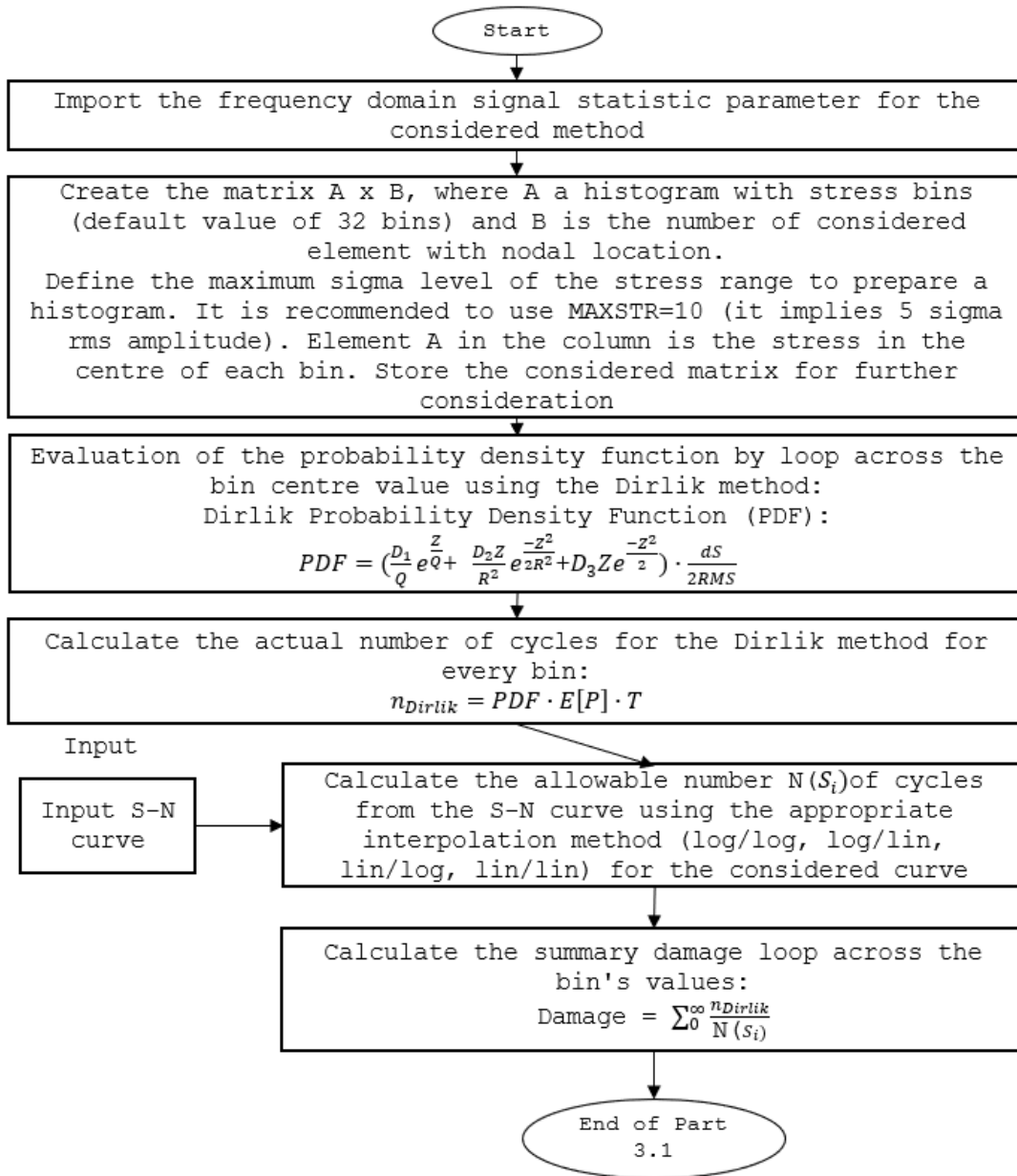


Figure 3-5 Part 3.1 of the algorithm for vibration damage assessment in the frequency domain, Dirlik method implementation

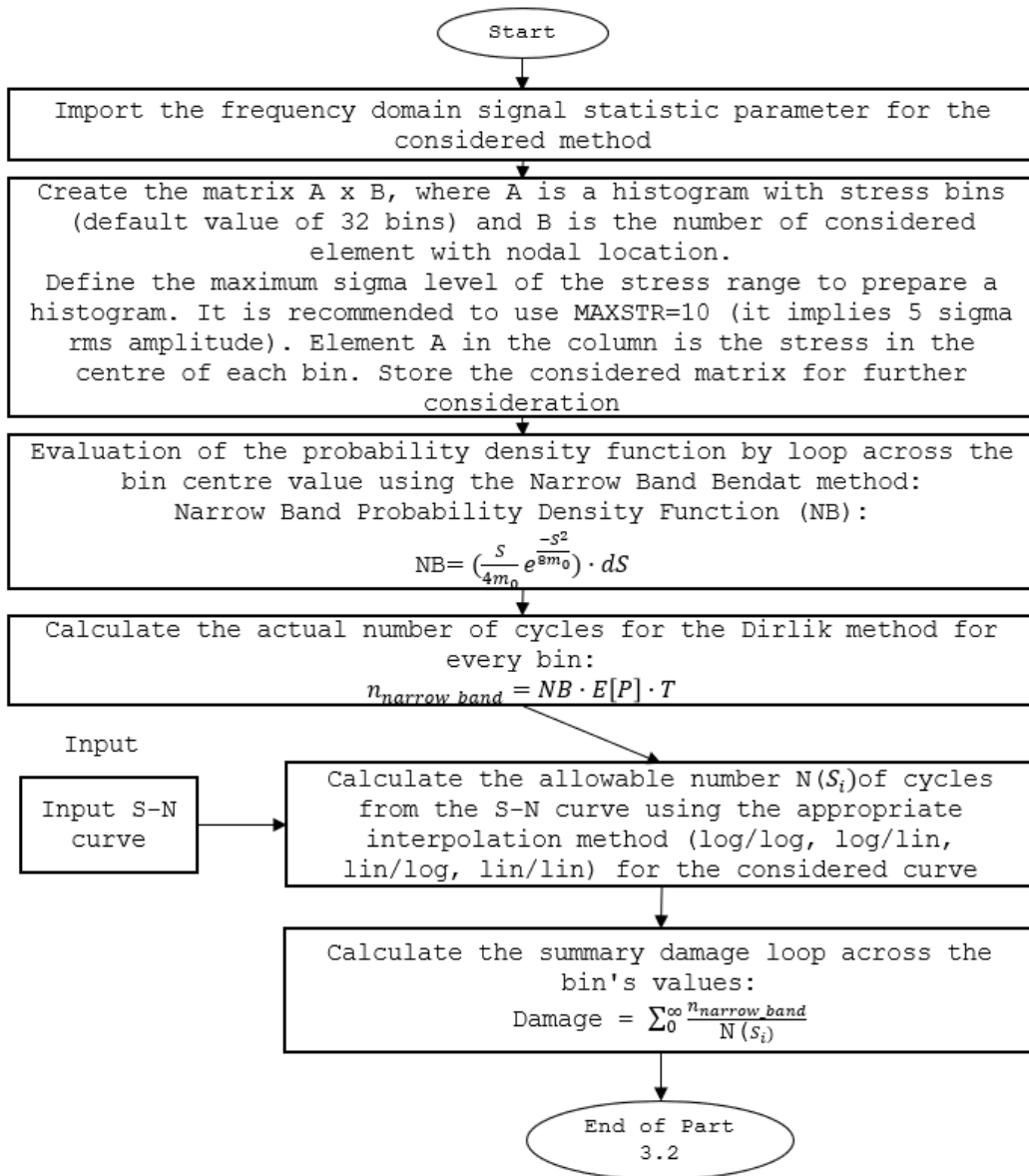


Figure 3-6 Part 3.2 of the algorithm for vibration damage assessment in the frequency domain, Bendat/Rice method implementation

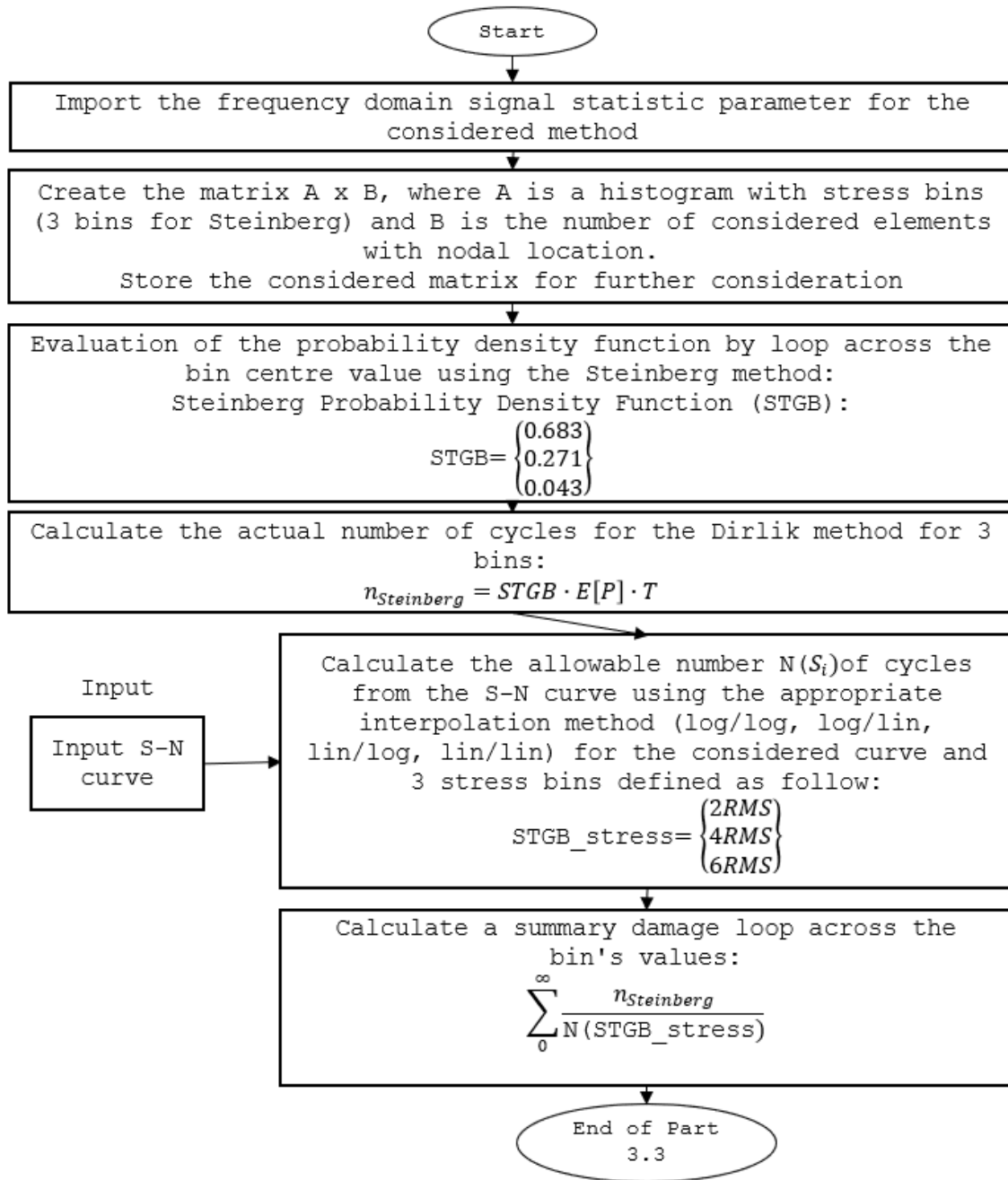


Figure 3-7 Part 3.3 of the algorithm for vibration damage assessment in the frequency domain, Steinberg method implementation

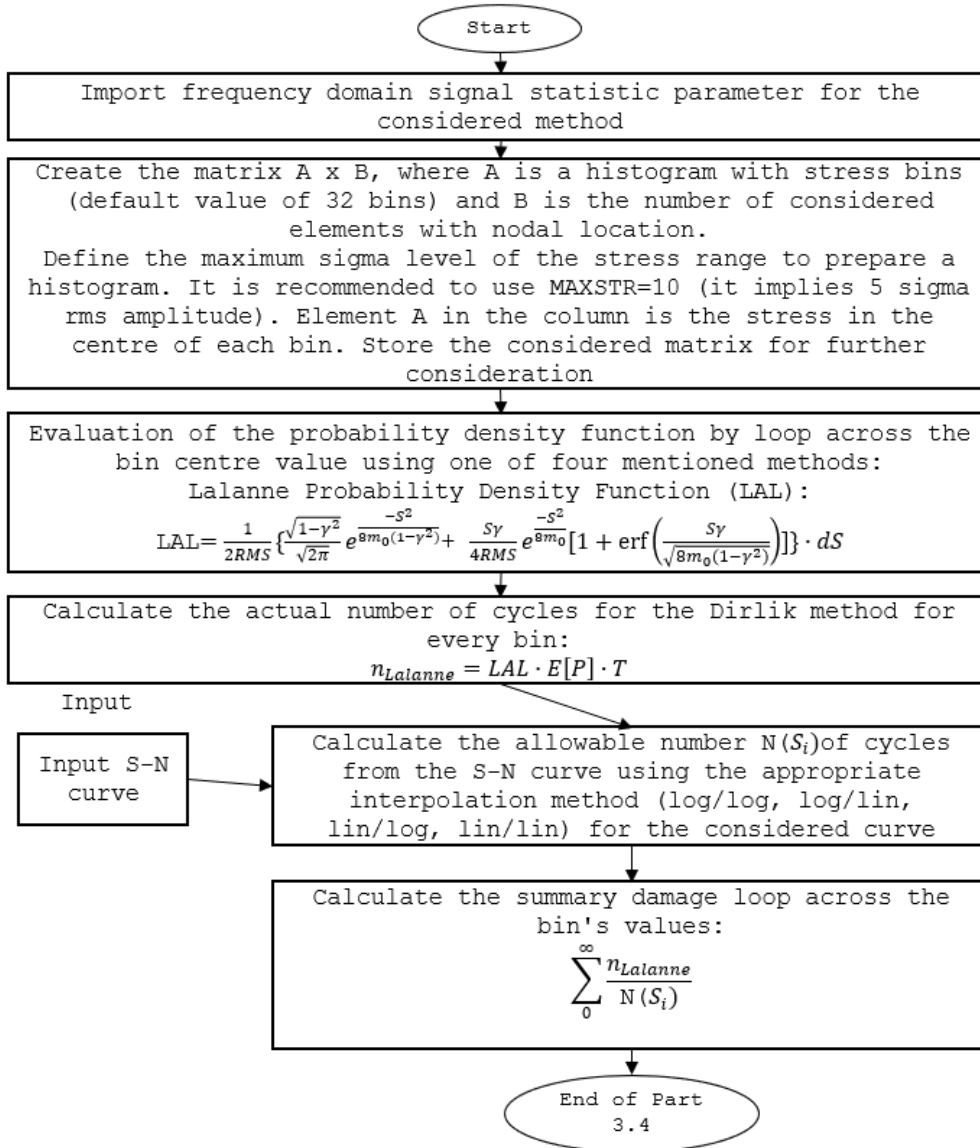


Figure 3-8 Part 3.4 of the algorithm for vibration damage assessment in the frequency domain, Lalanne method implementation

### 3.2 Spectral Moment estimation using different numerical integration methods

The algorithm, which estimates the vibration damage in the frequency domain, is based on spectral moments, and therefore the area of the algorithm requires further attention. Numerical integration techniques are used to evaluate spectral moments. In this section we describe the most popular integration methods and compare the results of the integration of an exemplary transfer function obtained based on Abaqus harmonic analysis and evaluated using the first part of the created algorithm. Numerical procedures of integration were implemented using Python programming language [45],[46] and [47].

#### 3.2.1 The Cumulative Trapezoidal integration method

This section presents exemplary spectral moment integration using the Cumulative Trapezoidal integration method used for convenience for tracking spectral moment values in the frequency domain. Figure 3-9, Figure 3-10, Figure 3-11 and Figure 3-12 show the exemplary cumulative integration process of the 0<sup>th</sup>, 1<sup>st</sup>, 2<sup>nd</sup> and 4<sup>th</sup> spectral moments respectively.

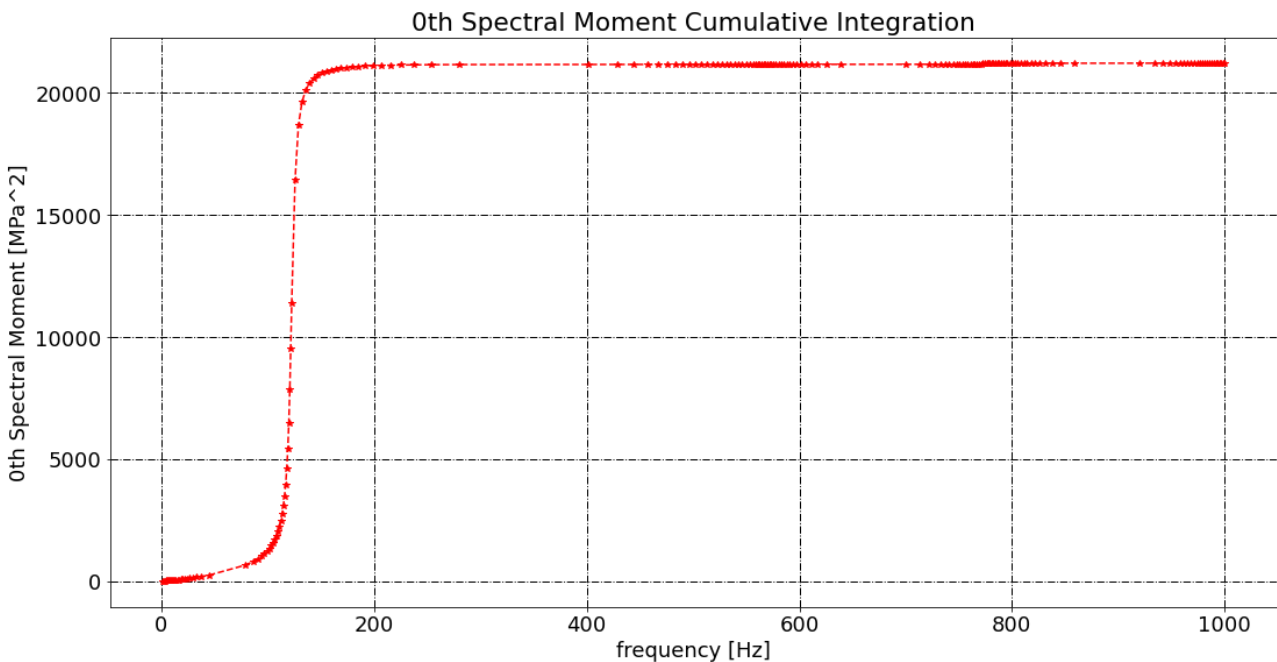


Figure 3-9 The 0 Spectral moment obtained using the cumulative trapezoidal integration transfer function method

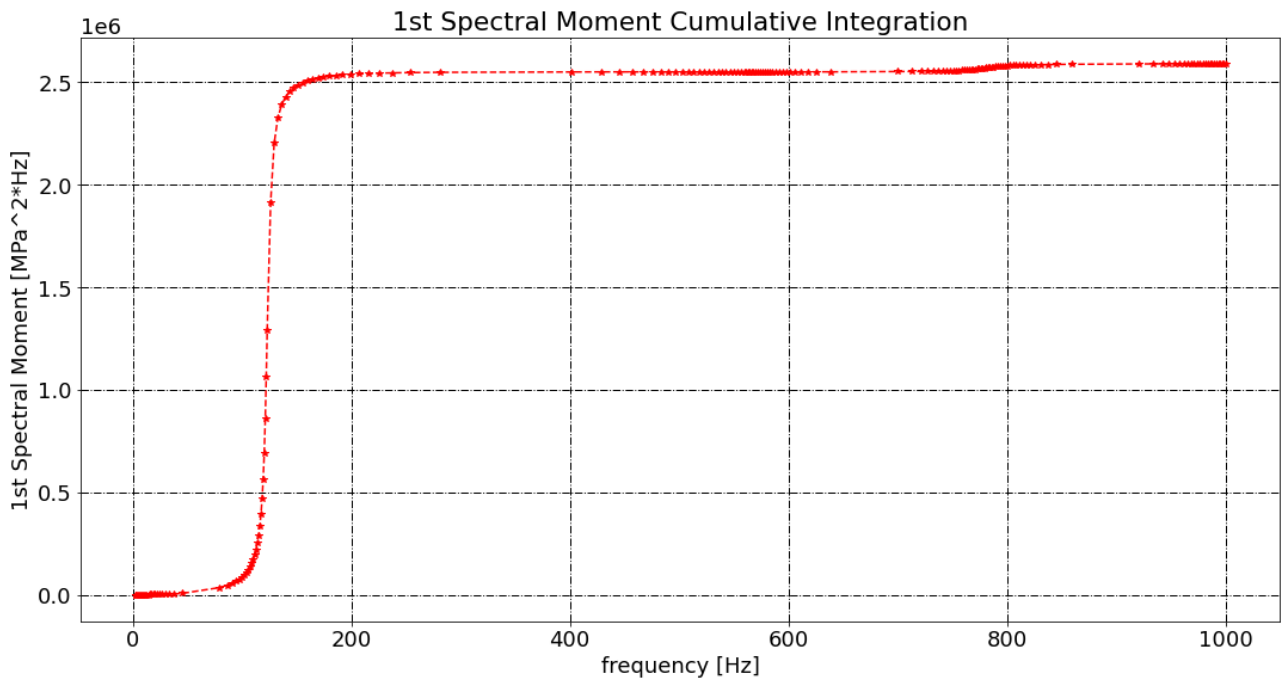


Figure 3-10 The 1<sup>st</sup> Spectral moment obtained using the cumulative trapezoidal integration method of the transfer function

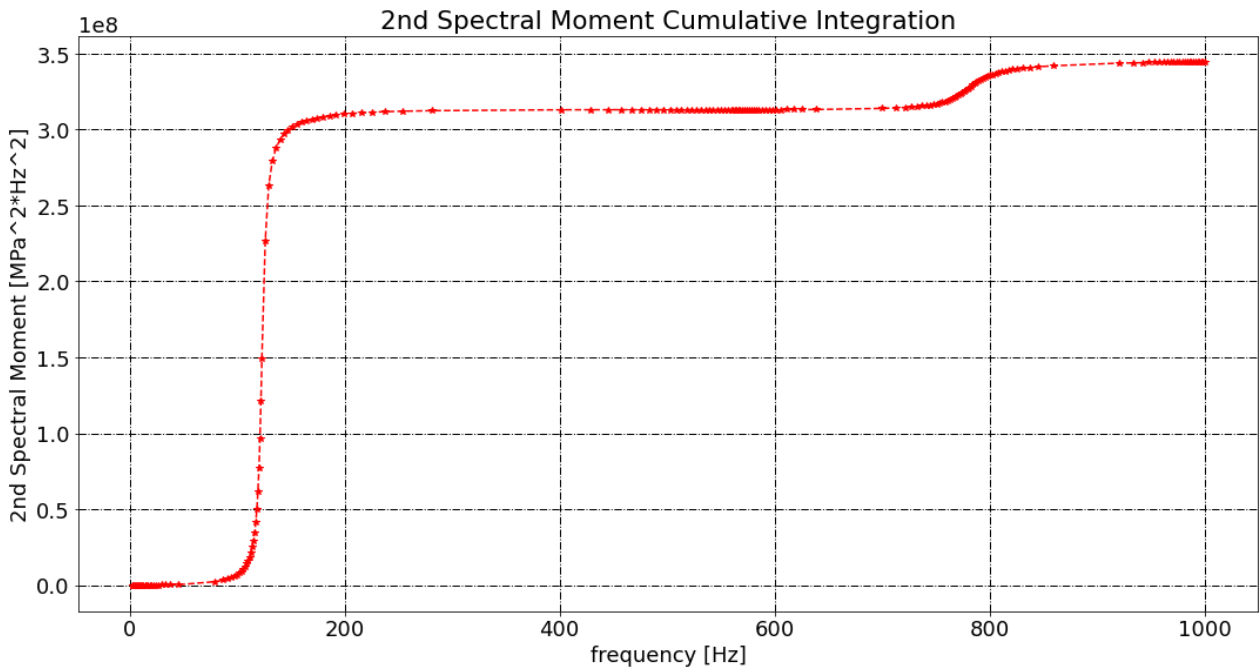


Figure 3-11 The 2<sup>nd</sup> Spectral moment obtained using the cumulative trapezoidal integration method of the transfer function

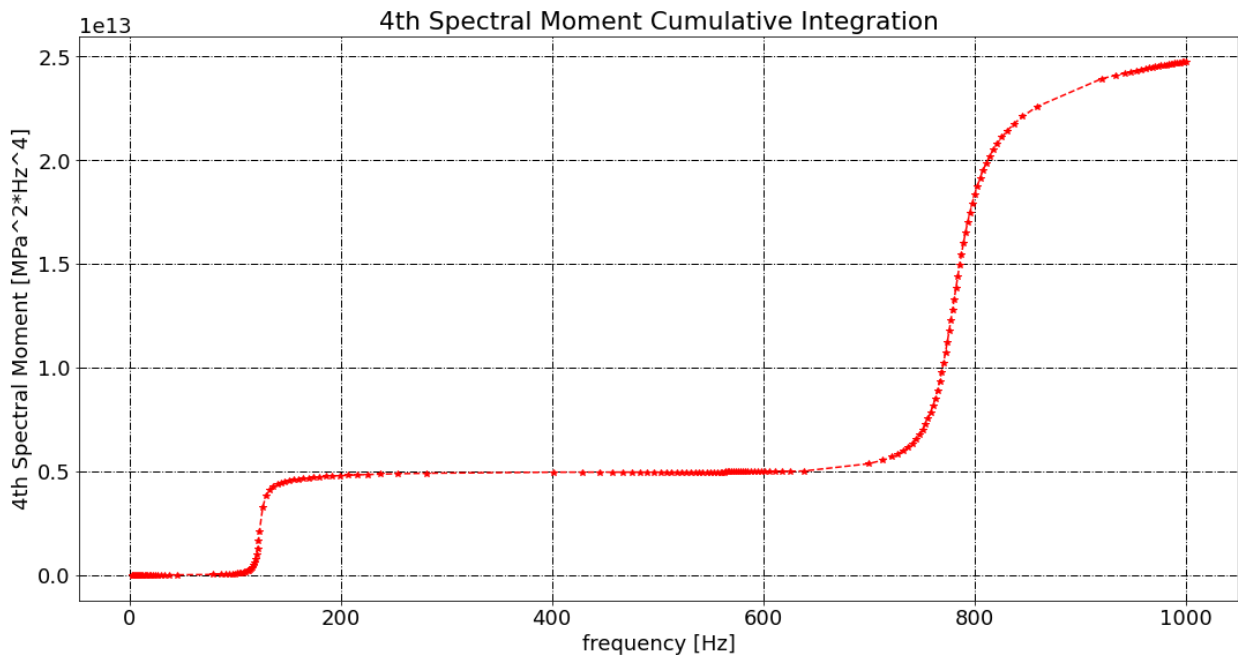


Figure 3-12 The 4<sup>th</sup> Spectral moment obtained using the cumulative trapezoidal integration method of the transfer function

### 3.2.2 Numerical integration methods used – summary

Vibration damage estimation in the frequency domain depends on the spectral analysis, as the whole signal statistic in the frequency domain depends on the accuracy of estimation spectral moments. Therefore, in this section we present the most common methods of integration spectral moments and compare the results.

Table 3-1 shows that the Cumulative Trapezoidal, Trapezoidal, Simpson, Romberg, and Gauss integration methods give close results of spectral moments (less than 2% of difference). Additionally, the Gauss quadrature integration method gives a high difference of the 0, 1<sup>st</sup> and 2<sup>nd</sup> spectral moments (around 30%) and visible differences for the 4<sup>th</sup> spectral moment (7.5% comparing to the other methods). It is therefore not recommended to use this method in further work. Based on the research results, further research will be based on the Gauss and Trapezoidal integration methods, as both methods are equally robust and give close results.

	$m_0$	$m_1$	$m_2$	$m_4$
Cumulative Trapezoidal integration method	21192	2567756	328497774	14815422714320
Trapezoidal integration method	21192	2567756	328497774	14815422714320
Simpson integration method	21528	2610383	333733189	14819449183349
Gauss quadrature integration method	14302	1759955	234317406	13714509525629
Romberg integration method	21239	2573605	329212209	14826155234242
Gauss integration method	21135	2560718	327629425	14800387051769
Percentage difference between the maximum and minimum value, including the Gauss Quadrature integration method	33.6%	32.6%	29.8%	7.5%
Percentage difference between the maximum and minimum value, excluding the Gauss Quadrature integration method	1.8%	1.9%	1.8%	0.2%

Table 3-1 Spectral moments integration using different integration methods

### **3.3 Python algorithm verification was created against the commercial MSC tool – CAE Fatigue**

The general approach presented in this paper is not to use commercial software for estimating vibration damage but create an original algorithm to control all the parameters and introduce further research results. The approach is therefore to create algorithms (with the current state of knowledge) and benchmark them with the commercial software MSC CAE Fatigue, which will be the basis of the research, later modified using research results.

Verification against commercial was made using CAE Fatigue software, which provide the damage result using the Dirlik, Bendat/Rice and Steinberg methods. In this case it is also based on Abaqus results sorted in .odb file, and damages were estimated for the element nodal value. To decrease the size of the considered task, we also created input data, such as a set of elements for damage estimation.

Python tools were created that quoted only the considered element number and sorted it in a .txt format file, and CAE Fatigue software based on this .txt 'guideline' can read/download only the result for quoted set of elements. This approach can make calculation much more effective than analysis of the whole model, additionally making the result more readable due to omitting results in the boundary condition and in low stress areas.

### 3.3.1 Sample description

Fatigue damage estimation is based on the FEM analysis [48] using a linear dynamic method in an Abaqus [34] environment. Modal and harmonic analysis for unit loading (1g acceleration) is performed in an Abaqus environment for components, allowing the resonance characteristic of the system to be obtained for further consideration using Rainflow Cycles Counting algorithms for damage estimation in the frequency domain. The research used a cantilever beam example with a cut U-notch. The geometry, discrete model and graphical support representation is presented in Figure 3-13, Figure 3-14 and Figure 3-15. The harmonic load input is a unit load (1g) acceleration applied to the base (supported region).

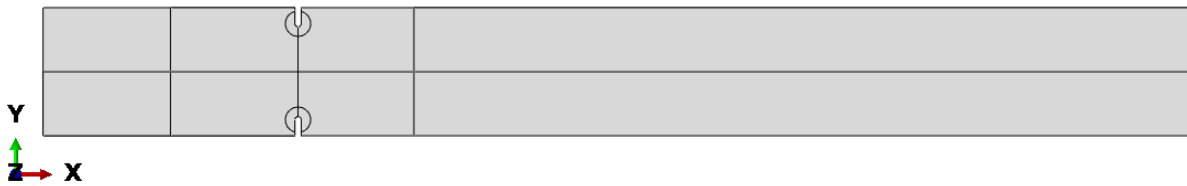


Figure 3-13 Sample geometry used for analysis

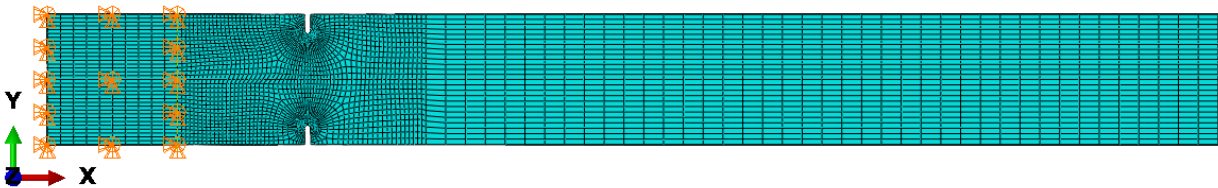


Figure 3-14 Geometry, the discrete model, and graphical support representation of a sample taken for visualisation of the research results

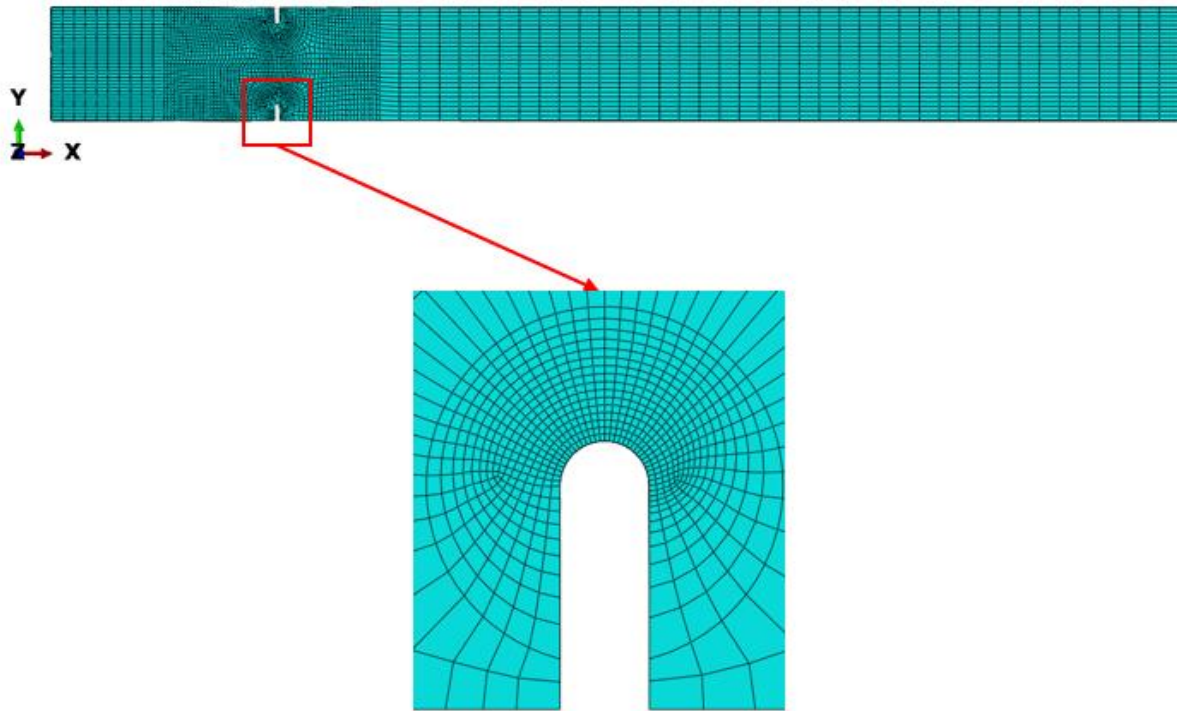


Figure 3-15 Discrete FEM model graphical representation details

For this research we assumed that the sample is made of steel 17-4PH (H1025) and used fatigue material properties from MMPDS-15, reference [49] for considered steel for  $K_t$  equals 3.

Steel 17-4PH (H1025)		
Young modulus E [MPa]	Poisson ratio $\nu$ [-]	Density $\rho$ [t/mm <sup>3</sup> ]
195000	0.27	7.89E-09

Table 3-2 Steel 17-4PH (H1025) material properties used for demonstrational analysis

For consideration, we assumed a critical damping ratio constant for the whole frequency bandwidth (0-1000Hz) and equal to 2.5% (Note that the created method and software need input, which consists of a model correlated against the test results, although as a benchmark we assumed artificial parameters of damping).

The total damage caused by the considered time series history can be obtained by aggregating the damage caused by each bin presented in the stress range histogram, see Eq. 3.5. This method is known as the Palmgren-Miner accumulated damage estimation [50] and [51].

$$Total\ Damage = \sum_0^{\infty} \frac{n_i}{N(S_i)} \quad Eq. 3.5$$

Where:

$n_i$  – the number of cycles for the considered stress in the bin on the fatigue histogram

$N(S_i)$  – the number of permissible cycles for the considered stress in the bin interpolated the form of the S-N curve.

The failure criterion corresponds to a total damage value exceeding 1.

Damage results can then be presented on a discrete model using the Abaqus [34] visualisation module and the author's scripts – see Figure 3-18, Figure 3-20 and Figure 3-22, and using commercial software – CAE Fatigue – see Figure 3-19, Figure 3-21 and Figure 3-23.

### 3.3.2 Material properties case study

To assess the fatigue damage life, samples made of stainless steel 17-4PH (H1025) were used for transmission shaft tubes to benchmark the algorithms, which use different methods for vibration damage assessment in the frequency domain i.e.: Dirlik, Lalanne, Steinberg, Bendat Narrow Band.

The material fatigue properties based on references MMPDS-15 ref [49]. The fatigue curve for the considered material is for  $K_t$  equals 3 and for the stress ration  $R = -1$  see Figure 3-16.

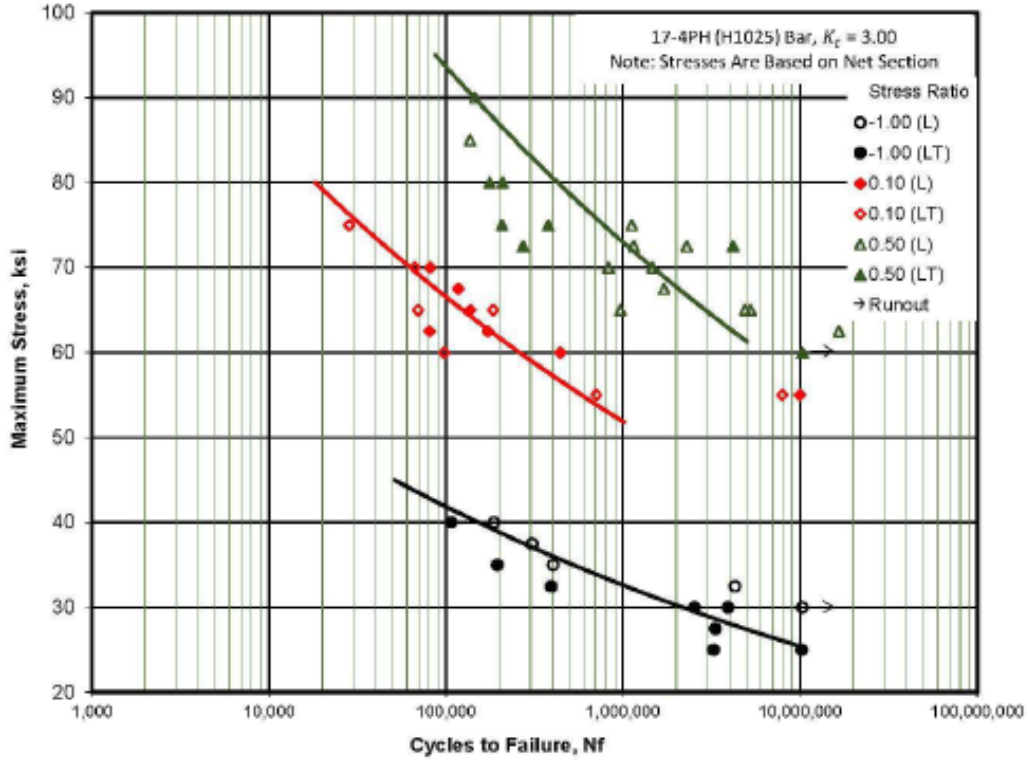


Figure 3-16 Best-fit S-N curves for notched,  $K_t=3.0$ , fatigue behaviours of 17-4PH (H1025) stainless steel bar, longitudinal and long transverse directions [49]

The S-N curve was created based on a logarithmic equation in logarithmic coordinates, graphical representation of the S–N curve is presented in Figure 3-17.

$$\log(N_f) = 21.60 - 9.24 \log(S_{eq}) \quad \text{Eq. 3.6}$$

where:

$S_{eq} = S_{max}(1 - R)^{0.581}$  – equivalent stress for different stress ratios

$R$  – stress ratio

$S_{max}$  – stress level for considered cycles to failure

$N_f$  – cycles to failure for considered equivalent stress

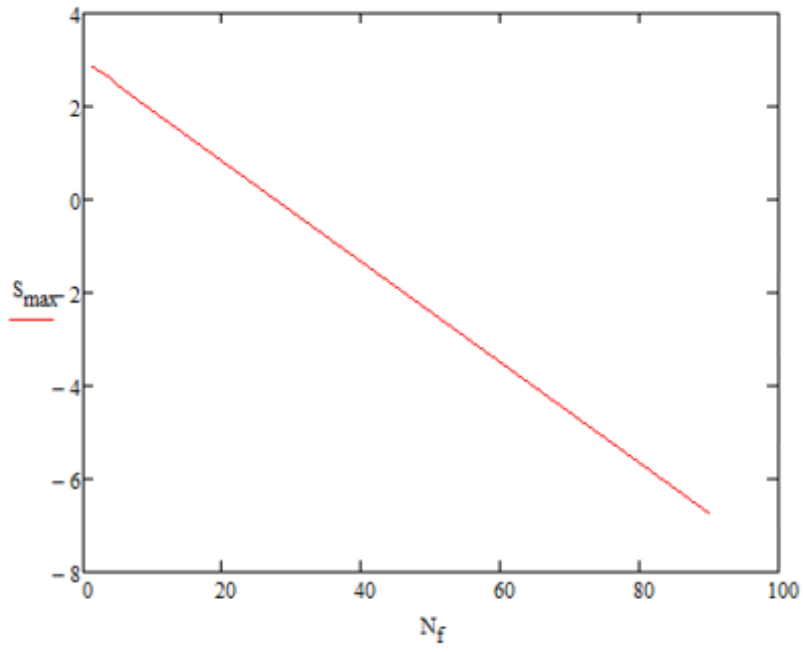


Figure 3-17 The S-N curve for vibration fatigue consideration for 17-4PH (H1025)  $K_t = 3$

### **3.3.3 Algorithm benchmarks against commercial software**

Damage values were estimated assuming a maximum sigma level of RMS stress equal to 10RMS for the range, therefore +/-5 for amplitude value. This setting is the default value of the CAE Fatigue software [28] and [29].

The stress bins used for damage estimation were set as default in CAE Fatigue software – equal to 32. Stress for each bin was calculated in the middle of the bin width, and the integration process was done using the trapezoidal numerical integration method.

The damage value was evaluated using an unaverage element nodal value (stress value extrapolated from integration points of elements of the element nodal location).

### 3.3.3.1 White noise signal – irregular factor 0.300

In Table 3-4 we quote the damage value for the irregular factor 0.585 using different methods of damage estimation in the frequency domain. The reference time exposure for the random vibration input for the considered irregular factor is 0.353h. Table 3-3 introduces the PSD input curve used for obtaining the white noise PSD response.

PSD input curve definition for the white noise signal	
Frequency [Hz]	PSD input [ $g^2/Hz$ ]
1	0.22
200	0.22
500	0.30
1000	0.30

Table 3-3 The PSD input curve definition used to obtain the white noise PSD response signal

Figure 3-18 shows exemplary damage results for the white noise signal using the Dirlik method and the author’s scripts. Analogical results has been presented using MSC CAE Fatigue software – see Figure 3-19.

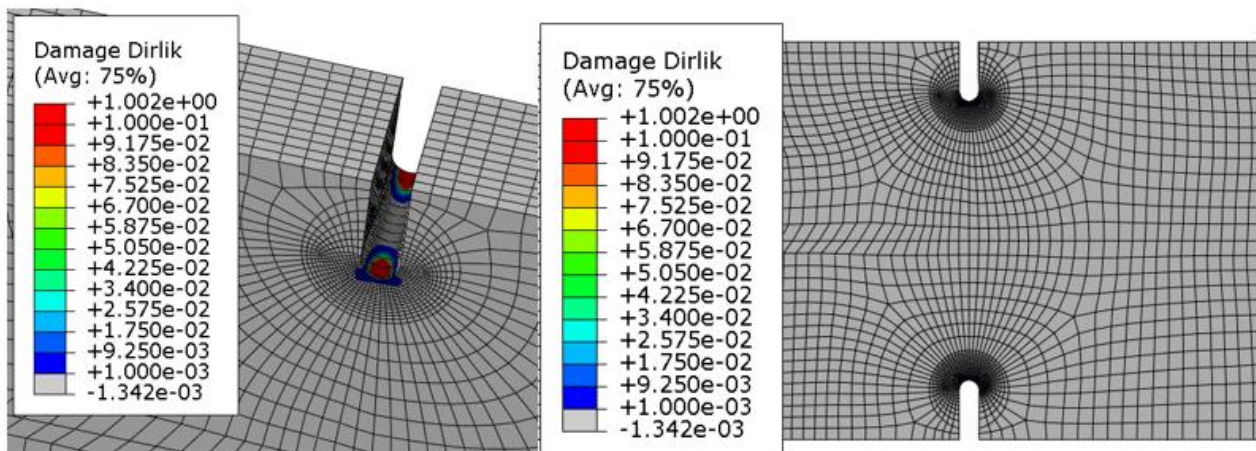


Figure 3-18 Visualisation of Dirlik Damage using a developed Python Algorithm at sample geometry using the Abaqus visualisation module and the author’s script – the white noise signal

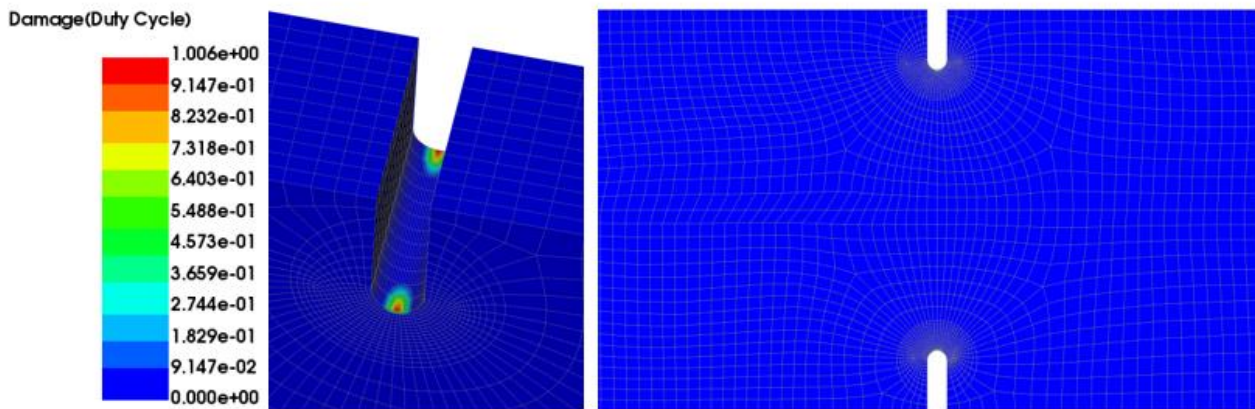


Figure 3-19 Visualisation of Dirlik Damage obtained in the MSC CAE Fatigue commercial software environment – the white noise signal

As a reference for vibration damage we used the Dirlik method, which is the best for general usage, for a general value of the irregular factor [3] and [4].

Dirlik damage quoted in Table 3-4 will be used also as a reference for the test setup as the most robust and general for all the methods used. Comparing the author’s algorithm for vibration damage estimation with MSC CAE Fatigue shows that for Dirlik and Narrow-Band (assuming use of the same approach with replacing EP with E0) obtained a great correlation. For the Steinberg method we obtained 11.78% in differences, however this method is much less robust than the two mentioned earlier. Additionally, the obtained results are very conservative for the white noise signal. The Lalanne method gives less accurate results – modification of this method will be introduced in section 3.4.

Method used for damage estimation	Dirlik	Narrow-Band	Lalanne	Steinberg
Damage values – Author’s Algorithm	1.0023	3.675 <sup>N*</sup> 1.142 <sup>N**</sup>	0.0013	8.321
Damage values – MSC CAE Fatigue Software	1.006	N/A* 1.147**	N/A	7.444
% Difference Author’s Algorithm versus MSC CAE Fatigue	0.36%	N/A* 0.43%**	N/A	11.78%

Table 3-4 Damages values for different methods used for vibration damage assessment in the frequency domain for the white noise signal

Note:

<sup>N\*</sup>Used EP – number of peaks in the spectrum value for Narrow Band cycles estimation as per equation Eq. 2.7.

<sup>N\*\*</sup>Used E0 – number of the upward zero crossing value, this approach is practiced in MSC CAE Fatigue software to decrease the conservatism of Narrow-Band method usage.

### 3.3.3.2 Wide band signal – irregular factor 0.585

In- Table 3-6 the quoted damage value for the irregular factor 0.585 uses a different method of damage estimation in the frequency domain. The reference time exposure for the random vibration input for the considered irregular factor is 0.229h. Table 3-5 introduces the PSD input curve used for obtaining the wide band PSD response.

The PSD input curve definition for the wide band signal	
Frequency [Hz]	PSD input [ $g^2/Hz$ ]
1	0.25
200	0.25
500	0.06
1000	0.06

Table 3-5 The PSD input curve definition used to obtain the wide band PSD response signal

Figure 3-20 shows exemplary damage results for the wide band signal using the Dirlik method and the author’s scripts. Analogical results are presented using MSC CAE Fatigue software – see Figure 3-21.

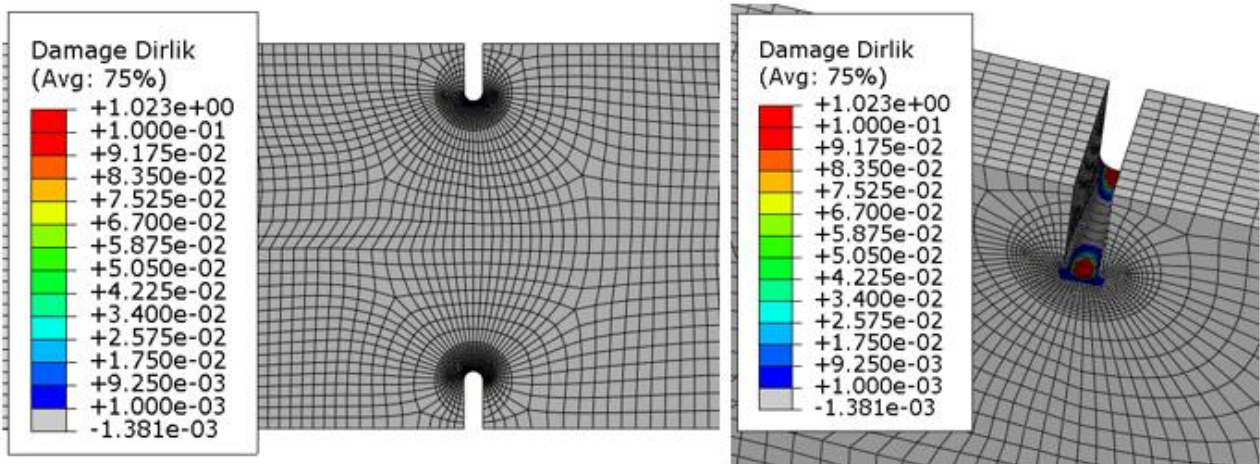


Figure 3-20 Visualisation of Dirlik Damage using a developed Python Algorithm as sample geometry using the Abaqus visualisation module and the author’s script – the wide band signal

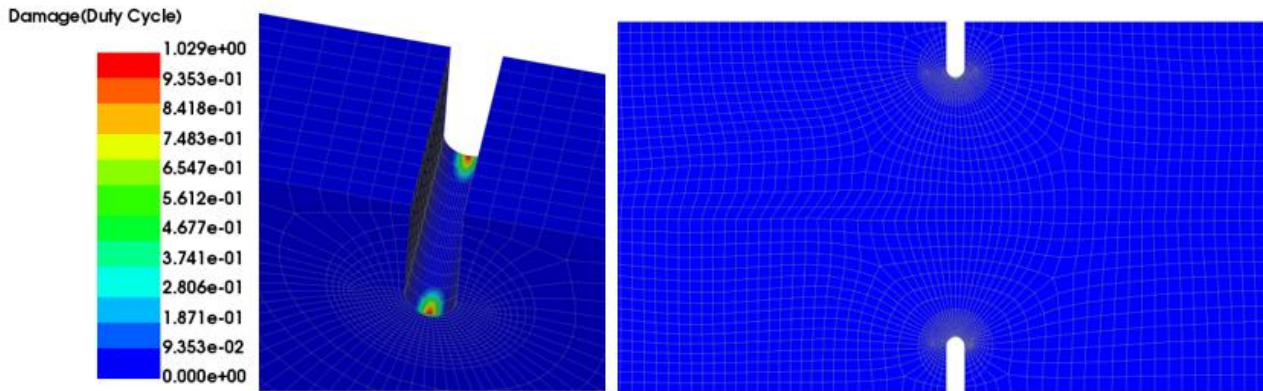


Figure 3-21 Visualisation of Dirlik Damage obtained in the MSC CAE Fatigue commercial software environment – the wide band signal

As the reference for vibration damage we used the Dirlik method, which is the best for general usage, for a general value of the irregular factor [3] and [4].

Dirlik damage quoted in Table 3-6 will be used also as a reference for the test setup as the most robust and general for all methods used. Comparing the author’s algorithm for vibration damage estimation with MSC CAE Fatigue shows that for Dirlik and Narrow-Band (assuming use of the same approach with replacing EP with E0) obtained a great correlation. For the Steinberg method we obtained 11.61% in differences, although this method is much less robust than the two mentioned earlier. Additionally, the obtained results are very conservative for the wide band signal. The Lalanne method gives less accurate results – modification of this method will be introduced in section 3.4.

Method used for damage estimation	Dirlik	Narrow-Band	Lalanne	Steinberg
Damage values – Author’s Algorithm	1.0236	2.2357* 1.0635**	3.5E-4	5.063
Damage values – MSC CAE Fatigue Software	1.0286	N/A* 1.0691**	N/A	4.536
% Difference Author’s Algorithm versus MSC CAE Fatigue	0.48%he	N/A* 0.52%**	N/A	11.61%

Table 3-6 Damage values for different methods used for vibration damage assessment in the frequency domain for – the wide band signal

Note:

\*Used EP – the number of peaks in the spectrum value for Narrow Band cycles estimation as per equation Eq. 2.7.

\*\*Used E0 – the number of upward zero crossing values, this approach is practiced in MSC CAE Fatigue software to decrease the conservatism of Narrow-Band method usage.

### 3.3.3.3 The Narrow band signal – the irregular factor 0.955

Table 3-8 shows the quoted damage value for the irregular factor 0.585 using different methods of damage estimation in the frequency domain. The reference time exposure for the random vibration input for considered irregular factor is 0.346h. Table 3-7 introduces the PSD input curve used for obtaining the narrow band PSD response.

The PSD input curve definition for the narrow band signal	
Frequency [Hz]	PSD input [ $g^2/Hz$ ]
1	0.23
200	0.23
500	1.00E-04
1000	1.00E-04

Table 3-7 The PSD input curve definition used to obtain the narrow band PSD response signal

Figure 3-22 shows exemplary damage results for the narrow band signal using the Dirlik method and the author’s scripts. Analogical results are presented using MSC CAE Fatigue software – see Figure 3-23.

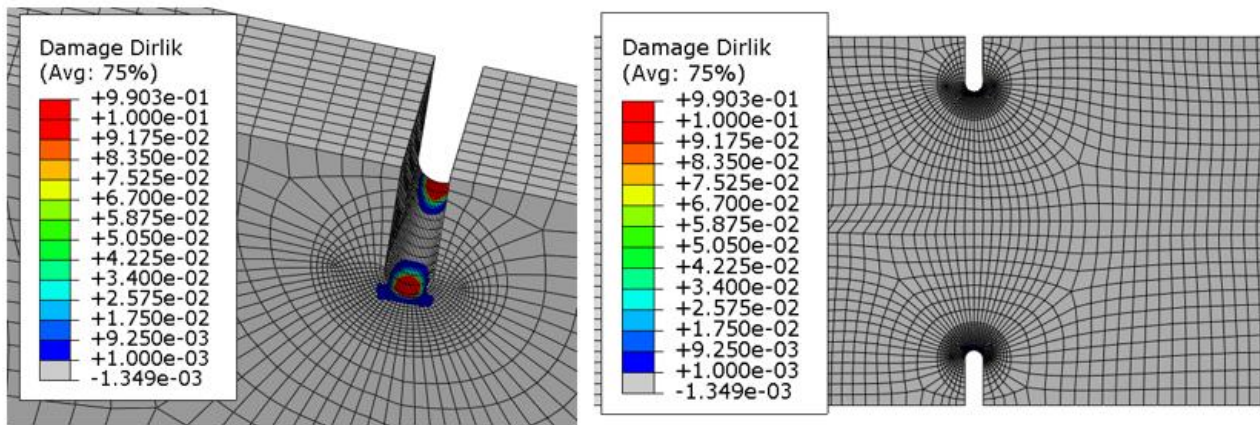


Figure 3-22 Visualisation of Dirlik Damage using a developed Python Algorithm as sample geometry using the Abaqus visualisation module and the author’s script – the narrow band signal

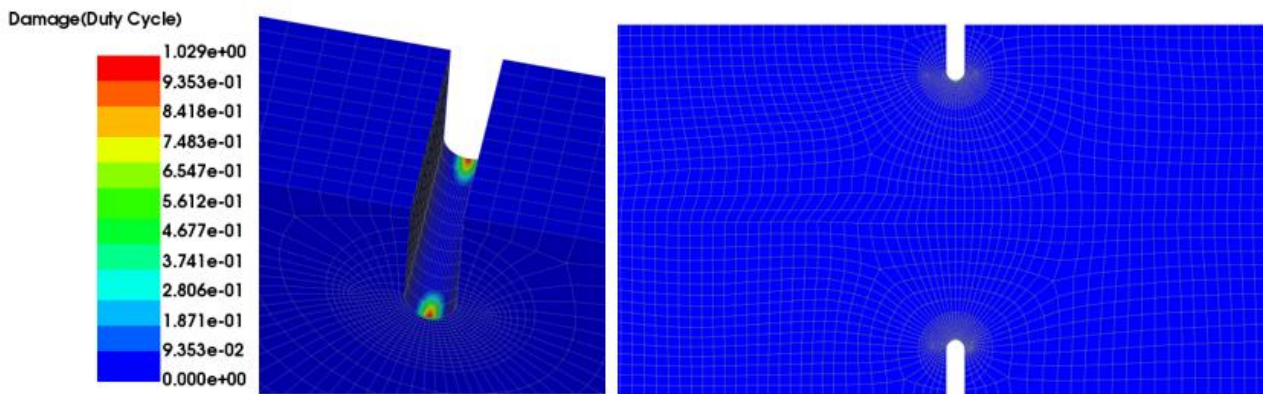


Figure 3-23 Visualisation of Dirlik Damage obtained in the MSC CAE Fatigue commercial software environment – the narrow band signal

As the reference for vibration damage the Dirlik method was used, as the best for general usage, for the general value of the irregular factor [3] and [4].

Dirlik damage quoted in Table 3-8 will also be used as a reference for the test setup, as it is the most robust and general method used. A comparison of the author’s algorithm for vibration damage estimation with MSC CAE Fatigue shows that the Dirlik and Narrow-Band methods (assuming using the same approach with replacing EP with E0) obtained a great correlation. With the Steinberg method we obtained 6.27% differences, although this method is much less robust than the two mentioned earlier. Additionally, the obtained results is very conservative for the narrow band signal. The Lalanne method gives less accurate results – modification of this method will be introduced in section 3.4.

Method used for damage estimation	Dirlik	Narrow-Band	Lalanne	Steinberg
Damage values – Author’s Algorithm	0.9910	1.0550* 1.0236**	4.86E-10	2.388
Damage values – MSC CAE Fatigue Software	1.0288	N/A* 1.0626**	N/A	2.247
% Difference Author’s Algorithm versus MSC CAE Fatigue	3.67%	N/A* 3.67%**	N/A	6.27%

Table 3-8 Damage values for different methods used for vibration damage assessment in the frequency domain for – the narrow band signal

Note:

\*Used EP – the number of peaks in the spectrum value for Narrow Band cycles estimation as per equation Eq. 2.7.

\*\*Used E0 – the number of upward zero crossing values, this approach is practiced in MSC CAE Fatigue software to decrease the conservatism of Narrow-Band method usage.

### 3.4 Lalanne method modification

Research results presented in Chapter 3 reveal that the Lalanne method gives underestimated damage values using Eq. 2.21 as per [20], [21] and [22]. Therefore, this section focuses on the modification of the Lalanne method and introduces changes to obtain a damage value aligned to the Dirlik method (as damage value using this method gives the closest result to damage value estimated using the Monte Carlo method).

#### 3.4.1 Integration of the PDF for the Dirlik, Lalanne and Narrow Band methods

The aim of the research is to integrate the PDF function for the Dirlik, Narrow Band and Lalanne methods to see if there are any differences on that stage. For these purposes an exemplary white noise signal is used, with statistic parameters presented in Table 3-9.

Signal statistic parameters in the frequency domain		
$m_0$ (0 <sup>th</sup> spectral moment) [MPa <sup>2</sup> ]	Irregular factor $\gamma$ [-]	i –Double Clipping Amplitude for the Histogram – with a signal clipped at 5RMS amplitude (10RMS double amplitude) [MPa]
773.8	0.265	278.17

Table 3-9 An exemplary signal statistic in frequency domain parameters

The following points were analysed to identify the issue:

- i. Evaluation of the Lalanne PDF function – LAL as per Eq. 2.21 gives a value of the integer equal to  $\int_0^i LAL(S)dS = 0.6326$ , and therefore does not reach the unity – it indicates that the proposed PDF equation needs to be modified. Figure 3-24 shows the Lalanne PDF in the function of the stress variable.

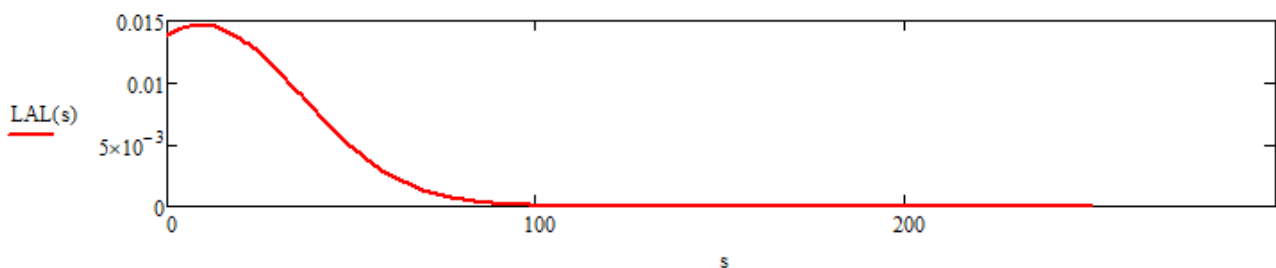


Figure 3-24 The Lalanne PDF in the function of the stress variable

- ii. Evaluation of the Bendat Narrow Band PDF function – NB as per Eq. 2.6 gives a value of the integer equal  $\int_0^i NB(S)dS = 0.9999$ , and therefore reaching the unity – it indicates that the proposed PDF equation is correct. Figure 3-25 shows the Lalanne PDF in the function of the stress variable.

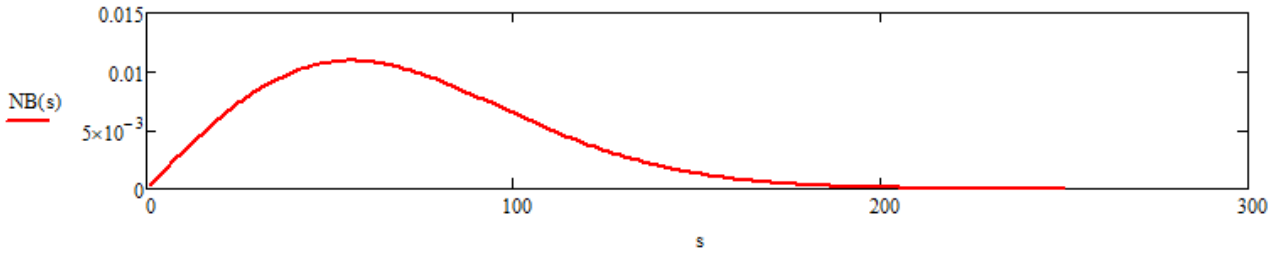


Figure 3-25 The Narrow Band Bendat PDF in the function of stress variable

- iii. Evaluation of the Dirlik PDF function – PDFD as per Eq. 2.8 gives a value of the integer equal to  $\int_0^t PDFD(S)dS = 0.9999$ , and therefore reaches the unity – it indicates that the proposed PDF equation is correct. Figure 3-26 shows the Dirlik PDF in the function of the stress variable.

Dirlik empirical variables for PDF estimation						
Variable	$X_m$ (Eq. 2.11) [-]	$D_1$ (Eq. 2.12) [-]	$D_2$ (Eq. 2.13) [-]	$D_3$ (Eq. 2.14) [-]	$Q$ (Eq. 2.15) [-]	$R$ (Eq. 2.16) [-]
Value	0.1688	0.1839	0.6547	0.1613	0.2299	0.1071

Table 3-10 Dirlik empirical variables for PDF estimation

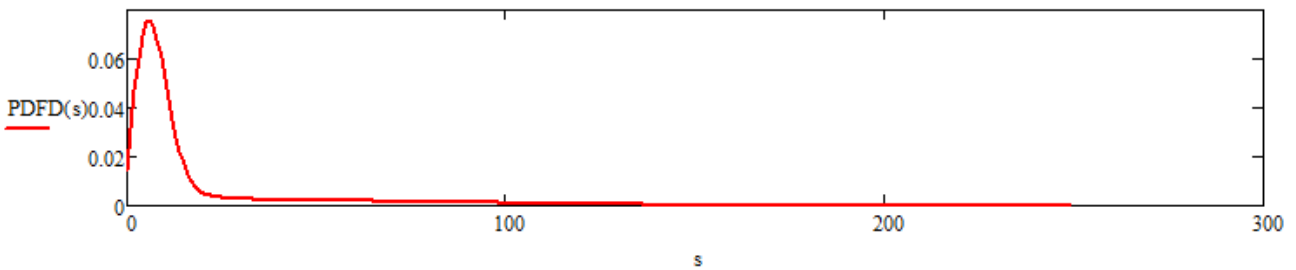


Figure 3-26 The Dirlik PDF in the function of the stress variable

### 3.4.2 Modification of the Lalanne PDF function - introduction

The PDF function introduced by Bendat in his work [15] in Rayleigh's part of function (see Eq. 3.7) used the complementary error function as per Eq. 3.9 (for erfc definition see Eq. 3.10)

$$W(z) = ze^{-\frac{z^2}{2}} \quad \text{Eq. 3.7}$$

Where z is a standardised variable defined by Eq. 3.8:

$$z = \frac{S}{RMS} \quad \text{Eq. 3.8}$$

Where:

S – Is the stress at the histogram bin

The Bendat formulation from reference [15] is as follows – see Eq. 3.9:

$$W(z) = \left\{ \frac{\sqrt{1-\gamma^2}}{\sqrt{2\pi}} e^{\frac{-S^2}{2m_0(1-\gamma^2)}} + \frac{S\gamma}{RMS} e^{\frac{-S^2}{2m_0}} \left[ 1 - \text{erfc}\left(\frac{S\gamma}{\sqrt{m_0(1-\gamma^2)}}\right) \right] \right\} \quad \text{Eq. 3.9}$$

The complementary error function can be defined as per equation Eq. 3.10 as per [56]. Figure 3-27 shows graphical representation of the error function and the complementary error function.

$$\text{erfc}(x) = \frac{2}{\sqrt{\pi}} \cdot \int_x^{\infty} e^{-t^2} dt \quad \text{Eq. 3.10}$$

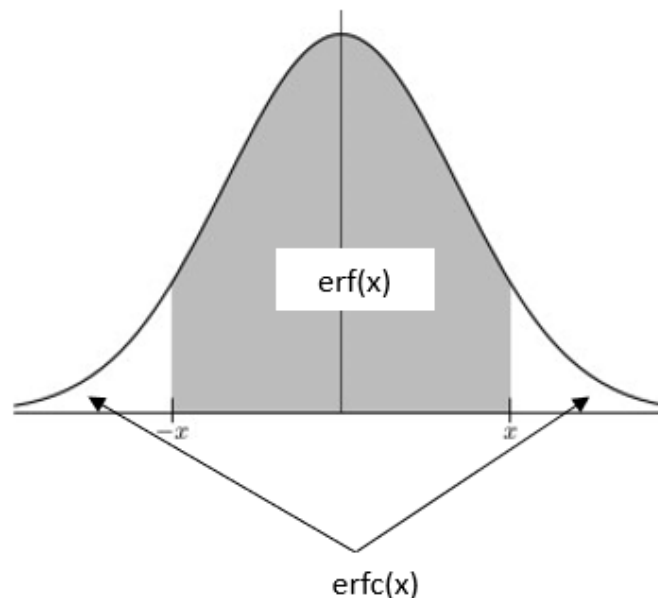


Figure 3-27 The error function erf(x) and the complementary error function – erfc(x), graphical representation

Therefore, the multiplication factor in Rayleigh’s part of the equation Eq. 3.9  $(1 - \operatorname{erfc}(\frac{S\gamma}{\sqrt{m_0(1-\gamma^2)}}))$  is equal to the error function, which can be defined as in equation Eq. 3.11 and equation Eq. 2.22 [56].

$$\operatorname{erf}(x) = 1 - \operatorname{erfc}(x) \tag{Eq. 3.11}$$

As a modification of equation Eq. 2.21 it is proposed to replace Rayleigh’s multiplication factor  $(1 - \operatorname{erfc}(\frac{S\gamma}{\sqrt{m_0(1-\gamma^2)}}))$  with the error function  $\operatorname{erf}(\frac{S\gamma}{\sqrt{m_0(1-\gamma^2)}})$ . Another modification uses Dirlik’s normalised stress variable  $(\frac{S}{2\sqrt{m_0}})$  instead of Bendat’s normalised stress variable  $(\frac{S}{\sqrt{m_0}})$ . These two modifications of the Lalanne PDF function were introduced in equation Eq. 3.11.

$$LALm = \frac{1}{RMS} \left\{ \frac{\sqrt{1-\gamma^2}}{\sqrt{2\pi}} e^{\frac{-s^2}{8m_0(1-\gamma^2)}} + \frac{S\gamma}{4RMS} e^{\frac{-s^2}{8m_0}} \left[ \operatorname{erf}\left(\frac{S\gamma}{\sqrt{8m_0(1-\gamma^2)}}\right) \right] \right\} \cdot ds \tag{Eq. 3.12}$$

Figure 3-28 shows the modified Lalanne (LALm) PDF function in the stress variable.

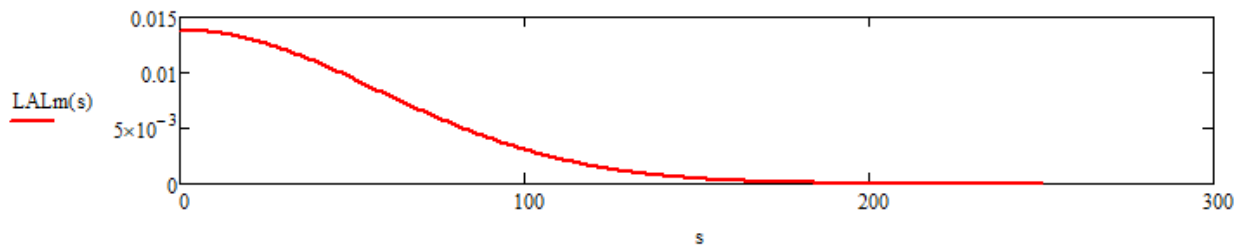


Figure 3-28 The modified Lalanne PDF in the function of the stress variable

Figure 3-29 shows the modified Lalanne (LALm) PDF function in the stress variable.

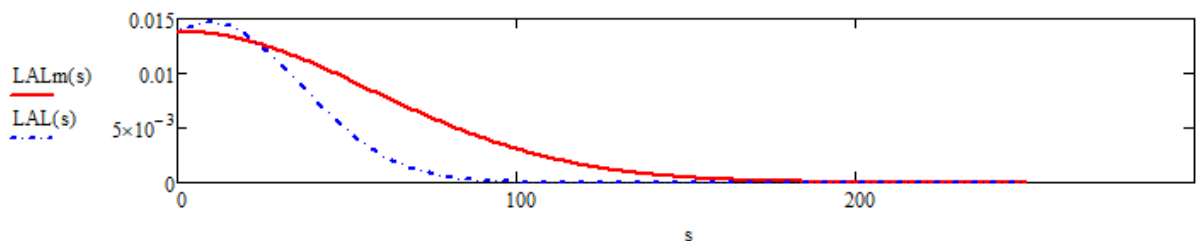


Figure 3-29 Graphical comparison of the Lalanne PDF – LAL(s) and the modified Lalanne PDF – LALm(s) in the function of the stress variable

Evaluation of the modified Lalanne PDF function – LALm defined by per Eq. 3.12 gives a value of the integer equal  $\int_0^i LALm(S)dS = 0.9999$ , and therefore obtained the correct value. Table 3-11 shows the damage values for the legacy Lalanne PDF, modified Lalanne PDF and using the Dirlik method as the reference. As per damage values presented in Table 3-11, the proposed modification allows to obtain damage values closer to the Dirlik method than using the legacy approach.

	Dirlik reference damage for the white noise signal	Damage value for the white noise signal	Dirlik reference damage for the wide band signal	Damage value for the wide band signal	Dirlik reference damage for the narrow band signal	Damage value for the narrow band signal
Damage value based on the legacy Lalanne PDF (LAL)	1.0023 (MSC CAE Fatigue damage 1.0060)	0.0013	1.0236 (MSC CAE Fatigue damage 1.0286)	3.5E-4	0.9910 (MSC CAE Fatigue damage 1.0288)	4.86E-10
Damage value based on the proposed modified Lalanne PDF (LALm)		1.4724		1.1333		1.0236

Table 3-11 Damages based on the legacy and proposed Lalanne PDF

The proposed modification gives a more conservative damage value for the narrow band signal (obtained ~50% more conservative than Dirlik) and for the wide band signal (obtained ~15% more conservative than Dirlik). For the white noise signal the proposed modification gives a result close to Dirlik – less than 5% of difference. Therefore, the proposed modified Lalanne method is recommended for use, especially when high conservatives in the analysis are desired, e.g., at the initial stage of the sizing unit, when test results are unavailable – the Transfer Function of the unit has not been correlated against the test results.

## CHAPTER 4 VIBRATION FATIGUE DAMAGE PREDITIONS UNDER STOCHASTIC LOADING – COMBINED FREQUENCY AND TIME DOMAIN CONSIDERATION

This section introduces combined frequency and time domains consideration for vibration damage estimation under random loading. The aim of the research is to analyse the unit in the frequency domain as presented in Chapter 3 using the linear dynamic approach to derive the transfer function. However, it is proposed that once the transfer function and then the PSD response have been derived, the signal should be retrieved in the time domain using the Monte Carlo method and IFFT. This section introduces the workflow used for switching from the frequency to time domain and final fatigue damage consideration in the time domain.

### 4.1 Time signal generation from the PSD Response function

The aim of using combined frequency and time domain consideration was introduced by Dirlik in his research [18]. For this purposes the Inverse Discrete Fast Fourier Transform (IDFFT) was used, (as the signal with one shape in the frequency domain can have infinite shapes in the time domain, which can cause different damage to the construction [52]) and the Monte Carlo method, which can be graphically presented in Figure 4-1.

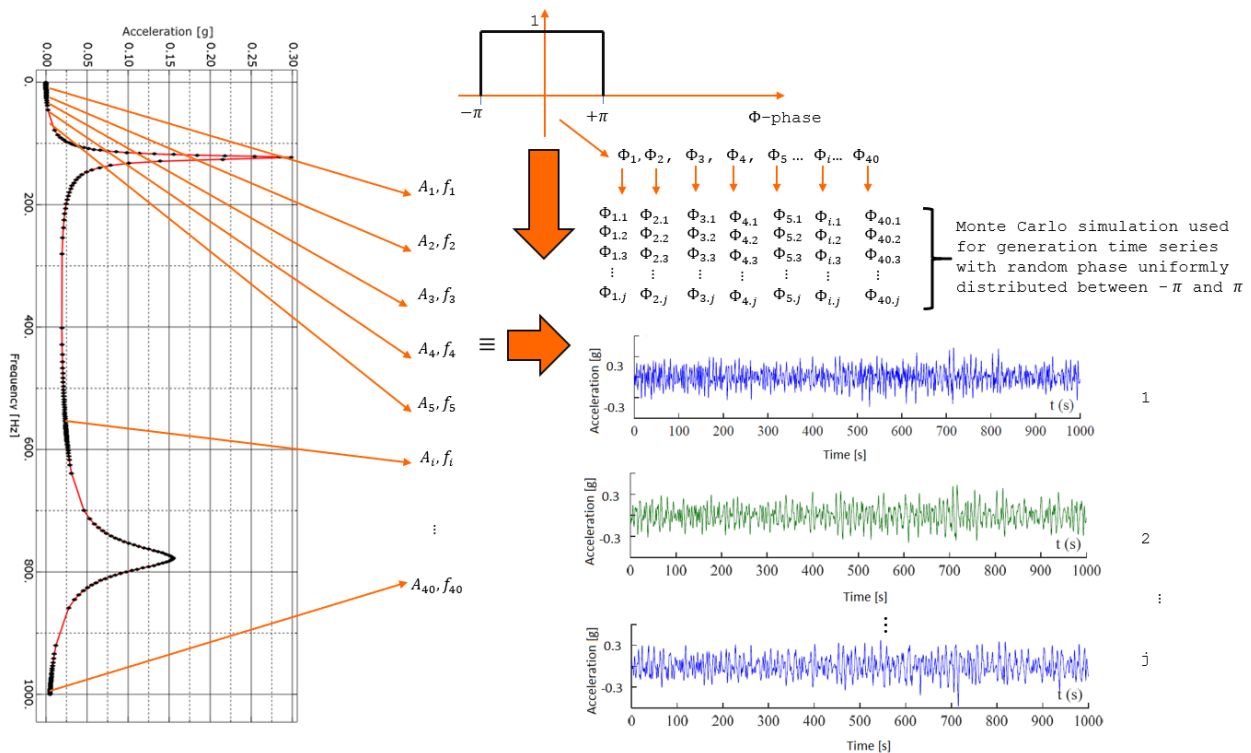


Figure 4-1 The process of recreating the time signals from the frequency using the Monte Carlo method

The basis for generating the time series data is the system response function [53], or the equivalent PSD response name estimated by the matrix summation process – see equation Eq. 3.3 for the multiple input.

For the single input – which will be considered in further research, the equation above can be reduced to the following equation Eq. 3.4, which will be used during research presented in this paper.

In order to verify the process of calculating the RMS stress based on the obtained/retrieved time domain signal, the RMS stress in the frequency domain must also be calculated as per equation Eq. 2.5.

The PSD response function and the frequency are the vector elements used in the next step for retrieving the time domain signal using Inverse Discrete Fourier transformation. The basic equation can be written as follows [18]:

$$S(k\Delta t) = \sum_{n=-\frac{N}{2}}^{\frac{N}{2}-1} \theta(j \cdot n2\pi f) \cdot e^{j \cdot 2\pi k n / N} \quad \text{Eq. 4.1}$$

where  $k$  can be written as per equation Eq. 4.3:

$$k = 0, 1, 2, 3, \dots, N - 1 \quad \text{Eq. 4.2}$$

$f$  – is the considered frequency

$N$  – is the natural number

and the  $\theta$  function can be written as Eq. 4.3 [54]:

$$\theta(j \cdot n2\pi f) = \sqrt{S(n \cdot 2\pi \Delta f)} e^{j\Phi_n} \quad \text{Eq. 4.3}$$

for  $n$  defined as in the equation Eq. 4.4:

$$n = 0, 1, 2, 3, \dots, N/2 - 1 \quad \text{Eq. 4.4}$$

The  $\Phi_n$  represents a random phase angle, defined as uniformly distributed in the bandwidth  $\langle -\pi; \pi \rangle$ . This definition implies that the time series is obtained using the Monte Carlo approach and inverse discrete Fourier transformation.

$N$  in equation Eq. 4.1 represent the total number of samples,  $\Delta f$  and  $\Delta t$  are linked with  $N$  as per the following equation Eq. 4.5 :

$$\Delta f = \frac{1}{\Delta t N} \quad \text{Eq. 4.5}$$

The time series signal is defined by function ( $S(k\Delta t)$ ) and needs to be a real function of time, in order to keep the sign for the Rainflow process, which would be omitted if the complex value of this function is not equal to zero, and therefore the magnitude would miss the sign of the signal. For this reason the spectrum defined by the function  $\theta$  in equation Eq. 4.3 has to exhibit the complex conjugate symmetry as per the below equation [54] and [55].

$$\theta(j \cdot n2\pi f) = \theta(-j \cdot n2\pi f) \quad \text{Eq. 4.6}$$

For  $n$  defined by equation Eq. 4.4.

What can be graphically shown as in the Figure 4-2.

An additional assumption for  $\theta$  function is presented in the equation Eq. 4.7.

$$\theta(0) = 0$$

Eq. 4.7

This ensures that the signal in the time domain  $S(k\Delta t)$  has a mean value equal to zero.

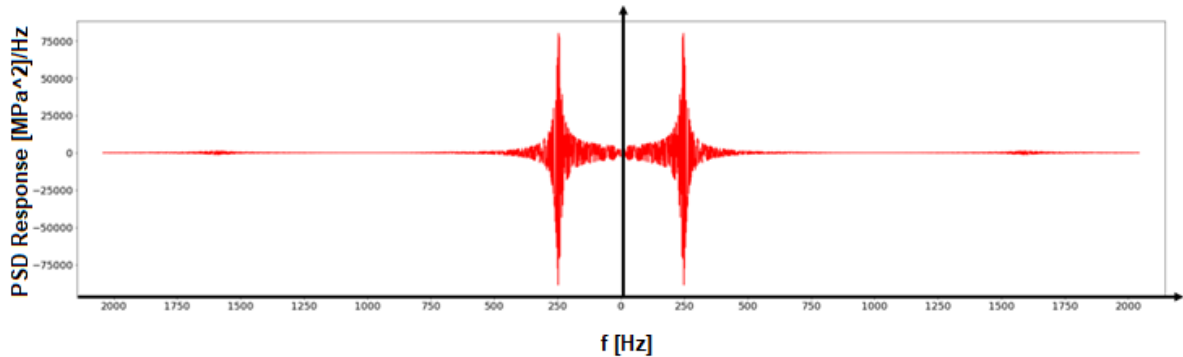


Figure 4-2 The complex conjugate symmetry of the  $\theta$  function

This ensures that the signal in time domain  $S(k\Delta t)$  has a mean value equal to zero.

It implies that the imaginary portion of the signal will be equal to zero, and therefore the magnitude of the signal will be equal to the real portion of this signal, which implies that the sign can be saved for further fatigue consideration.

To verify the obtained signal, we can recalculate the RMS of the time series signal  $S(k\Delta t)$  using the standard deviation equation, which can be written as follows:

$$RMS_{time\ series} = \sqrt{\frac{1}{N} \sum_{k=0}^{N-1} S(k\Delta t)^2} \quad \text{Eq. 4.8}$$

The obtained times signal has a zero mean value and standard deviation equal to the RMS estimated for the signal in the frequency domain, therefore the signal defined in the frequency domain retrieved to the time domain signal has been done successfully and will be used for retrieving the fatigue information using the time series Rainflow Cycle Counting algorithm implemented in Python language.

## 4.2 Time series Rainflow Cycle Counting algorithm

For fatigue consideration the time series retrieved from frequency domain PSD Response is the input for the Rainflow Cycle Counting algorithm [57], [58], [59], [60], [61] – to obtain pairs of maximum and minimum value of stress and an adequate number of cycles for the quoted stress range.

The time domain Rainflow Cycle Counting algorithm starts at the beginning of stress (or strain, load history) and goes through the inside of following peaks – see Figure 4-3. The ‘raindrops’ continue falling through an imaginary roof from the upper to the lower level until it reaches opposite a maximum more positive / minimum more negative than the maximum value / minimum value from start point. Additionally, the flow stops when it meets the rain from the roof above. The length of the following rainflow is registered in half cycle ranges.

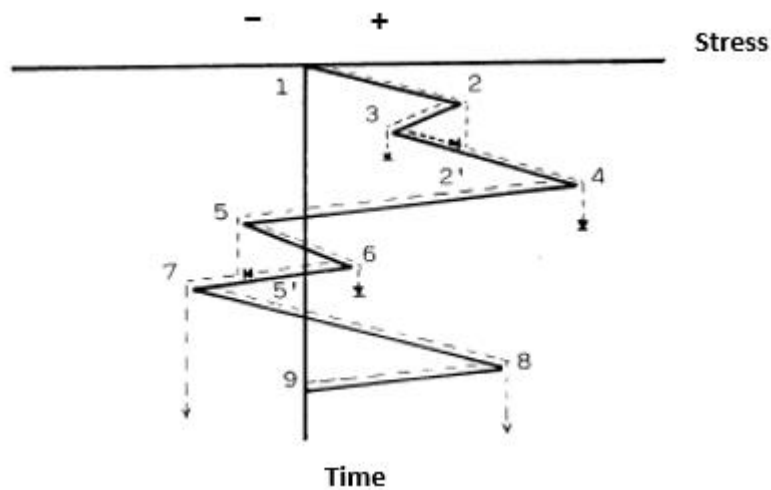


Figure 4-3 Rainflow Method graphical representation, [59]

Note: The dashed line represent the rain drop.

The rain drop starts at the 1<sup>st</sup> peak (minimum value), falls at the 2<sup>nd</sup> and 4<sup>th</sup> peaks, and stops at the opposite 5<sup>th</sup> peak – as this peak is more negative than the starting point – the 1<sup>st</sup> peak. Therefore, the range from the 1<sup>st</sup> peak to the 4<sup>th</sup> peak is registered as a half cycle. By analogy the 2<sup>nd</sup> peak and the 3<sup>rd</sup> peak are registered as a half cycle – as the rain drop started at the 2<sup>nd</sup> peak and stops at the 4<sup>th</sup> peak – this peak is more positive than the 2<sup>nd</sup> peak, although the rain drop that started at the 3<sup>rd</sup> peak stops at the 2<sup>nd</sup> peak, as in this point it meets the rain drop from the above roof. After meeting the second mentioned condition, there already exists a corresponding half cycle with equal magnitude extracted by the first condition – these two half cycles make a one full cycle. Therefore, the range consisting of the 3<sup>rd</sup> and 2<sup>nd</sup> peak make a full cycle, and the same with the range consisting of the 2<sup>nd</sup> peak and the 3<sup>rd</sup> peak.

This part of the research is creating the author’s algorithm using Python programming language. A flowchart of the Rainflow Cycle Counting Algorithm in the time domain is used in the author’s script introduced in Figure 4-4.

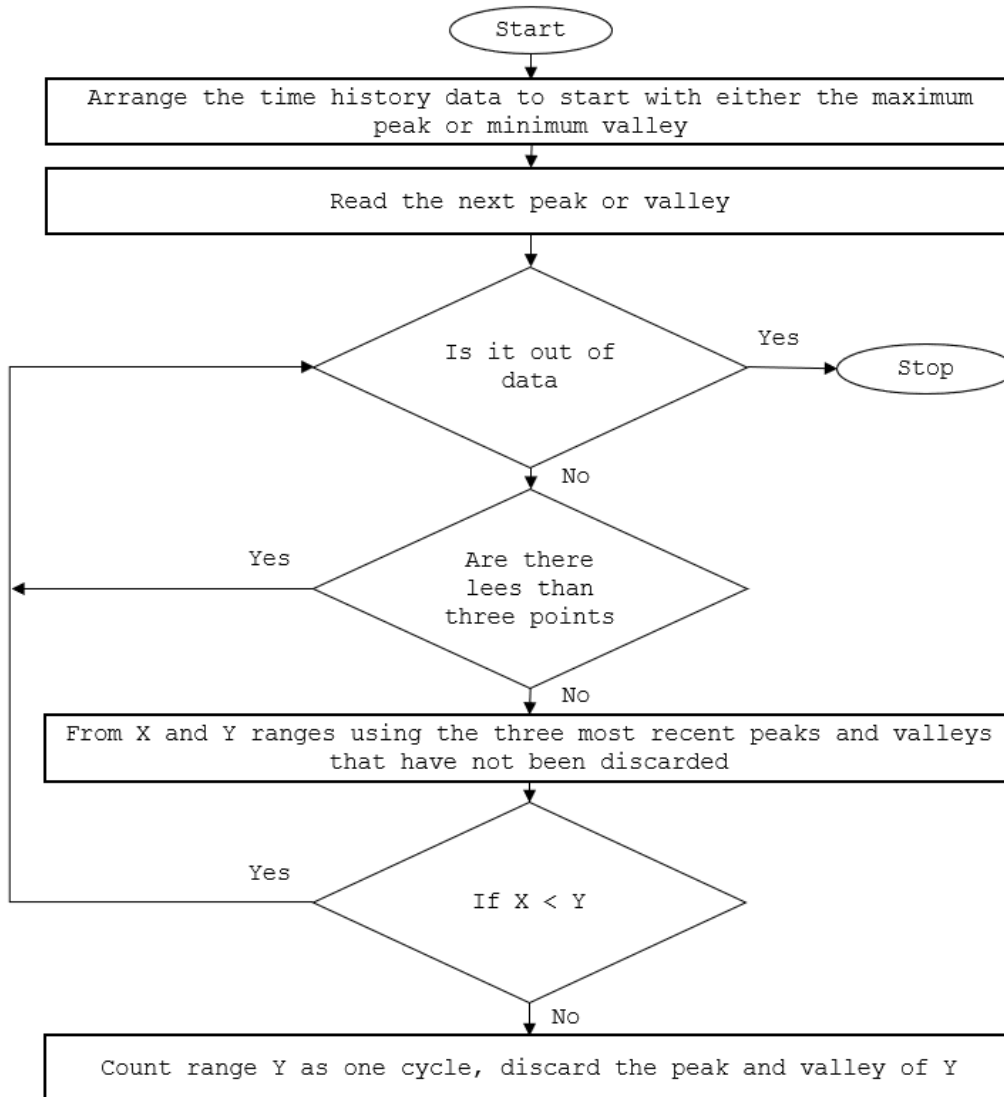


Figure 4-4 Flowchart of the Rainflow Cycle Counting Algorithm in the time domain

Figure 4-5, Figure 4-8 and Figure 4-11 show the retrieved time series from frequency domain signals using the Monte Carlo method and IFFT for white noise, wide band, and narrow band signals, respectively. These signals are the PSD response in time domain. The next step of processing these signals is extracting the peak and trough for the Rainflow Cycle Counting in the time domain (see Figure 4-6 for the white noise signal, Figure 4-9 for the wide band signal and Figure 4-12 for the narrow band signal). After the extraction process, the obtained series is processed using the Rainflow Cycle Counting algorithm in the time domain introduced in this section. The results are the pairs of minimum and maximum stress amplitude and adequate number of cycles for each pair. Graphical representation of this process is introduced using the author's script in Figure 4-7 for the white noise signal, Figure 4-10 for the wide band signal and Figure 4-13 for the narrow band signal.

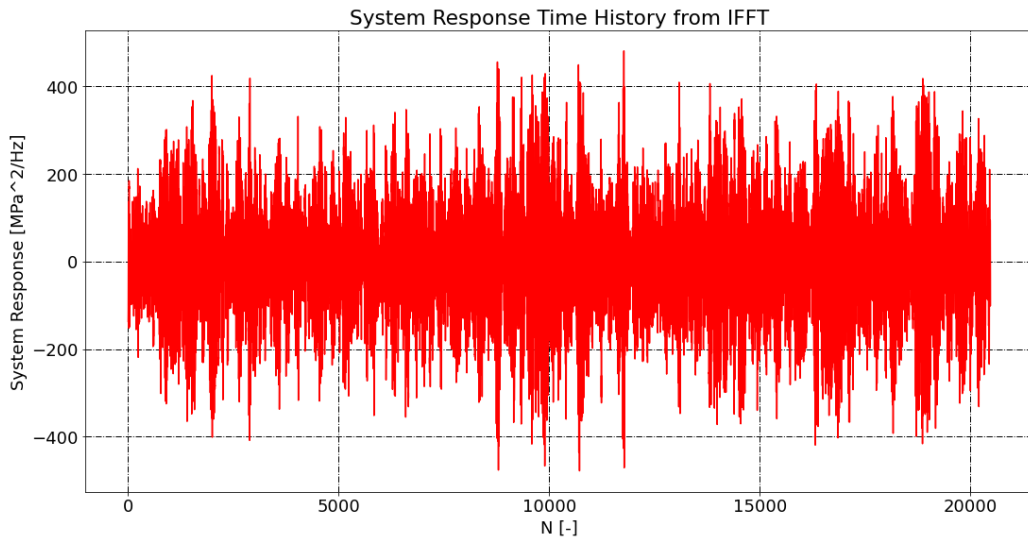


Figure 4-5 System response time history from IFFT and Monte Carlo Methods – the white noise signal

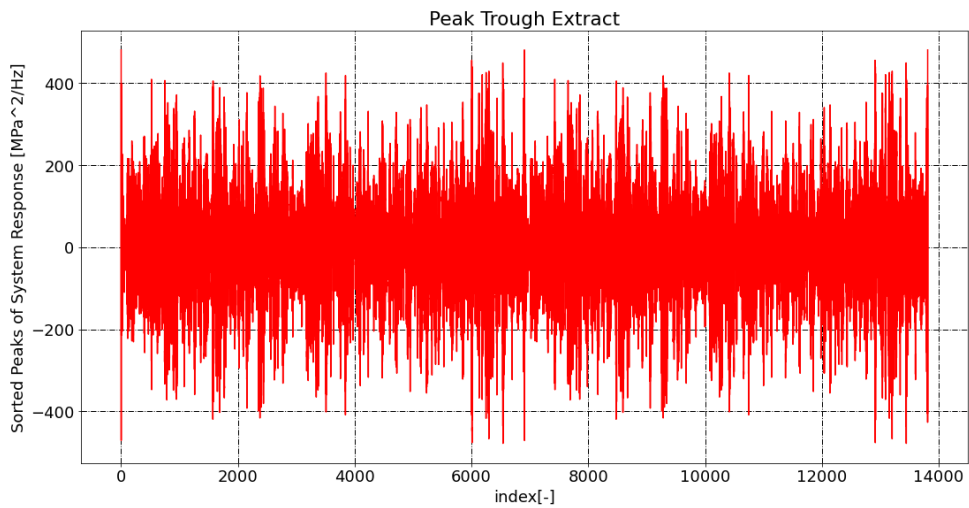


Figure 4-6 Initial time series processing extracting peak and trough for the Rainflow Counting Algorithm – the white noise signal

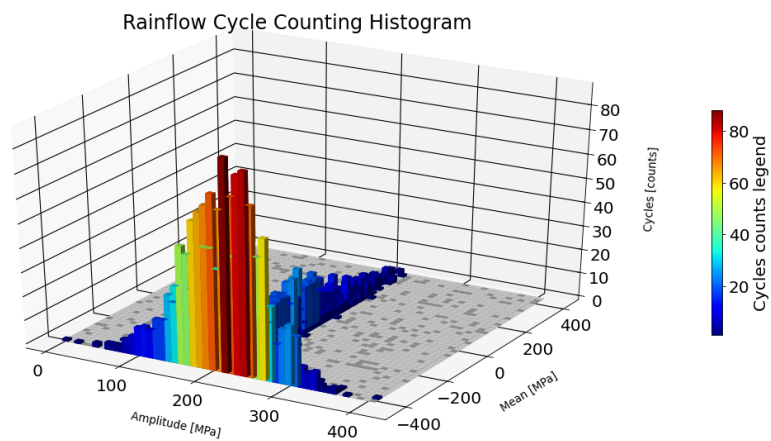


Figure 4-7 Rainflow Cycle Counting Algorithm Histogram – the white noise signal

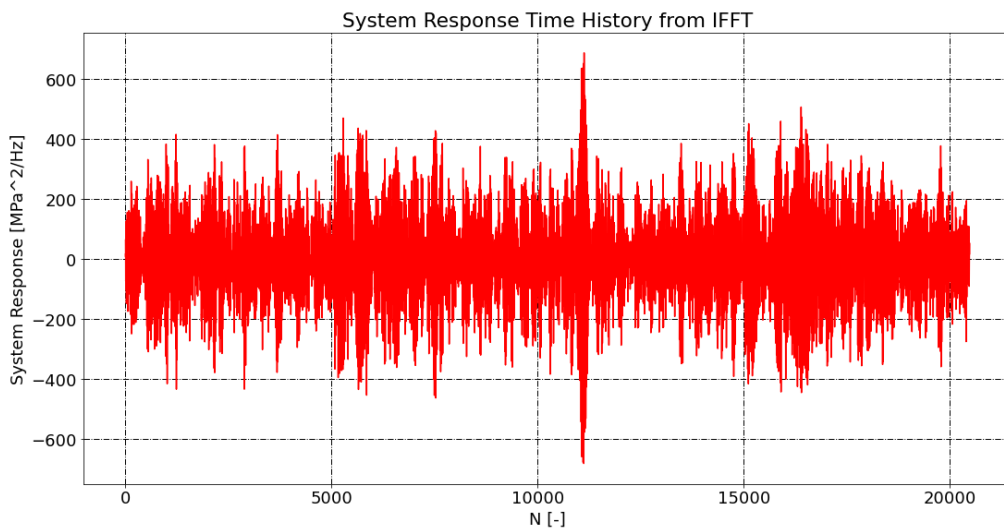


Figure 4-8 System response time history from the IFFT and Monte Carlo Methods – the wide band signal

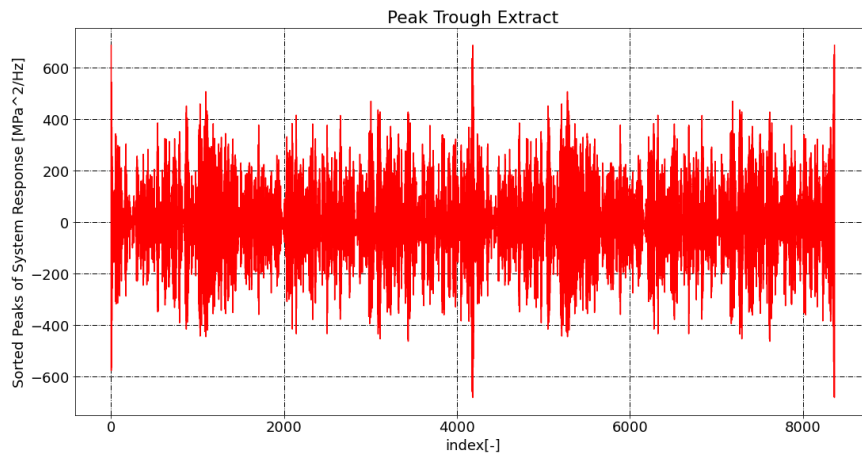


Figure 4-9 Initial time series processing extracting peak and trough for the Rainflow Counting Algorithm – the wide band signal

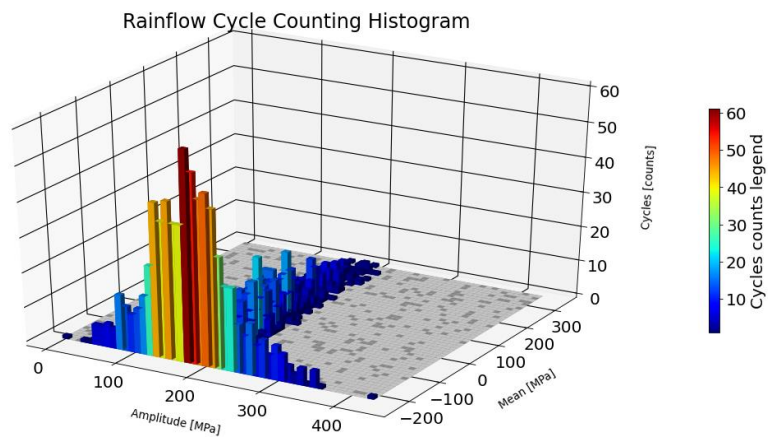


Figure 4-10 Rainflow Cycle Counting Algorithm Histogram – the wide band signal

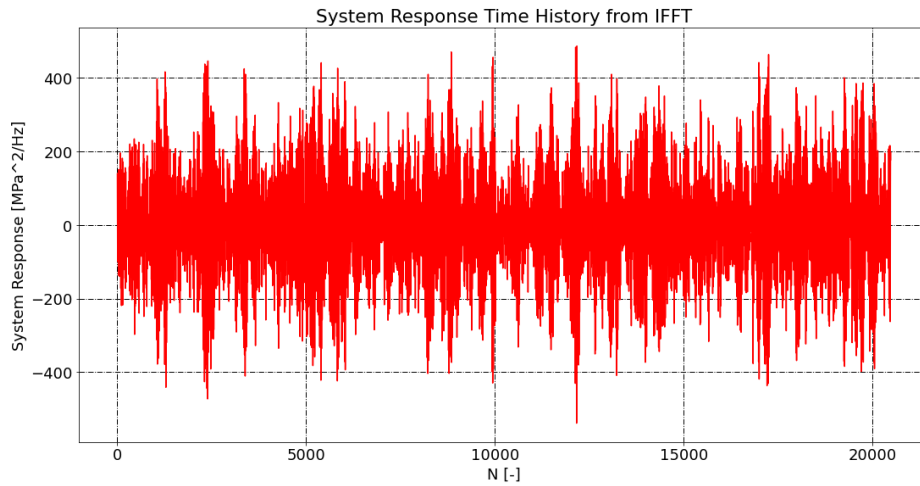


Figure 4-11 System response time history from the IFFT and Monte Carlo Methods – the narrow band signal

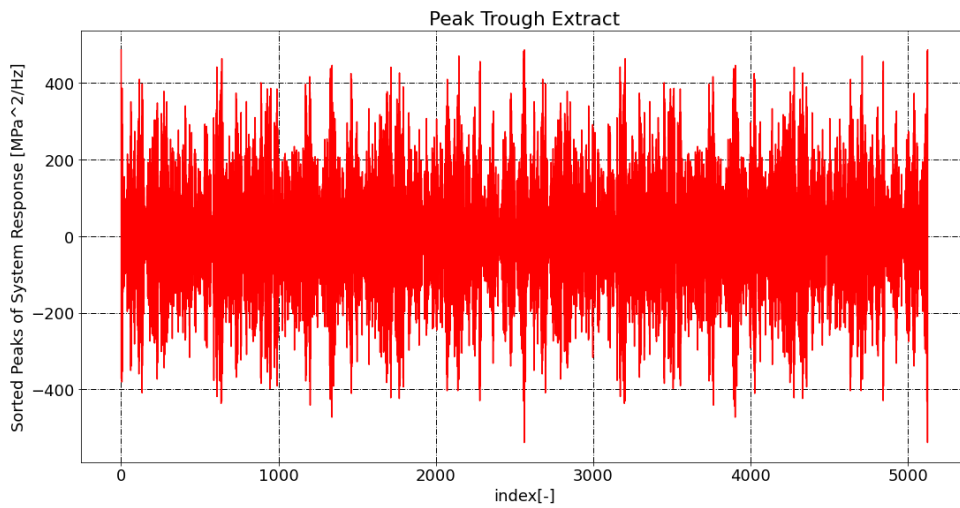


Figure 4-12 Initial time series processing extracting peak and trough for the Rainflow Counting Algorithm – the narrow band signal

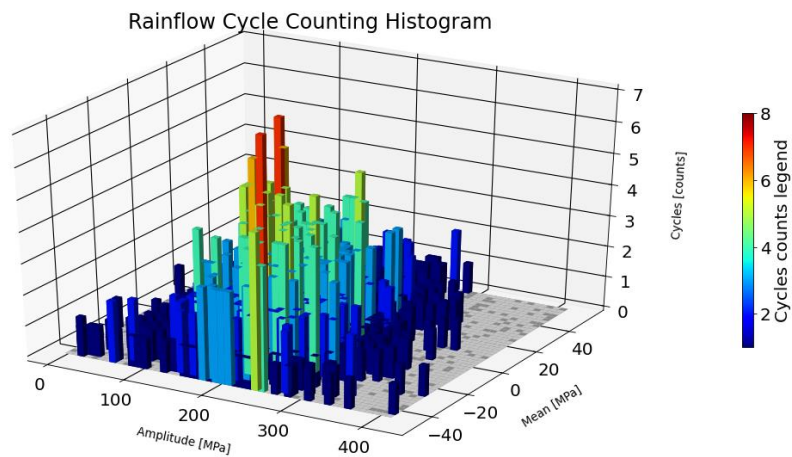


Figure 4-13 Rainflow Cycle Counting Algorithm Histogram – the narrow band signal

---

## CHAPTER 5 USING COMBINED TIME AND FREQUENCY DOMAINS CONSIDERATION FOR VERIFICATION AND MODIFICATION OF THE LEGACY THEORY

### 5.1 Signal statistics in the time domain as a benchmark of the signal statistic in frequency domain research results

Research results reveal that the signal statistics in the frequency domain give a different parameter result when the irregular factor decreases from 1 to 0 – moving from the narrow band to white noise signal – as introduced in [52]. Research has been extended to modify the existing signal statistics parameters in the frequency domain, to align them to the time domain signal statistic parameters. As the research object we used signals retrieved from the frequency domain using the Monte Carlo method, and the research was performed not on existing structure responses, but based on dummy system responses defined by a combination of two band pass filters in analytical form presented in equation Eq. 3.4. This approach allows for easily obtaining sixteen PSD responses with a different irregular factor from close to 1 (the narrow band signal) to close to 0.2 (the white noise signal).

$$PSD\_Response_i(f) = \left( \frac{A_1}{\sqrt{1 + \frac{(f-f_1)^2}{Q_1^2}}} + \frac{A_2}{\sqrt{1 + \frac{(f-f_2)^2}{Q_2^2}}} \right)^2 \quad \text{Eq. 5.1}$$

The parameters used in analytical form in equation Eq. 3.4, which define the PSD response function for further research, are presented in Table 5-1.

No.	A1	A2	f1	f2	Q1	Q2	fmax
1	3800	0	108	1.00E-30	3	0	250
2	3250	0	97	1.00E-30	6	0	250
3	2650	0	94	1.00E-30	8	0	250
4	2000	0	66	1.00E-30	5	0	250
5	2150	0	75	1.00E-30	14	0	250
6	2350	0	65	1.00E-30	16	0	250
7	2650	1800	42	106	5	4	250
8	2700	2000	32	105	5	3	250
9	2900	1700	34	109	5	2	250
10	3000	1500	31	107	5	1.8	250
11	3150	1000	29	115	6	2	250
12	2950	700	25	109	6	2	250
13	3050	600	21	110	6	2	250
14	3100	0	20	1.00E-30	5.5	0	250
15	3250	0	14	1.00E-30	5.3	0	250
16	3350	0	12	1.00E-30	4.8	0	250

Table 5-1 PSD response spectrum definition parameters

Figure 5-5 through Figure 5-7 show graphical representation of the PSD response function for exemplary samples from Table 5-1.

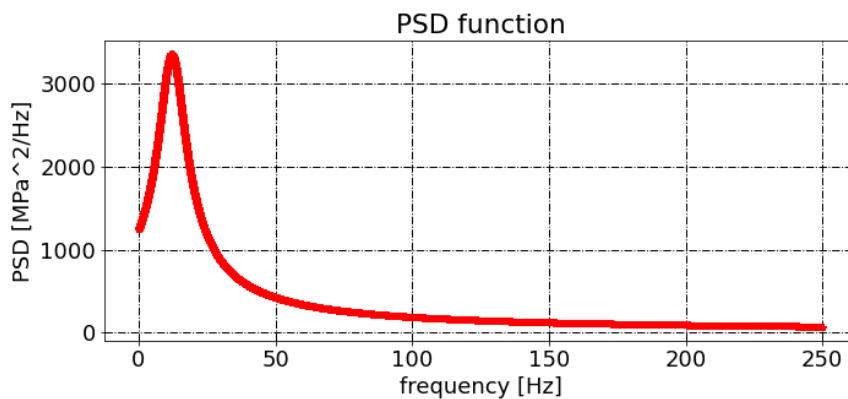


Figure 5-1 PSD response function for sample 1, irregular factor 0.975

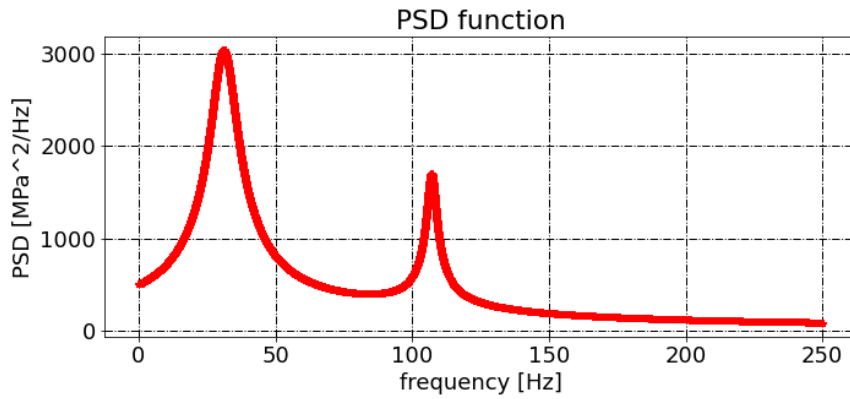


Figure 5-2 PSD response function for sample 11, irregular factor 0.486

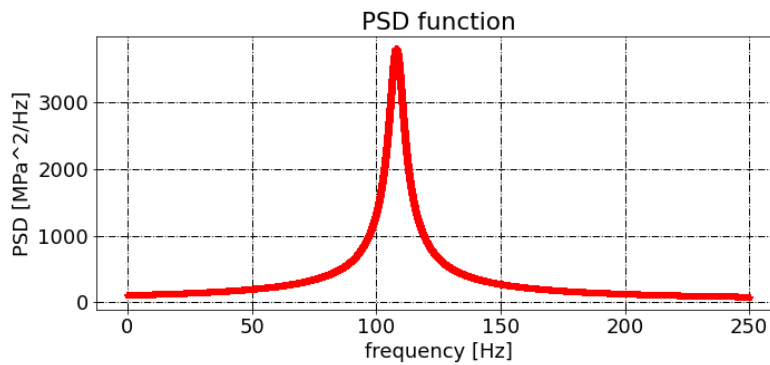


Figure 5-3 PSD response function for sample 16, irregular factor 0.258

The goal of the first stage of the research was to evaluate signal statistics in the frequency domain (irregular factor, number of upward zero crossings and number of peaks in the signal) using full integration of spectral moment and comparison against time domain signal statistics. The signal in the time domain was retrieved from the frequency domain signal using the Monte Carlo method as introduced in this paper in the section above. Table 5-2 shows the research results, which confirmed the previous assumption that the wide band and white noise signal statistic parameters tend to differ from their equivalent in the time domain, and that the narrow band signal obtained matched the results of signal statistic parameters – also as predicted.

No.	Time series variable			Frequency domain variables full integration			Full integration for frequency domain variables / time domain variables		
	Y	EP	E0	Y	EP	E0	Y	EP	E0
1	0.975	111.14	108.39	0.955	114.54	109.34	0.98	1.03	1.01
2	0.938	105.15	98.61	0.895	111.98	100.20	0.95	1.06	1.02
3	0.912	105.21	95.95	0.863	114.13	98.44	0.95	1.08	1.03
4	0.869	79.63	69.21	0.776	90.84	70.46	0.89	1.14	1.02
5	0.811	100.61	81.63	0.725	117.48	85.17	0.89	1.17	1.04
6	0.751	99.09	74.46	0.656	119.52	78.39	0.87	1.21	1.05
7	0.704	100.57	70.81	0.661	112.58	74.46	0.94	1.12	1.05
8	0.637	102.24	65.15	0.608	113.07	68.74	0.95	1.11	1.06
9	0.591	97.67	57.77	0.548	110.61	60.67	0.93	1.13	1.05
10	0.546	94.00	51.37	0.499	109.36	54.59	0.91	1.16	1.06
11	0.486	94.73	46.08	0.434	114.01	49.44	0.89	1.20	1.07
12	0.440	91.99	40.50	0.383	113.93	43.62	0.87	1.24	1.08
13	0.388	94.83	36.79	0.340	117.75	39.98	0.88	1.24	1.09
14	0.364	83.36	30.35	0.285	113.00	32.22	0.78	1.36	1.06
15	0.282	91.58	25.83	0.230	122.80	28.23	0.82	1.34	1.09
16	0.258	93.09	24.06	0.209	125.00	26.10	0.81	1.34	1.09

Table 5-2 Signal statistics in frequency domain parameters across irregular factor values, full spectral moment integration

The highest differences obtained for the white noise signal (irregular factor below 0.5) were for the number of peaks in the spectrum – a 36% difference. The wide band signal (irregular factor between 0.5 and 0.95) obtained a 21% maximum difference in the number of peaks in a signal. As the damage under random loading is proportional to the number of peaks, it is crucial to modify the empirical value to obtain proper results, which will result in a more accurate damage prediction. The maximum percentage differences in the assessment irregular factor are 22% and are observed for the white noise signal. The lowest exposure on the time and frequency domain signal statistic parameters can be observed for parameter E0 – upward zero crossing below 9% for the considered signal.

Additionally, the research results show that commercial software introduced a modification in the integration of the spectral moment, although the proposed solution provides results that only decrease the differences in the signal parameter in the time and frequency domain by a small number. It is therefore necessary to develop a method of modification of empirical parameters evaluated in the frequency domain.

Research resulted in modification of the integration of the 1<sup>st</sup>, 2<sup>nd</sup>, and 4<sup>th</sup> spectral moments, consisting of reducing the integration range from 1Hz to only 77.5% of the maximum considered frequency (see ref [52]), where the zero spectral moment or the RMS stress is calculated. This approach allows for obtaining the signal statistic parameter in the frequency domain close to the time domain parameters, i.e., up to 5% differences in the number of peaks, up to 4% in the irregular factor value, and up to 3% for the upward zero crossing of the considered signal. The results are shown in Table 5-3. The introduced changes will be used for modified algorithms, which will enable a precise estimation of the vibration damage – based on the signal statistic in the frequency domain equivalent to the signal statistic in the time domain.

No.	Time series variable			Frequency domain variables reduced integration range to (1Hz-77.5% <i>f</i> ) for <i>m</i> <sub>1</sub> , <i>m</i> <sub>2</sub> , <i>m</i> <sub>4</sub>			Reduced integration for frequency domain variables / time domain variables		
	Y	EP	E0	Y	EP	E0	Y	EP	E0
1	0.975	111.14	108.39	0.970	111.71	108.37	0.99	1.01	1.00
2	0.938	105.15	98.61	0.929	105.89	98.42	0.99	1.01	1.00
3	0.912	105.21	95.95	0.906	106.12	96.10	0.99	1.01	1.00
4	0.869	79.63	69.21	0.848	81.49	69.12	0.98	1.02	1.00
5	0.811	100.61	81.63	0.795	102.41	81.45	0.98	1.02	1.00
6	0.751	99.09	74.46	0.733	101.29	74.26	0.98	1.02	1.00
7	0.704	100.57	70.81	0.701	103.50	72.55	1.00	1.03	1.02
8	0.637	102.24	65.15	0.644	104.10	67.01	1.01	1.02	1.03
9	0.591	97.67	57.77	0.587	100.63	59.04	0.99	1.03	1.02
10	0.546	94.00	51.37	0.542	97.78	52.95	0.99	1.04	1.03
11	0.486	94.73	46.08	0.479	99.06	47.45	0.98	1.05	1.03
12	0.440	91.99	40.50	0.434	95.84	41.57	0.99	1.04	1.03
13	0.388	94.83	36.79	0.386	97.94	37.85	1.00	1.03	1.03
14	0.364	83.36	30.35	0.349	86.44	30.19	0.96	1.04	0.99
15	0.282	91.58	25.83	0.278	93.82	26.08	0.99	1.02	1.01
16	0.258	93.09	24.06	0.252	95.44	24.03	0.97	1.03	1.00

Table 5-3 Signal statistics in the frequency domain parameters across irregular factor values, reduced spectral moment *m*<sub>1</sub>, *m*<sub>2</sub>, *m*<sub>4</sub> integration

## 5.2 Narrow Band method modification

Theoretical derivation in section 5.1 using the methodology described in Chapter 4 allows for developing modified code for vibration damage estimation considering the reduced integration of the 1<sup>st</sup>, 2<sup>nd</sup> and 4<sup>th</sup> spectral moments. Reduced numerical integration implies that the signal statistic in the frequency domain, described empirically by Bendat, matches the signal statistic in the time domain – see section 5.1 (the signal in the time domain retrieved using the Monte Carlo method and block size  $2^{20}$ ). Additionally, a proposed new empirical formulation for the Narrow Bendat method replaces the equation Eq. 2.6. The new proposed formulation for calculating the actual number of cycles in each stress range bin is to be replaced by the number of peaks -  $E[P]$  with a variable zero upward crossing –  $E[0]$ , see equation Eq. 5.2. These changes in synergy with reduced integration imply modified damage results of the Narrow Band method (see Table 6) and are consistent with the Dirlik method damage value for the narrow band, wide band, and white noise signals. An additional benefit, in opposition to the Dirlik method, is that the new proposed technique is less empirically complicated, therefore less prone to error in engineering usage.

$$n_{Narrow\_Band} = NB(S) \cdot T \cdot E[0] \quad \text{Eq. 5.2}$$

### **5.3 Vibration damage estimation with modified integration of spectral moment results**

This section introduced the influence of reduced integration introduced in section 5.1 on the damage estimation in the frequency domain using the Dirlik, Lalanne and Narrow Band methods. Figure 5-4 shows Graphical representation of the proposed reduced integration of spectral moments (1<sup>st</sup>, 2<sup>nd</sup>, and 4<sup>th</sup>) for the exemplary PSD response function. Additionally, this section introduces modification of the Narrow Band and Lalanne methods introduced in section 5.2 and section 3.4.2 respectively. The research results presented in this section are an extension of the research results presented in the author's publication [53].

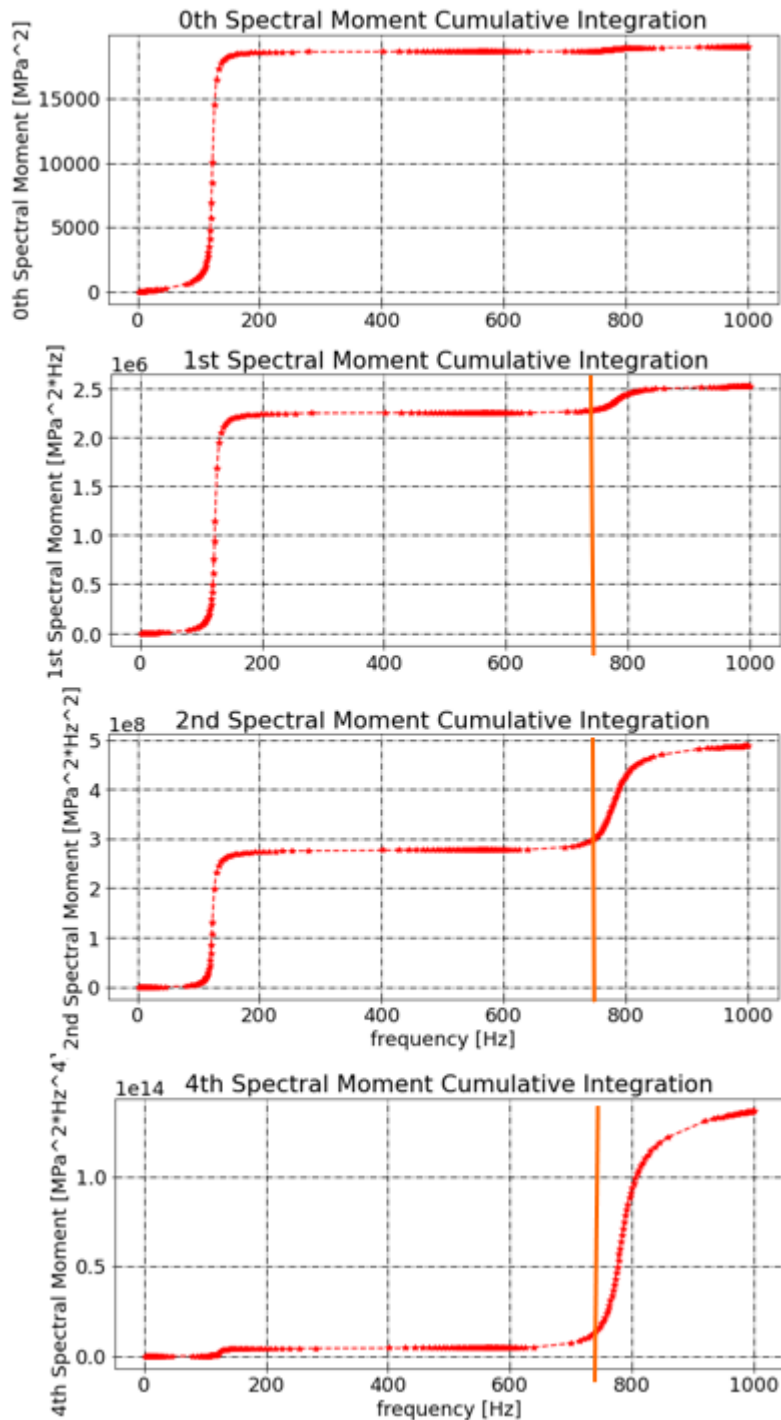


Figure 5-4 Graphical representation of the proposed reduced integration of spectral moments

Table 5-4 shows the summary of damage for the narrow band, wide band, and wide noise signal for full and reduced integration of spectral moments for PSD response clipped at five standard deviations. The obtained results show that reducing integration helps to obtain a great correlation of modified Lalanne and modified Narrow Band methods with the Dirlik method (note that the Dirlik method has the best correlation with the time domain damage estimation using the Monte Carlo method – see Table 5-4). Analogical observations were made for a signal clipped at three standard deviations as per Table 5-5.

Modification of the Narrow Band and Lalanne methods helps to obtain an equivalent method for the Dirlik legacy method by reducing complexity and reducing empirical variables. Using this method for commercial calculation makes it less exposed to error while keeping the same calculation accuracy.

<b>Signal clipped at five standard deviations</b>			
<b>White noise signal</b>			
<b>Damage estimation method</b>	<b>Full integration</b>	<b>Reduced integration (77.5%)</b>	<b>Full integration/Reduced integration</b>
<b>Legacy Narrow Band</b>	0.291	0.198	1.47
<b>Proposed modified Narrow Band (replaced EP with E0)</b>	0.090	0.079	1.14
<b>Dirlik</b>	0.080	0.081	0.98
<b>Legacy Lalanne</b>	3.688E-05	1.713E-05	2.15
<b>Proposed modified Lalanne</b>	0.106	0.085	1.25
<b>Time domain mean damage value</b>	0.074		
<b>Wide band signal</b>			
<b>Damage estimation method</b>	<b>Full integration</b>	<b>Reduced integration (77.5%)</b>	<b>Full integration/Reduced integration</b>
<b>Legacy Narrow Band</b>	0.185	0.129	1.43
<b>Proposed modified Narrow Band (replaced EP with E0)</b>	0.088	0.085	1.03
<b>Dirlik</b>	0.092	0.082	1.13
<b>Legacy Lalanne</b>	1.058E-05	1.552E-06	6.82
<b>Proposed modified Lalanne</b>	0.091	0.086	1.06
<b>Time domain mean damage value</b>	0.079		
<b>Narrow band signal</b>			
<b>Damage estimation method</b>	<b>Full integration</b>	<b>Reduced integration (77.5%)</b>	<b>Full integration/Reduced integration</b>
<b>Legacy Narrow Band</b>	0.088	0.085	1.03
<b>Proposed modified Narrow Band (replaced EP with E0)</b>	0.085	0.087	0.97
<b>Dirlik</b>	0.081	0.081	0.99
<b>Legacy Lalanne</b>	1.480E-11	7.149E-12	2.07
<b>Proposed modified Lalanne</b>	0.085	0.085	1.00
<b>Time domain mean damage value</b>	0.079		

Table 5-4 A summary of damage for the narrow band, wide band, and wide noise signal for full and reduced integration of spectral moments – signal clipped at five standard deviations

<b>Signal clipped at three standard deviations</b>			
<b>White noise signal</b>			
<b>Damage estimation method</b>	<b>Full integration</b>	<b>Reduced integration (77.5%)</b>	<b>Full integration/Reduced integration</b>
Legacy Narrow Band	0.158	0.108	1.47
Proposed modified Narrow Band (replaced EP with E0)	0.049	0.043	1.14
Dirlik	0.043	0.041	1.04
Legacy Lalanne	3.688E-05	1.713E-05	2.15
Proposed modified Lalanne	0.061	0.048	1.28
Time domain mean damage value	0.041		
<b>Wide band signal</b>			
<b>Damage estimation method</b>	<b>Full integration</b>	<b>Reduced integration (77.5%)</b>	<b>Full integration/Reduced integration</b>
Legacy Narrow Band	0.101	0.070	1.43
Proposed modified Narrow Band (replaced EP with E0)	0.048	0.046	1.03
Dirlik	0.047	0.044	1.05
Legacy Lalanne	1.058E-05	1.552E-06	6.82
Proposed modified Lalanne	0.050	0.047	1.07
Time domain mean damage value	0.044		
<b>Narrow band signal</b>			
<b>Damage estimation method</b>	<b>Full integration</b>	<b>Reduced integration (77.5%)</b>	<b>Full integration/Reduced integration</b>
Legacy Narrow Band	0.048	0.048	1.00
Proposed modified Narrow Band (replaced EP with E0)	0.046	0.046	1.00
Dirlik	0.044	0.045	0.99
Legacy Lalanne	1.480E-11	7.149E-12	2.07
Proposed modified Lalanne	0.046	0.046	1.00
Time domain mean damage value	0.043		

Table 5-5 A summary of damage for the narrow band, wide band, and wide noise signal for full and reduced integration of spectral moments – signal clipped at five standard deviations

#### **5.4 Populational research and expansion of the Dirlik method**

Research results made on the pure stochastic loading scenario show that the damage varies, and the variation depends on the block size (N) used in the Inverse Fourier Transformation. To obtain information about statistics of the damage, the research was extended to search large populations consisting of 5000 samples (for which observed stabilization distribution parameters) to obtain the damage distribution. Additionally, the research results presented in this section focused on selecting three different distributions, characterised by the best fitting damage variation description (Gaussian, Exponentiated Weibull and Generalised Extreme Value distributions).

Note that the populational analysis was performed for the critical integration point in the FEM discrete model.

### 5.4.1 White noise random signal analysis

Four different block sizes were introduced in the white noise signal research:  $2^{12}$ ,  $2^{14}$ ,  $2^{16}$  and  $2^{18}$ . The Kolmogorov-Smirnov criterium, which assesses the probability of distribution, was used to fit the distribution. Different distribution types available in the Python library [62] and [63] were used for the test. The best fitted distributions were narrowed to 3, with the highest fitting probability from: the Gaussian, Exponentiated Weibull and Generalised Extreme Value distributions.

It should be noted that the mean damage value is shown in Table 5-6 through Table 5-13 and 0.13% (taken -3 standard deviation in Gaussian distribution as a base) of the population has no lower damage and 9.73% (taken -3 standard deviation in Gaussian distribution as a base) of the population has no higher damage.

In Figure 5-5, Figure 5-7, Figure 5-9 and Figure 5-11 the corresponding damage values were presented for the searched population for the white noise signal for 4 mentioned block sizes for a signal clipped at 3 standard deviations. Per analogy the same results for a signal clipped at 5 standard deviations is presented in Figure 5-13, Figure 5-15, Figure 5-17 and Figure 5-19.

Visualisation of the best fitted distribution for a signal clipped at 3 standard deviations for 4 block sizes is presented in Figure 5-6, Figure 5-8, Figure 5-10 and Figure 5-12. Per analogy results for a signal clipped at 5 standard deviations are presented in Figure 5-14, Figure 5-16, Figure 5-18 and Figure 5-20.

Table 5-6 through Table 5-9 introduce a populational research results summary made for a white noise signal clipped at 3 standard deviations, and Table 5-10 through Table 5-13 show a summary of results for a signal clipped at 5 standard deviations.

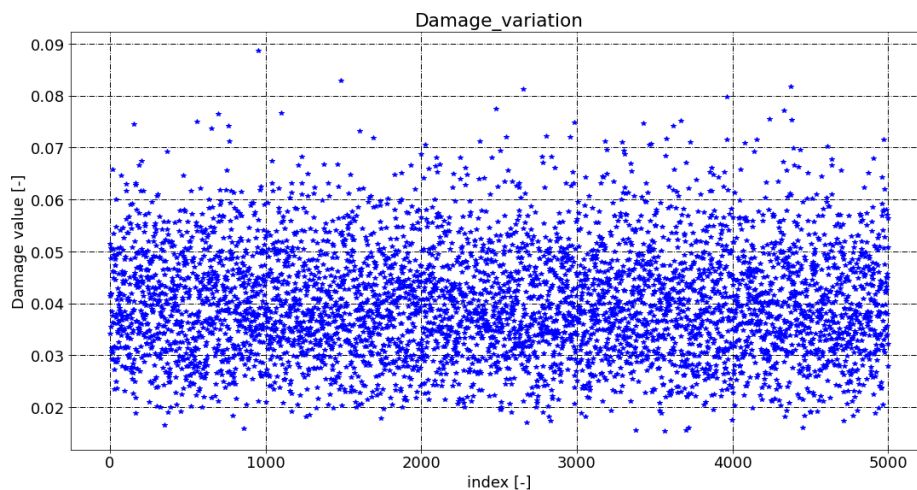


Figure 5-5 Damage values for the searched population for the white noise signal, with a signal clipped at 3 standard deviations, block size  $N=2^{12}$

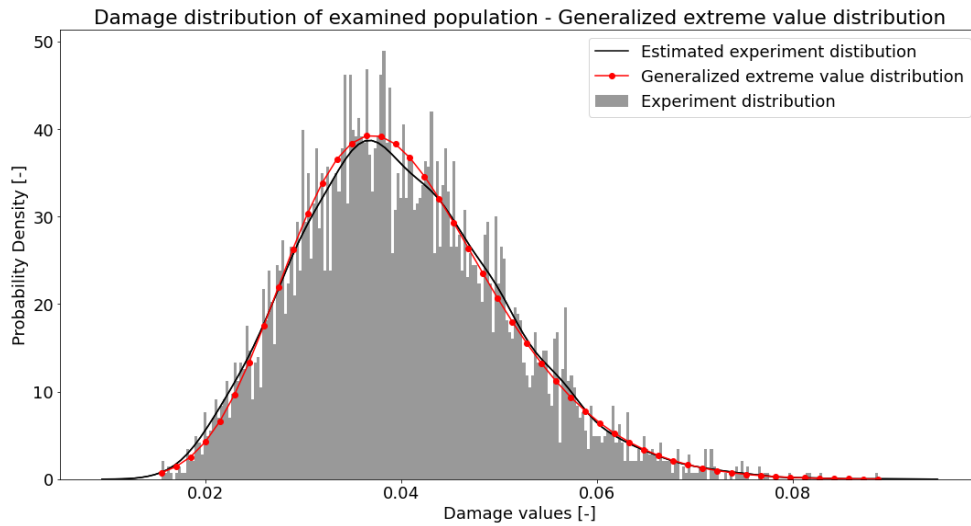


Figure 5-6 The best fitted distribution for the damage values for the searched population for the white noise signal, with a signal clipped at 3 standard deviations, block size  $N=2^{12}$  – Generalised Extreme Value distribution

Distribution type	Probability of the fitted distribution [-]	Mean damage [-]	Standard deviation of damage [-]	0.13% not lower than the quoted value of damage [-]	99.73% not exceeding the quoted value of damage [-]
Normal	0.00000	0.04010	0.01049	0.00866	0.06939
Exponentiated Weibull	0.70540	0.04010	0.01050	0.01692	0.07429
Generalised Extreme Value	0.77733	0.04010	0.01050	0.01543	0.07461

Table 5-6 Statistical parameters for a white noise signal clipped at 3 standard deviations, block size  $N=2^{12}$

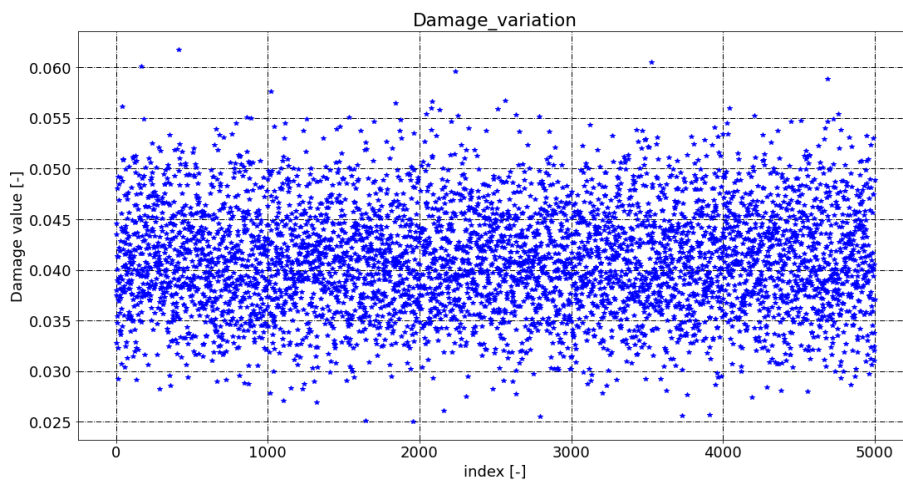


Figure 5-7 Damage values for the searched population for the white noise signal, with a signal clipped at 3 standard deviations, block size  $N=2^{14}$

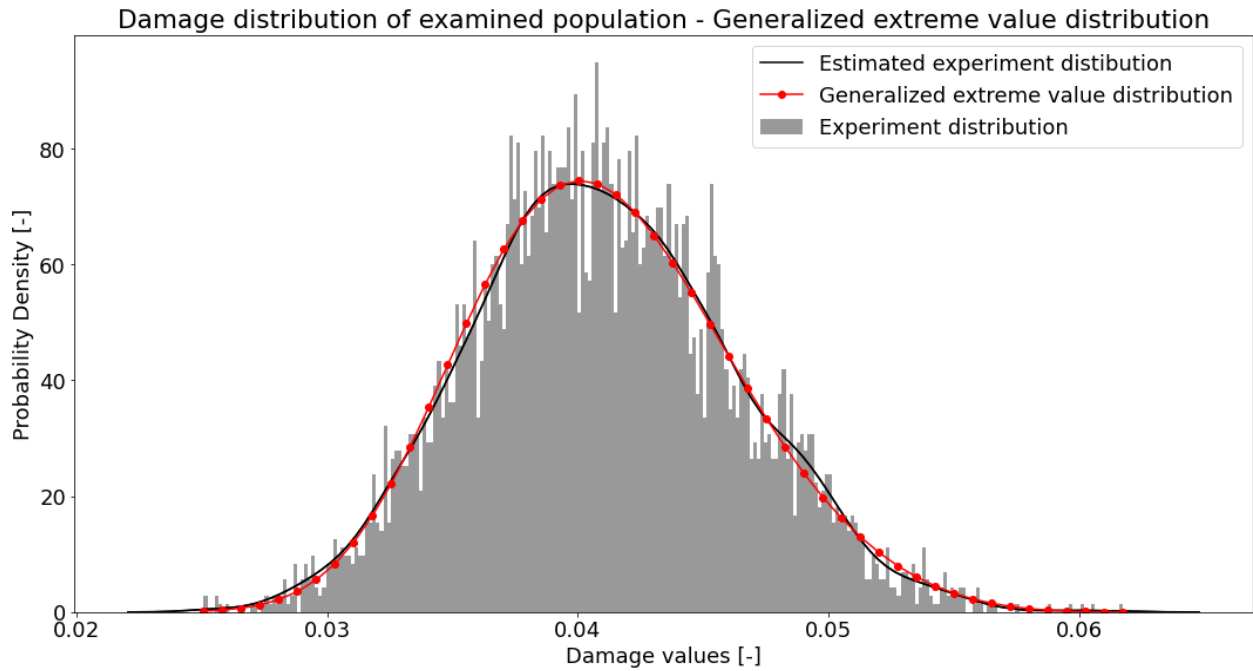


Figure 5-8 The best fitted distribution for damage values for the searched population for the white noise signal, with a signal clipped at 3 standard deviations, block size  $N=2^{14}$  – Generalised Extreme Value distribution

Distribution type	Probability of the fitted distribution [-]	Mean damage [-]	Standard deviation of damage [-]	0.13% not lower than the quoted value of damage [-]	99.73% not exceeding the quoted value of damage [-]
Normal	0.02058	0.04099	0.00524	0.02521	0.05557
Exponentiated Weibull	0.07518	0.04099	0.00532	0.02837	0.05824
Generalised Extreme Value	0.59687	0.04100	0.00529	0.02723	0.05618

Table 5-7 Statistical parameters for a white noise signal clipped at 3 standard deviations  $N=2^{14}$

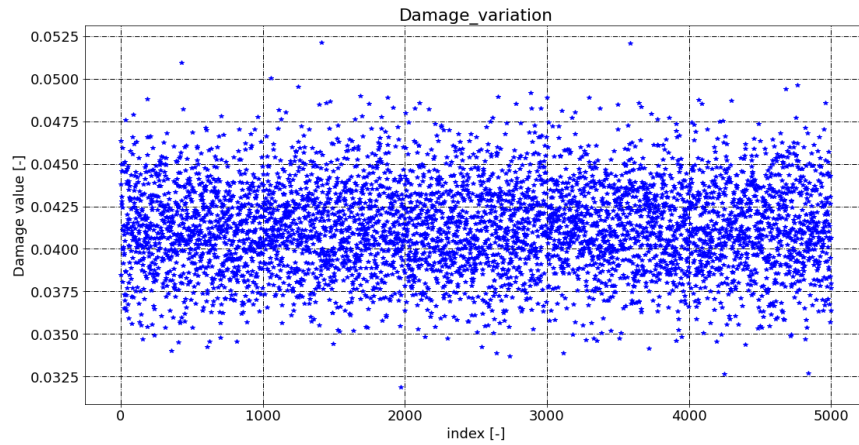


Figure 5-9 Damage values for the searched population for the white noise signal, with a signal clipped at 3 standard deviations, block size  $N=2^{16}$

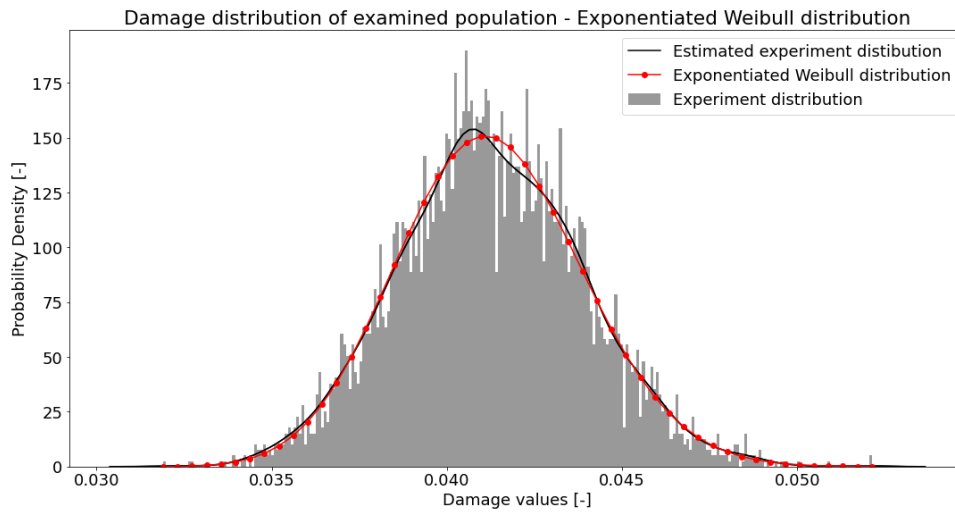


Figure 5-10 The best fitted distribution for damage values for the searched population for the white noise signal, with a signal clipped at 3 standard deviations, block size  $N=2^{16}$  – Exponentiated Weibull distribution

Distribution type	Probability of the fitted distribution [-]	Mean damage [-]	Standard deviation of damage [-]	0.13% not lower than the quoted value of damage [-]	99.73% not exceeding the quoted value of damage [-]
Normal	0.10940	0.04126	0.00263	0.03335	0.04856
Exponentiated Weibull	0.79453	0.04126	0.00263	0.03399	0.04887
Generalised Extreme Value	0.02990	0.04127	0.00268	0.03431	0.04900

Table 5-8 Statistical parameters for the white noise signal clipped at 3 standard deviations  $N=2^{18}$

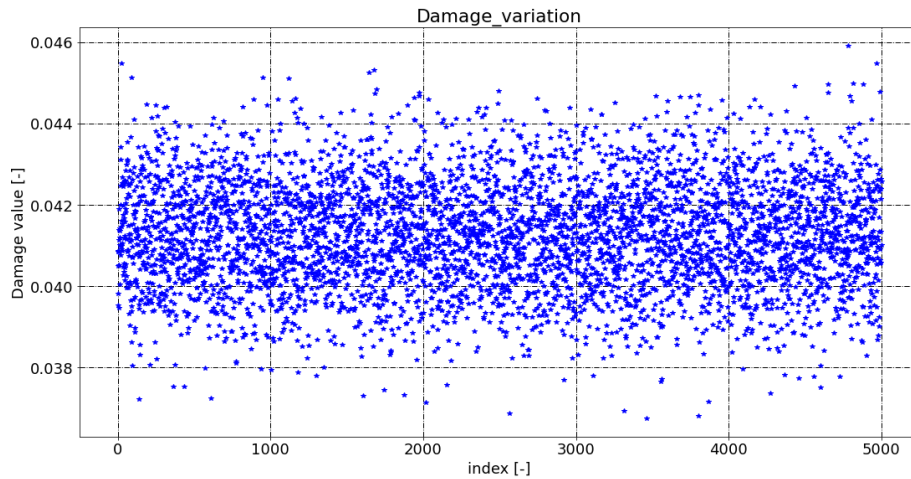


Figure 5-11 Damage values for the searched population for the white noise signal, with a signal clipped at 3 standard deviations, block size  $N=2^{18}$

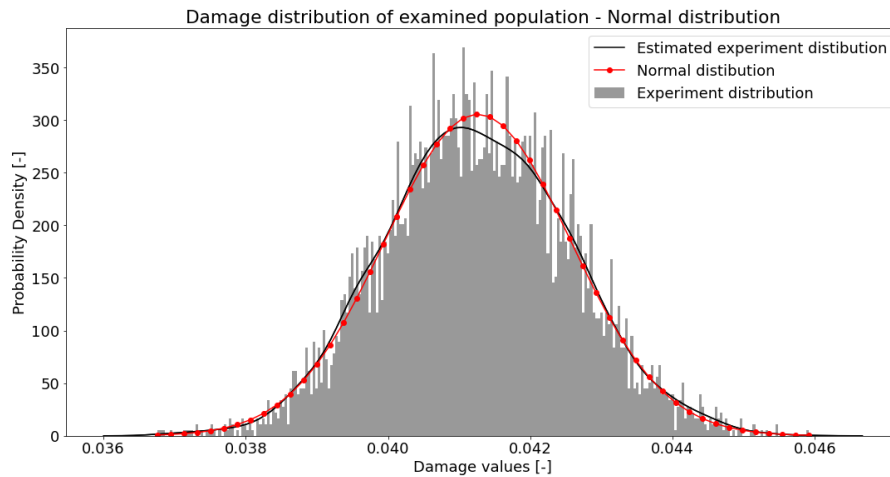


Figure 5-12 The best fitted distribution for damage values for the searched population for the white noise signal, with a signal clipped at 3 standard deviations, block size  $N=2^{18}$  – Normal distribution

Distribution type	Probability of the fitted distribution [-]	Mean damage [-]	Standard deviation of damage [-]	0.13% not lower than the quoted value of damage [-]	99.73% not exceeding the quoted value of damage [-]
Normal	0.67943	0.04126	0.00131	0.03733	0.04490
Exponentiated Weibull	0.00000	0.15614	0.18807	0.03670	N/A
Generalised Extreme Value	0.00000	0.04947	N/A	0.03759	0.31644

Table 5-9 Statistical parameters for a white noise signal clipped at 3 standard deviations  $N=2^{18}$

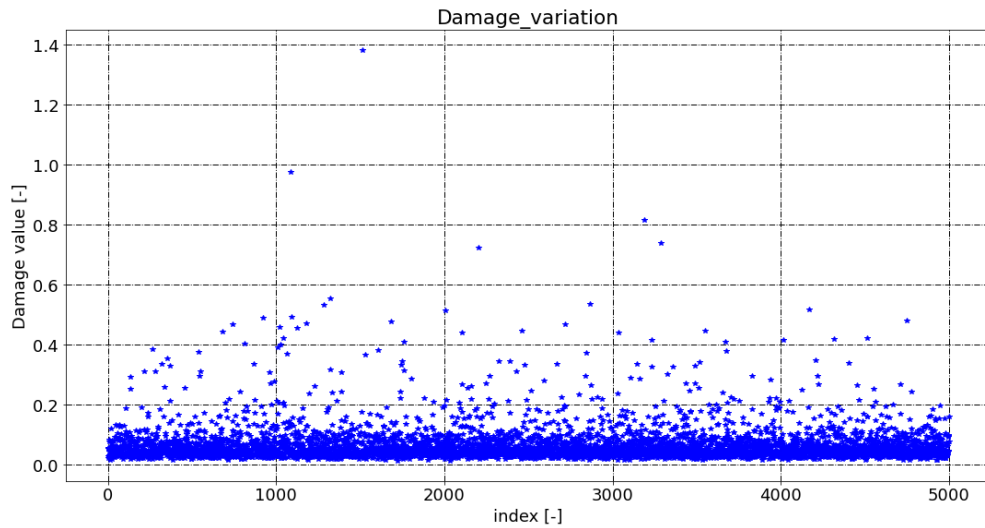


Figure 5-13 Damage values for the searched population for the white noise signal, with a signal clipped at 5 standard deviations, block size  $N=2^{12}$

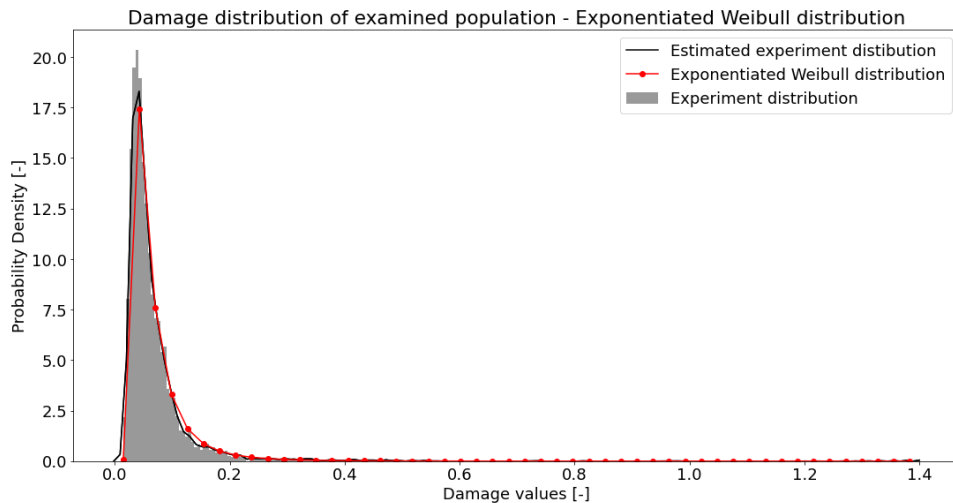


Figure 5-14 The best fitted distribution for damage values for the searched population for the white noise signal, with a signal clipped at 5 standard deviations, block size  $N=2^{12}$  – Exponentiated Weibull distribution

Distribution type	Probability of the fitted distribution [-]	Mean damage [-]	Standard deviation of damage [-]	0.13% not lower than the quoted value of damage [-]	99.73% not exceeding the quoted value of damage [-]
Normal	0.00000	0.06688	0.06161	0.00035	N/A
Exponentiated Weibull	0.38994	0.06596	0.05255	0.01695	0.34883
Generalised Extreme Value	0.00004	0.06728	0.08206	0.01777	2.30564

Table 5-10 Statistical parameters for a white noise signal clipped at 5 standard deviations, block size  $N=2^{12}$

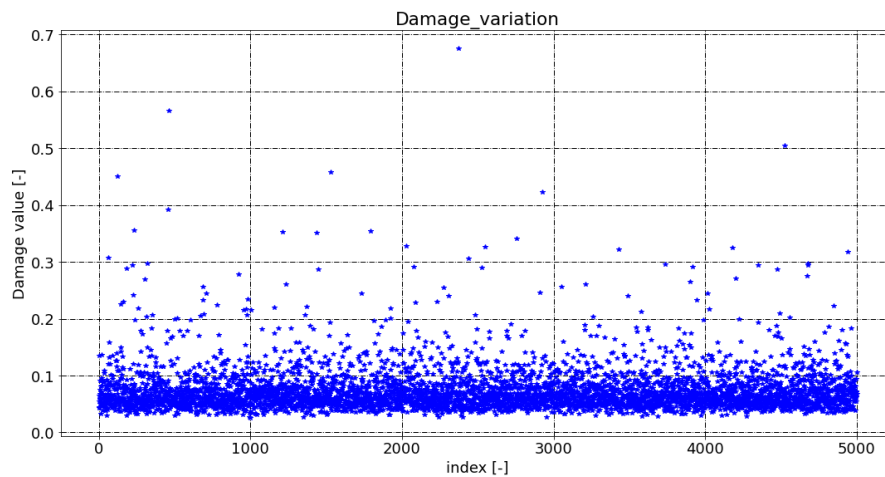


Figure 5-15 Damage values for the searched population for the white noise signal, with a signal clipped at 5 standard deviations, block size  $N=2^{14}$

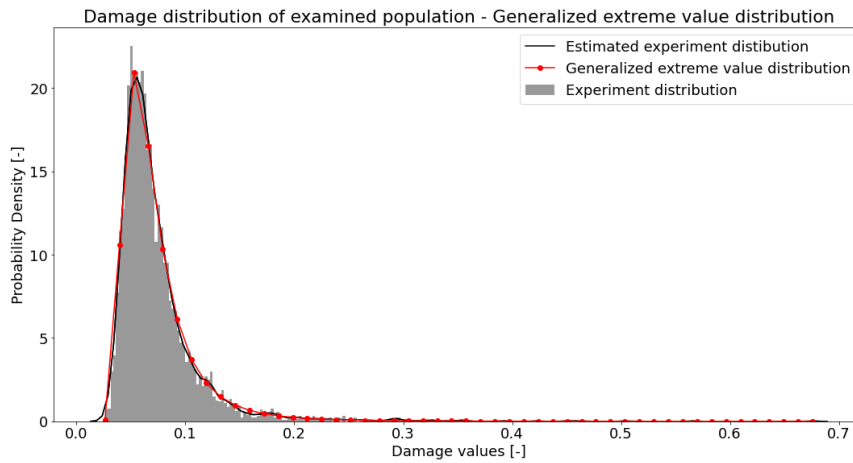


Figure 5-16 The best fitted distribution for damage values for a searched population for the white noise signal, with a signal clipped at 5 standard deviation, block size  $N=2^{14}$  – Generalised Extreme Value distribution

Distribution type	Probability of the fitted distribution [-]	Mean damage [-]	Standard deviation of damage [-]	0.13% not lower than the quoted value of damage [-]	99.73% not exceeding the quoted value of damage [-]
Normal	0.00000	0.07349	0.03908	0.00073	NA
Exponentiated Weibull	0.02981	0.07292	0.03322	0.03013	0.25528
Generalised Extreme Value	0.40506	0.07323	0.03732	0.02966	0.29918

Table 5-11 Statistical parameters for a white noise signal clipped at 5 standard deviations, block size  $N=2^{14}$

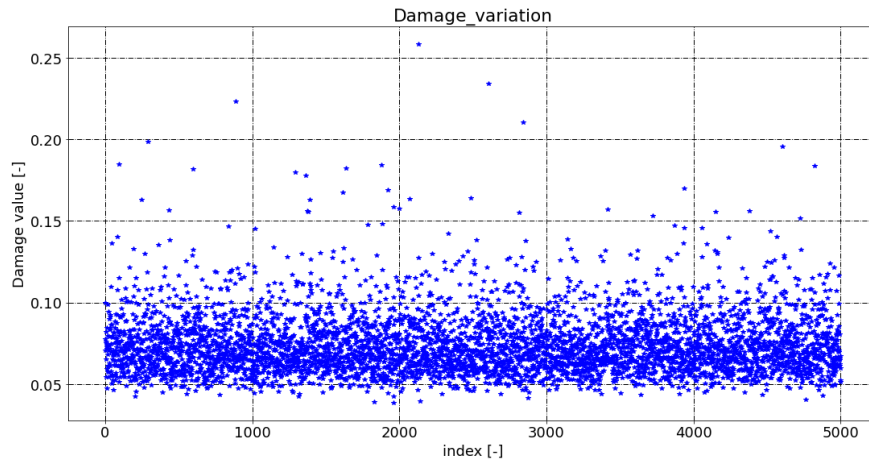


Figure 5-17 Damage values for the searched population for the white noise signal, with a signal clipped at 5 standard deviations, block size  $N=2^{16}$

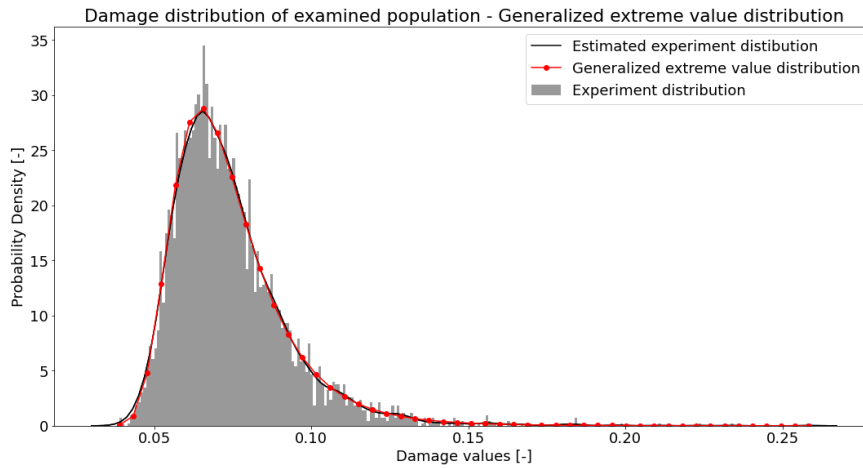


Figure 5-18 The best fitted distribution for damage values for the searched population for the white noise signal, with a signal clipped at 5 standard deviations, block size  $N=2^{16}$  – Generalised Extreme Value distribution

Distribution type	Probability of the fitted distribution [-]	Mean damage [-]	Standard deviation of damage [-]	0.13% not lower than the quoted value of damage [-]	99.73% not exceeding the quoted value of damage [-]
Normal	0.00000	0.07405	0.01859	0.01822	0.12584
Exponentiated Weibull	0.00000	0.11434	0.13545	0.04061	N/A
Generalised Extreme Value	0.97169	0.07405	0.01828	0.04307	0.16068

Table 5-12 Statistical parameters for the white noise signal clipped at 5 standard deviations, block size  $N=2^{16}$

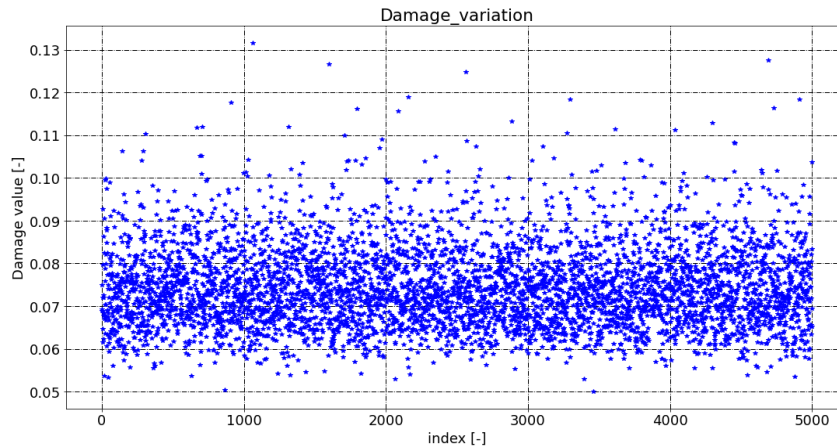


Figure 5-19 Damage values for the searched population for the white noise signal, with a signal clipped at 5 standard deviations, block size  $N=2^{18}$

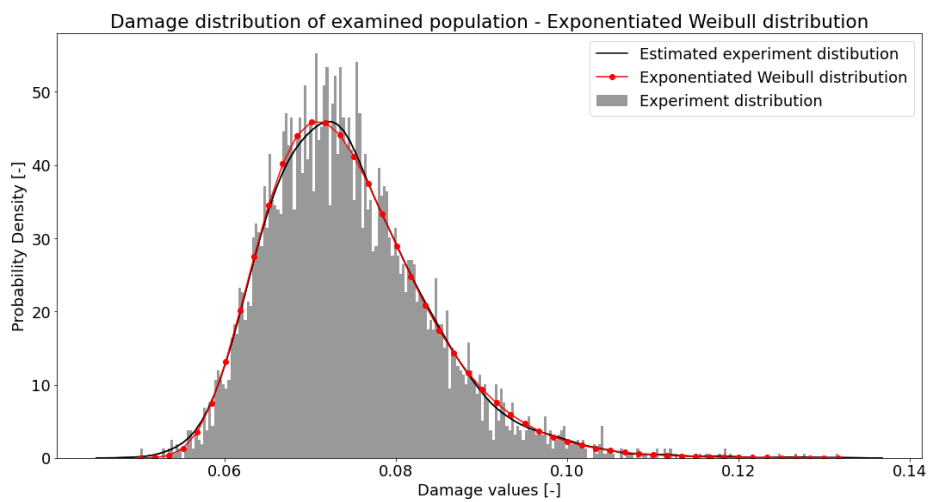


Figure 5-20 The The best fitted distribution for damage values for the searched population for the white noise signal, with a signal clipped at 5 standard deviations, block size  $N=2^{18}$  – Exponentiated Weibull distribution

Distribution type	Probability of the fitted distribution [-]	Mean damage [-]	Standard deviation of damage [-]	0.13% not lower than the quoted value of damage [-]	99.73% not exceeding the quoted value of damage [-]
Normal	0.00000	0.07443	0.00947	0.04591	0.10077
Exponentiated Weibull	0.83862	0.07442	0.00942	0.05495	0.10941
Generalised Extreme Value	0.81481	0.07445	0.00948	0.05448	0.11006

Table 5-13 Statistical parameters for the white noise signal clipped at 5 standard deviations, block size  $N=2^{18}$

### 5.4.2 Wide band random signal analysis

Research for the wide band signal introduced four different block sizes:  $2^{12}$ ,  $2^{14}$ ,  $2^{16}$  and  $2^{18}$ . The Kolmogorov-Smirnov criterium, which assesses the probability of a distribution, was used for fitting the distribution. For the test different distribution types available in Python library [62] and [63] were used. The best fitted distributions were narrowed down to 3 with the highest probability of fitting: Gaussian, Exponentiated Weibull and Generalised Extreme Value distributions.

It should be noted that the mean value of damage is presented in Table 5-14 through Table 5-21, and for which 0.13% (taken -3 standard deviation in Gaussian distribution as a base) of the population have no lower damage and 9.73% (taken -3 standard deviation in Gaussian distribution as a base) of the population have no higher damage.

In Figure 5-21, Figure 5-23, Figure 5-25 and Figure 5-27 corresponding damage values were presented for the searched population for the white noise signal for the 4 mentioned block sizes for a signal clipped at 3 standard deviations. Per analogy the same results for a signal clipped at 5 standard deviations is presented in Figure 5-29, Figure 5-31, Figure 5-33 and Figure 5-35.

The best fitted distributions visualisation for a signal clipped at 3 standard deviations for 4 block sizes is presented in Figure 5-22, Figure 5-24, Figure 5-26 and Figure 5-28. Per analogy results for a signal clipped at 5 standard deviations is presented in Figure 5-30, Figure 5-32, Figure 5-34 and Figure 5-36.

Table 5-14 through Table 5-17 introduce a populational research results summary made for a white noise signal clipped at 3 standard deviation, and Table 5-18 through Table 5-21 a summary of results for a signal clipped at 5 standard deviations.

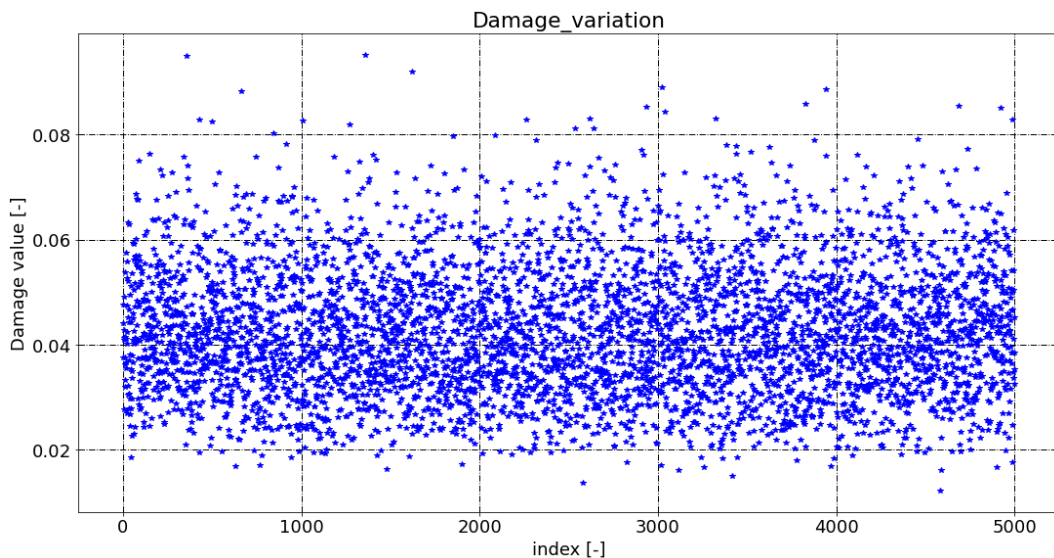


Figure 5-21 Damage values for the searched population for the wide band signal, with a signal clipped at 3 standard deviations, block size  $N=2^{12}$

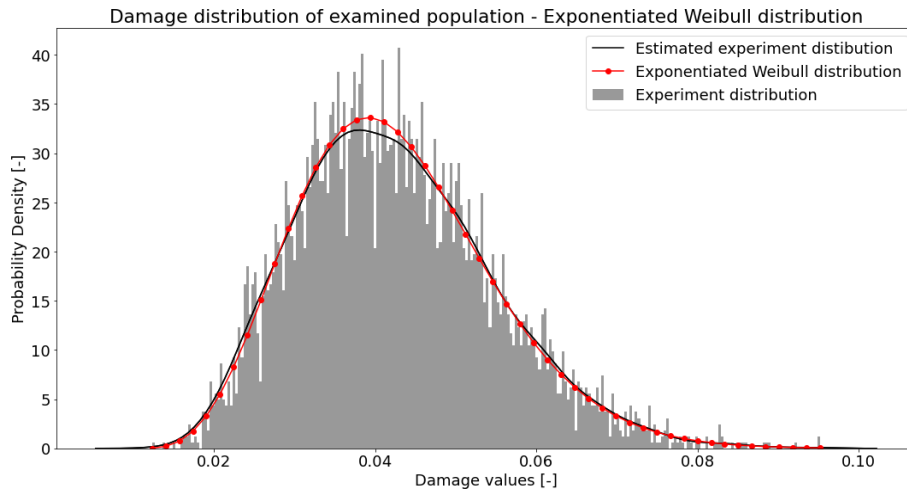


Figure 5-22 The best fitted distribution for damage values for the searched population for the wide band signal, with a signal clipped at 3 standard deviations, block size  $N=2^{12}$  – Exponentiated Weibull distribution

Distribution type	Probability of the fitted distribution [-]	Mean damage [-]	Standard deviation of damage [-]	0.13% not lower than the quoted value of damage [-]	99.73% not exceeding the quoted value of damage [-]
Normal	0.00000	0.04252	0.01208	0.00672	0.07645
Exponentiated Weibull	0.98142	0.04252	0.01208	0.01615	0.08288
Generalised Extreme Value	0.55531	0.04250	0.01207	0.01467	0.08307

Table 5-14 Statistical parameters for a wide band signal clipped at 3 standard deviations, block size  $N=2^{12}$

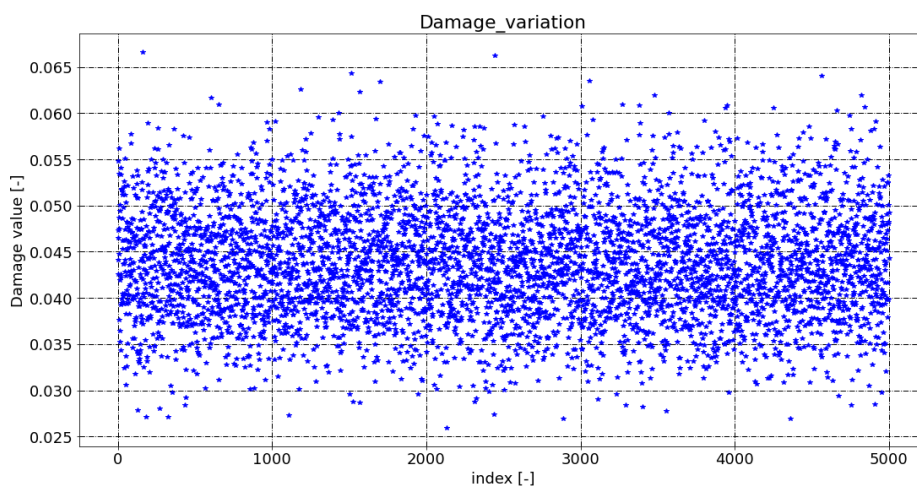


Figure 5-23 Damage values for the searched population for the wide band signal, with a signal clipped at 3 standard deviations, block size  $N=2^{14}$

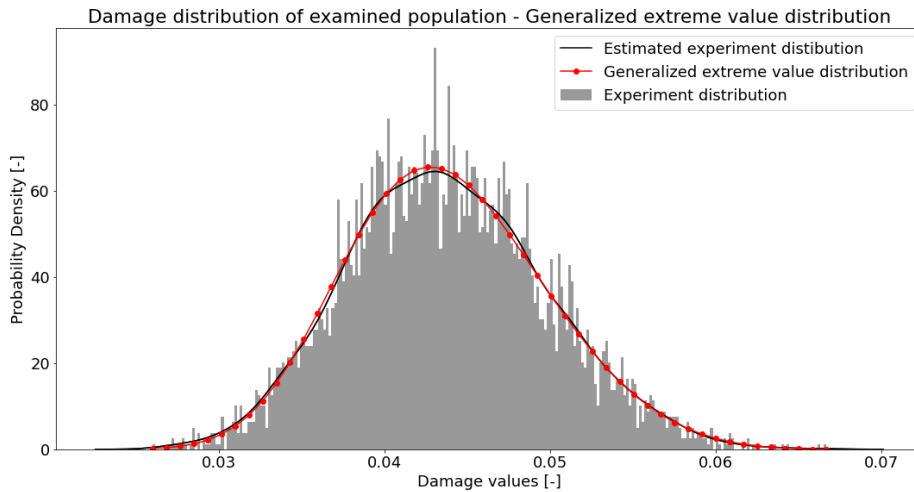


Figure 5-24 The best fitted distribution for damage values for the searched population for the wide band signal, with a signal clipped at 3 standard deviations, block size  $N=2^{14}$  – Generalised Extreme Value distribution

Distribution type	Probability of the fitted distribution [-]	Mean damage [-]	Standard deviation of damage [-]	0.13% not lower than the quoted value of damage [-]	99.73% not exceeding the quoted value of damage [-]
Normal	0.01451	0.04376	0.00598	0.02577	0.06039
Exponentiated Weibull	0.00000	0.04393	0.00710	0.03018	0.07194
Generalised Extreme Value	0.96553	0.04377	0.00601	0.02814	0.06105

Table 5-15 Statistical parameters for wide band signal clipped at 3 standard deviation  $N=2^{14}$

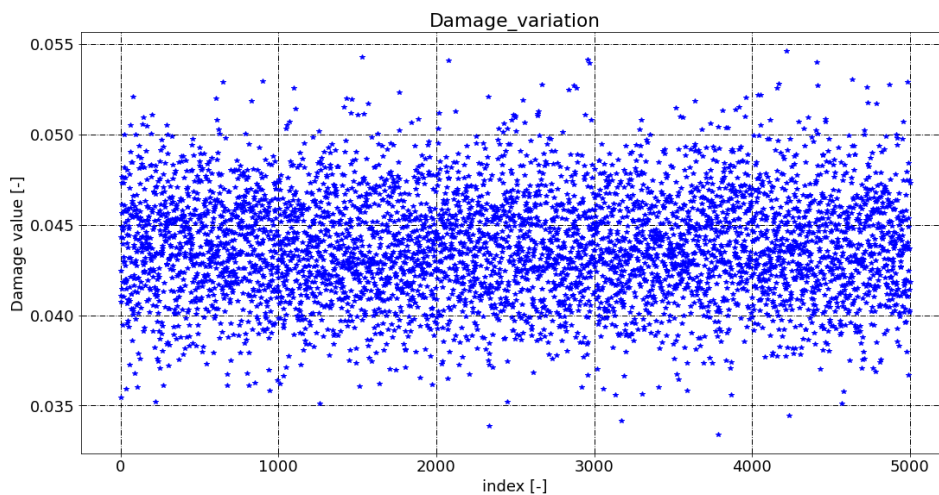


Figure 5-25 Damage values for the searched population for the wide band signal, with a signal clipped at 3 standard deviation, block size  $N=2^{16}$

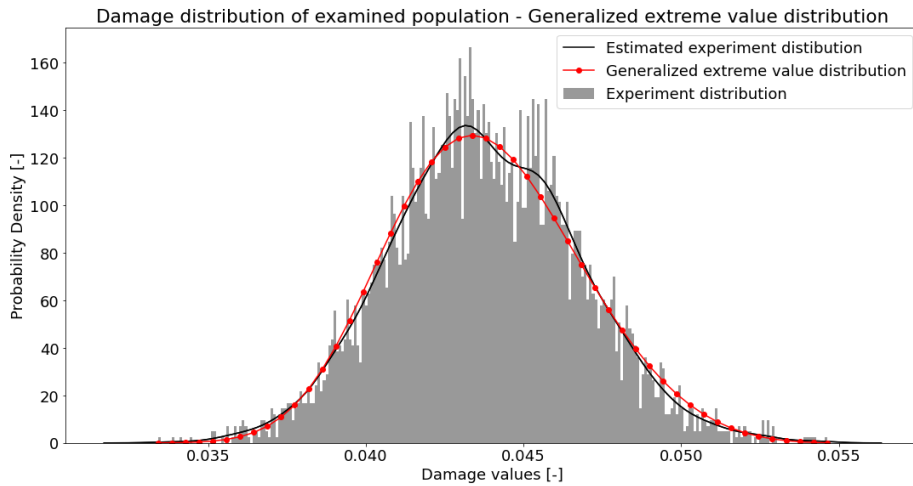


Figure 5-26 The best fitted distribution for damage values for the searched population for the wide band signal, with a signal clipped at 3 standard deviations, block size  $N=2^{16}$  – Generalised Extreme Value distribution

Distribution type	Probability of the fitted distribution [-]	Mean damage [-]	Standard deviation of damage [-]	0.13% not lower than the quoted value of damage [-]	99.73% not exceeding the quoted value of damage [-]
Normal	0.07936	0.04379	0.00298	0.03482	0.05208
Exponentiated Weibull	0.00068	0.04381	0.00301	0.03533	0.05154
Generalised Extreme Value	0.31657	0.04380	0.00302	0.03578	0.05225

Table 5-16 Statistical parameters for a wide band signal clipped at 3 standard deviations  $N=2^{16}$

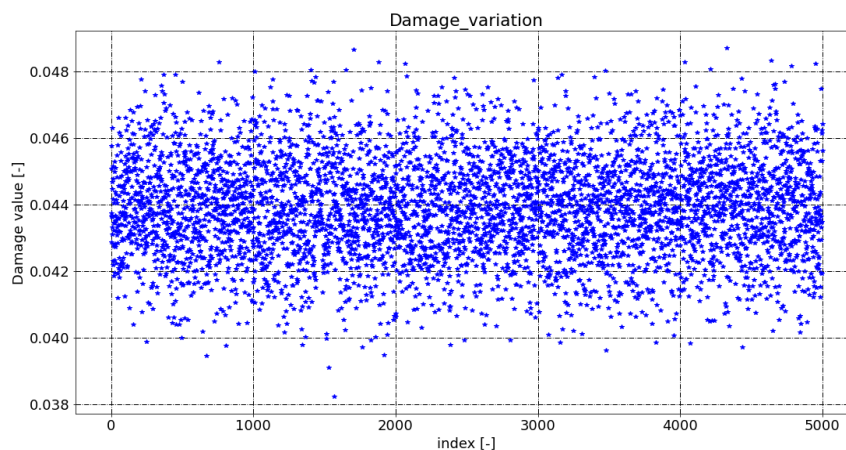


Figure 5-27 Damage values for the searched population for the wide band signal, with a signal clipped at 3 standard deviations, block size  $N=2^{18}$

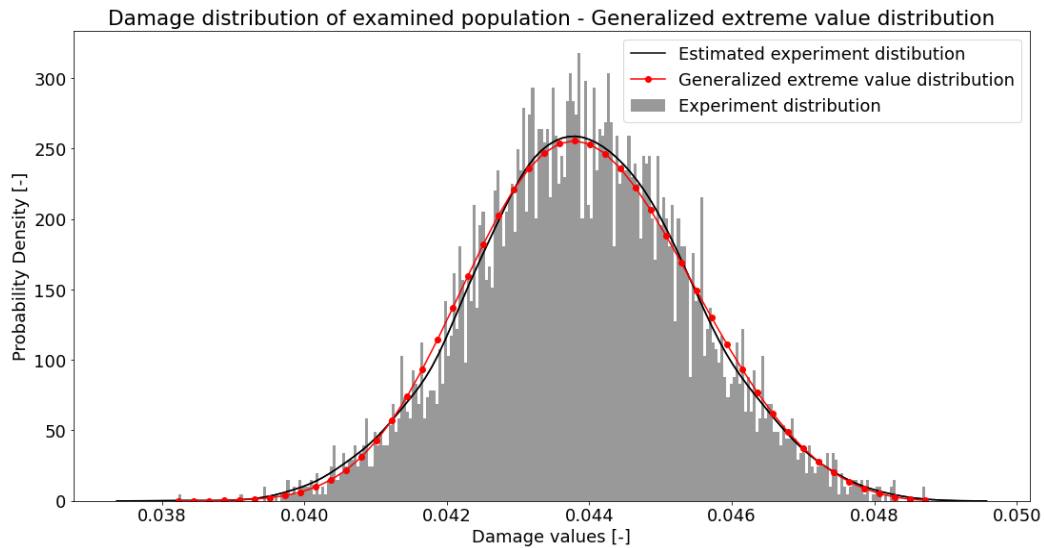


Figure 5-28 The best fitted distribution for damage values for the searched population for the wide band signal, with a signal clipped at 3 standard deviations, block size  $N=2^{18}$  – Generalised Extreme Value distribution

Distribution type	Probability of the fitted distribution [-]	Mean damage [-]	Standard deviation of damage [-]	0.13% not lower than the quoted value of damage [-]	99.73% not exceeding the quoted value of damage [-]
Normal	0.88312	0.04390	0.00150	0.03938	0.04808
Exponentiated Weibull	0.00000	0.04353	0.00199	0.03871	0.04876
Generalised Extreme Value	0.51925	0.04390	0.00151	0.03970	0.04788

Table 5-17 Statistical parameters for a wide band signal clipped at 3 standard deviations  $N=2^{18}$

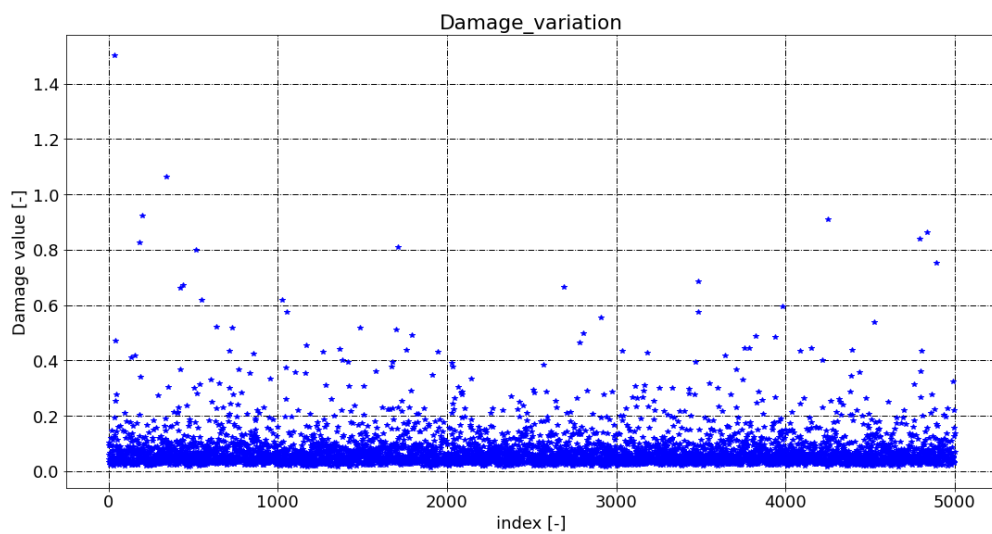


Figure 5-29 Damage values for the searched population for the wide band signal, with a signal clipped at 5 standard deviations, block size  $N=2^{12}$

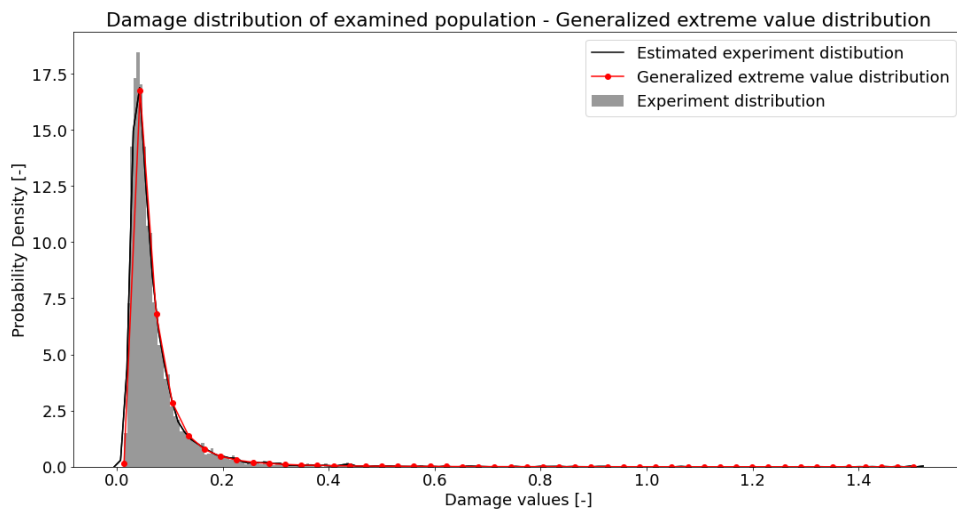


Figure 5-30 The best fitted distribution for damage values for the searched population for the wide band signal, with a signal clipped at 5 standard deviations, block size  $N=2^{12}$  – Generalised Extreme Value distribution

Distribution type	Probability of the fitted distribution [-]	Mean damage [-]	Standard deviation of damage [-]	0.13% not lower than the quoted value of damage [-]	99.73% not exceeding the quoted value of damage [-]
Normal	0.00000	0.07370	0.07526	0.00040	N/A
Exponentiated Weibull	0.14008	0.07230	0.06554	0.01693	0.50903
Generalised Extreme Value	0.94652	0.07474	0.13719	0.01630	0.70982

Table 5-18 Statistical parameters for a wide band signal clipped at 5 standard deviations, block size  $N=2^{12}$

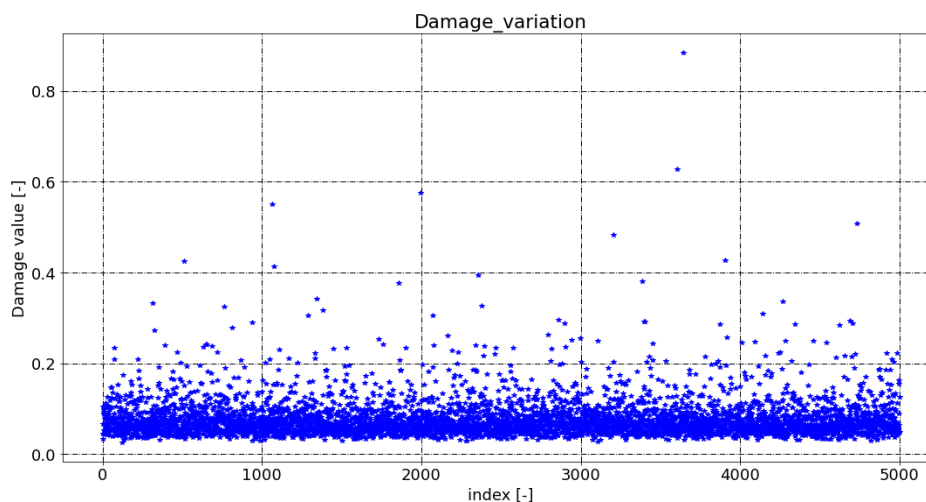


Figure 5-31 Damage values for the searched population for the wide band signal, with a signal clipped at 5 standard deviations, block size  $N=2^{14}$

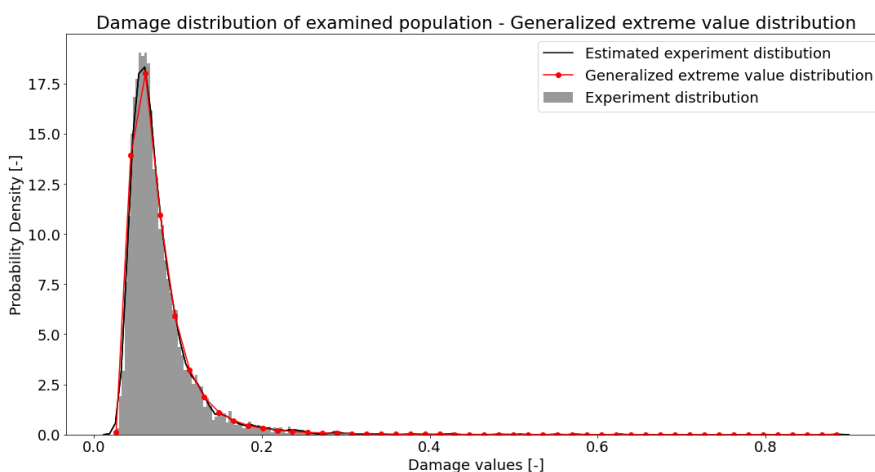


Figure 5-32 The best fitted distribution for damage values for the searched population for the wide band signal, with a signal clipped at 5 standard deviations, block size  $N=2^{14}$  – Generalised Extreme Value distribution

Distribution type	Probability of the fitted distribution [-]	Mean damage [-]	Standard deviation of damage [-]	0.13% not lower than the quoted value of damage [-]	99.73% not exceeding the quoted value of damage [-]
Normal	0.00000	0.07787	0.04330	0.00070	N/A
Exponentiated Weibull	0.30890	0.07729	0.03824	0.03053	0.29481
Generalised Extreme Value	0.91468	0.07779	0.04322	0.02998	0.34413

Table 5-19 Statistical parameters for a wide band signal clipped at 5 standard deviations, block size  $N=2^{14}$

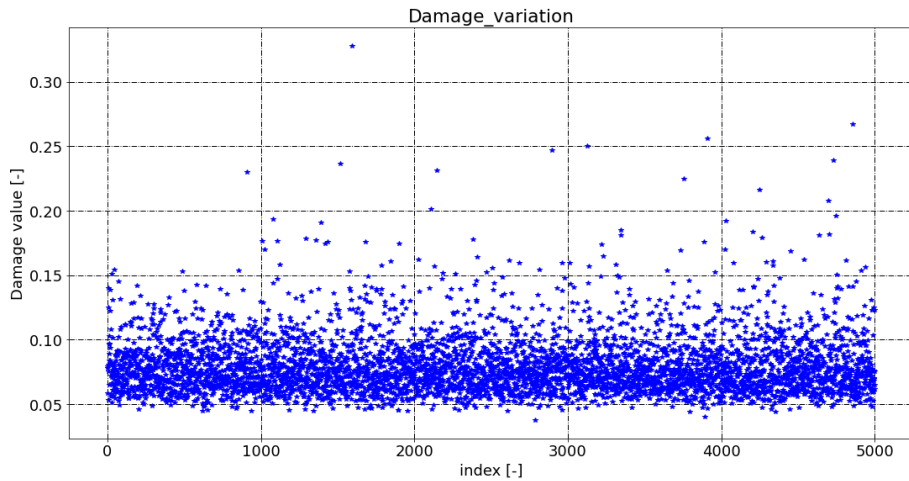


Figure 5-33 Damage values for the searched population for the wide band signal, with a signal clipped at 5 standard deviations, block size  $N=2^{16}$

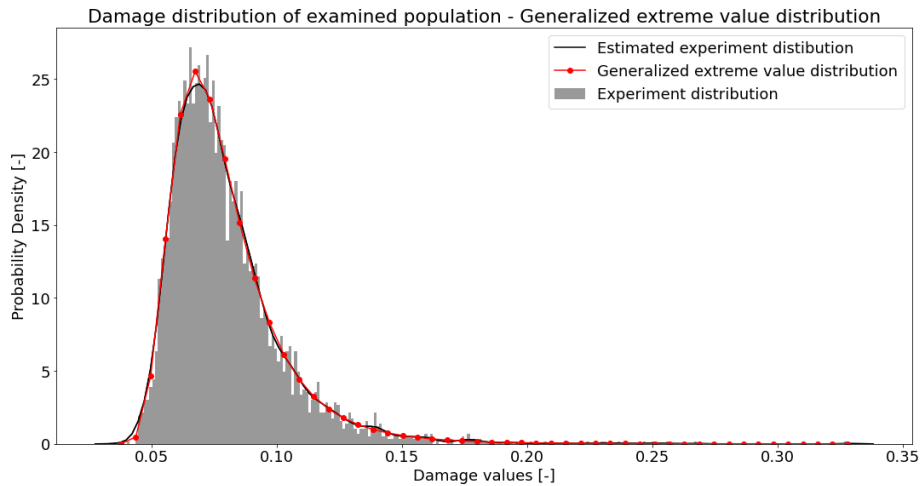


Figure 5-34 The best fitted distribution for damage values for the searched population for the wide band signal, with a signal clipped at 5 standard deviations, block size  $N=2^{16}$  – Generalised extreme distribution

Distribution type	Probability of the fitted distribution [-]	Mean damage [-]	Standard deviation of damage [-]	0.13% not lower than the quoted value of damage [-]	99.73% not exceeding the quoted value of damage [-]
Normal	0.00000	0.07959	0.02271	0.01232	0.14343
Exponentiated Weibull	0.75042	0.07949	0.02194	0.04491	0.18512
Generalised Extreme Value	0.99548	0.07958	0.02251	0.04467	0.19482

Table 5-20 Statistical parameters for a wide band signal clipped at 5 standard deviations, block size  $N=2^{16}$

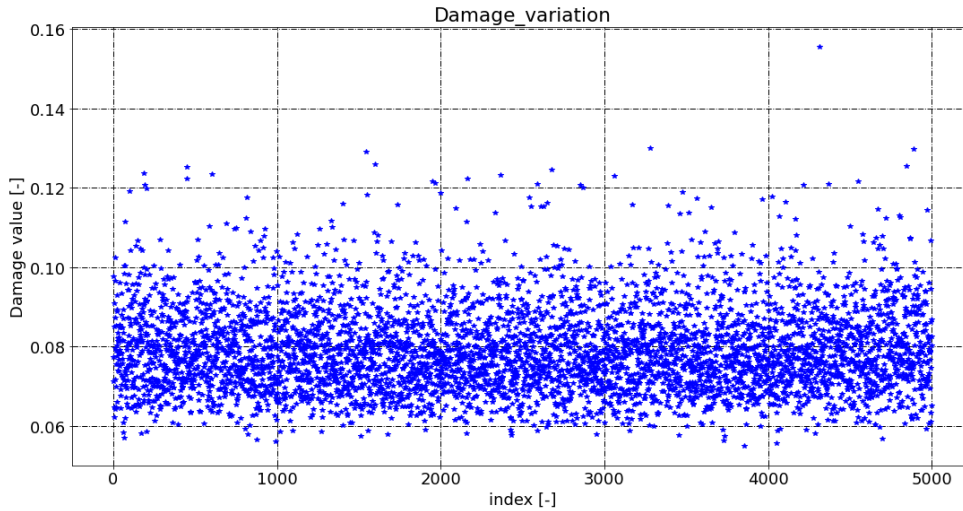


Figure 5-35 Damage values for the searched population for the wide band signal, with a signal clipped at 5 standard deviations, block size  $N=2^{18}$

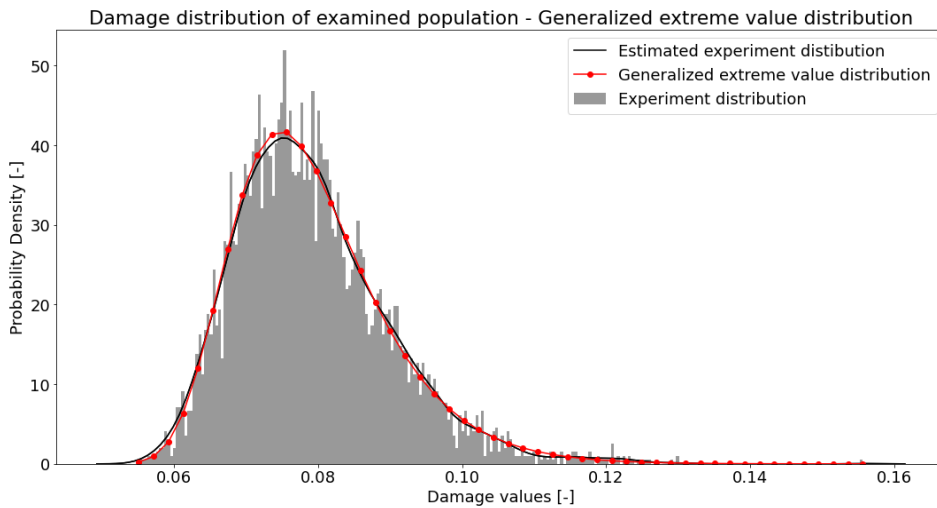


Figure 5-36 The best fitted distribution for damage values for the searched population for the wide band signal, with a signal clipped at 5 standard deviations, block size  $N=2^{18}$  – Generalised Extreme Value distribution

Distribution type	Probability of the fitted distribution [-]	Mean damage [-]	Standard deviation of damage [-]	0.13% not lower than the quoted value of damage [-]	99.73% not exceeding the quoted value of damage [-]
Normal	0.00000	0.07919	0.01075	0.04683	0.10909
Exponentiated Weibull	0.00000	0.48911	0.79548	0.05511	N/A
Generalised Extreme Value	0.97556	0.07920	0.01075	0.05712	0.12081

Table 5-21 Statistical parameters for a wide band signal clipped at 5 standard deviations, block size  $N=2^{18}$

### 5.4.3 Narrow Band random signal analysis

Research for the narrow band signal introduced four different block sizes:  $2^{12}$ ,  $2^{14}$ ,  $2^{16}$  and  $2^{18}$ . The Kolmogorov-Smirnov criterium, which assesses the probability of a distribution, was used for fitting the distribution. For testing different distribution types available in Python library [62] and [63] were used. The best fitted distributions were narrowed down to 3 with the highest probability of fitting: Gaussian, Exponentiated Weibull and Generalised Extreme Value distributions.

It is worth noting that the mean value of damage is presented in Table 5-22 through Table 5-29 and 0.13% (taken -3 standard deviation in Gaussian distribution as a base) of the population have no lower damage and 9.73% (taken -3 standard deviation in Gaussian distribution as a base) of the population have no higher damage.

In Figure 5-37, Figure 5-39, Figure 5-41 and Figure 5-43 corresponding damage values are presented for the searched population for the white noise signal for the 4 mentioned block sizes for a signal clipped at 3 standard deviations. Per analogy the same results for a signal clipped at 5 standard deviations are presented in Figure 5-45, Figure 5-47, Figure 5-49 and Figure 5-51.

The best fitted distributions visualisation for a signal clipped at 3 standard deviations for the 4 block sizes are presented in Figure 5-38, Figure 5-40, Figure 5-42 and Figure 5-44. Per analogy results for a signal clipped at 5 standard deviations are presented in Figure 5-46, Figure 5-48, Figure 5-50 and Figure 5-52.

Table 5-14 through Table 5-25 introduce a populational research results summary made for a white noise signal clipped at 3 standard deviations, and Table 5-26 through Table 5-29 a summary of results for a signal clipped at 5 standard deviations.

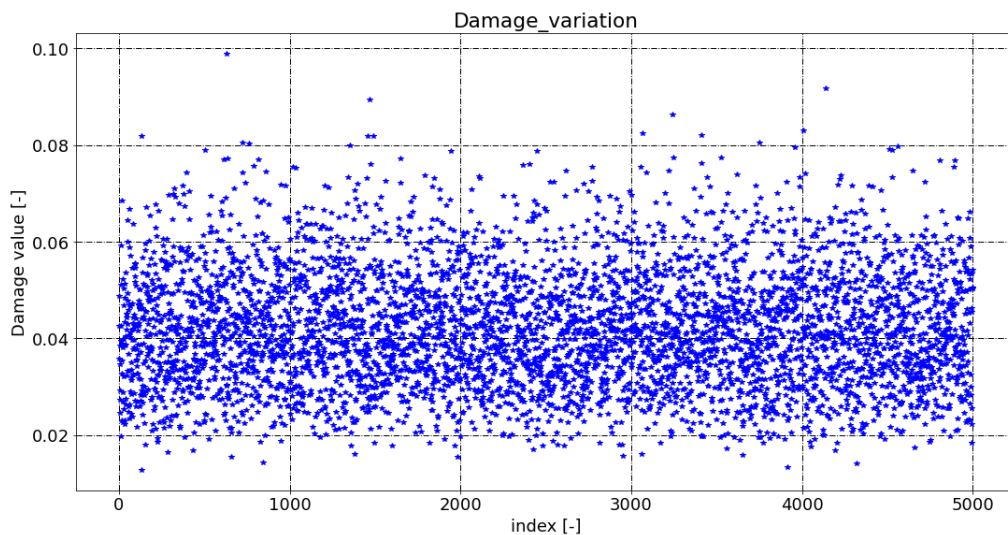


Figure 5-37 Damage values for the searched population for the narrow band signal, with a signal clipped at 3 standard deviations, block size  $N=2^{12}$

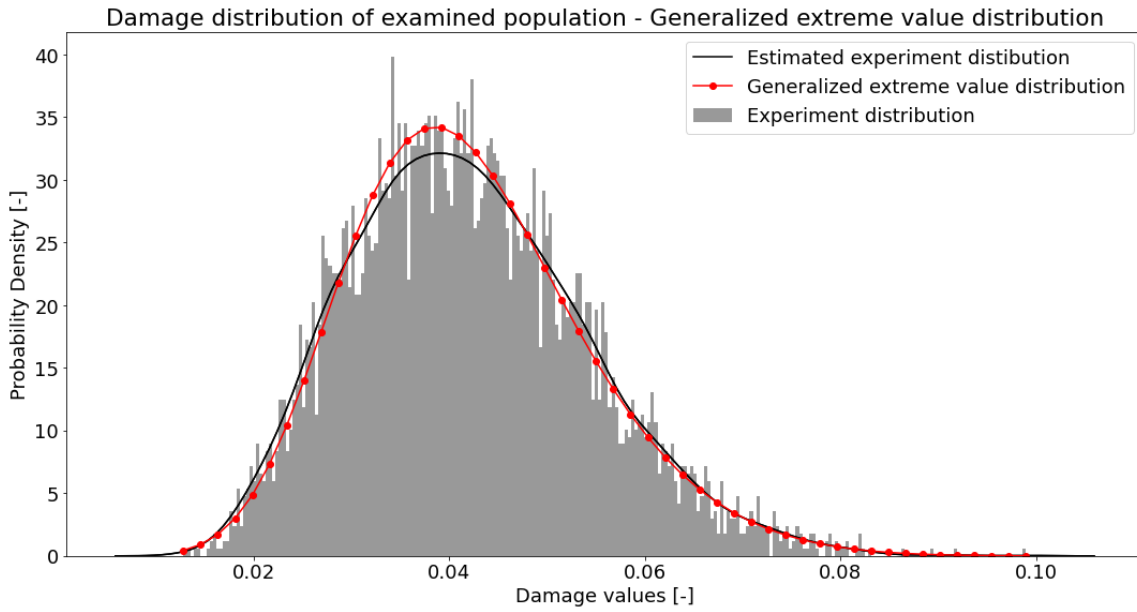


Figure 5-38 The best fitted distribution for damage values for the searched population for the narrow band signal, with a signal clipped at 3 standard deviations, block size  $N=2^{12}$  – Generalised Extreme Value distribution

Distribution type	Probability of the fitted distribution [-]	Mean damage [-]	Standard deviation of damage [-]	0.13% not lower than the quoted value of damage [-]	99.73% not exceeding the quoted value of damage [-]
Normal	0.00001	0.04197	0.01204	0.00636	0.07583
Exponentiated Weibull	0.00000	0.35253	0.54951	0.01281	N/A
Generalised Extreme Value	0.41095	0.04195	0.01202	0.01362	0.08131

Table 5-22 Statistical parameters for a narrow band signal clipped at 3 standard deviations, block size  $N=2^{12}$

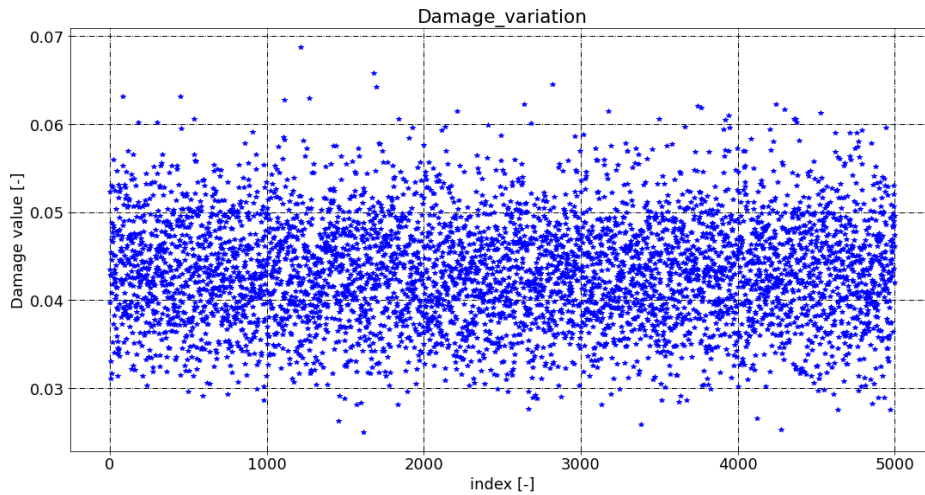


Figure 5-39 Damage values for the searched population for the narrow band signal, with a signal clipped at 3 standard deviations, block size  $N=2^{14}$

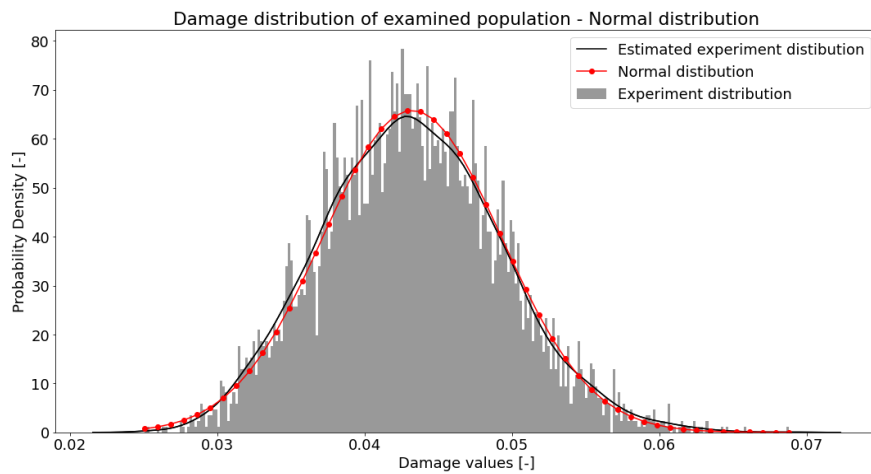


Figure 5-40 The best fitted distribution for damage values for the searched population for the narrow band signal, with a signal clipped at 3 standard deviations, block size  $N=2^{14}$  – Normal distribution

Distribution type	Probability of the fitted distribution [-]	Mean damage [-]	Standard deviation of damage [-]	0.13% not lower than the quoted value of damage [-]	99.73% not exceeding the quoted value of damage [-]
Normal	0.48454	0.04320	0.00606	0.02496	0.06006
Exponentiated Weibull	0.00000	0.04398	0.00680	0.02598	0.05774
Generalised Extreme Value	0.09376	0.04322	0.00614	0.02746	0.06117

Table 5-23 Statistical parameters for a narrow band signal clipped at 3 standard deviations  $N=2^{14}$

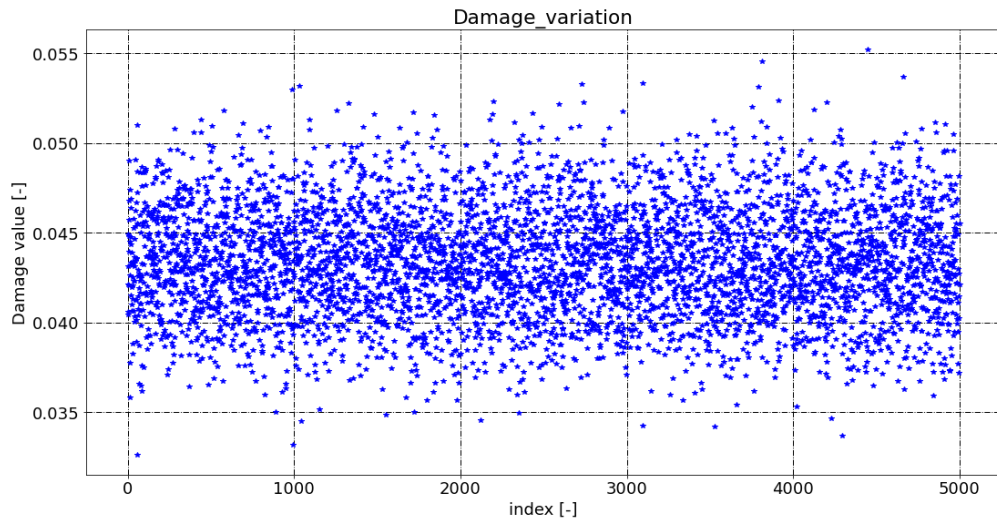


Figure 5-41 Damage values for the searched population for the narrow band signal, with a signal clipped at 3 standard deviations, block size  $N=2^{16}$

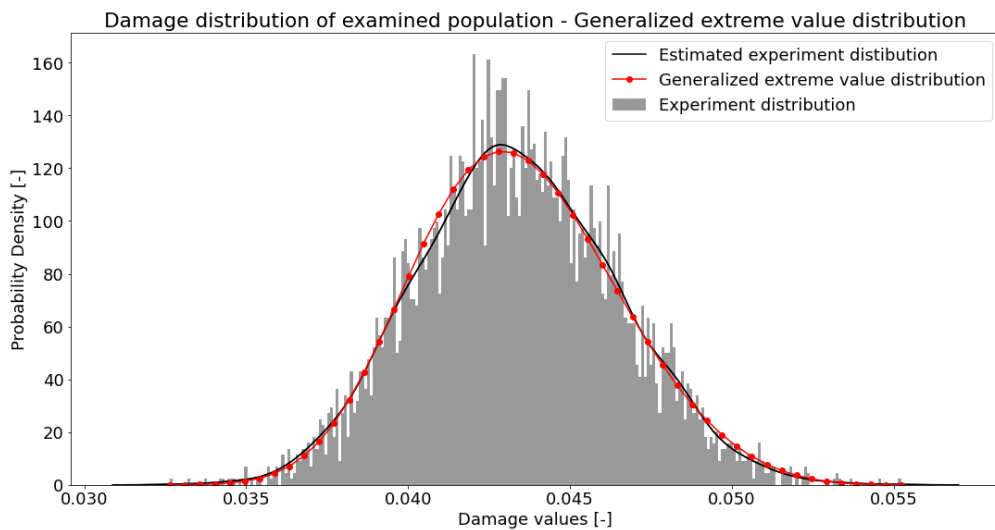


Figure 5-42 The best fitted distribution for damage values for the searched population for the narrow band signal, with a signal clipped at 3 standard deviations, block size  $N=2^{16}$  – Generalised Extreme Value distribution

Distribution type	Probability of the fitted distribution [-]	Mean damage [-]	Standard deviation of damage [-]	0.13% not lower than the quoted value of damage [-]	99.73% not exceeding the quoted value of damage [-]
Normal	0.09135	0.04338	0.00306	0.03416	0.05190
Exponentiated Weibull	0.00000	0.39407	0.74436	0.03261	N/A
Generalised Extreme Value	0.34343	0.04339	0.00310	0.03520	0.05210

Table 5-24 Statistical parameters for a narrow band signal clipped at 3 standard deviations  $N=2^{16}$

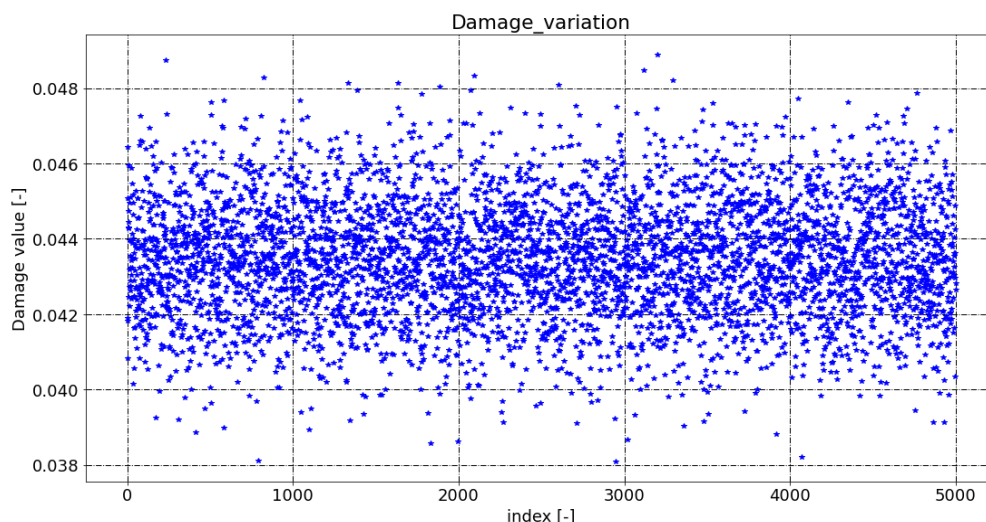


Figure 5-43 Damage values for the searched population for the narrow band signal, with a signal clipped at 3 standard deviations, block size  $N=2^{18}$

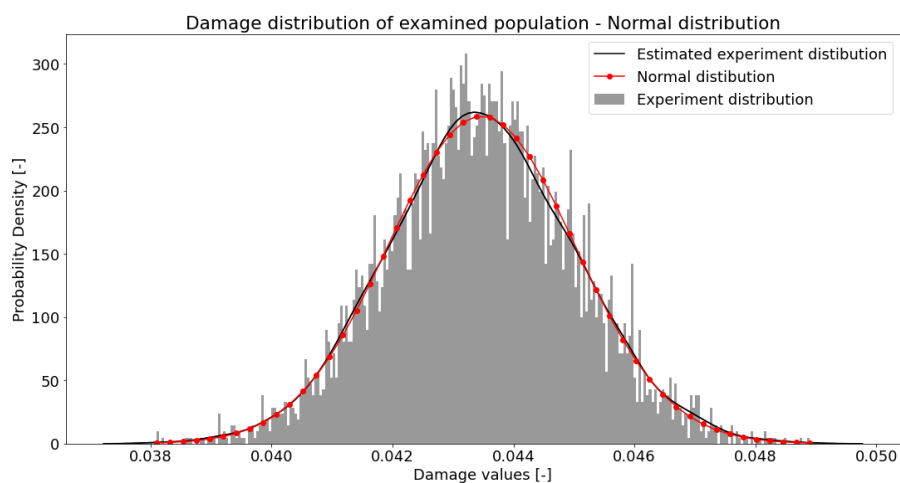


Figure 5-44 The best fitted distribution for damage values for the searched population for the narrow band signal, with a signal clipped at 3 standard deviations, block size  $N=2^{18}$  – Exponentiated Weibull distribution

Distribution type	Probability of the fitted distribution [-]	Mean damage [-]	Standard deviation of damage [-]	0.13% not lower than the quoted value of damage [-]	99.73% not exceeding the quoted value of damage [-]
Normal	0.83739	0.04347	0.00154	0.04776	0.03883
Exponentiated Weibull	0.00142	0.04349	0.00155	0.03910	0.04739
Generalised Extreme Value	0.06752	0.04348	0.00156	0.03921	0.04770

Table 5-25 Statistical parameters for a narrow band signal clipped at 3 standard deviations  $N=2^{18}$

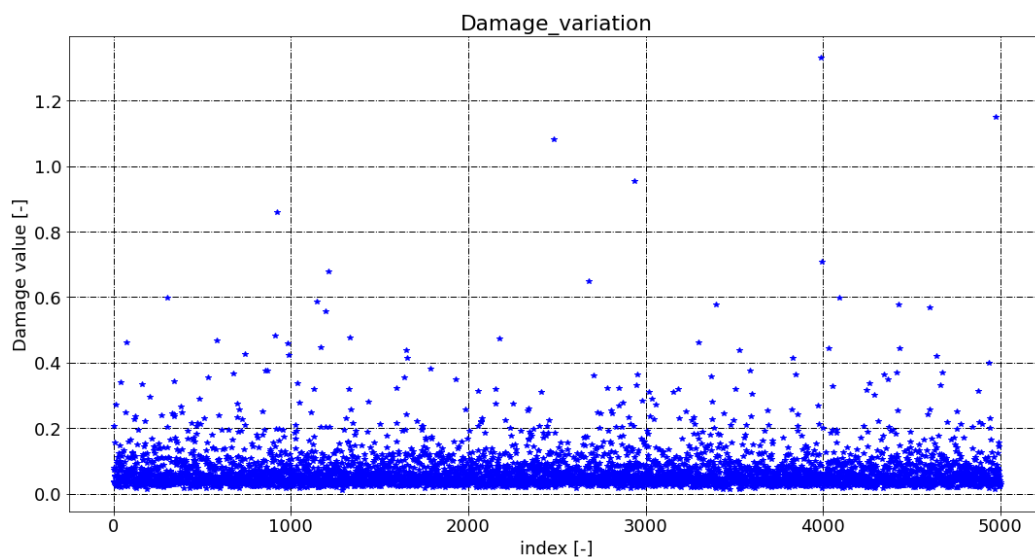


Figure 5-45 Damage values for the searched population for the narrow band signal, with a signal clipped at 5 standard deviations, block size  $N=2^{12}$

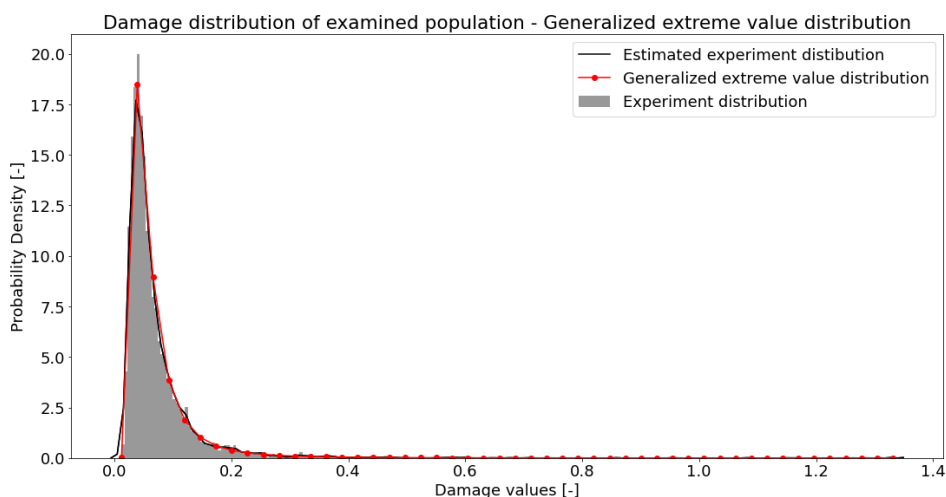


Figure 5-46 The best fitted distribution for damage values for the searched population for the narrow band signal, with a signal clipped at 5 standard deviations, n block size  $N=2^{12}$  – Generalised Extreme Value distribution

Distribution type	Probability of the fitted distribution [-]	Mean damage [-]	Standard deviation of damage [-]	0.13% not lower than the quoted value of damage [-]	99.73% not exceeding the quoted value of damage [-]
Normal	0.00000	0.07023	0.06723	0.00038	N/A
Exponentiated Weibull	0.05966	0.06896	0.05749	0.01649	0.44323
Generalised Extreme Value	0.44168	0.07087	0.09430	0.01584	0.60087

Table 5-26 Statistical parameters for a narrow band signal clipped at 5 standard deviations, block size  $N=2^{12}$

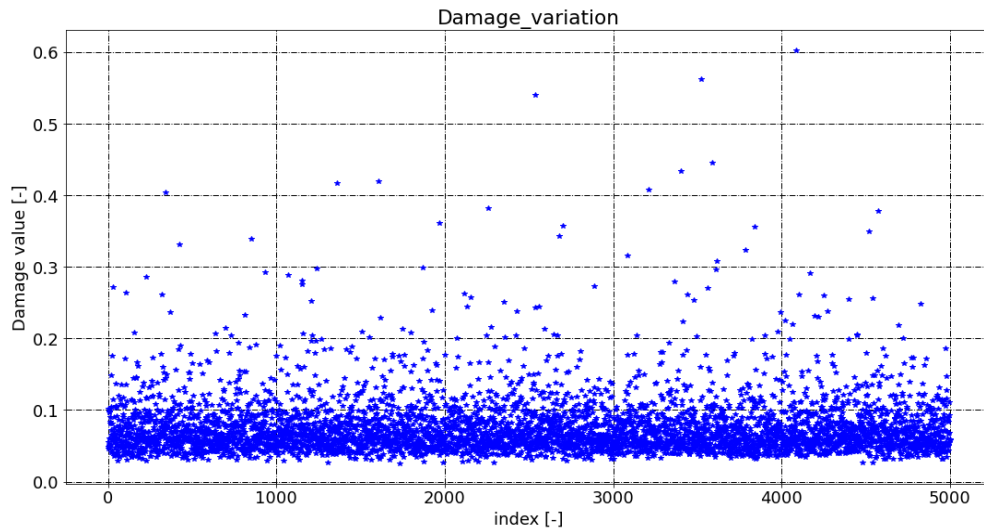


Figure 5-47 Damage values for the searched population for the narrow band signal, with a signal clipped at 5 standard deviations, block size  $N=2^{14}$

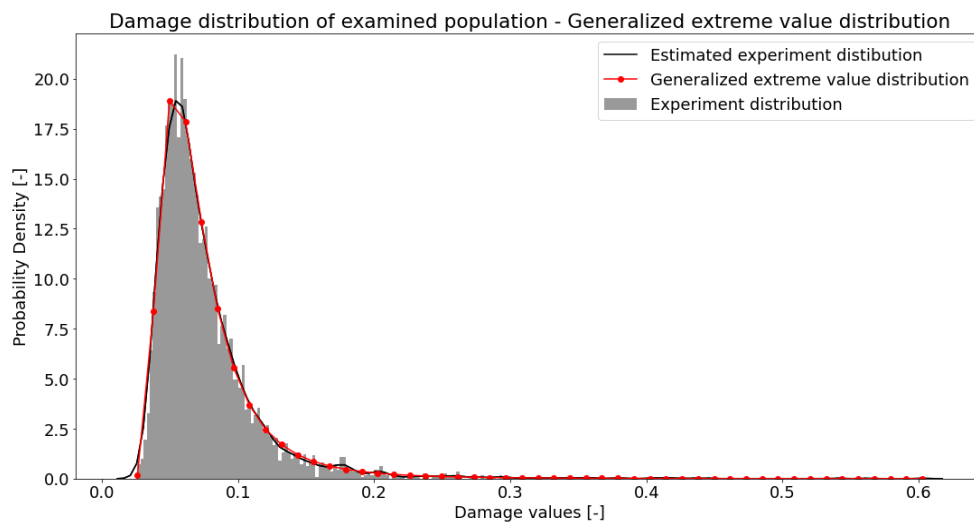


Figure 5-48 The best fitted distribution for the damage values for the searched population for the narrow band signal, with a signal clipped at 5 standard deviations, block size  $N=2^{14}$  – Generalised Extreme Value Distribution

Distribution type	Probability of the fitted distribution [-]	Mean damage [-]	Standard deviation of damage [-]	0.13% not lower than the quoted value of damage [-]	99.73% not exceeding the quoted value of damage [-]
Normal	0.00000	0.07571	0.04098	0.00072	N/A
Exponentiated Weibull	0.20369	0.07473	0.03573	0.02783	0.26912
Generalised Extreme Value	0.96212	0.07567	0.04147	0.02880	0.32958

Table 5-27 Statistical parameters for narrow band signal clipped at 5 standard deviation, block size  $N=2^{14}$

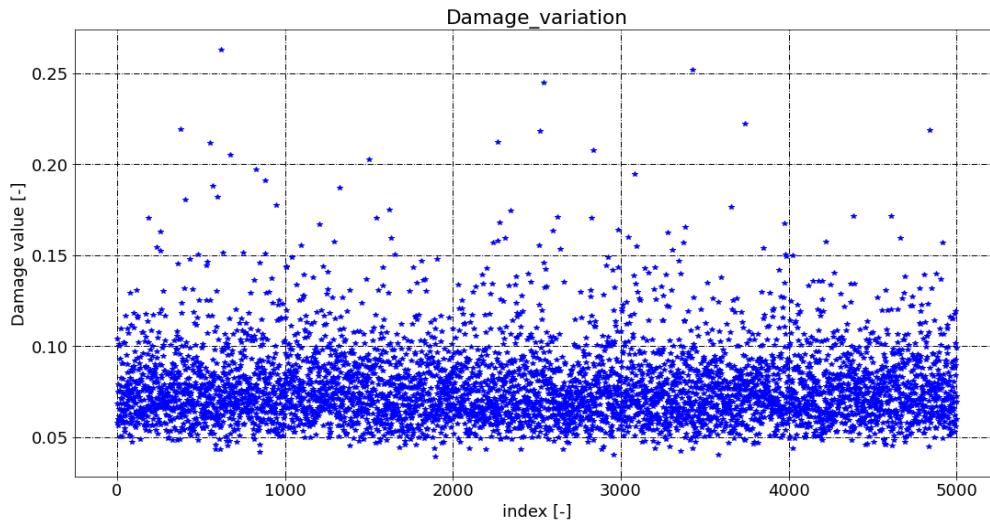


Figure 5-49 Damage values for the searched population for the narrow band signal, with a signal clipped at 5 standard deviations, block size  $N=2^{16}$

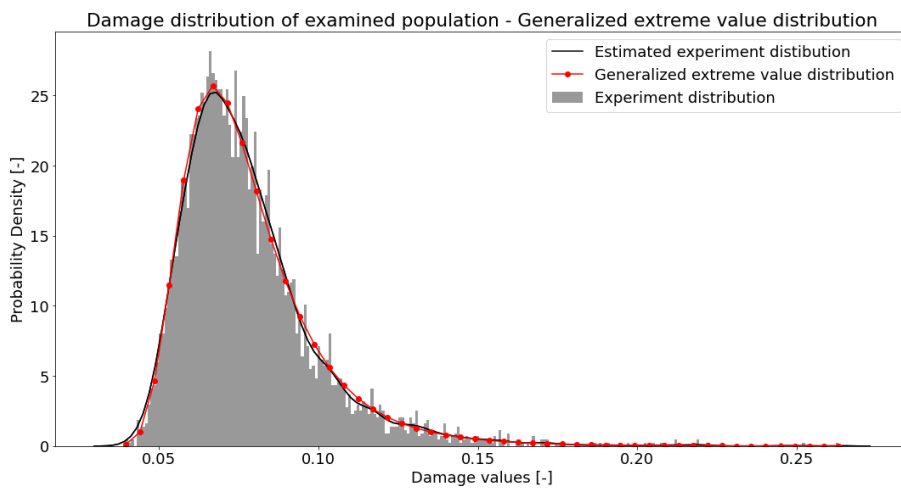


Figure 5-50 The best fitted distribution for the damage values for the searched population for the narrow band signal, with a signal clipped at 5 standard deviations, block size  $N=2^{16}$  – Generalised Extreme Value Distribution

Distribution type	Probability of the fitted distribution [-]	Mean damage [-]	Standard deviation of damage [-]	0.13% not lower than the quoted value of damage [-]	99.73% not exceeding the quoted value of damage [-]
Normal	0.00000	0.07803	0.02162	0.01365	0.13861
Exponentiated Weibull	0.00000	0.07488	0.02568	0.03951	0.15844
Generalised Extreme Value	0.57211	0.07802	0.02135	0.04329	0.18299

Table 5-28 Statistical parameters for a narrow band signal clipped at 5 standard deviations, block size  $N=2^{16}$

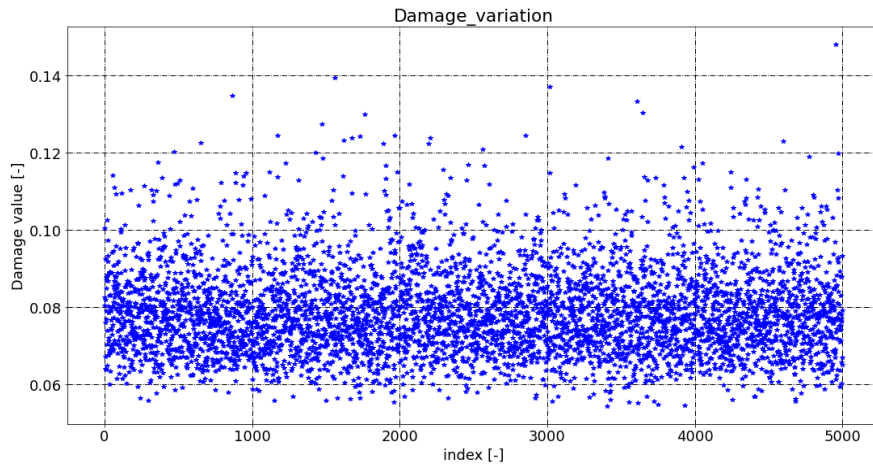


Figure 5-51 Damage values for the searched population for the narrow band signal, with a signal clipped at 5 standard deviations, block size  $N=2^{18}$

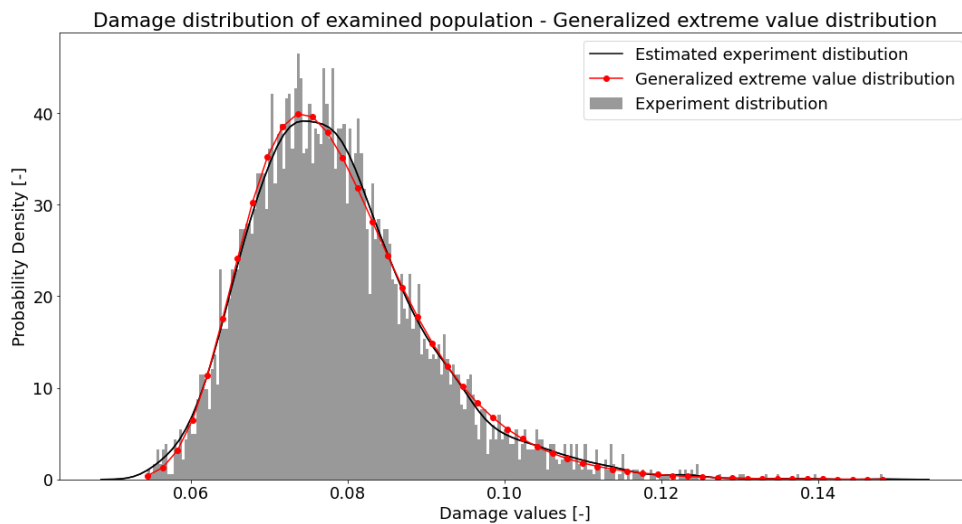


Figure 5-52 The best fitted distribution for damage values for the searched population for the narrow band signal, with a signal clipped at 5 standard deviations, block size  $N=2^{18}$  – Generalised Extreme Value Distribution

Distribution type	Probability of the fitted distribution [-]	Mean damage [-]	Standard deviation of damage [-]	0.13% not lower than the quoted value of damage [-]	99.73% not exceeding the quoted value of damage [-]
Normal	0.00000	0.07877	0.01128	0.04480	0.11015
Exponentiated Weibull	0.00000	0.53129	0.94674	0.05451	N/A
Generalised Extreme Value	0.63124	0.07879	0.01126	0.05571	0.12250

Table 5-29 Statistical parameters for a narrow band signal clipped at 5 standard deviations, block size  $N=2^{18}$

#### 5.4.4 Summary and conclusions of the populational research

The summary of conducted computer experiments using two combined methods: FEM, the Monte Carlo method and Python programming, allows to identify the high variability of the damage value depending on the frequency resolution used in IFFT. This phenomenon was not introduced by Dirlik.

Research results presented in this paper show that the legacy methods (Narrow Band, Lalanne, Dirlik) used in commercial software for stochastic loading scenarios provide an accurate mean value of damage but have no opportunity to assess the variability of damage, which depends on e.g., the block size in IFFT.

Introducing a new method of calculation (based on the combined frequency and time approach) of the damage under the random loading scenario allows for more robust damage estimation in the time domain while keeping the efficiency benefit related to the frequency domain calculation (the basis of the time domain calculation are results from the linear dynamic harmonic analysis). The new proposed approach allows to estimate the mean value of damage, distribution of damage and variation, which depends on the IFFT block size. Using the novel method introduced in this paper allows to obtain higher accuracy of the results than with the legacy method, and a higher efficiency of computation than with the legacy method. The novel method also enables analysis of time series population to assess the damage variation, which is not possible using the legacy method.

The research results reveal that damage variation occurs (damage variability depends on the block size used in IFFT), and therefore the conclusion is that for the considered test equipment the frequency resolution parameter defines the variability of the damage. This issue should be considered when sizing the unit and developing a test procedure taking into account the test aperture used for final testing of the considered unit.

An additional conclusion is that for the populational analysis it is recommended to use the best fitting among three proposed methods of distribution: Exponentiated Weibull, Gaussian and Generalised Extreme Value. The research shows that for different block sizes for different signal types it is possible to use one distribution from these three, which accurately describes the damage distribution.

The research results show that for a white noise signal clipped at three standard deviations, the best fitted distribution for low block size is Generalised Extreme Value distribution, but when the block size increases a better distribution method is Weibull, while for a block size higher than  $N=2^{16}$ , normal distribution fits the damage distribution (see Figure 5-6, Figure 5-8, Figure 5-10, Figure 5-12 and Table 5-6 through Table 5-9). For a signal clipped at five standard deviations, we observed that Exponentiated Weibull and Generalised Extreme Value distributions best fit the experiment damage distribution (see Figure 5-14, Figure 5-16, Figure 5-18, Figure 5-20 and Table 5-10 through Table 5-13).

The research results shows that for a wide band signal clipped at three standard deviations, Generalised Extreme Value distribution fits well for a low value of block size  $N=2^{12}$  (Exponentiated Weibull is also characterised by fitting the experiment damage well) – see Figure 5-22, Figure 5-24, Figure 5-26, Figure 5-28 and Table 5-14 through Table 5-17. For a signal clipped at five standard deviations the Generalised Extreme Value distribution fits best to the experiment damage distribution – see Figure 5-30, Figure 5-32, Figure 5-34, Figure 5-36 and Table 5-18 through Table 5-21.

The research results show that for a narrow band signal clipped at three standard deviations, the Generalised Extreme Value and Normal distribution methods fit well – see Figure 5-38, Figure 5-40, Figure 5-42, Figure 5-44 and Table 5-22, Table 5-14 through Table 5-25. For a signal clipped at five standard deviations, Generalised Extreme Value distribution best fits the experiment damage distribution – see Figure 5-46, Figure 5-48, Figure 5-50, Figure 5-52 and Table 5-26 through Table 5-29.

These three distributions can be applied for statistical consideration in all cases where a signal is clipped at three and five standard deviations and for a non-clipped signal, as this set of distribution allows to describe the damage variability process and derived the damage range, which depend on IFFT block size (see Table 5-6 through Table 5-29). These distributions can be applied for white noise, wide band, and narrow band signals.

Another aspect is that the algorithm can also be adjusted to the frequency resolution (block size) during real testing to assess the variability of damage to the test equipment. As for a block size smaller than  $N=2^{14}$  the variability might increase, which can imply under-testing. In real testing there is a limitation for N used for defining 'Block size', and applying a high value of N can imply an increasing variation PSD profile from the predefined one, therefore it is proposed to apply the low value of N and modify the PSD reference input curve to meet following criteria:

$$D_{i_{0.13\%}}(N_{2^i}) \geq D_{20_{99.73\%}}(N_{2^{20}}) \tag{Eq. 5.3}$$

Where:

N– Block size

$D_{i_{0.13\%}}(N_{2^i})$  – damage for which 0.13% of the population has no lower damage – for the block size used during the testing

$D_{20_{99.73\%}}(N_{2^{20}})$  – damage for which 99.73% of the population has no higher damage – when N is equal to  $1048576 = 2^{20}$

Meeting the above criteria ensures that the unit will not be under-tested during real testing, when the block size used during the testing is limited. Graphical representation of the proposed criteria is presented in Figure 5-53, Figure 5-54 and Figure 5-55 respectively for the white noise, wide band and narrow band signals.

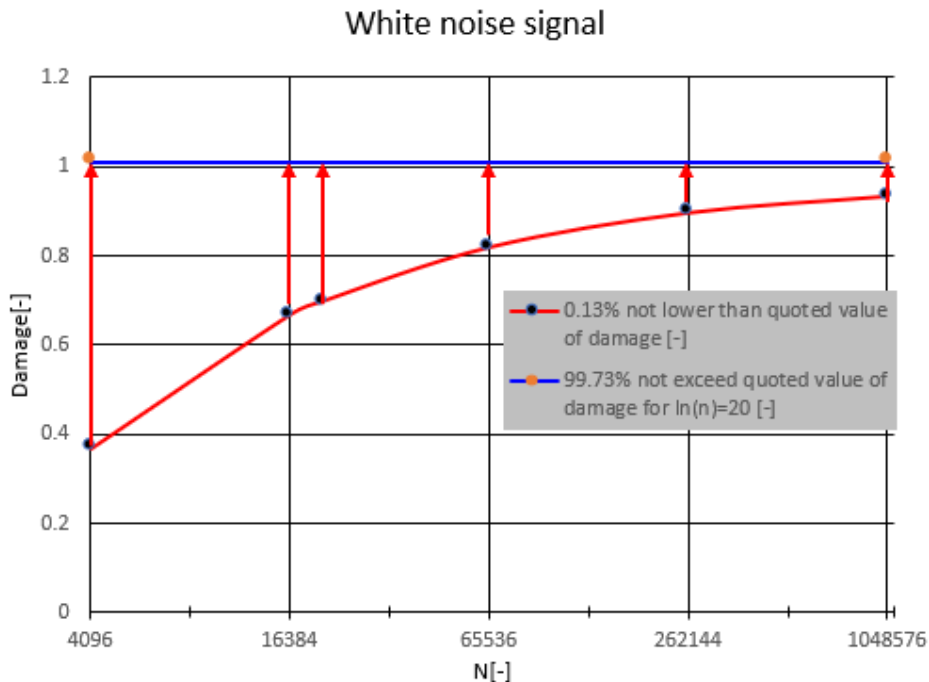


Figure 5-53 Damage correction for a different number of block sizes in IFFT – the white noise signal

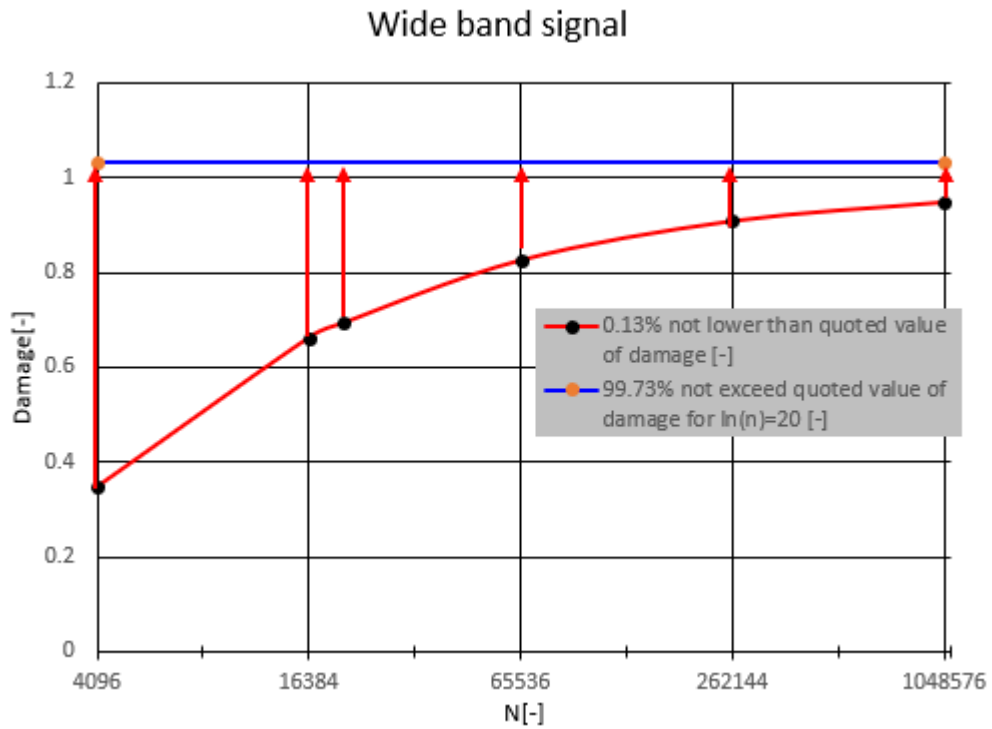


Figure 5-54 Damage correction for a different number of block sizes in IFFT – the wide band signal

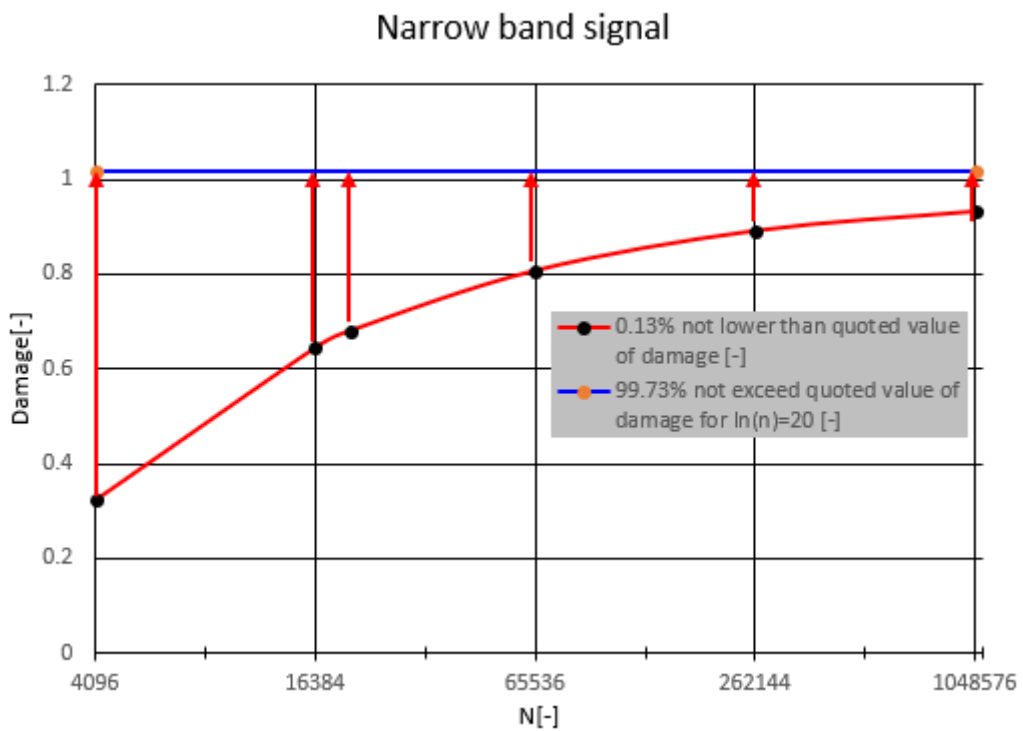


Figure 5-55 Damage correction for a different number of block sizes in IFFT – the narrow band signal

---

## **CHAPTER 6     DEVELOPING A METHOD FOR VIBRATION DAMAGE ESTIMATION UNDER COMBINED RANDOM AND DETERMINISTIC LOADING**

### **6.1     Research for developing a new method - introduction**

The Rainflow Cycle Counting algorithm in the frequency domain is commonly used for vibration damage estimation under stochastic loading of linear systems in synergy with FEM analysis. The precursor of Rainflow Cycle Counting algorithm in frequency domain were Bendat and Rice [15], [16], [17] and [19], who provided a method used for narrow band signals. The next milestone was the development of the Rainflow Cycle Counting algorithm in the frequency domain made by Dirlik, using the Monte Carlo method [18]. This approach is now considered one of the most accurate techniques used in commercial software ([28], [30]) for assessment of damage under random loading. Other researchers included Lalanne ([20], [21] and [22]) and Steinberg [23], who provided methods for Rainflow Cycle Counting in the frequency domain. All of these methods have been tested by Halfpenny ([6], [13] and [14]), although only for evaluation damage under pure stochastic loading.

The methods were developed for vibration damage estimation purely for stochastic loading. However these methods have been adopted for more general usage, i.e. damage estimation under combined stochastic and deterministic loading by the Bishop, Sweitzer, Schlesinger, Woodward, Kerr, Murthy, Datta, Atkins in their publications ([3], [4], [5], [8], [9], [10], [11], [64] and [65]). The loading scenario for using this method are e.g., the simultaneous deterministic sine sweep and random load – see Figure 6-1. This combination is required by the US Department of Defence Test Method Standard [66] or other specific requirements driven by military aircraft manufacturers.

The first stage of research introduced in this paper shows that using the abovementioned methods resulting in high conservative damage results.

The second stage of research was development of a novel method for precise damage estimation under combined loads, which introduces the combined frequency and time domain calculation instead of only frequency domain for vibration damage estimation in legacy methods. The superposition of stochastic and deterministic loading approach was introduced by NASA [67]. The novel method presented in this paper assumes extension of this approach for analysis of the PSD response of the system, making the stochastic and deterministic signals superposition and damage analysis using the Monte Carlo Method. The novel method introduced in this paper is much more accurate, and can replicate the test parameter, e.g., a clipping stochastic signal at considered sigma level. Additionally, this method allows to consider a large population of time series to assess the damage distribution for the considered PSD input curve.

In this paper, for combined loads we used a simultaneous deterministic linear sine sweep – which represents, e.g. shooting with a variable firing gun installed on an aircraft or helicopter and stochastic loads defined by a PSD input curve (Figure 6-1) – which represent normal operating dynamic loading, e.g. turbulences.

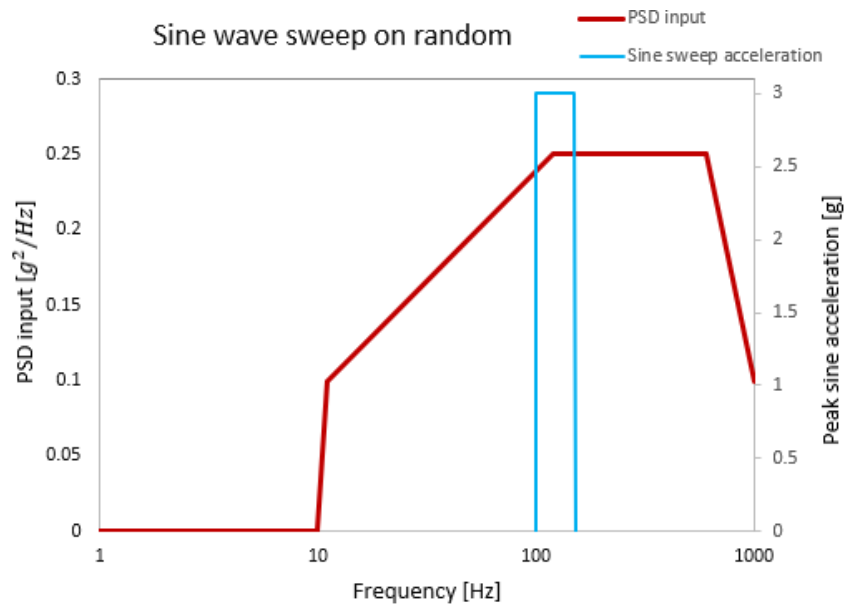


Figure 6-1 Sine waves sweep simultaneous with a random background

The novel technique introduced in this paper expands research done by Dirlik with regards to the frequency resolution, populational studies [52] and [68], a combination of stochastic and deterministic loading and additionally using FEM for transfer function estimation.

## 6.2 Legacy methods – vibration damage estimation under combined stochastic and deterministic loading in the frequency domain

The methodology introduced in Chapter 2 of this paper is the basis for damage estimation only under stochastic loading. Research done by Bishop, Sweitzer, Schlesinger, Woodward, Kerr, Murthy, Datta, and Atkins in their publications ([3], [4], [5], [8], [9], [10], [11], [64] and [65]), describe the aim of damage estimation based on superimposing spectral moments generated by random and deterministic loads. The abovementioned approach was used.

The Transfer Function ( $H_i(f)$ ), which consist of e.g., Huber-Mises-Hencky complex stress or critical plane stress, needs to be evaluated for finite –  $i$  numbers of frequency sub-ranges, e.g., for a sweep between 100-150Hz it needs to be evaluated for the considered sub-range size, e.g., 0.1Hz. For each subrange a single sine wave is considered, and a signal statistic needs to be introduced.

The response function –  $S(f)$  is then evaluated based on the Transfer Function –  $H(f)$ , and sine sweep amplitude ( $G(f)$ ) as in the equation Eq. 6.1.

$$S_i(f_i) = \sqrt{H_i(f_i)} \cdot G_i(f_i) \quad \text{Eq. 6.1}$$

The Root Mean Square of the single sine wave (RMS) can be evaluated as in the equation Eq. 6.2

$$\text{RMS} = \frac{\sqrt{2}}{2} \cdot S_i(f_i) \quad \text{Eq. 6.2}$$

The next step is evaluation of spectral moments for every considered single sine wave function using the following equation for the 0, 1st, 2nd, 4th spectral moments (see equation Eq. 6.3 through equation Eq. 6.6).

$$m_{0\_sine\_wave}(f_i) = \text{RMS}^2 \quad \text{Eq. 6.3}$$

$$m_{1\_sine\_wave}(f_i) = m_0(f_i) \cdot f_i \quad \text{Eq. 6.4}$$

$$m_{2\_sine\_wave}(f_i) = m_0(f_i) \cdot f_i^2 \quad \text{Eq. 6.5}$$

$$m_{4\_sine\_wave}(f_i) = m_0(f_i) \cdot f_i^4 \quad \text{Eq. 6.6}$$

Where:

$f_i$  – is the considered frequency

Signal statistics in the frequency domain are based on a spectral analysis performed iteratively for the considered frequency sub-ranges e.g., 0.1Hz sub-ranges width. Spectral moments from deterministic loading ( $m_{0\_sine\_wave}$ ,  $m_{1\_sine\_wave}$ ,  $m_{2\_sine\_wave}$ ,  $m_{4\_sine\_wave}$ ) need to be the sum of the spectral moments from a stochastic background ( $m_0$ ,  $m_1$ ,  $m_2$ ,  $m_4$ ) as introduced in equation Eq. 6.7 through equation Eq. 6.10.

$$m_{0\_mixed\_mode}(f_i) = m_0 + m_{0\_sine\_wave}(f_i) \quad \text{Eq. 6.7}$$

$$m_{1\_mixed\_mode}(f_i) = m_1 + m_{1\_sine\_wave}(f_i) \quad \text{Eq. 6.8}$$

$$m_{2\_mixed\_mode}(f_i) = m_2 + m_{2\_sine\_wave}(f_i) \quad \text{Eq. 6.9}$$

$$m_{4\_mixed\_mode}(f_i) = m_4 + m_{4\_sine\_wave}(f_i) \quad \text{Eq. 6.10}$$

Where:

$m_{0\_mixed\_mode}(f_i)$  – is the spectral 0 moment for the superimposed signal at the considered frequency  
 $m_{1\_mixed\_mode}(f_i)$  – is the spectral 1<sup>st</sup> moment for the superimposed signal at the considered frequency  
 $m_{2\_mixed\_mode}(f_i)$  – is the spectral 2<sup>nd</sup> moment for the superimposed signal at the considered frequency  
 $m_{4\_mixed\_mode}(f_i)$  – is the spectral 4<sup>th</sup> moment for the superimposed signal at the considered frequency

It is worth noting that in the superposition of the spectral moment, the sum used for the full moment from the stochastic part of the load ( $m_0, m_1, m_2, m_4$ ) as the allowable number of cycles is also calculated iteratively for the considered  $T_i$  which is equal to the total time of exposure to random and deterministic loading –  $T_{Total}$ , divided by the number of sub-ranges – see equation Eq. 6.11.

$$T_i = \frac{T_{Total}}{n} \quad \text{Eq. 6.11}$$

where:

$n$  – is the number of sub-ranges

Rainflow Cycle Counting in the frequency domain evaluated by the Dirlik or Narrow Band Method / damage assessment are provided for each sub-range in the same way as introduced in section 2 of this paper:

The number of actual cycles as per Dirlik Rainflow Cycle Counting in the frequency domain –  $n_i$  – see equation Eq. 6.12.

$$n_i = PDF_i(S) \cdot T_i \cdot E_i[P] \quad \text{Eq. 6.12}$$

Where:

$PDF_i(S)$  – is the Probability Density Function at the considered stress bin

$E_i[P]$  – is the number of peaks at the considered stress bin

The damage value for the considered sub-range ( $D_i$ ) – see equation Eq. 6.13.

$$D_i = \frac{n_i}{N(S)_i} \quad \text{Eq. 6.13}$$

Where:

$N(S)_i$  – is the allowable number of cycles at the considered stress bin based on the considered S-N curve

The total damage ( $D_{Total}$ ) under combined stochastic and deterministic loading is the sum of damage from each sub-range – see equation Eq. 6.14.

$$D_{Total} = \sum_{i=1}^n D_i \quad \text{Eq. 6.14}$$

The damage value obtained by created an algorithm has been benchmarked against the damage value obtained using commercial software and obtained a good correlation (exemplary results are presented in section 6.4 of this paper).

### 6.3 Combined frequency and time domain vibration damage estimation under combined stochastic and deterministic loading – the new proposed method

The frequency domain stochastic signal is retrieved in the time domain using the approach presented in Chapter 4 of this paper.

The specified linear sine sweep frequency ( $f_{spec}(t)$ ) dependence from time can be written as a function of time and frequency – see equation Eq. 6.15, [52].

$$f_{spec}(t) = f_1 + K \cdot T \quad \text{Eq. 6.15}$$

Where:

T – is the total sweep time

K – is the sweep rate

$f_1$  – is the initial sweep frequency

The specified frequency ( $f_{spec}(t)$ ) can be written in alternative form as in the equation Eq. 6.16):

$$f_{spec}(t) = f_1 + (f_2 - f_1) \frac{t}{T} \quad \text{Eq. 6.16}$$

$f_2$  – is the end sweep frequency

t – is the time variable

The sine sweep frequency ( $f(t)$ ) is the integral of the specified frequency and can be written as in the equation Eq. 6.17.

$$f(t) = \int f_{spec}(t) dt = f_1 \cdot t + \frac{f_2 - f_1}{T} \cdot \frac{t^2}{2} \quad \text{Eq. 6.17}$$

The input sine sweep ( $G(t)$ ) with a constant acceleration amplitude can be written as in the equation Eq. 6.18.

$$G(t) = u(t) \cdot \sin(\omega t) = u(t) \cdot \sin(2\pi f(t) \cdot t) \quad \text{Eq. 6.18}$$

Where:

$u(t)$  – is the displacement in time

$\omega$  – circular frequency

And an equivalent version for implementation in Python programming language ([62] and [63]) can be written as in the equation Eq. 6.19.

$$G(t) = u(t) \cdot \sin\left(2\pi \cdot t \cdot \left(f_1 + \frac{f_2 - f_1}{T} \cdot \frac{t}{2}\right)\right) \quad \text{Eq. 6.19}$$

The sine sweep frequency is deterministic, and depends on time, therefore the sine sweep function can be scaled by the transfer function  $H(f)$  to obtain a time series sweep including the system response as presented in Figure 6-2.

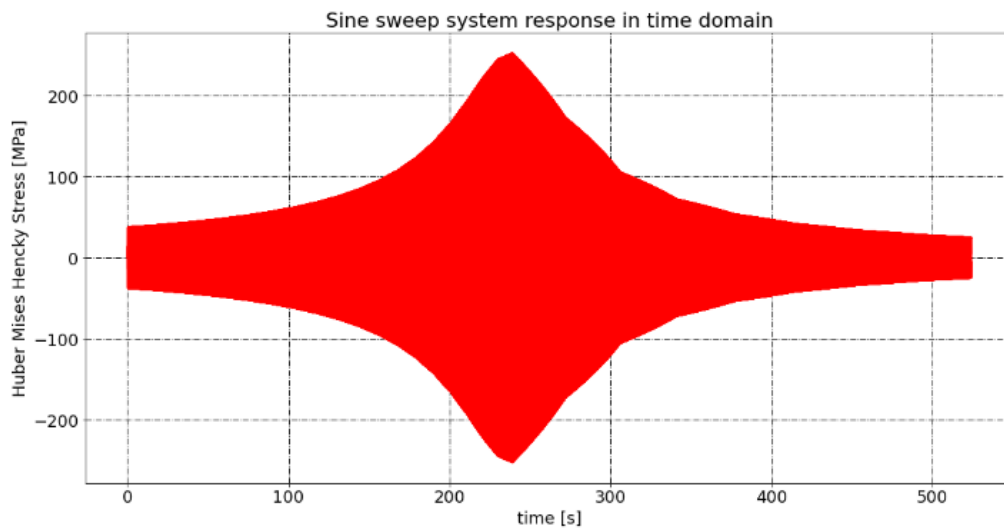


Figure 6-2 Sine sweep system response in the time domain, with a sweep rate  $K=0.095367$  Hz/s

The sine sweep response ( $S(t)$ ) can be written as in the equation Eq. 6.20.

$$S(t) = \sqrt{H(t)} \cdot G(t) \quad \text{Eq. 6.20}$$

Where:

$H(f)$  – is the transfer function

$G(t)$  – is the input sine sweep acceleration

This signal, which consists of the PSD response stress values, can now be superimposed to a random time series PSD response retrieved with the Monte Carlo method (assuming linearity of system, with restriction that the time sequence of the retrieved random signal matches the time sequence of the sine sweep) – see Figure 6-3.

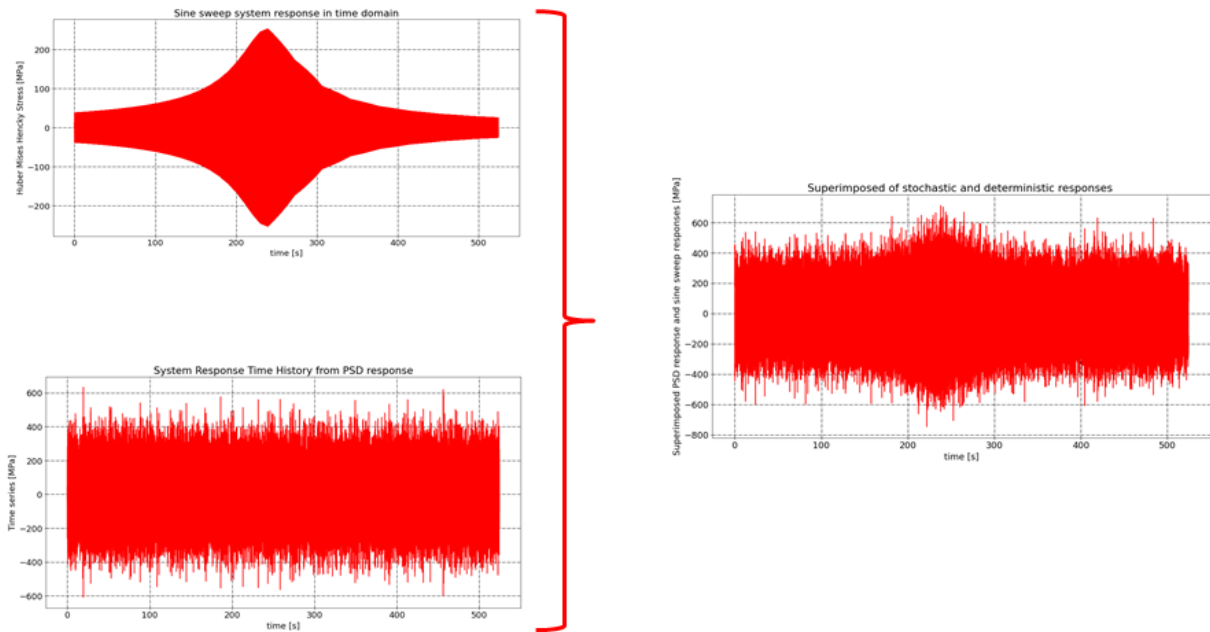


Figure 6-3 The superimposed stochastic and deterministic responses in the time domain

For the superimposed signal, the Rainflow Cycle Counting algorithm in the time domain can be used, the SN curve for stress life method needs to be introduced, and the damage for combined stochastic-deterministic input can be evaluated.

It should also be noted that the sweep rate can be fitted to background random loading to obtain one sweep during an operating random load if there is no specific requirement driven by the aircraft manufacturer.

It has been checked that n number of sine sweeps with n times higher than the reference sweep rate (see Figure 6-4 for n=2 and Figure 6-5 for n=4) causes the same theoretical damage as one sweep with the reference sweep rate. The reference signals have been integrated in a theoretical way – there is no continuous link between sweeps, however it has negligible impact on the quoted damage as the maximum stress cycles for the considered samples is much higher than in the linked area. It should be emphasised that only one sweep acting during the duration of the random loading should give a high level of damage, as an increasing sweep rate can cause the system to not respond with full amplitude during the resonance, with the maximum resonance amplitude decreasing.

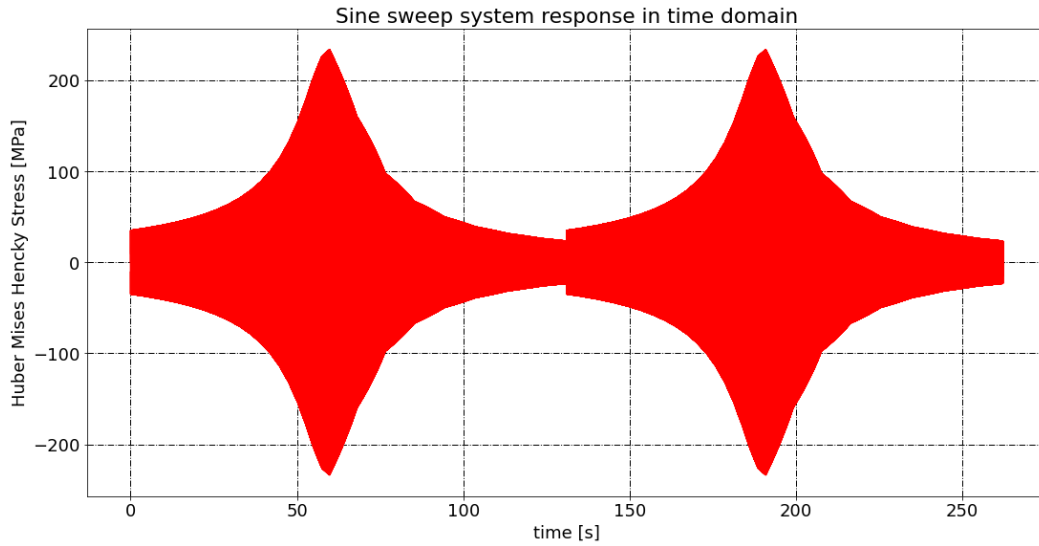


Figure 6-4 Sine sweep system response in the time domain, with a sweep rate  $K \cdot 2 = 0.190735$  Hz/s

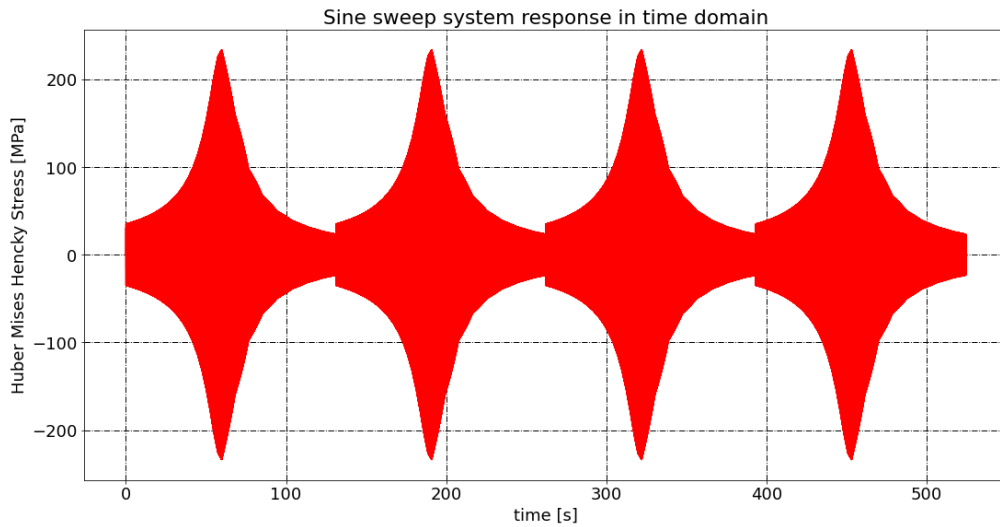


Figure 6-5 Sine sweep system response in the time domain, with a sweep rate  $K \cdot 4 = 0.38147$  Hz/s

The proposed algorithm flow chart for damage estimation under combined stochastic and deterministic loading in the time domain is presented in Figure 6-6.

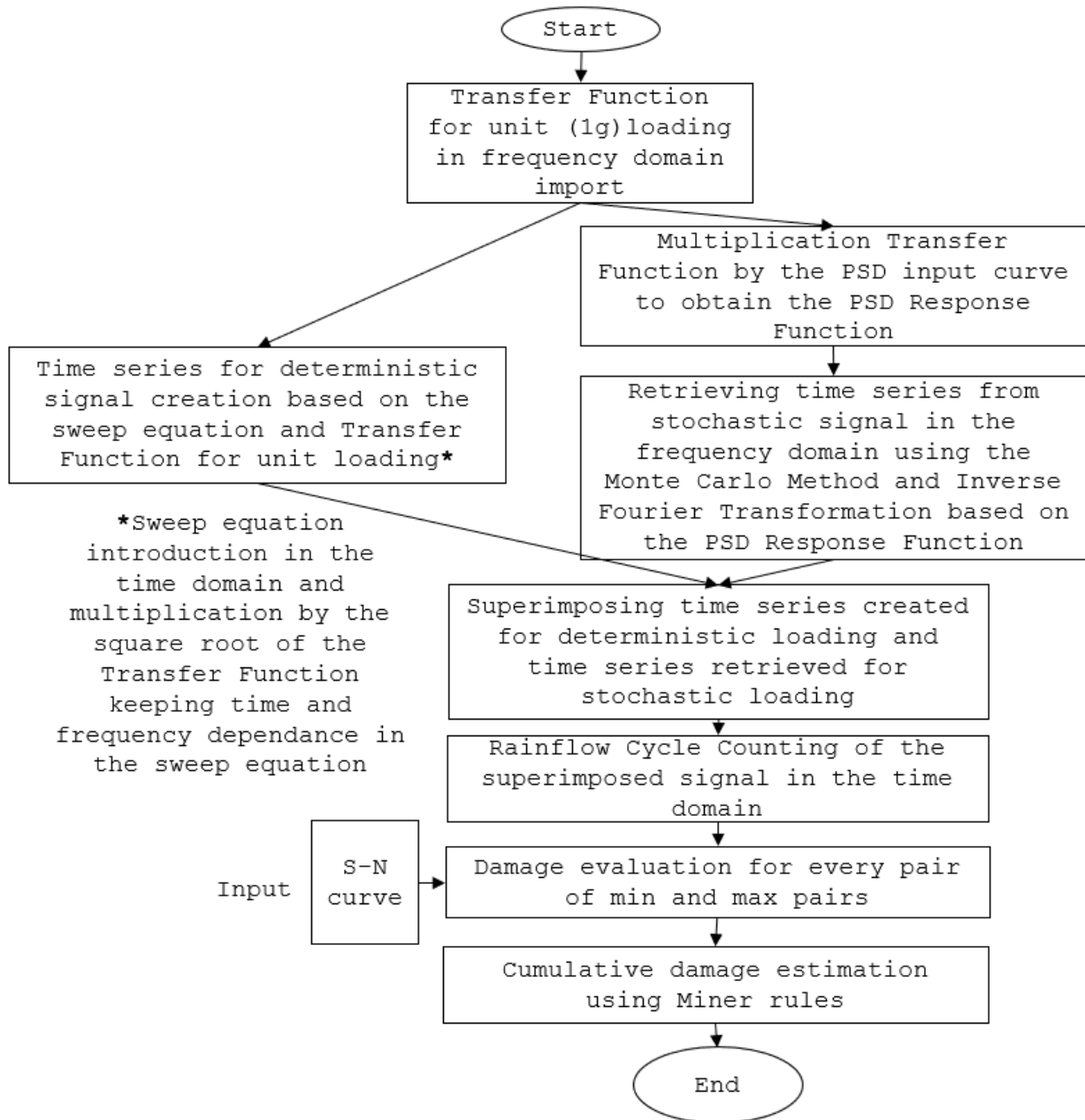


Figure 6-6 Algorithm flow chart for damage estimation under combined stochastic and deterministic loading in the time domain

#### 6.4 Comparison results obtained for the legacy method and the proposed method

The above-mentioned legacy method for combined stochastic deterministic loading proved to be highly conservative. Two loops of analysis under vibration loading were calculated. The 1<sup>st</sup> Loop, based on algorithms for vibration damage estimation under deterministic loading (pure sine sweep), obtained a damage value of 0.009 for the critical integration point. The 2<sup>nd</sup> Loop was based on algorithms for combined stochastic deterministic loading and a low level non-damaging random load (giving 0 damage after evaluation using the algorithm for pure random loading, peaking at 9MPa of 5 $\sigma$  stress). For the combined load scenario, a damage of 0.58 was calculated for the same sine sweep as in the 1st Loop (resulting in 0.009 of damage). The results above show that the legacy approach is highly conservative and initialised further research. A summary of the obtained result is in Table 6-1.

Note: Even if we assume that the maximum stress from resonance for the sine sweep (258MPa) occurs for every cycle in the sweep (conservatively assuming that maximum peak in the resonance occurs through 50Hz) and superimposes a 5 $\sigma$  stress amplitude equal to 9MPa, the obtained damage is equal 0.21.

No.	Damage proposed method	Damage legacy method with the author's algorithm for combined loading	Damage legacy method using the MSC CAE Fatigue algorithm for combined loading	Damage for the sine sweep only using the author's algorithm for deterministic harmonic loading	Damage for the sine sweep only using the MSC CAE Fatigue algorithm for deterministic harmonic loading
1	0.00875	0.58110	0.60804	0.00875	0.00944
2	0.06718	1.00792	1.07479	0.00875	0.00944

Table 6-1 Comparison damage evaluated using the spectral method in the frequency domain (legacy method) and the new proposed method (damage evaluated in the time domain)

Note: In this section we used the FEM model and material model presented in section 3.3.1 and section 3.3.2 for consideration.

The research results show that the legacy method is highly conservative, and therefore there is a need to develop a new method for this loading scenario, to remove the conservatism during damage estimation. This is important for aerospace, especially with regard to military application, where e.g., the mass of the component can be reduced.

## 6.5 Additional considerations on the proposed method

Research results from the pure stochastic loading scenario shows that the damage can vary, and the variation depends on the block size (N) used in Inverse Fourier Transformation. To obtain information about statistics of the damage, the research was extended to search a large population consisting of 5000 samples (for which observed stabilization distribution parameters), to obtain the damage distribution. This section presents the research results quoted in the author's publication [69], which intruded a white noise signal and extended these considerations to the narrow band and wide band signal.

It should be noted that the populational analysis was performed for a critical integration point in the FEM discrete model.

### 6.5.1 White noise random signal analysis

Research for the white noise signal introduced 3 different block sizes:  $2^{12}$ ,  $2^{14}$  and  $2^{16}$ . The Kolmogorov-Smirnov criterium, which assesses the probability of a distribution, was used for fitting the distribution. Different distribution types available in the Python library [62] were used for the testing. The best fitted distributions were narrowed down to 3 with the highest probability of fitting: Gaussian, Exponentiated Weibull and Generalised Extreme Value distributions.

It is worth noting that the mean value of damage is quoted in Table 8-2 through Table 6-7 and 0.13% (taken -3 standard deviation in Gaussian distribution as a base) of the population has no lower damage and 9.73% (taken -3 standard deviation in Gaussian distribution as a base) of the population has no higher damage.

In Figure 6-7, Figure 6-9 and Figure 6-11 corresponding damage values are presented for the searched population for the white noise signal for the 3 mentioned block sizes for a signal clipped at 3 standard deviations. Per analogy the same results for a signal clipped at 5 standard deviations are presented in Figure 6-13, Figure 6-15 and Figure 6-17.

The best fitted distributions visualisation for a signal clipped at 3 standard deviations for 3 block sizes is presented in Figure 6-8, Figure 6-10 and Figure 6-12. Per analogy results for a signal clipped at 5 standard deviations are presented in Figure 6-14, Figure 6-16 and Figure 6-18.

In Table 6-2 through Table 6-4 a populational research results summary for a white noise signal clipped at 3 standard deviations is presented, and in Table 6-5 through Table 6-7 the summary of results for a signal clipped at 5 standard deviations.

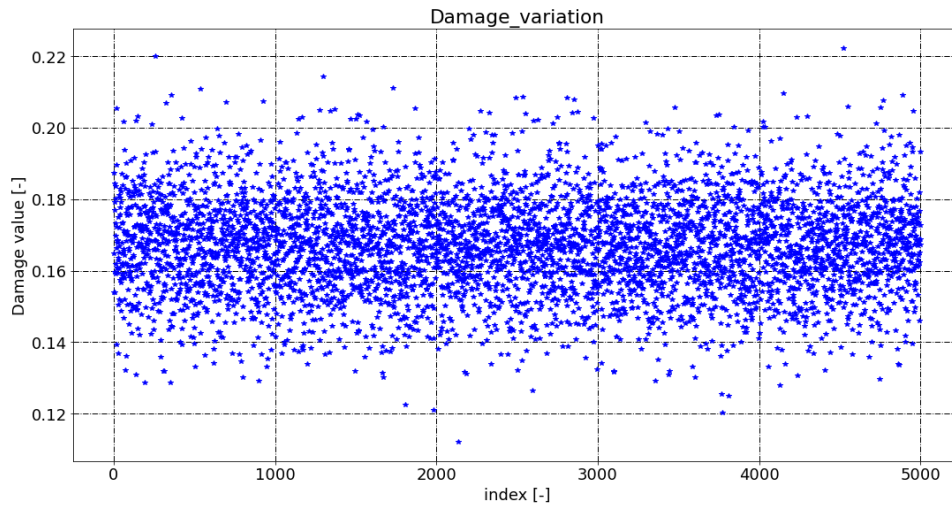


Figure 6-7 Damage values for the searched population for the white noise signal, with a signal clipped at 3 standard deviations, block size  $N=2^{12}$

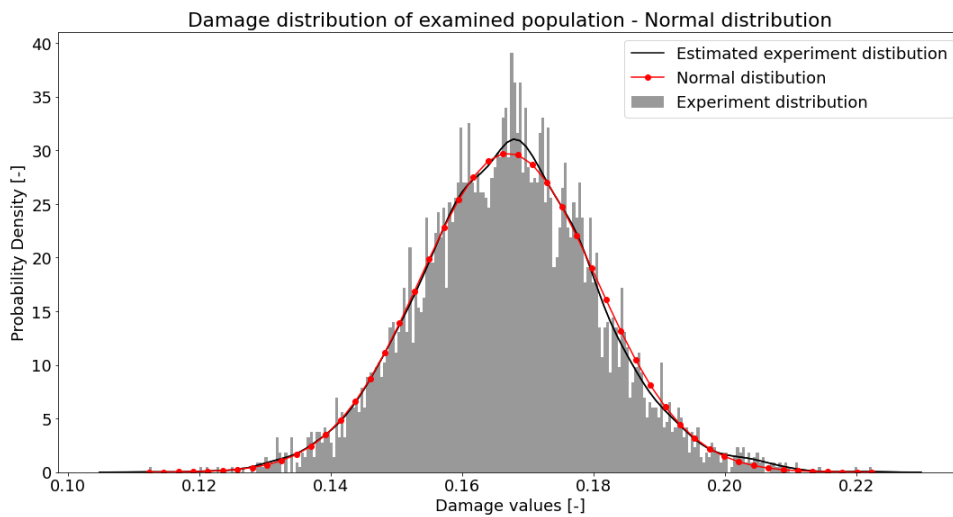


Figure 6-8 The best fitted distribution for damage values for the searched population for the white noise signal, with a signal clipped at 3 standard deviations, block size  $N=2^{12}$  – Normal distribution

Distribution type	Distribution fitting probability [-]	Mean damage [-]	Standard deviation of damage [-]	0.13% of samples not lower than the quoted value of damage [-]	99.73% of samples not higher than the quoted value of damage [-]
Normal	0.27452	0.16697	0.01341	0.12660	0.20427
Exponentiated Weibull	0.00000	0.15973	0.04217	0.11231	0.33518
Generalised Extreme Value	0.00091	0.16708	0.01380	0.13093	0.20641

Table 6-2 Statistical parameters for a white noise signal clipped at 3 standard deviations, block size  $N=2^{12}$

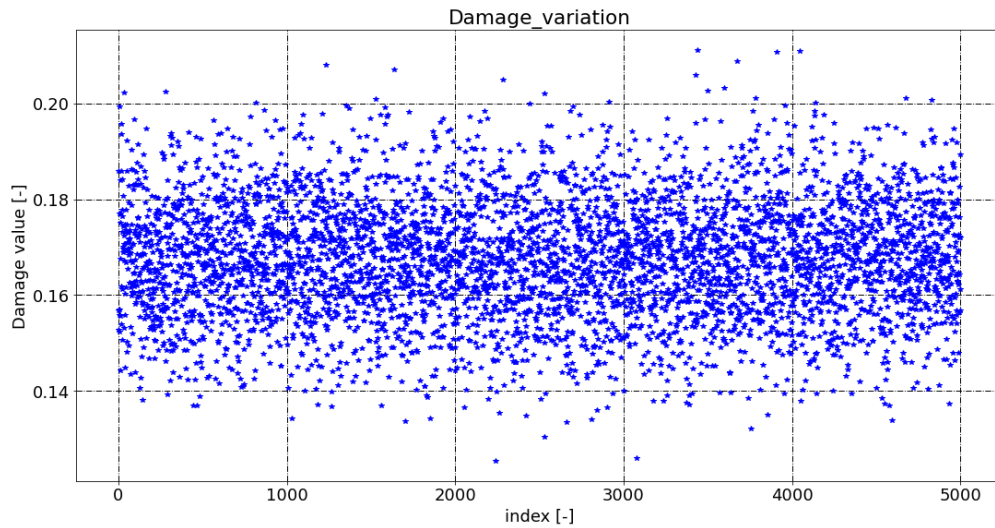


Figure 6-9 Damage values for the searched population for the white noise signal, with a signal clipped at 3 standard deviations, block size  $N=2^{14}$

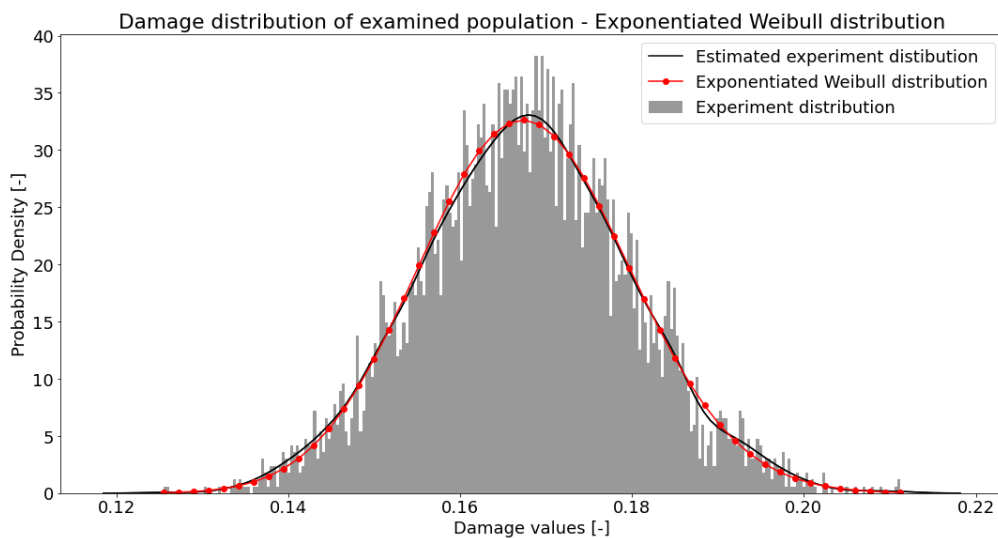


Figure 6-10 The best fitted distribution for damage values for the searched population for the white noise signal, with a signal clipped at 3 standard deviations, block size  $N=2^{14}$  – Exponentiated Weibull distribution

Distribution type	Distribution fitting probability [-]	Mean damage [-]	Standard deviation of damage [-]	0.13% of samples not lower than the quoted value of damage [-]	99.73% of samples not higher than the quoted value of damage [-]
Normal	0.80900	0.16763	0.01217	0.13098	0.20149
Exponentiated Weibull	0.90471	0.16763	0.01217	0.13269	0.20201
Generalised Extreme Value	0.05506	0.16768	0.01235	0.13450	0.20164

Table 6-3 Statistical parameters for a white noise signal clipped at 3 standard deviations  $N=2^{14}$

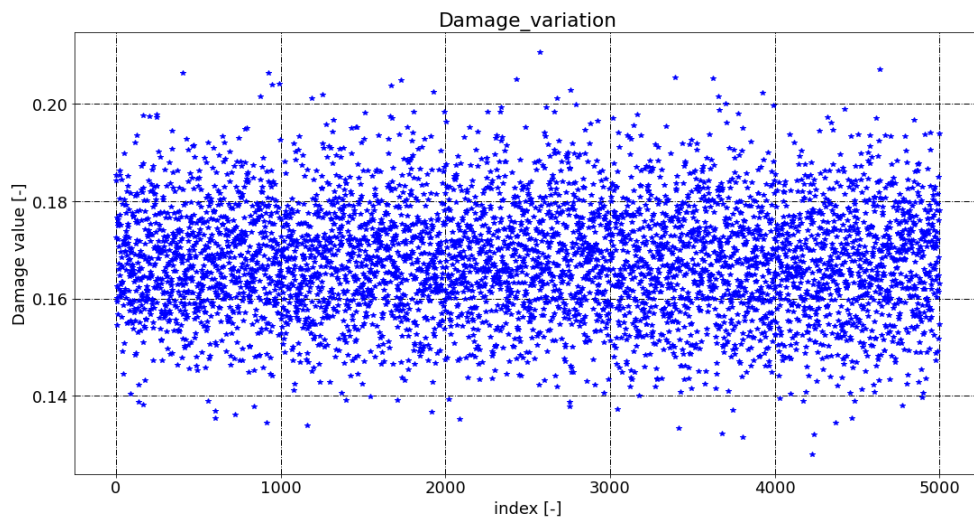


Figure 6-11 Damage values for the searched population for the white noise signal, with a signal clipped at 3 standard deviations, block size  $N=2^{16}$

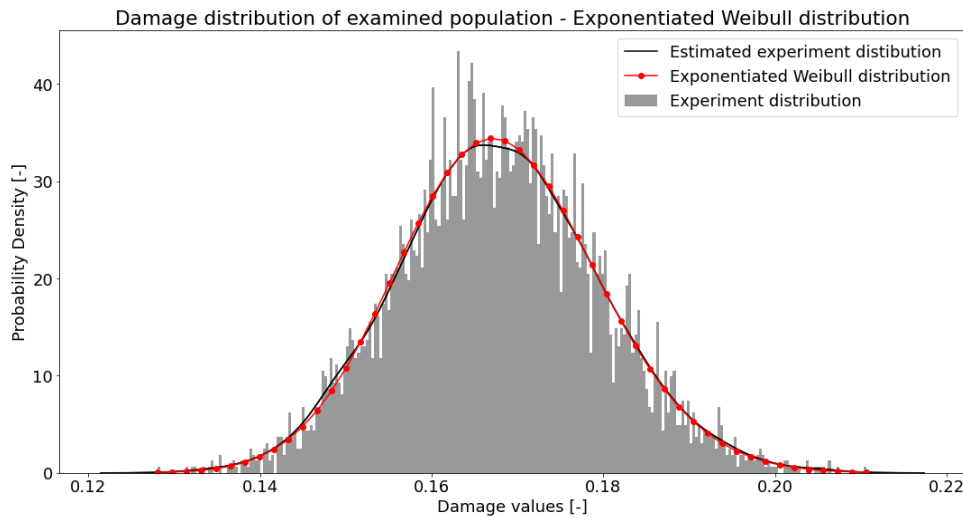


Figure 6-12 The best fitted distribution for damage values for the searched population for white the noise signal, with a signal clipped at 3 standard deviations, block size  $N=2^{16}$  – Exponentiated Weibull distribution

Distribution type	Distribution fitting probability [-]	Mean damage [-]	Standard deviation of damage [-]	0.13% of samples not lower than the quoted value of damage [-]	99.73% of samples not higher than the quoted value of damage [-]
Normal	0.49042	0.16785	0.01161	0.13287	0.20016
Exponentiated Weibull	0.99708	0.16783	0.01162	0.13473	0.20152
Generalised Extreme Value	0.26514	0.16789	0.01175	0.13660	0.20064

Table 6-4 Statistical parameters for a white noise signal clipped at 3 standard deviations  $N=2^{16}$

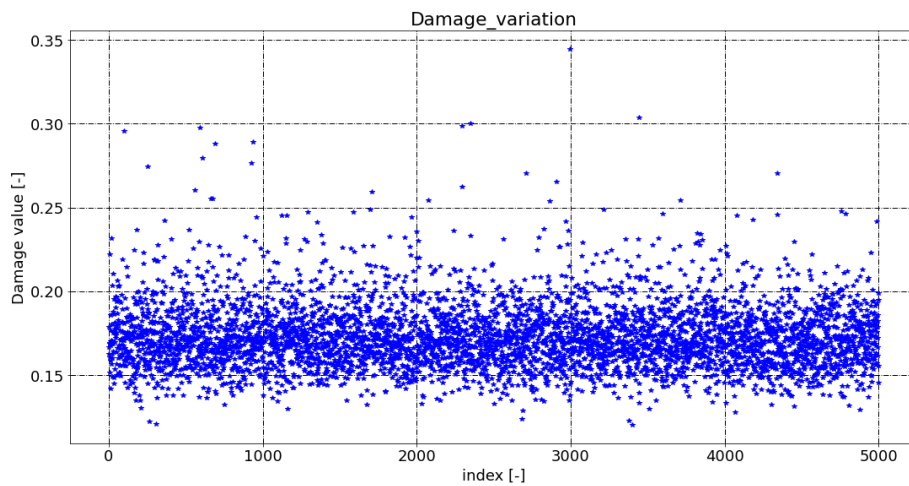


Figure 6-13 Damage values for the searched population for the white noise signal, with a signal clipped at 5 standard deviation, block size  $N=2^{12}$

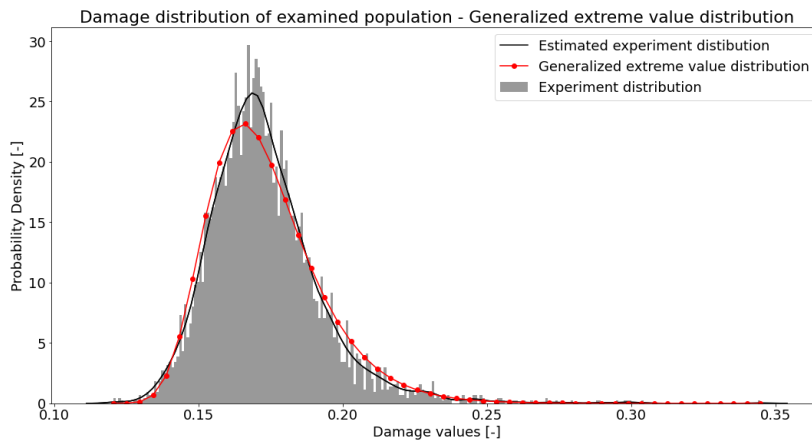


Figure 6-14 The best fitted distribution for damage values for the searched population for the white noise signal, with a signal clipped at 5 standard deviations, block size  $N=2^{12}$  – Generalised Extreme Value distribution

Distribution type	Distribution fitting probability [-]	Mean damage [-]	Standard deviation of damage [-]	0.13% of samples not lower than the quoted value of damage [-]	99.73% of samples not higher than the quoted value of damage [-]
Normal	0.00000	0.17292	0.01933	0.11472	0.22669
Exponentiated Weibull	0.00001	0.17277	0.01827	0.12702	0.23245
Generalised Extreme Value	0.00049	0.17313	0.01932	0.13327	0.24754

Table 6-5 Statistical parameters for a white noise signal clipped at 5 standard deviations, block size  $N=2^{12}$

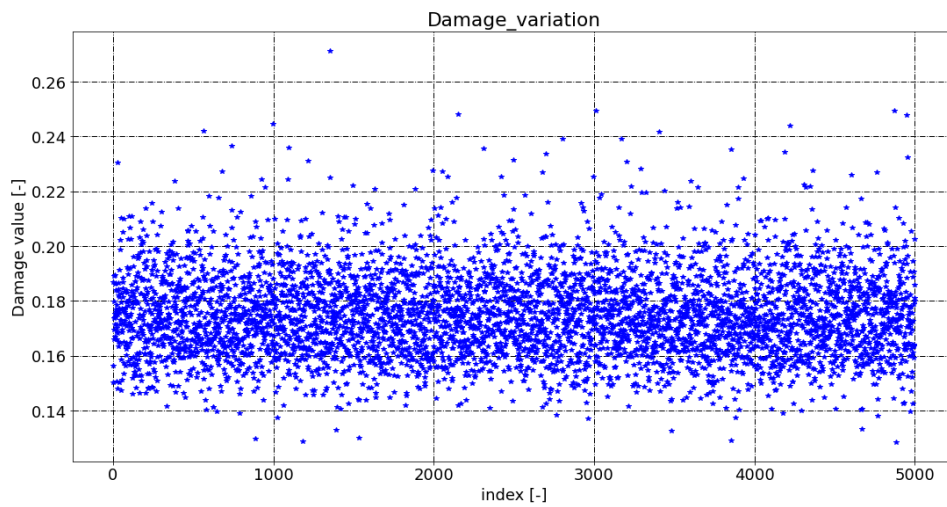


Figure 6-15 Damage values for the searched population for the white noise signal, with a signal clipped at 5 standard deviations block size  $N=2^{14}$

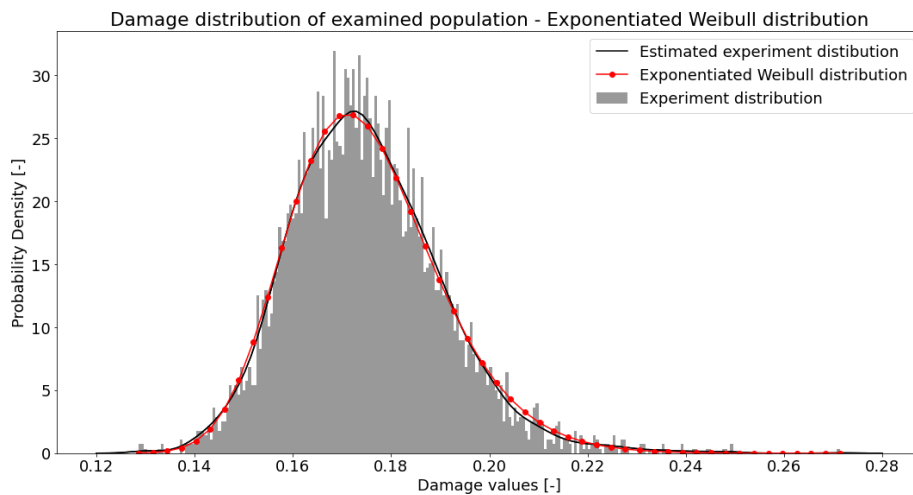


Figure 6-16 The best fitted distribution for damage values for the searched population for the white noise signal, with a signal clipped at 5 standard deviations, block size  $N=2^{14}$  – Exponentiated Weibull distribution

Distribution type	Distribution fitting probability [-]	Mean damage [-]	Standard deviation of damage [-]	0.13% of samples not lower than the quoted value of damage [-]	99.73% of samples not higher than the quoted value of damage [-]
Normal	0.00000	0.17498	0.01547	0.12840	0.21801
Exponentiated Weibull	0.68282	0.17495	0.01541	0.13748	0.22694
Generalised Extreme Value	0.07246	0.17512	0.01576	0.13901	0.22855

Table 6-6 Statistical parameters for a white noise signal clipped at 5 standard deviations, block size  $N=2^{14}$

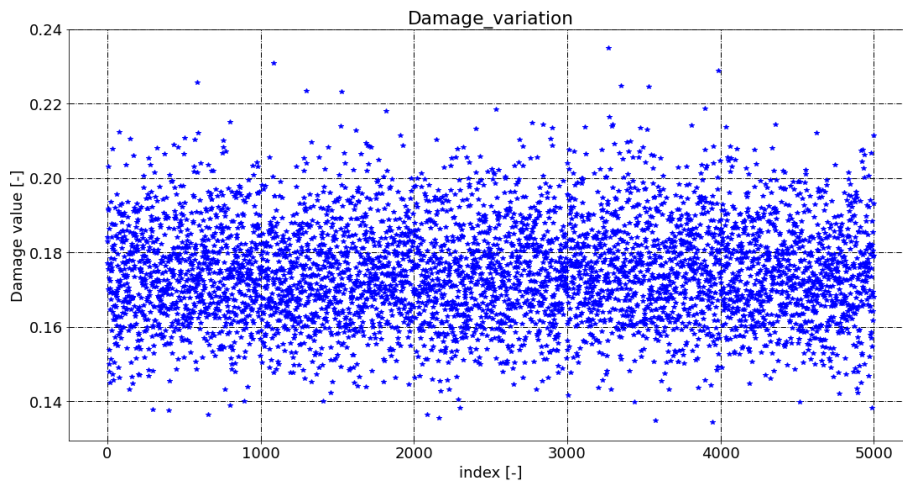


Figure 6-17 Damage values for the searched population for the white noise signal, with a signal clipped at 5 standard deviations, block size  $N=2^{16}$

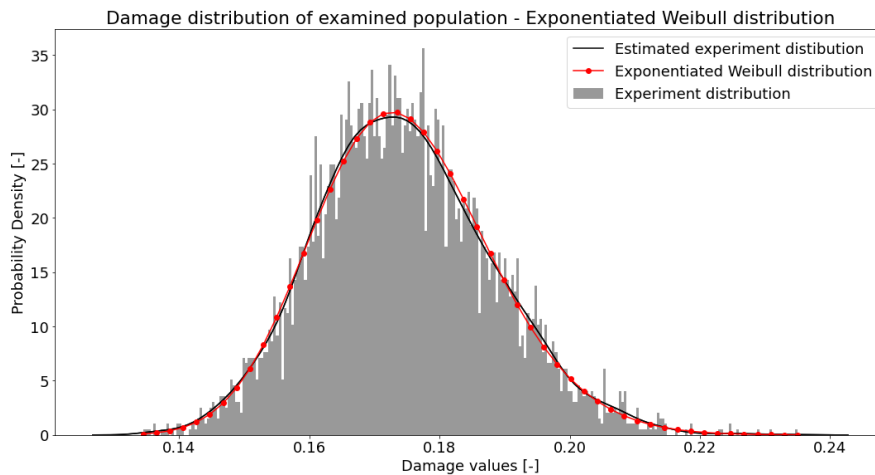


Figure 6-18 The best fitted distribution for damage values for the searched population for the white noise signal, with a signal clipped at 3 standard deviations, block size  $N=2^{16}$  – Exponentiated Weibull distribution

Distribution type	Distribution fitting probability [-]	Mean damage [-]	Standard deviation of damage [-]	0.13% of samples not lower than the quoted value of damage [-]	99.73% of samples not higher than the quoted value of damage [-]
Normal	0.00193	0.17462	0.01354	0.13384	0.21230
Exponentiated Weibull	0.83692	0.17463	0.01354	0.13902	0.21650
Generalised Extreme Value	0.52516	0.17467	0.01370	0.14047	0.21627

Table 6-7 Statistical parameters for a white noise signal clipped at 5 standard deviations, block size  $N=2^{16}$

### 6.5.2 Wide band random signal analysis

Research for the wide band signal introduced 3 different block sizes:  $2^{12}$ ,  $2^{14}$  and  $2^{16}$ . The Kolmogorov-Smirnov criterium, which assesses the probability of a distribution, was used for fitting the distribution. Different distribution types available in the Python library [62] were used for testing. The best fitted distributions were narrowed down to 3 with the highest probability of fitting: Gaussian, Exponentiated Weibull and Generalised Extreme Value distributions.

It is worth noting that the mean value of damage is quoted in Table 6-8 through Table 6-13 and 0.13% (taken -3 standard deviation in Gaussian distribution as a base) of the population has no lower damage and 9.73% (taken -3 standard deviation in Gaussian distribution as a base) of the population has no higher damage.

In Figure 6-19, Figure 6-21 and Figure 6-23 the corresponding damage values are presented for the searched population for the wide band signal for the 3 mentioned block sizes, for a signal clipped at 3 standard deviations. Per analogy the same results for a signal clipped at 5 standard deviations are presented in Figure 6-25, Figure 6-27 and Figure 6-29.

The best fitted distribution visualisation for a signal clipped at 3 standard deviations for the 3 block sizes are presented in Figure 6-20, Figure 6-22 and Figure 6-24. Per analogy, the results for a signal clipped at 5 standard deviations are presented in Figure 6-26, Figure 6-28 and Figure 6-30.

Table 6-8 through Table 6-10 present a populational research results summary for a white noise signal clipped at 3 standard deviations, and Table 6-11 through Table 6-13 show a summary of results for a signal clipped at 5 standard deviations.

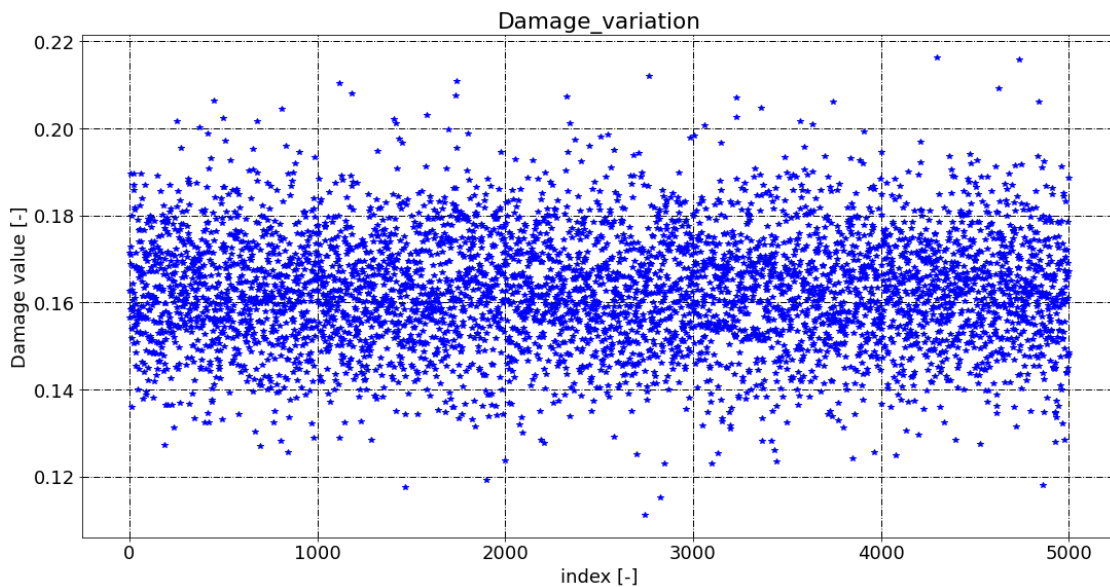


Figure 6-19 Damage values for the searched population for the wide band signal, with a signal clipped at 3 standard deviations, block size  $N=2^{12}$

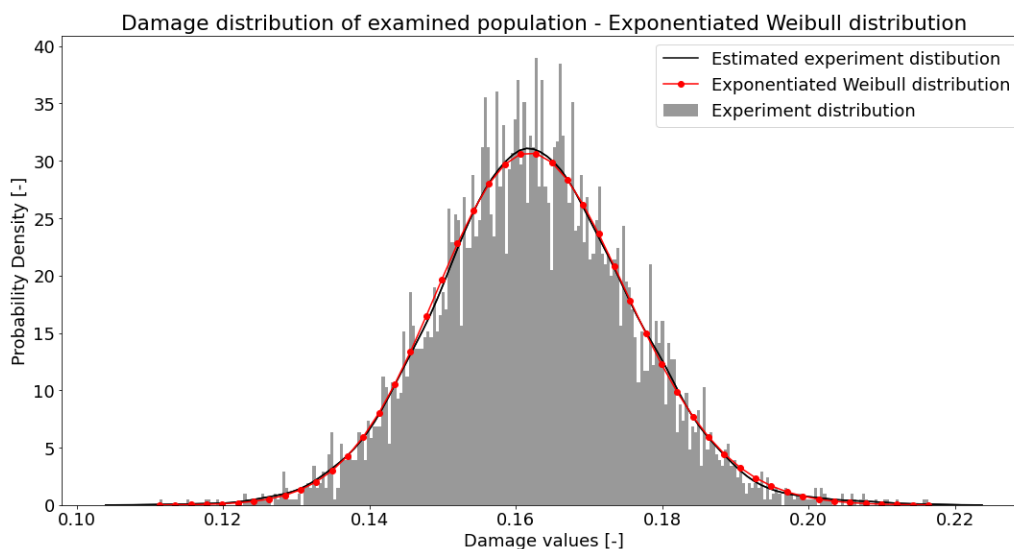


Figure 6-20 The best fitted distribution for damage values for the searched population for the wide band signal, with a signal clipped at 3 standard deviations, block size  $N=2^{12}$  – Exponentiated Weibull distribution

Distribution type	Probability of the fitted distribution [-]	Mean damage [-]	Standard deviation of damage [-]	0.13% not lower than the quoted value of damage [-]	99.73% not exceeding the quoted value of damage [-]
Normal	0.29958	0.16262	0.01308	0.12324	0.19900
Exponentiated Weibull	0.78456	0.16261	0.01308	0.12452	0.20055
Generalised Extreme Value	0.00821	0.16273	0.01346	0.12774	0.20147

Table 6-8 Statistical parameters for a wide band signal clipped at 3 standard deviations, block size  $N=2^{12}$

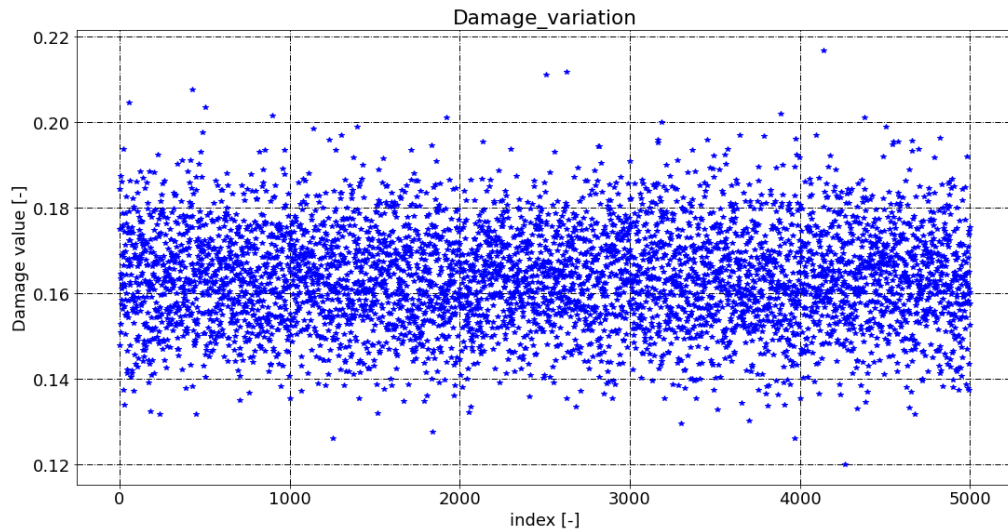


Figure 6-21 Damage values for the searched population for the wide band signal, with a signal clipped at 3 standard deviations, block size  $N=2^{14}$

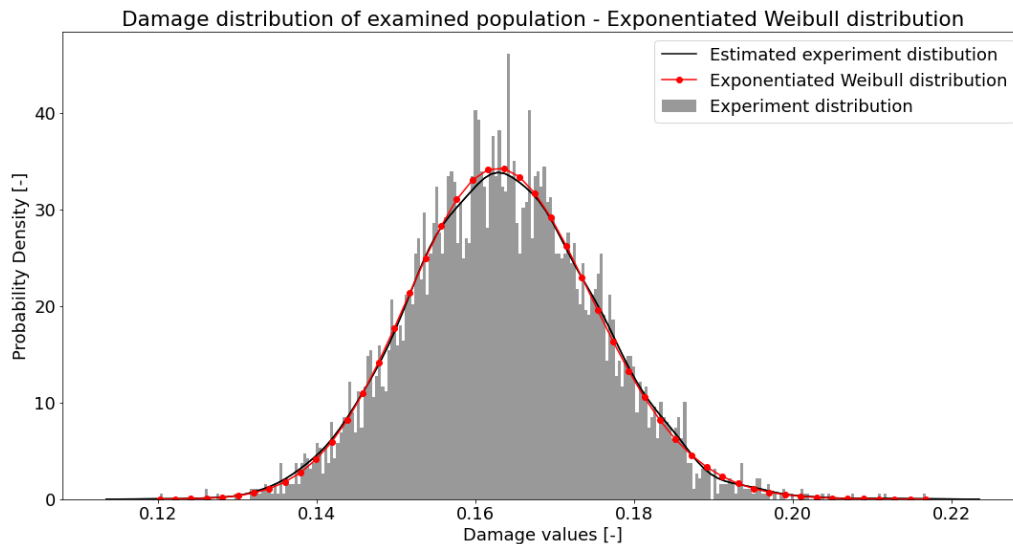


Figure 6-22 The best fitted distribution for damage values for the searched population for the wide band signal, with a signal clipped at 3 standard deviations, block size  $N=2^{14}$  – Exponentiated Weibull distribution

Distribution type	Probability of the fitted distribution [-]	Mean damage [-]	Standard deviation of damage [-]	0.13% not lower than the quoted value of damage [-]	99.73% not exceeding the quoted value of damage [-]
Normal	0.47102	0.16359	0.01166	0.12789	0.19635
Exponentiated Weibull	0.94591	0.16355	0.01164	0.12845	0.19709
Generalised Extreme Value	0.01435	0.16367	0.01200	0.13121	0.19658

Table 6-9 Statistical parameters for a wide band signal clipped at 3 standard deviations  $N=2^{14}$

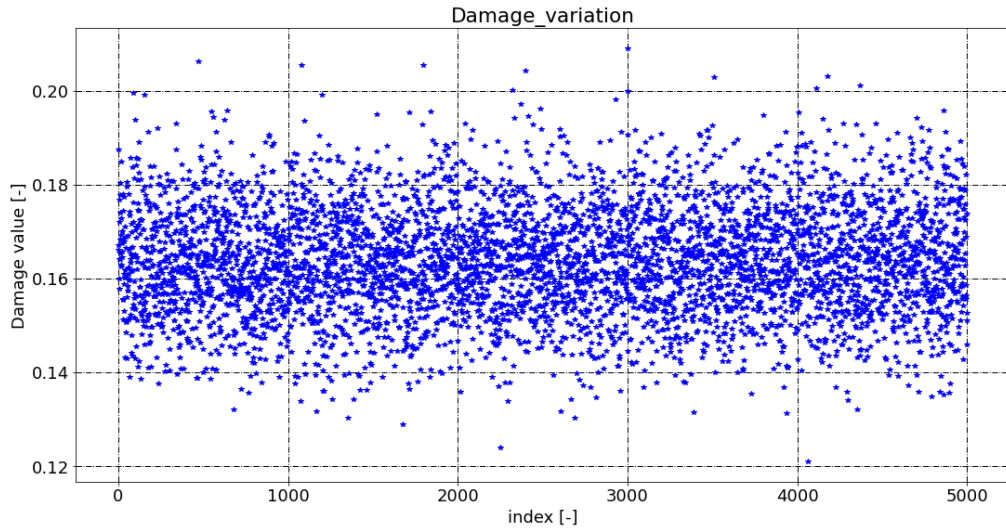


Figure 6-23 Damage values for the searched population for the wide band signal, with a signal clipped at 3 standard deviations, block size  $N=2^{16}$

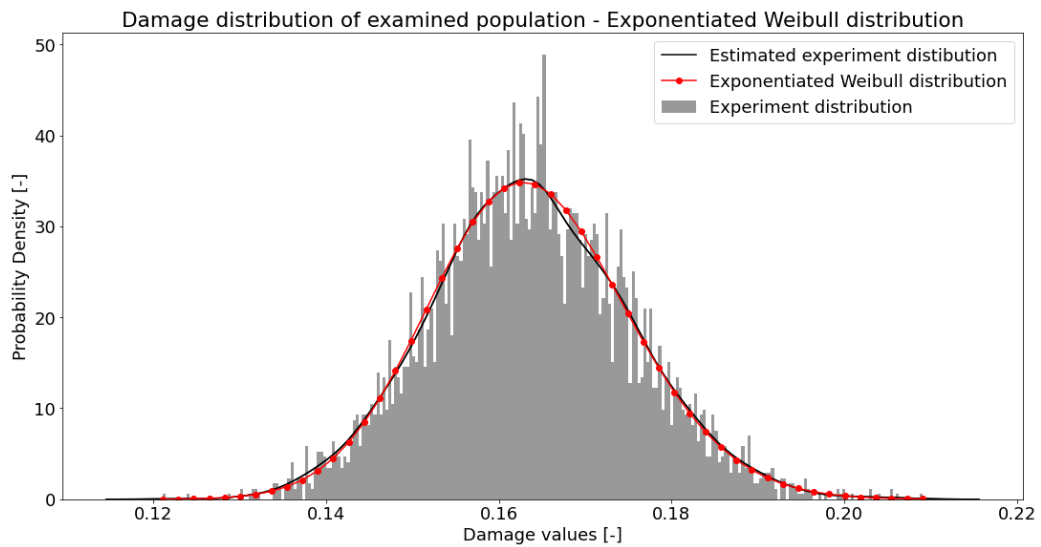


Figure 6-24 The best fitted distribution for damage values for the searched population for the wide band signal, with a signal clipped at 3 standard deviations, block size  $N=2^{16}$  – Exponentiated Weibull distribution

Distribution type	Probability of the fitted distribution [-]	Mean damage [-]	Standard deviation of damage [-]	0.13% not lower than the quoted value of damage [-]	99.73% not exceeding the quoted value of damage [-]
Normal	0.04568	0.16371	0.01150	0.12907	0.19572
Exponentiated Weibull	0.79828	0.16370	0.01151	0.13097	0.19755
Generalised Extreme Value	0.11025	0.16377	0.01169	0.13317	0.19711

Table 6-10 Statistical parameters for a wide band signal clipped at 3 standard deviations  $N=2^{16}$

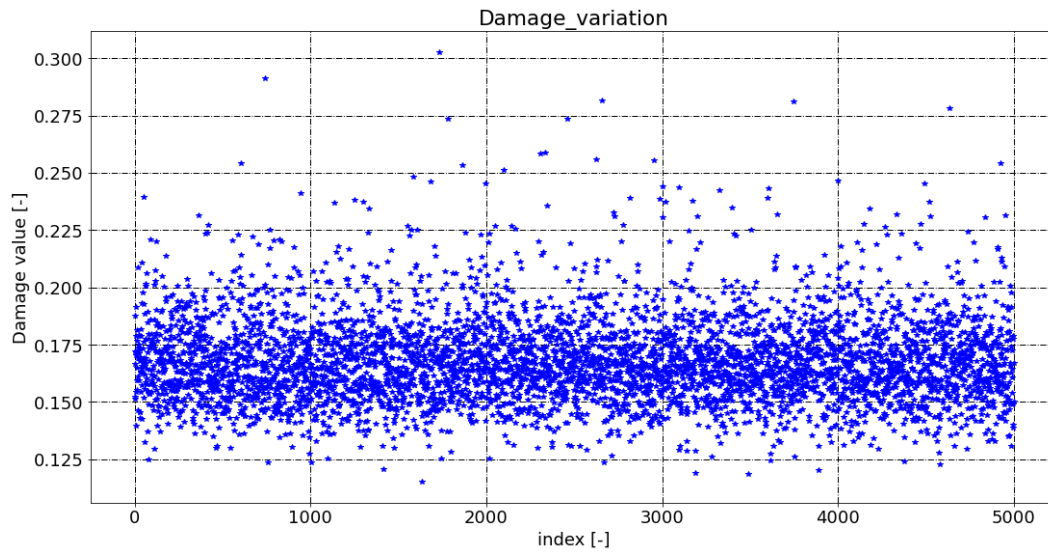


Figure 6-25 Damage values for the searched population for the wide band signal, with a signal clipped at 5 standard deviations, block size  $N=2^{12}$

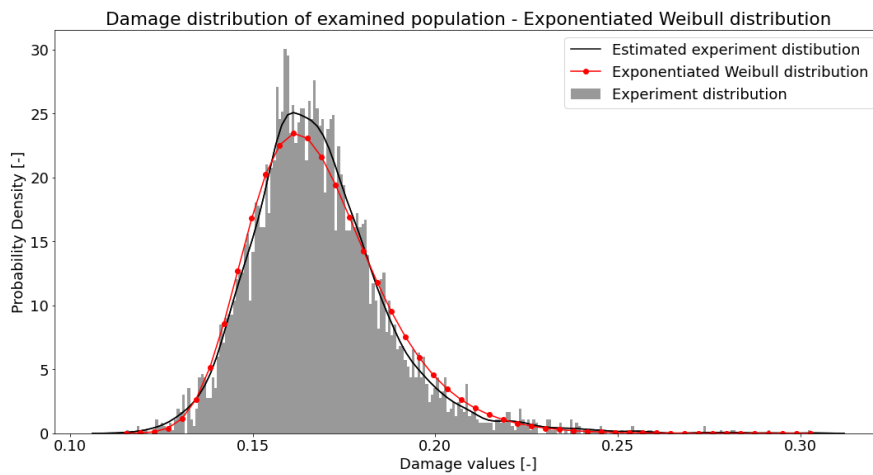


Figure 6-26 The best fitted distribution for damage values for the searched population for the wide band signal, with a signal clipped at 5 standard deviations, block size  $N=2^{12}$  – Exponentiated distribution

Distribution type	Probability of the fitted distribution [-]	Mean damage [-]	Standard deviation of damage [-]	0.13% not lower than the quoted value of damage [-]	99.73% not exceeding the quoted value of damage [-]
Normal	0.00000	0.16800	0.01872	0.11161	0.22009
Exponentiated Weibull	0.00125	0.16808	0.01842	0.12710	0.23543
Generalised Extreme Value	0.00015	0.16820	0.01883	0.12819	0.23822

Table 6-11 Statistical parameters for a wide band signal clipped at 5 standard deviations, block size  $N=2^{12}$

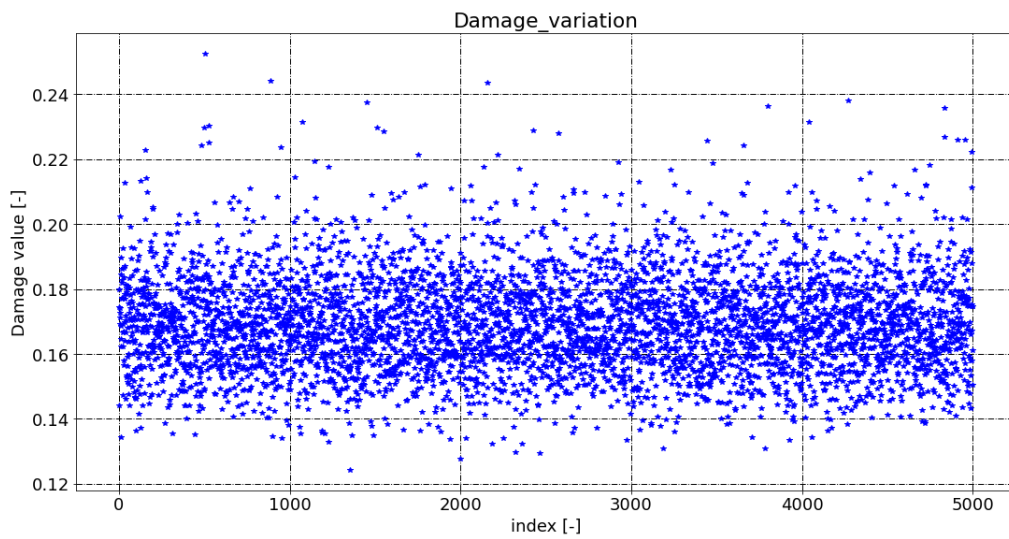


Figure 6-27 Damage values for the searched population for the wide band signal, with a signal clipped at 5 standard deviations, block size  $N=2^{14}$

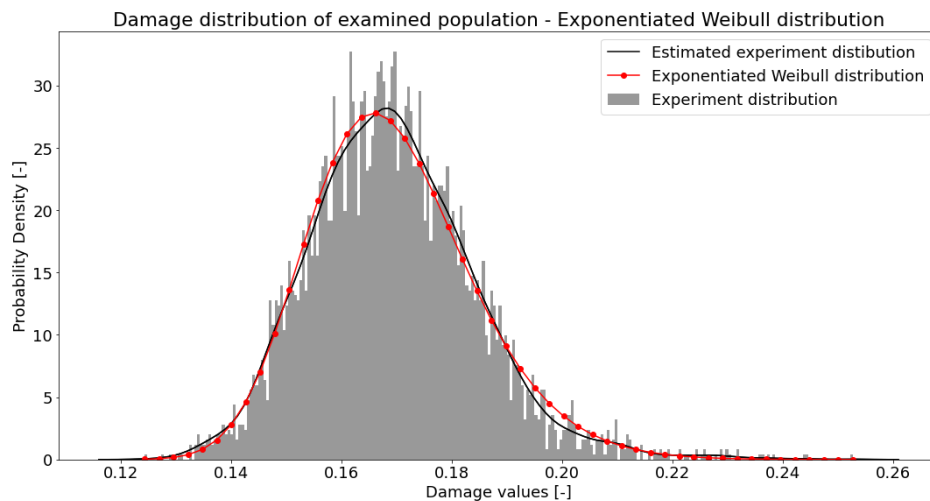


Figure 6-28 The best fitted distribution for damage values for the searched population for the wide band signal, with a signal clipped at 5 standard deviations, block size  $N=2^{14}$  – Exponentiated Weibull distribution

Distribution type	Probability of the fitted distribution [-]	Mean damage [-]	Standard deviation of damage [-]	0.13% not lower than the quoted value of damage [-]	99.73% not exceeding the quoted value of damage [-]
Normal	0.00003	0.16934	0.01492	0.12440	0.21086
Exponentiated Weibull	0.23695	0.16936	0.01490	0.13266	0.21921
Generalised Extreme Value	0.02024	0.16947	0.01521	0.13422	0.22032

Table 6-12 Statistical parameters for a wide band signal clipped at 5 standard deviations, block size  $N=2^{14}$

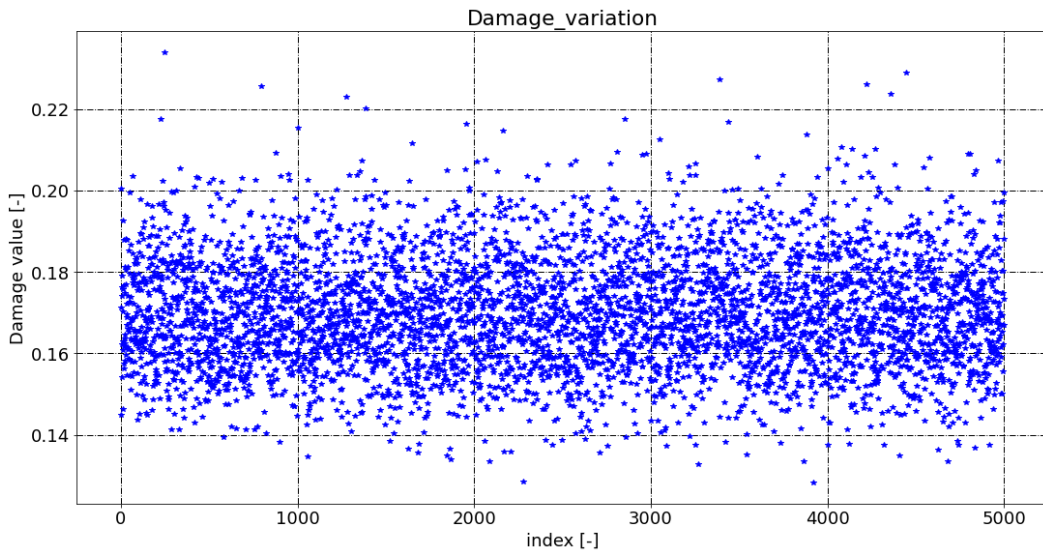


Figure 6-29 Damage values for the searched population for the wide band signal, with a signal clipped at 5 standard deviations, block size  $N=2^{16}$

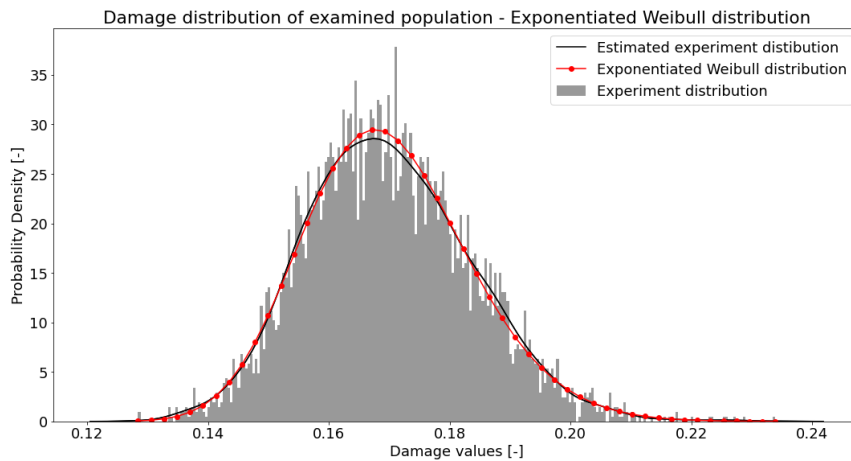


Figure 6-30 The best fitted distribution for damage values for the searched population for the wide band signal, with a signal clipped at 3 standard deviations, block size  $N=2^{16}$  – Exponentiated Weibull distribution

Distribution type	Probability of the fitted distribution [-]	Mean damage [-]	Standard deviation of damage [-]	0.13% not lower than the quoted value of damage [-]	99.73% not exceeding the quoted value of damage [-]
Normal	0.00133	0.16994	0.01369	0.12870	0.20804
Exponentiated Weibull	0.95236	0.16990	0.01370	0.13447	0.21289
Generalised Extreme Value	0.53781	0.17000	0.01389	0.13581	0.21295

Table 6-13 Statistical parameters for a wide band signal clipped at 5 standard deviations, block size  $N=2^{16}$

### 6.5.3 Narrow Band random signal analysis

Research for the narrow band signal introduced 3 different block sizes:  $2^{12}$ ,  $2^{14}$  and  $2^{16}$ . The Kolmogorov-Smirnov criterium, which assesses the probability of a distribution, was used for fitting the distribution. Different distribution types available in the Python library [62] were used for testing. The best fitted distributions were narrowed down to 3 with the highest probability of fitting: Gaussian, Exponentiated Weibull and Generalised Extreme Value distributions.

It is worth noting that mean the value of damage is presented in Table 6-14 through Table 6-19 and 0.13% (taken -3 standard deviation in Gaussian distribution as a base) of the population has no lower damage and 9.73% (taken -3 standard deviation in Gaussian distribution as a base) of the population has no higher damage.

In Figure 6-31, Figure 6-33 and Figure 6-35, the corresponding damage values are presented for the searched population for the white noise signal for the 3 mentioned block sizes for a signal clipped at 3 standard deviations. Per analogy the same results for a signal clipped at 5 standard deviations is presented in Figure 6-37, Figure 6-39 and Figure 6-41.

The best fitted distribution visualisation for a signal clipped at 3 standard deviations for the 3 block sizes is presented in Figure 6-32, Figure 6-34 and Figure 6-36. Per analogy results for a signal clipped at 5 standard deviations are presented in Figure 6-38, Figure 6-40 and Figure 6-42.

Table 6-14 through Table 6-16 present a populational research results summary made for a white noise signal clipped at 3 standard deviations, and Table 6-17 through Table 6-19 show a summary of results for a signal clipped at 5 standard deviations.

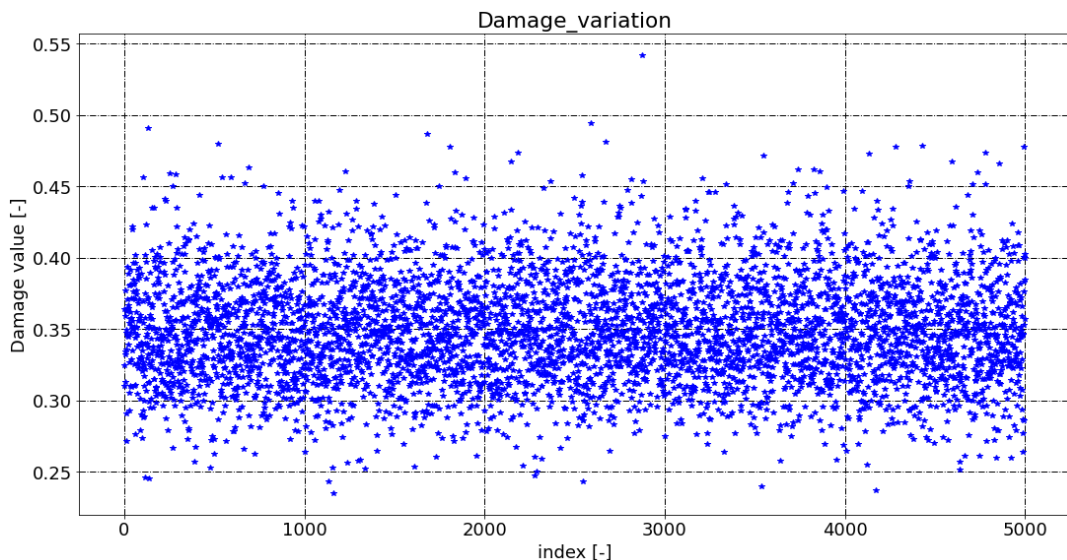


Figure 6-31 Damage values for the searched population for the narrow band signal, with a signal clipped at 3 standard deviations, block size  $N=2^{12}$

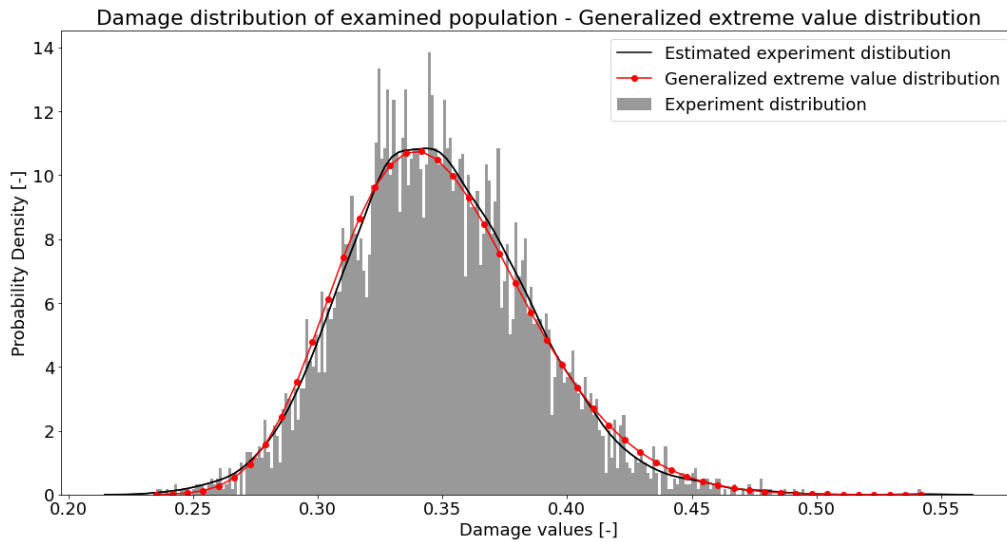


Figure 6-32 The best fitted distribution for damage values for the searched population for the narrow band signal, with a signal clipped at 3 standard deviations, block size  $N=2^{12}$  – Generalised Extreme Value distribution

Distribution type	Probability of the fitted distribution [-]	Mean damage [-]	Standard deviation of damage [-]	0.13% not lower than the quoted value of damage [-]	99.73% not exceeding the quoted value of damage [-]
Normal	0.00083	0.34861	0.03687	0.23757	0.45120
Exponentiated Weibull	0.00000	0.33173	0.07133	0.23564	0.60820
Generalised Extreme Value	0.03591	0.34886	0.03767	0.25722	0.46721

Table 6-14 Statistical parameters for a narrow band signal clipped at 3 standard deviations, block size  $N=2^{12}$

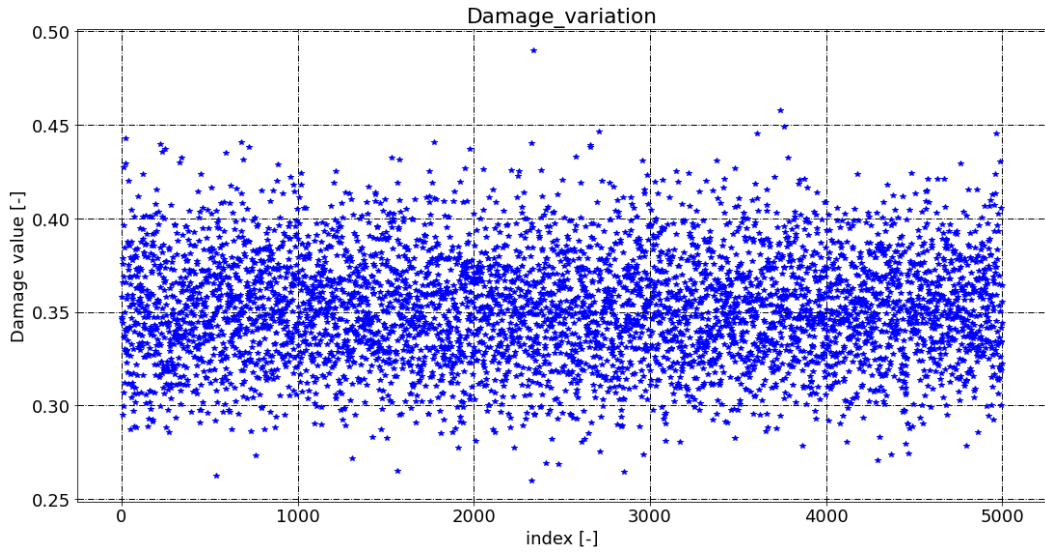


Figure 6-33 Damage values for the searched population for the narrow band signal, with a signal clipped at 3 standard deviations, block size  $N=2^{14}$

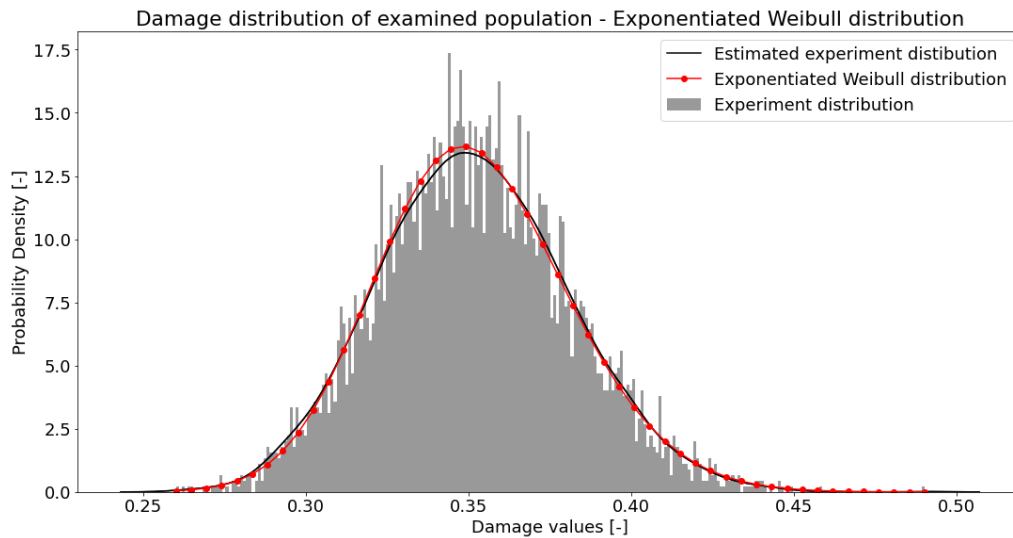


Figure 6-34 The best fitted distribution for damage values for the searched population for the narrow band signal, with a signal clipped at 3 standard deviations, block size  $N=2^{14}$  – Exponentiated Weibull distribution

Distribution type	Probability of the fitted distribution [-]	Mean damage [-]	Standard deviation of damage [-]	0.13% not lower than the quoted value of damage [-]	99.73% not exceeding the quoted value of damage [-]
Normal	0.22580	0.35176	0.02916	0.26395	0.43289
Exponentiated Weibull	0.96216	0.35188	0.02948	0.27058	0.44086
Generalised Extreme Value	0.05754	0.35192	0.02992	0.27664	0.44180

Table 6-15 Statistical parameters for a narrow band signal clipped at 3 standard deviations  $N=2^{14}$

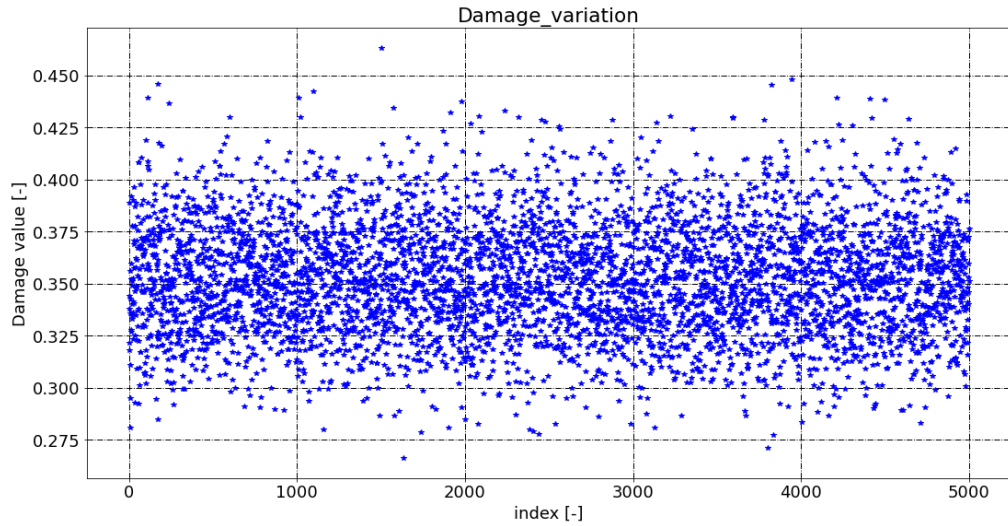


Figure 6-35 Damage values for the searched population for the narrow band signal, with a signal clipped at 3 standard deviations, block size  $N=2^{16}$

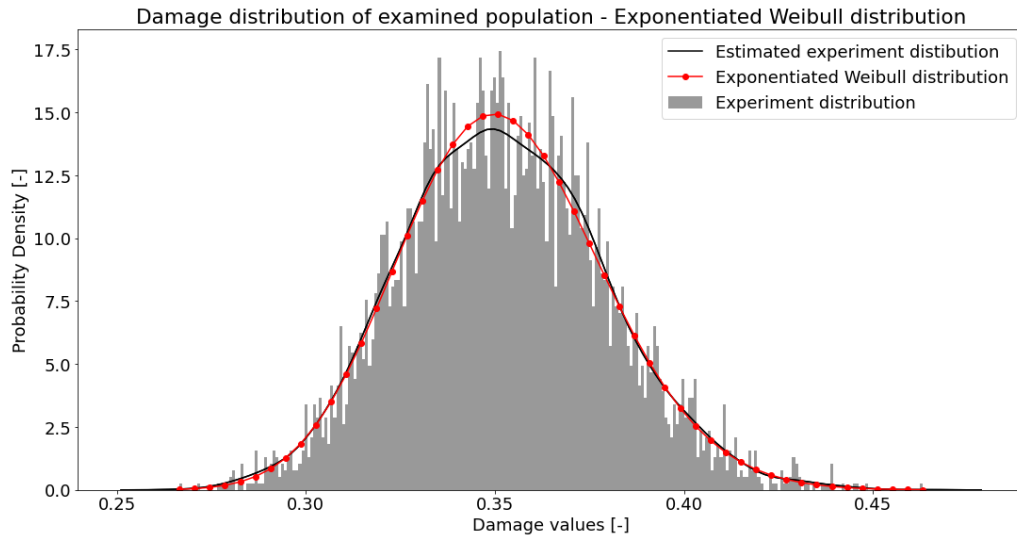


Figure 6-36 The best fitted distribution for damage values for the searched population for the narrow band signal, with a signal clipped at 3 standard deviations, block size  $N=2^{16}$  – Exponentiated Weibull distribution

Distribution type	Probability of the fitted distribution [-]	Mean damage [-]	Standard deviation of damage [-]	0.13% not lower than the quoted value of damage [-]	99.73% not exceeding the quoted value of damage [-]
Normal	0.11812	0.35225	0.02672	0.27180	0.42658
Exponentiated Weibull	0.86662	0.35226	0.02672	0.27958	0.43174
Generalised Extreme Value	0.38807	0.35234	0.02706	0.28253	0.43104

Table 6-16 Statistical parameters for a narrow band signal clipped at 3 standard deviations  $N=2^{16}$

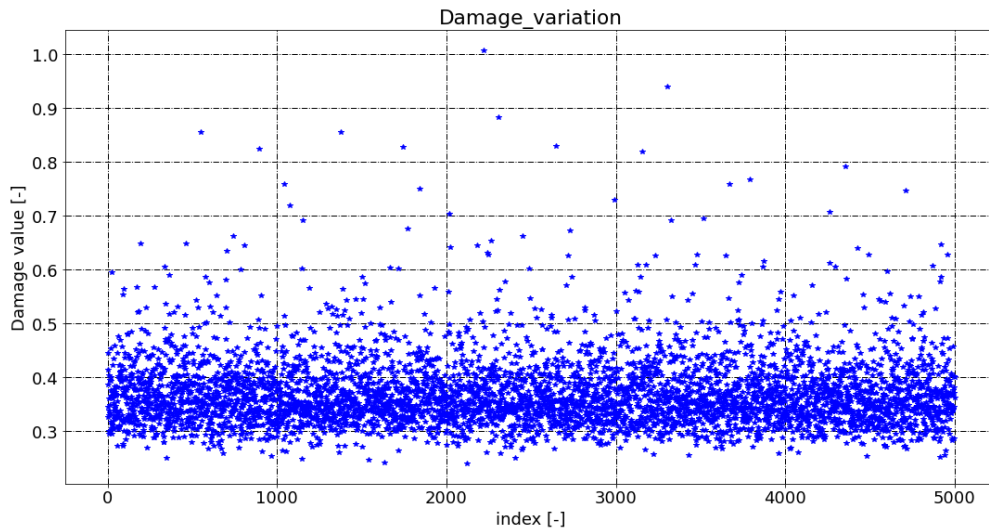


Figure 6-37 Damage values for the searched population for the narrow band signal, with a signal clipped at 5 standard deviations, block size  $N=2^{12}$

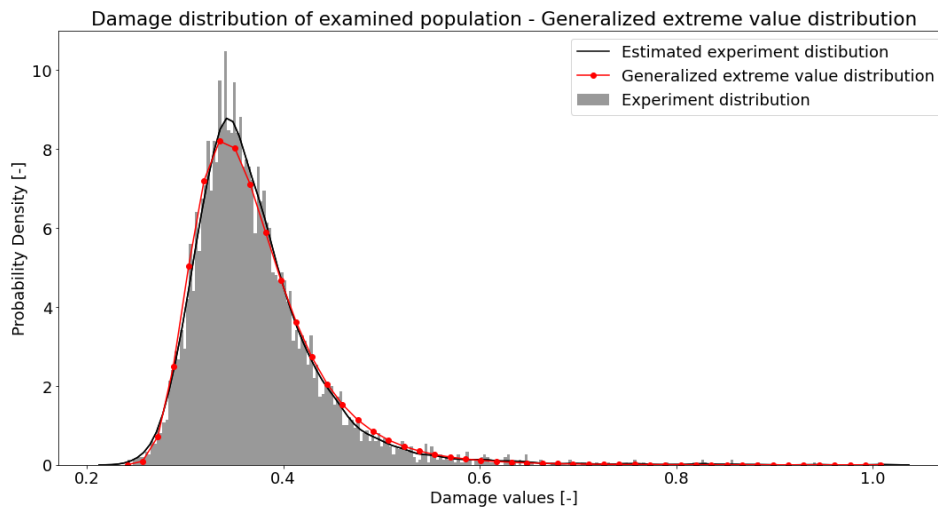


Figure 6-38 The best fitted distribution for damage values for the searched population for the narrow band signal, with a signal clipped at 5 standard deviations, block size  $N=2^{12}$  – Generalised Extreme Value distribution

Distribution type	Probability of the fitted distribution [-]	Mean damage [-]	Standard deviation of damage [-]	0.13% not lower than the quoted value of damage [-]	99.73% not exceeding the quoted value of damage [-]
Normal	0.00000	0.37092	0.06488	0.17315	0.55046
Exponentiated Weibull	0.02536	0.37100	0.06116	0.23792	0.57440
Generalised Extreme Value	0.05581	0.37100	0.06214	0.25992	0.64275

Table 6-17 Statistical parameters for a narrow band signal clipped at 5 standard deviations, block size  $N=2^{12}$

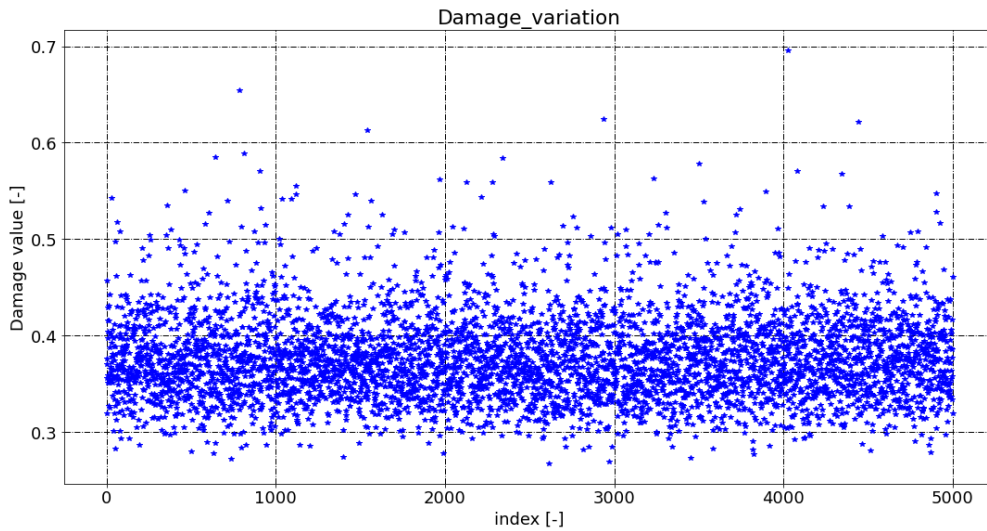


Figure 6-39 Damage values for the searched population for the narrow band signal, with a signal clipped at 5 standard deviations, block size  $N=2^{14}$

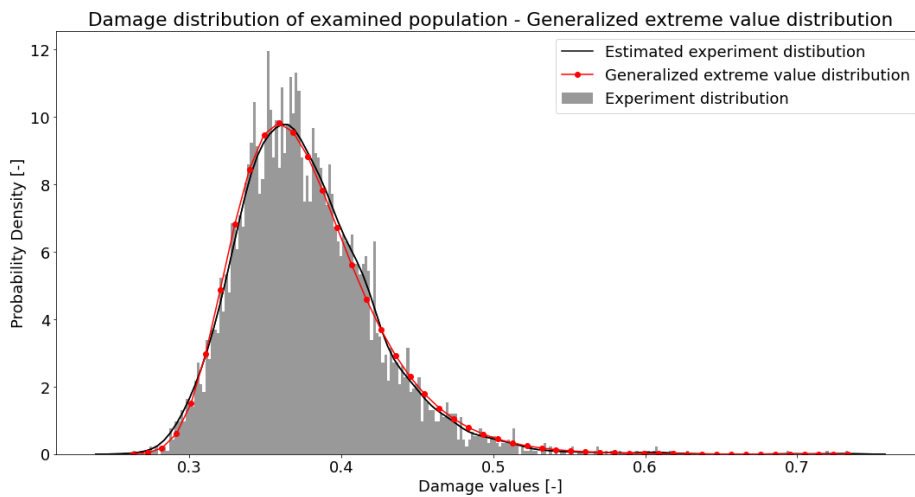


Figure 6-40 The best fitted distribution for damage values for the searched population for the narrow band signal, with a signal clipped at 5 standard deviations, block size  $N=2^{14}$  – Generalised Extreme Value Distribution

Distribution type	Probability of the fitted distribution [-]	Mean damage [-]	Standard deviation of damage [-]	0.13% not lower than the quoted value of damage [-]	99.73% not exceeding the quoted value of damage [-]
Normal	0.00000	0.37690	0.04532	0.24042	0.50299
Exponentiated Weibull	0.00000	0.38449	0.05469	0.26607	0.51474
Generalised Extreme Value	0.15329	0.37714	0.04549	0.28295	0.55160

Table 6-18 Statistical parameters for a narrow band signal clipped at 5 standard deviations, block size  $N=2^{14}$

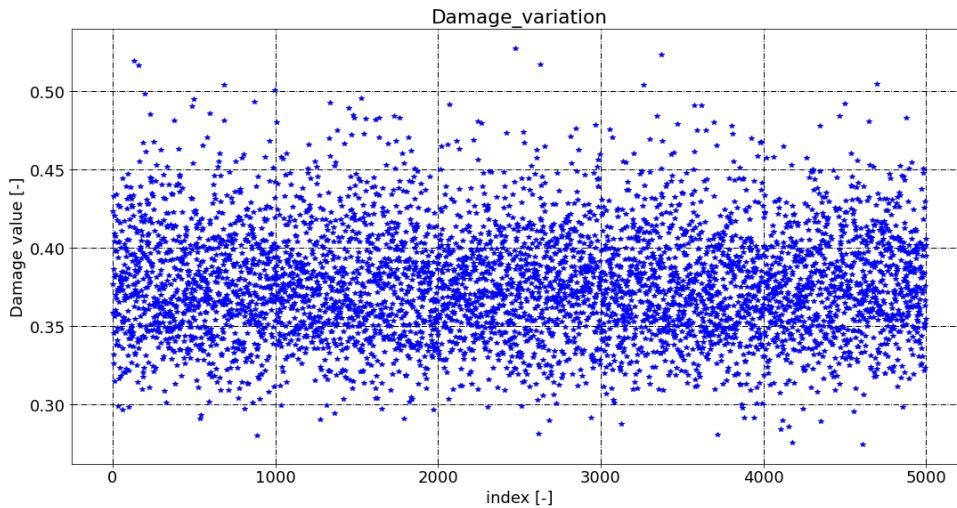


Figure 6-41 Damage values for the searched population for the narrow band signal, with a signal clipped at 5 standard deviations, block size  $N=2^{16}$

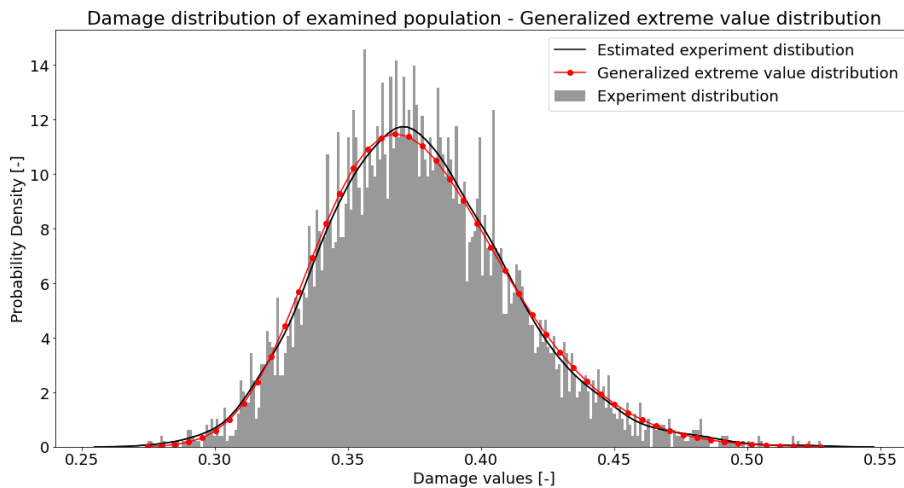


Figure 6-42 The best fitted distribution for damage values for the searched population for the narrow band signal, with a signal clipped at 3 standard deviations, block size  $N=2^{16}$  – Generalised Extreme Value Distribution

Distribution type	Probability of the fitted distribution [-]	Mean damage [-]	Standard deviation of damage [-]	0.13% not lower than the quoted value of damage [-]	99.73% not exceeding the quoted value of damage [-]
Normal	0.00003	0.37701	0.03514	0.27120	0.47476
Exponentiated Weibull	0.14226	0.37657	0.03452	0.27863	0.47898
Generalised Extreme Value	0.39537	0.37714	0.03539	0.29151	0.48909

Table 6-19 Statistical parameters for a narrow band signal clipped at 5 standard deviations, block size  $N=2^{16}$

#### 6.5.4 Summary and conclusions for the new proposed method

A summary of the conducted computer experiments using two combined methods: FEM, the Monte Carlo method and Python programming allows to identify the high conservatism of the legacy frequency domain-based method. Research results presented in this paper show that the legacy method used by commercial software for combined stochastic-deterministic loading scenario gives high conservative damage results, which can result in oversizing military aircraft or helicopter units and any other unit exposed to this load scenario.

The introduction of a new method of calculating damage (based on the combined frequency and time approach) in the aforementioned loading scenario allows for precise damage estimation in the time domain while keeping the efficiency benefit related to the frequency domain calculation (as the base for the time domain calculation is the result of a linear dynamic harmonic analysis). The novel method introduced in this paper allows to obtain more accurate results than the legacy method and as high efficiency of computation as with the legacy method.

The research results reveal that the damage variation decreases when the block size in IFFT increases (the same phenomena as quoted in related research [68] and Chapter 5 of this paper for only stochastic loading). The novel method also allows for analysis of the time series population to assess the damage variation, which is impossible using the legacy method. An additional conclusion is that for the populational analysis it is recommended to use the best fitted distribution from the three selected during the research (see Table 6-2 through Table 6-19; Figure 6-8, Figure 6-10, Figure 6-12, Figure 6-14, Figure 6-16 and Figure 6-18 for white noise signal; Figure 6-20, Figure 6-22, Figure 6-24, Figure 6-14, Figure 6-16 and Figure 6-18 for the wide band signal; Figure 6-32, Figure 6-34, Figure 6-36 Figure 6-38, Figure 6-40 and Figure 6-42 for the narrow band signal): Exponentiated Weibull, Generalised Extreme Value and Gaussian distributions for statistical consideration for all cases where a signal is clipped at three and five standard deviations for the white noise, wide band, and narrow band signal.

An additional benefit related to using the proposed method is that a signal can be clipped with a requested standard deviation level, e.g., in the aerospace industry it is common to clip the input to 3 standard deviations. Therefore, this method can replicate real test conditions, which is not possible using the spectral method.

Another aspect is that the algorithm can also be fitted to align with the frequency resolution (block size) during a real test to assess the variability of damage to the test rig equipment. As for a block size smaller than  $N=2^{14}$ , the variability could increase, which would imply under testing.

Additionally, equation Eq. 5.3 should also be met for this loading scenario, with the exception that value of the  $\log_2(N)$  might be lower than 20 if we observe a low damage variation for the lower value of block size – this is only to reduce the cost of the computation.

## CHAPTER 7 USAGE DEVELOPED ALGORITHMS FOR VIBRATION DAMAGE PREDICTION OF AIRCRAFT TRANSMISSION SHAFTS

This chapter introduces an assessment of the impact of the dynamic load at an exemplary transmission shaft. For these purposes tools and algorithms used for vibration damage assessment under stochastic loading and combined loading (stochastic and deterministic) are presented and expanded in Chapter 3 through Chapter 6. Legacy methods (used by commercial software, e.g., MSC CAE Fatigue) were used for the analysis, which were then compared against a modified legacy method (e.g., the Narrow Band and Lalanne method) or a new method was developed from scratch – Chapter 6 presents a new method for vibration damage assessment using combined time and frequency domains. The analysis provided in this section aims to demonstrate the developed methods on the example of a transmission shaft.

### 7.1 The transmission shaft geometry model and discrete model description

Figure 7-1 shows a simplified shaft geometry, which replicates the dynamic characteristics of a real transmission shaft. It should be noted that simplified geometry was used also to avoid sharing any confidential technical company data.

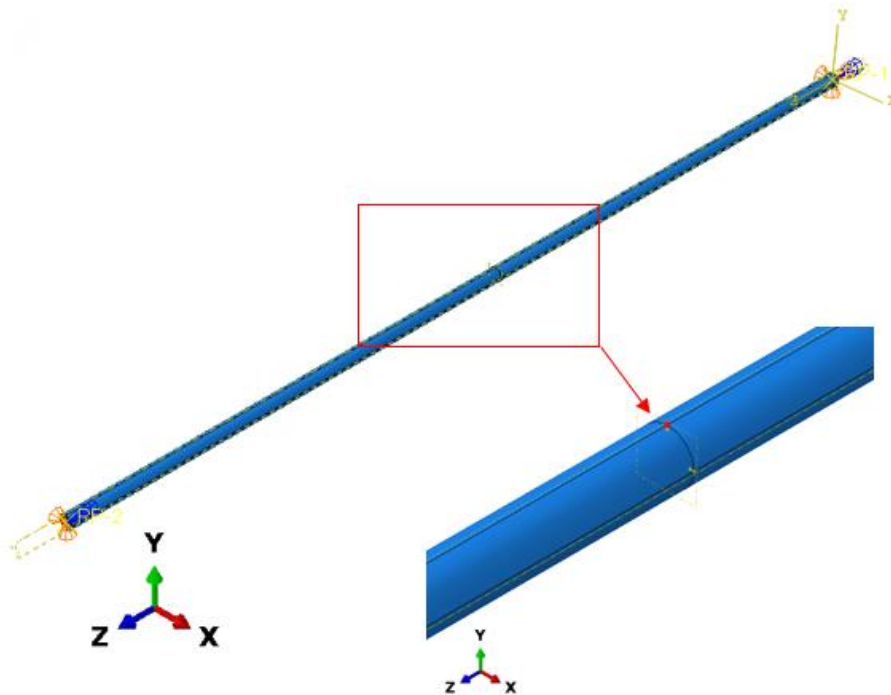


Figure 7-1 Transmission shaft simplified geometry and graphical representation of the control point and boundary condition

The shaft was simplified to just a tube, with the end fitting not modelled – it is worth noting that the resonance characteristics for simplified assembly had a good correlation with the test results. Additionally, the simplified model is used to provide information about the impact of the dynamic load on shaft itself – the end fitting is not part of the consideration to reduce the task size.

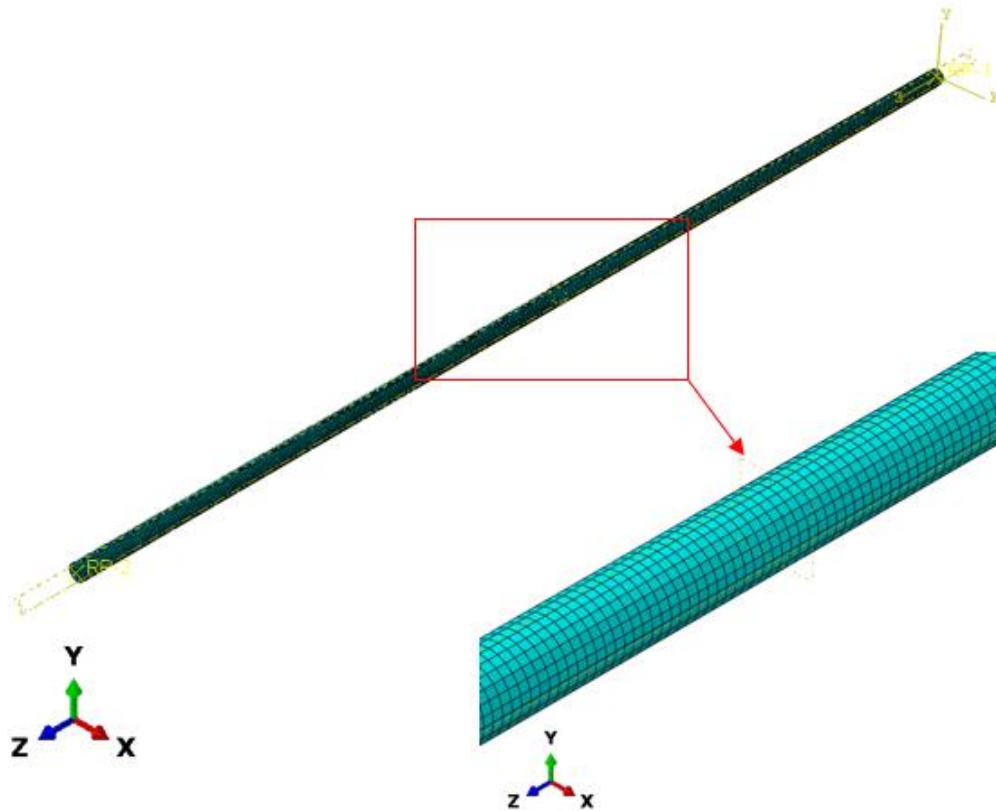


Figure 7-2 Discrete model, element C3D8R, 8-nodes linear brick, reduced integration

Figure 7-2 shows a discrete model of the considered transmission shaft. The quadratic shape function of the element prevents the shear locking phenomena that can occur in linear elements with full integration and can therefore replicate the resonance characteristic stress in the considered area. Using linear function element with full integration can help obtain equivalent Huber-Mises-Hencky stress 94.38 MPa versus 93.38 MPa (as per Figure 7-3) for the quadratic element for the first most significant mode in the considered frequency bandwidth. Therefore, to build a discrete model we used 8-node brick hexagonal elements with a reduced integration shape function with to reduce the task size and demonstrate the results of the created algorithms. Using these elements allowed us to obtain resonance characteristics consistent with the test results, as shown in the following section`.

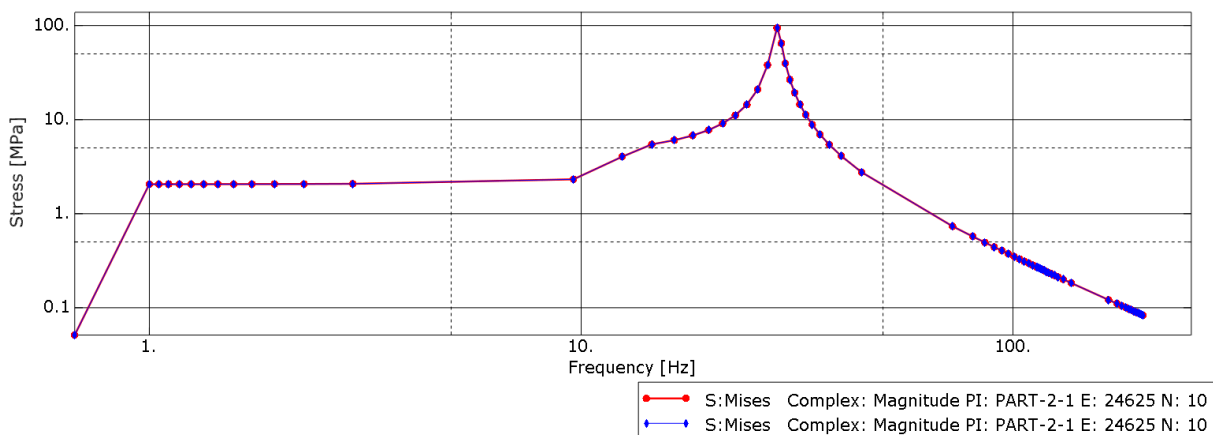


Figure 7-3 Red curve – the Huber-Mises-Hencky stress quadratic shape function, the blue curve Huber-Mises-Hencky stress linear shape function

## 7.2 Numerical environment correlation with test results

For the initial loop of correlation, we used the Half-Power Bandwidth method [70] to assess the critical damping value. After the first loop, the FEM model was tuned to obtain a matching resonance frequency and amplification level to the test results. The critical damping value for the obtained aligned response is 2.1%.

Figure 7-4 shows initial resonance characteristics real unit test results for the Y direction of the transmission shaft assembly.

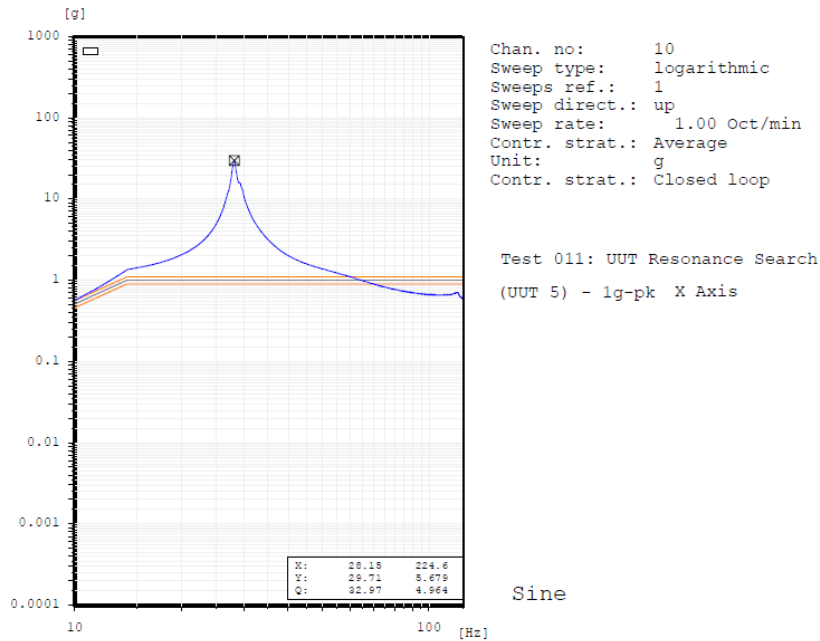


Figure 7-4 Test resonance characteristics of the transmission shaft

Note: The initial resonance search was made using a logarithmic sweep rate of 0.0167 octave/min.

Figure 7-5 shows the resonance characteristic obtained using the correlated FEM model in the Abaqus environment – resonance frequency and amplification differences in the FEM model are below 1% versus the test results.

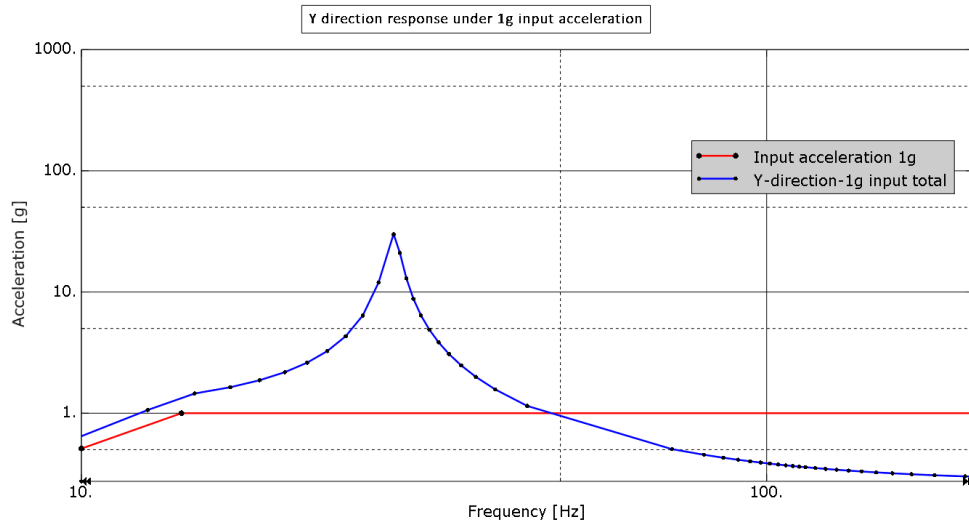


Figure 7-5 FEM resonance characteristics obtained from the correlated numerical environment (critical damping 2.1%)

### 7.3 Assessment of the impact of a stochastic dynamic load on an exemplary transmission shaft using the developed methods – damage estimation under stochastic loading

This section presents a vibration damage assessment of a transmission shaft under stochastic dynamic loading using a legacy approach – frequency domain damage estimation, and the proposed approach – combined frequency domain consideration. Additionally, we present the results for vibration damage estimation in the frequency domain using modification of the legacy methods introduced in this paper (e.g., modified Lalanne and Narrow Band methods or the new approach for integration spectral moments).

#### 7.3.1 Frequency domain damage estimation

For frequency domain damage estimation, we used the same material as in Chapter 3, however for  $K_t$  equals 1 (as the hot spot area is in the centre of the shaft – an area without stress concentration). The S–N curve of considered material is presented in Table 7-1 .

S-N curve definition steel 17-4PH (H1025)	
Cycles N [-]	Stress [MPa]
1.00E+02	1020
1.00E+03	845
1.00E+05	610
1.00E+06	479
1.00E+07	375
1.00E+08	307
1.00E+09	252
1.00E+10	206
4.97E+10	6

Table 7-1 The S-N curve definition for steel 17-4PH (H1025) [49]

Table 7-2 shows the PSD input curve for Loop 1 and Loop 2 in the case under consideration. Loop 1 in this case is the initial input for the frequency domain calculation, and combined frequency and time domain consideration. As the original theoretical PSD input\* implies that the PSD response signal is a narrow band signal for which modification of the legacy method proposed in this paper gives a similar result as for legacy methods (except Lalanne), we added new theoretical PSD input\* curve definition, which makes the PSD response signal a wide band signal. For the wide band signal the differences of the legacy approach for the signal statistic in the frequency domain and time domain increased – as shown in Chapter 5 of this paper.

\*It should be noted that the theoretical PSD input and new theoretical PSD input were selected to obtain a not negligible damage value, and for which the stress amplitudes are within the range of use of the stress life method. These theoretical PSD input curves are not consistent with the normative curve [2], [66], and are used only demonstration of the tools and algorithm created within this paper.

<b>PSD input curve definition Loop 1</b>	
Frequency [Hz]	PSD input [g <sup>2</sup> /Hz]
1	1.8
200	1.8
<b>PSD input curve definition Loop 2</b>	
Frequency [Hz]	PSD input [g <sup>2</sup> /Hz]
1	0.5
100	0.5
101	20
200	20

Table 7-2 PSD input curves for Loop 1 and Loop 2 of the considered vibration damage

Table 7-3 shows Loop 1 of the damage estimation in the frequency domain under consideration for the critical integration point of the element. The considered PSD curve and shaft transfer function obtained a narrow band PSD response signal, therefore based on the research presented in this paper the legacy method and the method with proposed modifications gives a close damage value (except Lalanne method). All the considered method – modified Lalanne, Dirlik and Narrow Band methods, give close damage results for the narrow band PSD response. The damage results evaluated in the frequency domain are close to the mean damage value estimated in the time domain using the Monte Carlo method – a PSD response with less than 10% differences for a signal clipped with 5 and 3 standard deviations.

It should be noted that the mean value of damage comes from the populational research presented in 7.3.2 of this paper.

Although the results for all the aforementioned methods give close results to the mean of the time series damage value, the deviation of damages need to be taken into account. This study is presented in section 7.3.2.

<b>Impact of stochastic dynamic loading on an exemplary transmission shaft Loop 1</b>			
<b>A signal clipped at five standard deviations</b>			
<b>Damage estimation method</b>	<b>Full integration</b>	<b>Reduced integration (77.5%)</b>	<b>Full integration/Reduced integration</b>
<b>Legacy Narrow Band</b>	0.110	0.108	1.02
<b>Proposed modified Narrow Band (replaced EP with E0)</b>	0.102	0.102	1.00
<b>Dirlik</b>	0.101	0.101	1.00
<b>Legacy Lalanne</b>	2.436E-06	1.868E-06	1.30
<b>Proposed modified Lalanne</b>	0.102	0.102	1.00
<b>Time domain mean damage value</b>	0.094		
<b>A signal clipped at three standard deviations</b>			
<b>Damage estimation method</b>	<b>Full integration</b>	<b>Reduced integration (77.5%)</b>	<b>Full integration/Reduced integration</b>
<b>Legacy Narrow Band</b>	0.036	0.036	1.02
<b>Proposed modified Narrow Band (replaced EP with E0)</b>	0.036	0.034	1.08
<b>Dirlik</b>	0.033	0.032	1.03
<b>Legacy Lalanne</b>	2.436E-06	1.868E-06	1.30
<b>Proposed modified Lalanne</b>	0.034	0.034	1.00
<b>Time domain mean damage value</b>	0.031		

Table 7-3 A summary of the vibration damage estimation results for Loop 1 of the case under consideration

Figure 7-6 and Figure 7-7 show exemplary Dirlik damage results on a discrete model using the author’s tool for signals slipped a five standard deviations and three standard deviations.

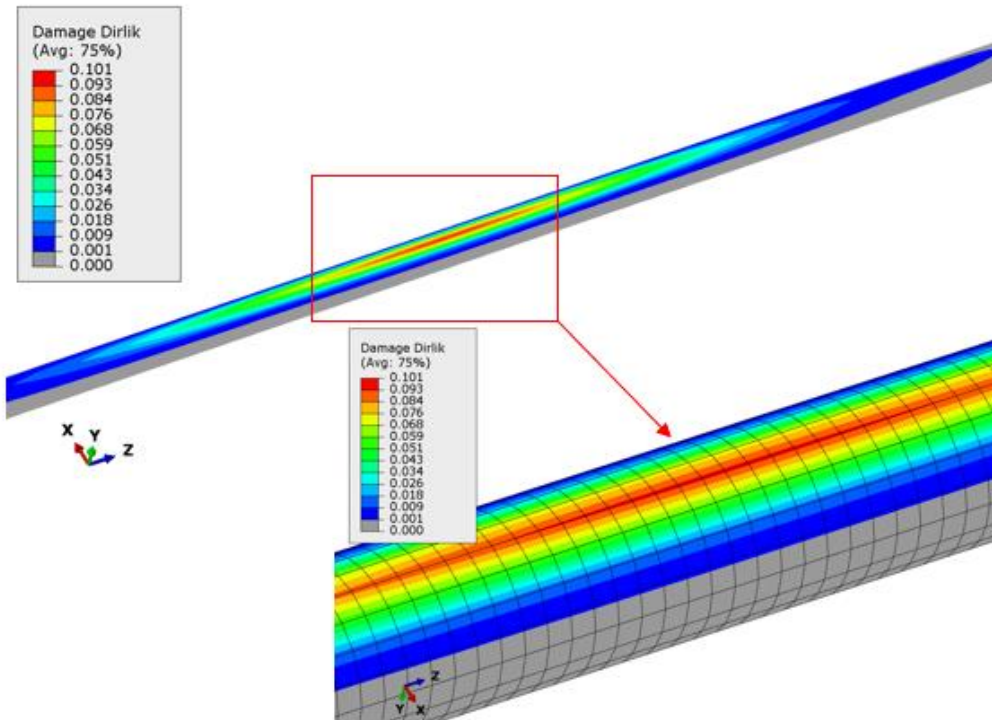


Figure 7-6 Vibration damage estimation using the Dirlik method with reduced spectral moments integration for a PSD Response clipped at five standard deviations using the author's tool

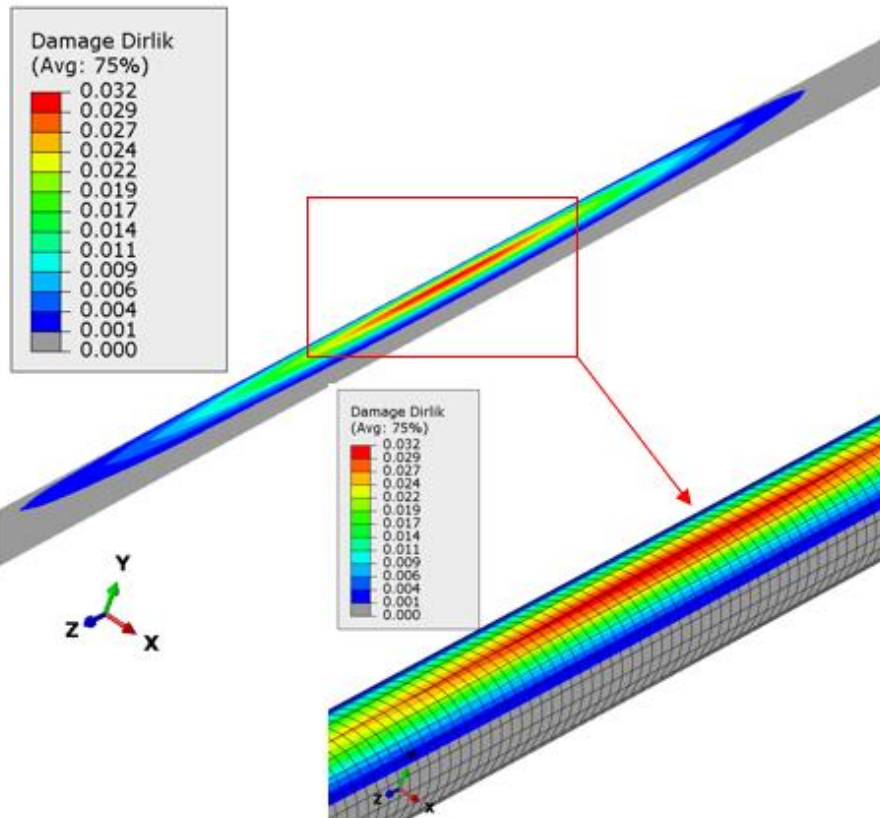


Figure 7-7 Vibration damage estimation using the Dirlik method with reduced spectral moments integration for a PSD Response clipped at three standard deviations using the author's tool

To show the benefits of modification of the legacy method we present Loop 2 of the research only within the frequency domain calculation (without quoting the time series damage value as we did not present the populational research for Loop 2, while the populational research for the wide band and white noise signals can be found in Chapter 5 of this paper – the research shows that the conclusion reached for the narrow band signal is analogical with that for the wide band and white noise signal). Table 7-4 shows a summary of the damage result for a three and five standard deviations PSD response signal clipping, using frequency domain-based methods. The result show that modifying the legacy methods provides damage results close to the Dirlik method (this method gives damage results close to the time domain damage results using the Monte Carlo method as per Chapter 5 of this paper). The results show the modification of the Narrow Band method allow to obtain two times less conservative damage results, and for the modified Lalanne method give a much more accurate damage value than for the Legacy Lalanne method.

<b>Impact of stochastic dynamic loading on an exemplary transmission shaft Loop 2</b>			
<b>A signal clipped at five standard deviations</b>			
<b>Damage estimation method</b>	<b>Full integration</b>	<b>Reduced integration (77.5%)</b>	<b>Full integration/Reduced integration</b>
<b>Legacy Narrow Band</b>	0.482	0.398	1.21
<b>Proposed modified Narrow Band (replaced EP with E0)</b>	0.252	0.247	1.02
<b>Dirlik</b>	0.283	0.240	1.18
<b>Legacy Lalanne</b>	2.170E-05	1.492E-05	1.45
<b>Proposed modified Lalanne</b>	0.254	0.248	1.03
<b>A signal clipped at three standard deviations</b>			
<b>Damage estimation method</b>	<b>Full integration</b>	<b>Reduced integration (77.5%)</b>	<b>Full integration/Reduced integration</b>
<b>Legacy Narrow Band</b>	0.117	0.097	1.21
<b>Proposed modified Narrow Band (replaced EP with E0)</b>	0.061	0.060	1.02
<b>Dirlik</b>	0.059	0.057	1.03
<b>Legacy Lalanne</b>	2.170E-05	1.492E-05	1.45
<b>Proposed modified Lalanne</b>	0.063	0.061	1.04

Table 7-4 A summary of the vibration damage estimation results for Loop 2 of the case under consideration

### 7.3.2 Combined frequency and time domain damage estimation under stochastic loading

This section presents the populational research made on 5000 samples (for which observed stabilization distribution parameters), the calculation was provided based on the transfer function for the critical integration point in the transmission shaft. The input loading is the same as defined in section 7.3.1. The populational research aims to obtain the distribution of the damage and assess the variability of damage, as the research introduced in section 5.4 reveals a high variability of the damage value, which depends on the frequency resolution used in IFFT. Table 7-5 shows a summary of the damage for a PSD response clipped at three and five standard deviations for different frequency resolutions in IFFT. The damage results as presented using the three best fitted distributions recommended in Chapter 5 (Exponentiated Weibull, Generalised Extreme Value and Gaussian distributions). The obtained results show that the damage variation stabilises for  $N=2^{16}$  for the three standard deviations signal clipping. For the low frequency resolution, the damage variability is very high – the maximum damage for which 99.73% of samples have lower damage is around two times higher than the mean value. This shows that the damage results estimated using the frequency domain-based method quoted damage value of 0.031 are consistent with the mean damage. However, the damage can vary within the range 0.010 to 0.059, e.g., if during the test a low resolution was, such as  $N=2^{12}$ . A value close to the 0.059 suggests over-testing, although a value of 0.010 suggests under-testing and can be critical in terms of structural integrity. Therefore, the modification of the PSD input curve proposed in 5.4.4 – which proposes to increase the PSD input value to meet the condition that the damage value for which 0.13% of the test sample has no lower damage, will be higher than the damage for which 99,73% of the population does not exceed the quoted damage value for the reference PSD input curve for IFFT block size  $N=2^{20}$ .

For a signal clipped at five standard deviations, we can observe that the mean damage value for block size  $N=2^{12}$  is not representative, showing stabilisation of the mean damage value at  $N=2^{18}$ . Additionally for this clipping we can observe far more damage variability – a damage value for which 0.13% of the population has no lower damage is 38% lower than the mean value, damage value for which 99.73% of population have higher damage is 171% higher than mean value (a comparison made for block size  $N=2^{20}$ ). The same comparison for a three sigma PSD response clipping is 6% and 5% respectively.

A graphical representation of the obtained result is presented in Figure 7-8 and Figure 7-9.

Three standard deviations clipping				
$\log_2(N)$ [-]	N [-]	Mean damage [-]	0.13% not lower than the quoted value of damage [-]	99.73% not exceeding the quoted value of damage [-]
12	4096	0.02988	0.01006	0.05926
14	16384	0.03070	0.01842	0.04446
16	65536	0.03077	0.02437	0.03730
18	262144	0.03084	0.02735	0.03406
20	1048576	0.03086	0.02911	0.03249
Five standard deviations clipping				
$\log_2(N)$ [-]	N [-]	Mean damage [-]	0.13% not lower than the quoted value of damage [-]	99.73% not exceeding the quoted value of damage [-]
12	4096	0.06872	0.01072	1.07656
14	16384	0.08322	0.01963	1.00431
16	65536	0.08875	0.03184	0.66266
18	262144	0.09211	0.04519	0.41469
20	1048576	0.09397	0.05785	0.25467

Table 7-5 A summary of the damage results for combined frequency and time domains vibration damage estimation

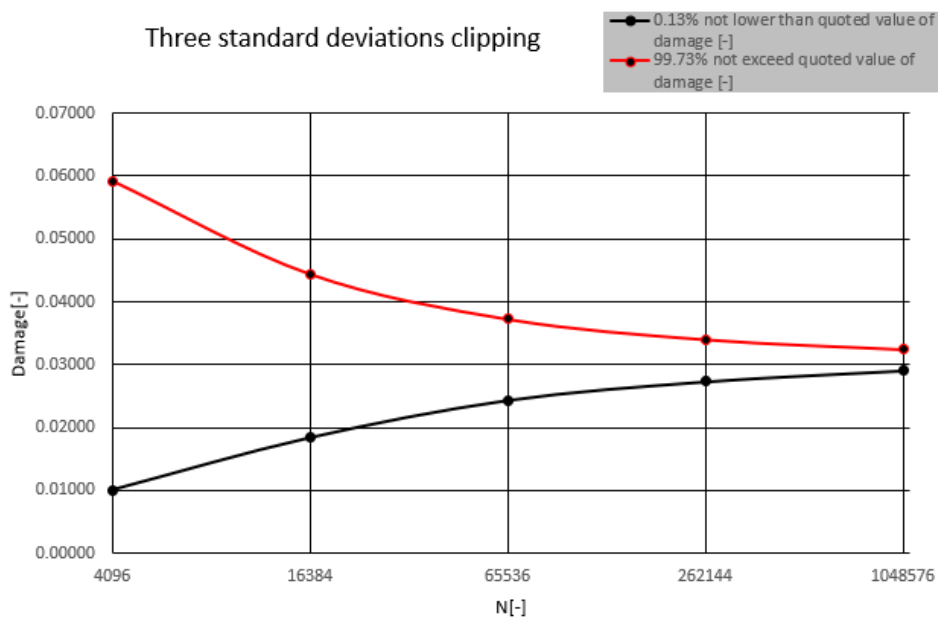


Figure 7-8 Graphical representation of the damage deviation for different IFFT frequency resolution for a signal clipped at three standard deviations

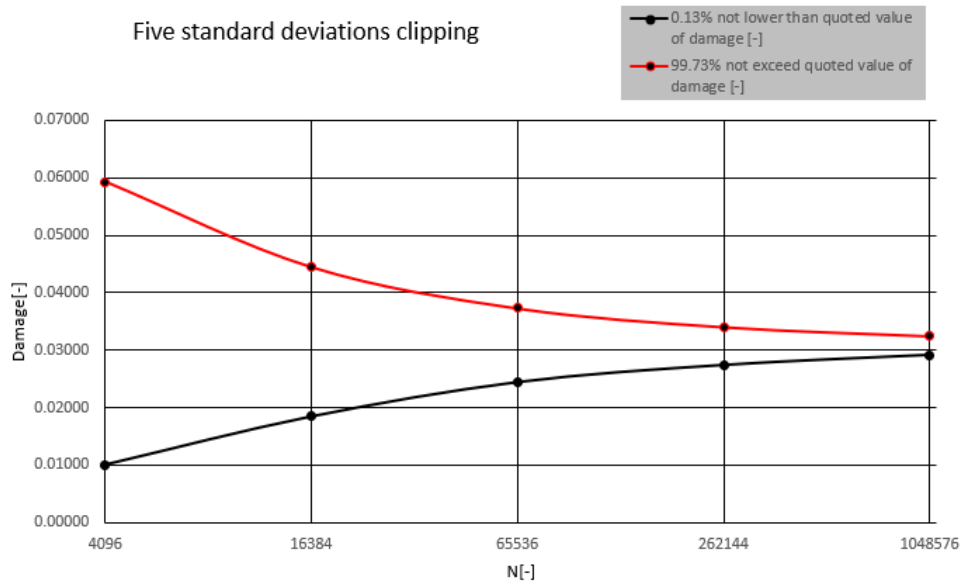


Figure 7-9 Graphical representation of the damage deviation for different IFFT frequency resolution for a signal clipped at five standard deviations

**7.4 An assessment of the impact of combined stochastic and deterministic dynamic loading on an exemplary transmission shaft – damage estimation under combined stochastic and deterministic loading**

This section presents the impact of combined stochastic and deterministic loading on an exemplary transmission shaft using the current state of knowledge – a legacy method and the new proposed author’s method introduced originally in [69] and developed further in Chapter 6 of this paper. As an example, we used the PSD input curve and constant amplitude sine sweep defined in Table 7-6. The research assumed that a random background is applied at frequency range 1-200Hz with a simultaneous sine sweep with amplitude 5g, acting at 15-35Hz (the frequency range for the sine selected to overlap the sine sweep input with a resonance frequency to obtain high damage value). As an example, we used the linear sine sweep.

<b>Stochastic signal definition in the frequency domain</b>		
<b>Frequency [Hz]</b>	<b>PSD input [g<sup>2</sup>/Hz]</b>	<b>Total time of exposure [s]</b>
1	1.0	2621
200	1.0	2621
<b>Deterministic signal definition in the frequency domain at frequency bandwidth &lt;15Hz; 35Hz&gt;</b>		
<b>Frequency [Hz]</b>	<b>Sine sweep amplitude [g]</b>	<b>Linear sine sweep rate [Hz/s]</b>
15	5	0.00763
35	5	0.00763

Table 7-6 The stochastic and deterministic signal definition for vibration damage estimation under combined loading

### 7.4.1 Frequency domain damage estimation under combined stochastic and deterministic loading

The first loop of the research used a legacy technique – a calculation based purely on the frequency domain. As introduced in the author’s publication [69] and Chapter 6, this method is highly conservative and the damage is quoted here as a reference for the new developed method. Table 7-7 shows a summary of the damage results using the legacy method – frequency based. Using the Dirlik method the obtained damage exceeded 1 and is therefore quoted also for 0.75% of the amplitude of the initial deterministic sine sweep. As introduced in Chapter 5 and Chapter 6, the Dirlik damage is consistent with the mean value of the sample population under consideration. Based on the results quoted in the table below, the damage for the initial sine sweep amplitude exceeds 1, however the mean damage value for a large population for block size  $N=2^{16}$  is 0.081 (see section 7.4.2, Table 7-8). Even when applying 0.75% of the initial sine sweep amplitude, we obtained damage of 0.691 for reduced integration. This shows that the legacy technique overestimates the damage value. It should be noticed that also the damage variation should be considered – see 7.4.2.

<b>The impact of combined deterministic and stochastic dynamic loading on an exemplary transmission shaft</b>			
<b>A non-clipped signal</b>			
<b>Damage estimation method</b>	<b>Full integration</b>	<b>Reduced integration (77.5%)</b>	<b>Full integration/Reduced integration</b>
<b>Dirlik full deterministic signal amplitude</b>	>1	>1	N/A
<b>Dirlik 0.75% of deterministic signal amplitude</b>	0.6930	0.6909	1.00
<b>The time domain mean damage value for a non-clipped signal</b>	0.081		

Table 7-7 A summary of the damage under combined stochastic and deterministic loading using the frequency domain methods (the time domain results are presented as a reference)

#### 7.4.2 Combined time and frequency domain damage estimation under combined stochastic and deterministic loading

This section introduces the second loop of assessment of combined stochastic and deterministic loading on a transmission shaft, based on the new proposed combined frequency and time domain calculation method – as introduced in Chapter 6.

Figure 7-10 shows the response of the transmission shaft in the time domain for combined random loading and a sine sweep for the considered example. Figure 7-11 shows a Rainflow Cycle Counting histogram for Rainflow response presented in Figure 7-10 using the author’s Rainflow Cycle Counting algorithm introduced in section 4.2.

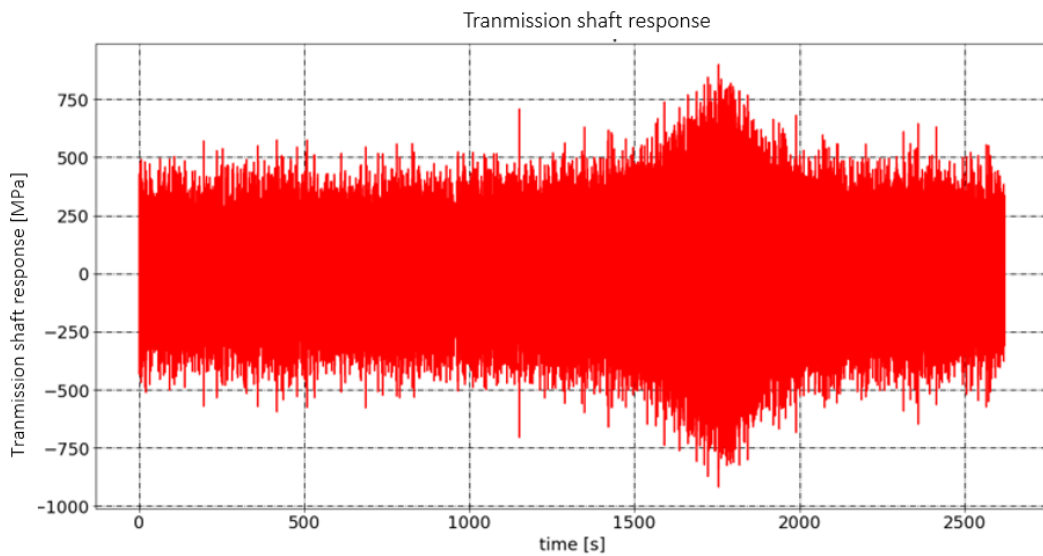


Figure 7-10 A combined stochastic and deterministic response of the transmission shaft in the time domain

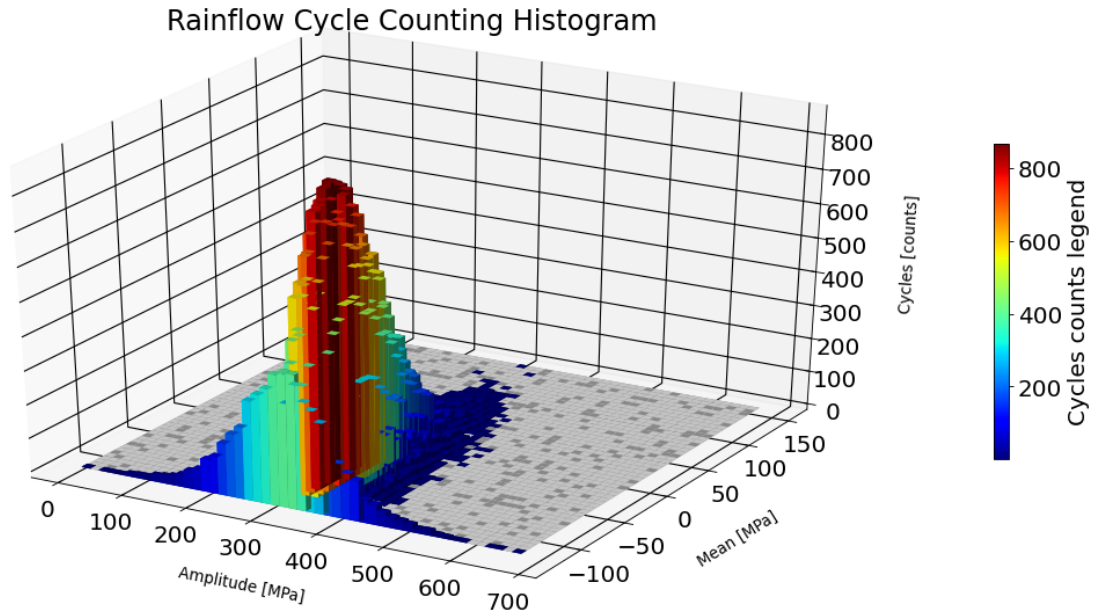


Figure 7-11 A Rainflow Cycle Counting histogram for combined stochastic and deterministic loading

Table 7-8 shows a summary of the populational damage analysis (based on 5000 samples for which observed stabilization distribution parameters) under combined simultaneous random loading and the linear sine sweep for the considered shaft example. The considered case takes into account signals clipped with three and five standard deviations and a non-clipped signal (to compare the new method with the legacy method). Three block sizes were used in all the cases, and we observed stabilisation of the mean damage and variation of damage. For a signal clipped with three standard deviations the differences between the mean and the damage, for which 0.13% of the population had no lower value, is 43%. The differences between the mean and damage value, for which 99.73% of the considered population has no higher damage value, is 63%. The response same differences for a signal clipped with five standard deviations are 61% and 584% respectively, and for a non-clipped signal 60% and 591% respectively. These results imply that, especially assuming a non-clipped signal or a low-clipped signal, the damage variation is high, which show how important it is to search the population of the example to properly assess the damage mean value and the potential damage variation. Additionally, taking into account the damage variability, the legacy technique (frequency domain based) is much more conservative than the proposed method (for the legacy technique the damage exceeds 1, while for the proposed method the damage, for which 99.73% of the considered population has a lower value, is 0.56 assuming that the signal is not clipped). Normally, for most aerospace application, the signal is clipped at three standard deviations, but the conservatism of the legacy technique is very high and implies oversizing of the unit for this load condition requirement. The new proposed method allows for precise damage estimation consistent with the requirement (e.g., many aerospace requirements allow for a signal clipped with three standard deviations), which implies reducing the conservatism and oversizing the unit in terms of vibration requirements.

Figure 7-12 through Figure 7-14 show a graphical representation of the transmission shaft damage variability under combined stochastic and deterministic loading presented in a summary presented in Table 7-8. These figures show that the damage, for which 0.13% of the population has a lower value, is stable in opposition to the damage value for which 99.73% of the population has a lower damage value.

<b>A stochastic signal clipped with three standard deviations</b>				
$\log_2(N)$ [-] [-]	N [-]	Mean damage [-]	0.13% not lower than the quoted value of damage [-]	99.73% not exceeding the quoted value of damage [-]
12	4096	0.04966	0.02636	0.10112
14	16384	0.05011	0.02776	0.08478
16	65536	0.05014	0.02871	0.08191
<b>A stochastic signal clipped with five standard deviations</b>				
$\log_2(N)$ [-]	N [-]	Mean damage [-]	0.13% not lower than the quoted value of damage [-]	99.73% not exceeding the quoted value of damage [-]
12	4096	0.07257	0.02787	0.67955
14	16384	0.07890	0.03123	0.58560
16	65536	0.08159	0.03162	0.55803
<b>A non-clipped stochastic signal</b>				
$\log_2(N)$ [-]	N [-]	Mean damage [-]	0.13% not lower than the quoted value of damage [-]	99.73% not exceeding the quoted value of damage [-]
12	4096	0.07354	0.02753	0.70834
14	16384	0.08025	0.03110	0.64071
16	65536	0.08136	0.03267	0.56250

Table 7-8 A damage summary for combined stochastic deterministic dynamic loading for a signal clipped with three, five standard deviations, and a non-clipped signal

Note that the non-clipped signal was mentioned in this section only as a direct comparison with the legacy method, as for the legacy method clipping a random signal is not allowed. Normally in the aerospace industry it is allowed to clip a random signal at three standard deviations [2].

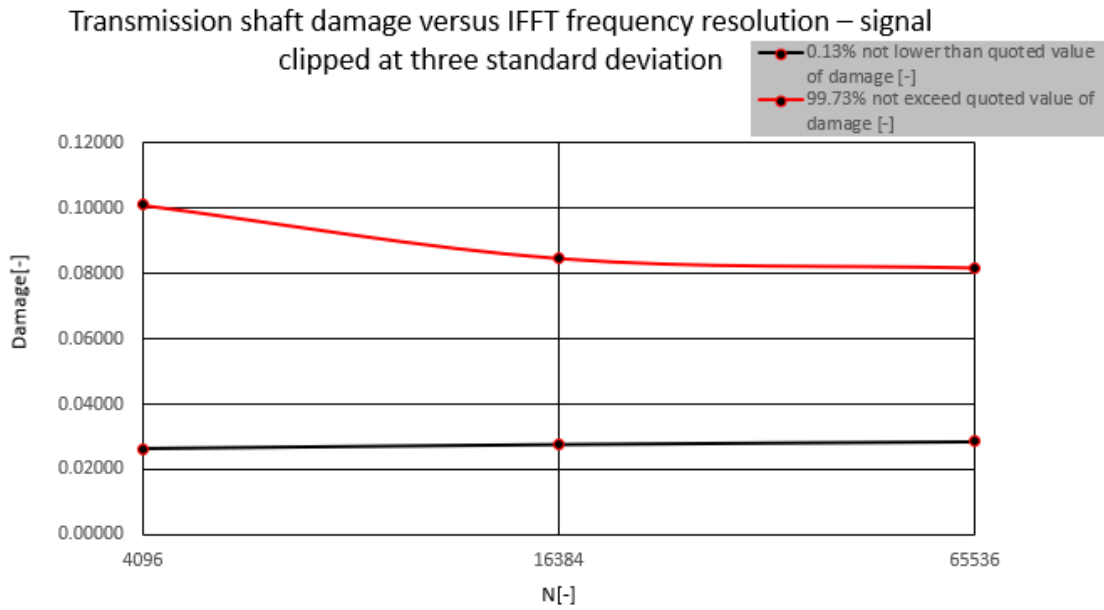


Figure 7-12 Graphical representation of the damage deviation under combined stochastic and deterministic loading for different IFFT frequency resolutions for a signal clipped at three standard deviations

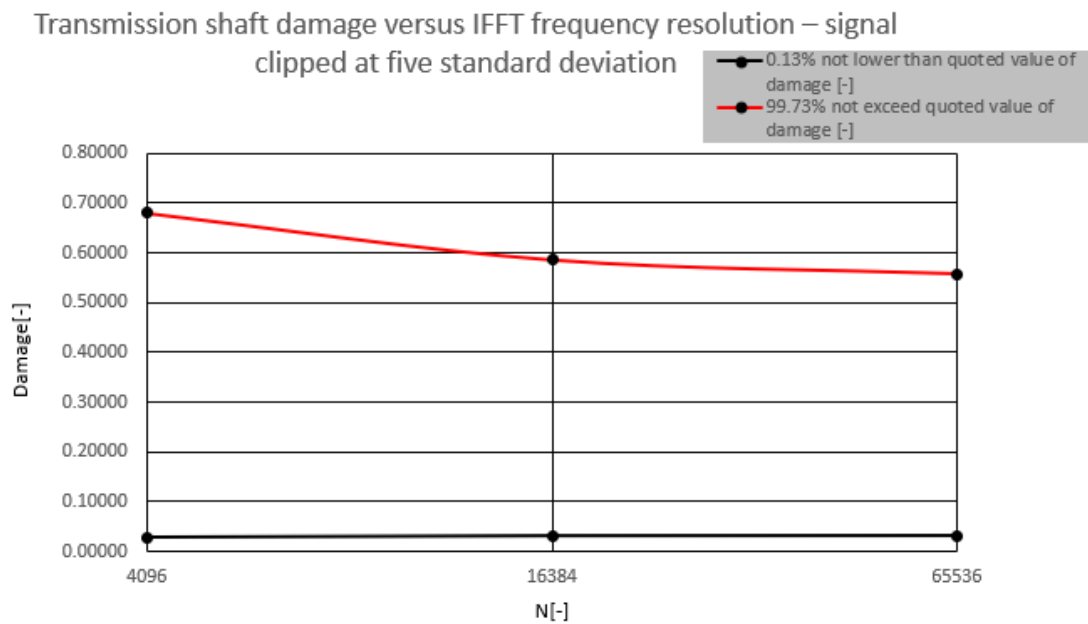


Figure 7-13 Graphical representation of the damage deviation under combined stochastic and deterministic loading for different IFFT frequency resolutions for a signal clipped at five standard deviations

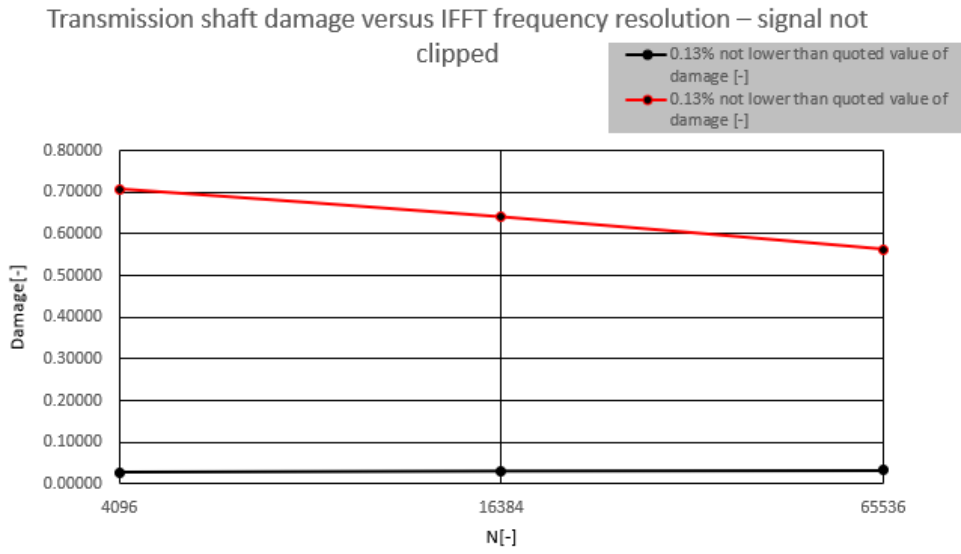


Figure 7-14 Graphical representation of the damage deviation under combined stochastic and deterministic loading for different IFFT frequency resolutions for a non-signal clipped response

## CHAPTER 8 CONCLUSIONS AND FURTHER RESEARCH

A summary of the conducted computer experiments using two combined methods: FEM and the Monte Carlo method and Python programming allows for identifying gaps in the empirical description of the signal statistic in the frequency domain for signals other than the narrow band. For the white noise signal, the number of peaks obtained using empirical equations is more than 50% different than the number of peaks obtained in the time domain signal retrieved using the Monte Carlo and IFFT methods (for the narrow band signal empirical parameters in the frequency domain match the signal parameters in the time domain). The research results help to modify the existing method for vibration damage assessment via modification of the equation for evaluation of the PDF function (Lalanne method), modifying the equation for the actual number of cycles calculation (Bendat method). Additionally, the proposed new approach for integrating spectral moments uses the Monte Carlo and IFFT methods, which helps to obtain signal statistic parameters in the frequency domain matched to signal statistics in the time domain – which is not the case for the wide band signal and the white noise signal using the legacy theory (only the narrow band signal statistic parameters in the frequency domain matched to the signal statistic parameters in the time domain). Reduced integration of the 1<sup>st</sup>, 2<sup>nd</sup> and 4<sup>th</sup> spectral moments allows for precise derivation of signal statistics in the frequency domain and using this approach with the modified Lalanne and Bendat methods (based on research introduced in this paper) allows to obtain close damage results with the Dirlik method. It is worth noting that the damage evaluated using the Dirlik method is treated as a reference, as it is the best for general usage, for a general value of the irregular factor based on publications [3] and [4] and based on conducted research. The research result therefore helps to developed two methods –based on the legacy Bendat and Lalanne method, which enables precise damage estimation for all signals (narrow band, wide band, white noise) with accuracy close to the Dirlik method. The new modified method has a much less complicated empirical formulation – which is important in engineering usage in Collins Aerospace Company.

The research revealed that the damage variation depends on the block size (N) used in IFFT – this phenomenon was not research by Dirlik. This reveals that the legacy method for vibration damage estimation under stochastic loading estimates the mean damage, however in reality the damage values variate and the damage ranges (which depend on the block size) need to be estimated. In his research, Dirlik used a relatively low value of block size –  $N = 20 \times 2^{10}$ , and in the current research noticed that the damage variability is close to +/-60%. This can be critical in terms of the accuracy of the Dirlik method, which does not consider a frequency resolution variable during real testing. What needs to be noticed is the fact that Dirlik' s examined population was only 10 samples, which was potentially not enough to obtain a good statistical description of the examined population. Therefore, the research presented in this paper has been extended to taken into account a large population of sample (5000, for which observed stabilization distribution parameters) – using computer techniques for testing, based on the Monte Carlo and IFFT methods. This helps to assess the impact of the population size and block size on the damage statistic and damage distribution. An additional aspect taken into account is the impact on the tested units with apertures, which normally have a limited frequency resolution (limited block size) – This could imply significant under-testing for the low value of the frequency resolution used for testing.

To estimate the damage range, it is recommended to use one of three best fitted distribution types: Generalised Extreme Value, Exponentiated Weibull and Gaussian distributions – as these distributions characterise the best fitting damage distributions from among many others taken into account. Additionally, it was proposed to use the criteria defined in Eq. 5.3, which says that damage for which 0.13% of the population has no lower damage – for the block size used during the testing –  $D_{i,0.13\%}(N_{2^i})$  needs to be higher than the damage for which 99.73% of the population has no higher damage – when N is equal to  $1048576 = 2^{20} - (D_{20,99.73\%}(N_{2^{20}}))$ . Meeting the criteria introduced above guarantees that there is no under-testing during real testing, when the block size used during the testing is limited. The graphical representation of the proposed criteria is shown in Figure 5-53, Figure 5-54 and Figure 5-55 for the white noise, wide band and narrow band signals respectively.

Another important aspect of the presented work was developing a method for precise vibration damage assessment, originally presented in the author's publication [69], for the white noise signal and extended for the wide band and narrow band signals in this document. The new approach is to use combined frequency and time domain consideration and Rainflow Cycle Counting in the time domain instead of the legacy technique to process all calculations in the frequency domain. This approach helps keep the legacy efficiency of the linear dynamic method analysis in the frequency domain with a high level of accuracy of the time domain approach of Rainflow Cycle Counting in time domain. This work introduced how conservative is the legacy method and might implies oversizing aerospace units to meet dynamic loading requirement. Using the new method is a milestone for analysis this loading scenario for Collins Aerospace Company. Proposed novel method can be used for civilian and military aircrafts as well. Using this method will help to reduce weight, increase reliability and safety of aircraft units.

Additionally, this approach helps to assess the damage ranges (damage variability) – in a similar way as the damage assessment for pure random loading. To estimate the damage ranges, it is recommended to use one of the three best fitted distribution types: Generalised Extreme Value, Exponentiated Weibull and Gaussian distribution – as these distributions best fit the experiment damage distribution from among many others taken into account as per analogy to vibration damage estimation under pure random loading. For simultaneous random and deterministic loading it is also proposed to meet the condition described by inequality presented in Eq. 5.3 – as meeting this criteria guarantees not under-testing during real testing, when the block size used during the testing is limited.

All the developed methods were used for assessment of the dynamic loading impact on an exemplary transmission shaft in Chapter 7, where two cases were considered. The first related to the pure random loading impact on a transmission shaft, and the second assume a simultaneous random and deterministic sine sweep loading scenario. This analysis aims to demonstrate the author's tools and method with using the research results and methods introduced in this document. The demonstration was made on a transmission shaft, which was tested – the test results were used for correlation of the FEM model used for derivation of the transfer function. The obtained transfer function of the transmission shaft was used as the input for the created tools. The conducted analysis shows that using the legacy method for vibration damage estimation under random loading can be critical in terms of the structural integrity of the considered unit, as it does not take into account the damage variation, which depends on the block size. In terms of the second load scenario – the vibration damage estimation under combined stochastic and deterministic loading, the legacy technique is very conservative and could imply oversizing the units. The new proposed method derived an accurate damage value taking into account random signal clipping and block size using during real testing. The new method also allows for estimating the damage ranges, not just the mean value as with the legacy method.

The stress-based approach was used for demonstrating the algorithm, and additionally this approach is widely used in the related research ([3] through [14]), and commercial software as nCode [30] and MSC CAE Fatigue [28], for isotropic material. Future research will also focus on developing an algorithm using the Critical Plane approach, which is treated as a more robust approach for multiaxial fatigue damage assessment ([28], [29], [30], [35], [36], [37] and [38]). This approach is much more computationally intensive, as calculations need to be provided per each e.g., 10°, from 0° to 180°, as proposed in commercial software [30]. It should be noted that expanding the new developed method for vibration damage estimation under simultaneous random and deterministic sine sweep loading is allowed – a suitable calculation procedure needs to be developed.

Additionally, further research will focus also on the possibility to use the proposed method in synergy with the energetic fracture mechanics model, as used in publication [39], [40] and [41], where the Cohesive Zone Model was used for assessing damage and life prediction.

It should be noted that this method was originally developed for isotropic, metallic material, and any other consideration to use this method for orthotropic material will be the subject of future research.

The research presented in this paper introduced the stress life method as an example. Further research and publication will focus on using the strain life method, using e.g. Morrow or Smith-Watson-Topper Mean Stress Correction and Neuber correction [42], [43] and [44] for expanding the proposed method to allow fatigue consideration, when a local plasticity region occurs due to the high level of loading occurrence.

---

## BIBLIOGRAPHY

- [1] Australian Government: Tyre failure and flap asymmetry event involving Boeing 787, VH-VKA. Australian Transport Safety Bureau. Singapore 2017
- [2] Environmental Conditions and Test Procedures for Airborne Equipment, RTCA DO-160G, Washington US, 2010
- [3] Bishop N., Kerr S., Murthy P., Sweitzer K.: Advances Relating to Fatigue Calculations for Combined Random and Deterministic Loads. SAE Technical Paper 2014-01-0725, 2014, doi:10.4271/2014-01-0725
- [4] Bishop N., Murthy P., Sweitzer K., Kerr S.: Time vs frequency domain analysis for large automotive systems. SAE Technical Paper 2015-01-0535, 2015, doi: 10.4271/2015-01-0535
- [5] Ferreira W., Meehan T., Cardoso V., Bishop N.: A comparative study of automotive system fatigue models processed in the time and frequency domain. SAE Technical Paper 2016-01-0377, 2016, doi 10.4271/2016-01-0377
- [6] Halfpenny A., Kichim F.: Rainflow cycle counting and acoustic fatigue analysis technique for random loading. 10<sup>th</sup> International Conference RASD, Southampton UK, 2010
- [7] Bishop N., Sherratt F.: Fatigue life prediction from power spectral density data. Environmental Engineering, vol. 2, 1989
- [8] Bishop N., Sherratt F.: Finite Element Based Fatigue Calculation. NAFEMS Ltd., 2000
- [9] Sweitzer K., Bishop N., Genberg V.: Efficient computation of spectral moments for determination of random response statistics. International Conference on Noise and Vibration Engineering - ISMA, Leuven, BE, 2004
- [10] Bishop N.: Methods for the rapid evaluation of fatigue damage on the Howden HWP330 wind turbine. *Proceedings of the 13th British Wind Energy Conference, Swansea, UK*, p. 317-321, 1991
- [11] Datta S., Bishop N., Sweitzer K., Atkins A.: Simultaneous durability assessment and relative random analysis under base shake loading conditions. SAE Technical Paper 2017-01-0339, 2017
- [12] Halfpenny A.: Rainflow Cycle Counting and fatigue analysis from PSD. Proceedings of the ASTELAB conference, France, 2007
- [13] Halfpenny A., Bishop N.: *Vibration Fatigue*, HBM-nCode, UK, 1997
- [14] Halfpenny A., Kichim F.: Rainflow cycle counting and acoustic fatigue analysis technique for random loading. 10<sup>th</sup> International Conference RASD, Southampton UK, 2010
- [15] Bendat J.: Probability functions for random responses. NASA report contract NAS-5-4590, 1964
- [16] Bendat J.: Random data: Analysis and measurement procedures. John Wiley & Sons Inc., New York United States 2010

- 
- [17] Bendat J.: Principles and Applications of Random Noise Theory. John Wiley, New York, 1958
- [18] Dirlik T.: Application of computers to fatigue analysis, PhD Thesis, Warwick University, 1985
- [19] Rice S.: Mathematical analysis of random noise. Selected papers on noise and stochastic processes, Dover, New York, 1954
- [20] Lalanne C.: Mechanical vibration and shock, Vol. 4, Hermes Penton Science, London, 2009
- [21] Lalanne C.: Mechanical vibration and shock analysis: Specification Development, 3rd edition, Vol. 5, Wiley, London, 2014
- [22] Lalanne C.: Mechanical vibration and shock analysis: Fatigue Damage, 3<sup>rd</sup> edition, Vol. 4, Wiley, London, 2014
- [23] Steinberg D.: Vibration analysis for electronic equipment (2nd edition). Jon Wiley & Sons, New York, 1988
- [24] Wirshing P.: Paez T. Ortiz K.: Random Vibration, John Wiley & Sons Inc., New York 1995
- [25] Chaudhury G., Dover W.: Fatigue analysis offshore platforms subjected to sea wave loadings. International Journal of Fatigue, Vol. 7, No. 1, p.13-19, 1985
- [26] Gall D., Hancock J.: Fatigue crack growth under narrow and broad band stationary loading. Glasgow University, Marine Technology Centre, 1985
- [27] Tuna J.: Fatigue life prediction for Gaussian random loads at the design stage. Fatigue and Fracture of Engineering Materials & Structures, Vol. 9 No. 3, p. 169-184, 1986
- [28] CAEfatigue VIBRATION (CFV) User Guide & Verification Manual (Release 2014). CAEfatigue Limited, UK, March 2014
- [29] CAEfatigue VIBRATION (CFV) User Guide & Verification Manual (Release 2020). CAE fatigue Limited, UK, Nov 2020
- [30] nCode 2022.0 documentation, HBK 2020
- [31] Papoulis A.: Probability, Random Variables and Stochastic Processes. McGraw-Hill Inc., New York, 1965
- [32] Lindgren B.: Statistical Theory. Macmillan Publishing Co. Inc., New York, 1968
- [33] Benson H.: Principles of Vibration. Oxford University Press, New York, Oxford (1996)
- [34] ABAQUS User Manual V2018. Dassault Systems (2017)
- [35] Delprete C., Sesana R., Vercelli A.: Multiaxial damage assessment and life estimation: application to an automotive exhaust manifold. Procedia Engineering Vol. 2, April 2010, p. 725-734.
- [36] Engin Z., Coker D.: Comparison of Equivalent Stress Method with Critical Plane Approaches for Multiaxial High Cycle Fatigue Assessment. 2nd International Conference on Structural Integrity, ICSI 2017, 4-7 September 2017, Funchal, Madeira, Portugal. Procedia Structural Integrity Vol. 5 2017, p. 1229-1236

- 
- [37] Weber B.: Fatigue multiaxiale des structures industrielles sous chargements quelconque, PhD Thesis, l'Institut National des Sciences Appliquées de Lyon, 1999
- [38] Billaudeau T., Nadot Y., Bezine G.: Multiaxial fatigue limit for defective materials: mechanism and experiments. *Acta Materialia* 52, p. 3911-3920, 2004.
- [39] Smolnicki M., Ptak M., Lesiuk G.: Static failure load predictions in notched steel components using a combined experimental-numerical approach. *International Journal of Structural Integrity*. 2017, vol. 8, no. 6, p. 683-693.
- [40] Wang J. T.: Relating Cohesive Zone Models to Linear Elastic Fracture Mechanics. NASA/TM-2010-216692, May 2010.
- [41] Kucharski P., Lesiuk G., Czaplinski T., Fratzczak R., Maciejewski Ł: Numerical Estimation of Stress Intensity Factors and Crack Propagation in Lug Connector with Existing Flaw. AIP Conference Proceedings. Fatigue Failure and Fracture Mechanics XXVI: Proceedings of the XXVI Polish National Conference on Fatigue Failure and Fracture Mechanics 17-20 May 2016 Fojutowo, Poland.
- [42] Dowling N.E.: Local Strain Approach to Fatigue. *Comprehensive Structural Integrity*, Vol 4, 2003 p. 77-94.
- [43] Meggiolaro M. A., Castro J. T. P.: Statistical evaluation of strain-life fatigue crack initiation predictions. *International Journal of Fatigue*, Vol 26, Issue 5, May 2004, p. 463-476.
- [44] Lee Y. L., Hathaway R., Barkey M.: Fatigue Testing and Analysis. Theory and Practice. Elsevier Butterworth Heinemann, 1st Edition July 29, 2004.
- [45] Langtangen H.: Python Scripting for Computational Science, Third Edition, Simula Research Laboratory. Springer, Berlin, Heidelberg, 2009
- [46] McKinney W.: Python for Data Analysis, 2nd Edition, William McKinney, Beijing Cambridge, Farnham, Kohl, Sebastopol, Tokyo 2018
- [47] McKinney W.: Data Science from Scratch, Joel Grus, Beijing Cambridge, Farnham, Kohl, Sebastopol, Tokyo 2015
- [48] Zienkiewicz O.C.: Finite Element Method. McGraw-Hill, Dallas (1977)
- [49] Metallic Materials Properties Development and Standardization (MMPDS-15), Battelle Memorial Institute, July 2020.
- [50] Palmgren A.: Die lebensdauer von kugellagern, *zeitschrift des vereinesdeutscher ingenierure*, Vol. 68, No. 14, 1924, pp. 339-341, 1924
- [51] Miner A.: Cumulative damage in fatigue. *J Applied Mechanics*, Vol. 67, 1945, pp A159-A164, 1945
- [52] Ptak M., Czmochocki J.: Using computer techniques for vibration damage estimation under stochastic loading using the Monte Carlo Method for aerospace applications. *Probabilistic Engineering Mechanics*. 2023, vol. 72, p. 1-13.

- [53] Ptak M., Czmochoowski J.: Using computer techniques for vibration damage estimation of aircraft structures under stochastic loading. W: Computer Aided Engineering. Nauka i przemysł / red. Tadeusz Smolnicki. Wrocław: Oficyna Wydawnicza Politechniki Wrocławskiej, 2022. p. 169-179.
- [54] Newland D.: An introduction to random vibrations, spectral & wavelet analysis. Longman Inc., England 1995
- [55] Newland, D.: *Mechanical Vibrations Analysis and Computation*. Dover Publications, 3rd Edition, 2006
- [56] Chevillard S.: The functions erf and erfc computed with arbitrary precision and explicit error bounds. Information and Computation Vol. 216, July 2012, Pages 72-95.
- [57] ESDU 06010 Cycle counting methods for the estimation on fatigue life
- [58] Downing S., Socie D.: Simple Rainflow counting algorithms. International Journal of Fatigue, January 1982
- [59] Matsuishi M, Endo T.: Fatigue of metals subject to varying stress. Japan Society of Mechanical Engineers, Fukuoka, March 1968
- [60] Sutherland H.: On the Fatigue Analysis of Wind Turbines. Sandia National Laboratories, Albuquerque, New Mexico, June 1999
- [61] Watson P., Dabell B.: Cycle counting and fatigue damage. Society of Environmental Engineers, September 1976
- [62] Python 3.8.12 Documentation (<https://docs.python.org/3.8/>)
- [63] Python 2.7.3 Documentation (<https://docs.python.org/release/2.7.3/>)
- [64] Bishop N., Sweitzer K., Schlesinger D., Woodward A.: Fatigue calculation for multi input random and deterministic loads in the frequency domain. UK NAFEMS Conference, Oxford UK, Accelerating the Future of CAE, 10-11 June 2014
- [65] Bishop N., Murthy P, Sweitzer K.: Advances Relating to Fatigue Calculation for Combined Random and Deterministic Loads. 13<sup>th</sup> International ASTM/ESIS Symposium on Fatigue and Fracture Mechanics (39<sup>th</sup> National Symposium on Fatigue and Fracture Mechanics), November 13-15, 2013, Jacksonville, FL
- [66] MIL-STD-810H, Department of Defence Test Method Standard: Environmental Brown A.M., McGhee D. S.: Statistical Evaluation and Improvement of Method for Combining Random and Harmonic Loads. Marshall Space Flight Centre, Alabama 35812, 2003.
- [67] Engineering Consideration and Laboratory Test, USA, 2019
- [68] Brown A.M., McGhee D. S.: Statistical Evaluation and Improvement of Method for Combining Random and Harmonic Loads. Marshall Space Flight Centre, Alabama 35812, 2003.
- [69] Ptak M., Czmochoowski J.: Using computer technique for developing method for vibration damage estimation under combined random and deterministic loading. Computational Technologies in Engineering TKI 2022, Acta Mechanica et Automatica vol. 17, No 4, 2023.

- [70] Ptak M., Czmochowski J.: Analysis of the impact of dynamic loads on transmission shafts of a civil aircraft. W: Modelling in engineering 2020: applied mechanics / eds. Arkadiusz Mężyk [i in.]. Cham: Springer, cop. 2021. s. 245-257.  
(Advances in Intelligent Systems and Computing, ISSN 2194-5357; vol. 1336)